The role of hypoxic preconditioning in protection against the cardiotoxic effects of the anthracycline compound Doxorubicin.

Angshuman Maulik

Thesis submitted for award of the degree of MD (Research)

University College London

DECLARATION.

I, Angshuman Maulik, confirm that the work presented in this report is my own. Where information has been derived from other sources, I confirm that this has been indicated in the thesis.

Signed: (Angshuman Maulik)

ACKNOWLEDGEMENTS.

My mother Gopa, my brother Anirban and his wife Madhumita, and my friend Mlle Laurence Jacob are the foremost people who deserve acknowledgement for their encouragement, patience and sacrifice in supporting me through this work. The advice, guidance, patience and encouragement of the following people are also acknowledged, without which the work described below would remain incomplete. Particular acknowledgement is deserved for the help and guidance provided by Dr I Piowtrowska, who provided help, guidance and advice on technical aspects at all times without hesitation or reserve, helped guide experimental designs, and very helpfully provided feedback and advice in constructing this thesis. It ought to be acknowledged that Dr S Davidson provided some limited advice and guidance in experimental planning and also reviewed this thesis while it was being prepared. The advice and help of Dr S Chakraborti at University of Massachusetts Medical School in the preparation of this report deserves highlighted. Overview and broad guidance during this project was provided by Prof Derek M Yellon, who also provided the facilities and funding for this work. It is understood this work was supported by funding from the British Heart Foundation (grant number PG/15/52/31598) and the Biomedical Research Centre (grant number BRC233/CM/SD/101320). This work was undertaken at UCLH/UCL who received a proportion of funding from the Department of Health's National Institute for Health Research Biomedical Research Centres funding scheme.

Dr J Vicencio

Dr S Subrayan

Dr J McGowan

Contents

Table of Figures

Abstract

Introduction: Anthracyclines (ANTC) are potent chemotherapy agents, but may cause chronic irreversible cardiac failure. Recent data suggest cardiac damage due to ANTC begins early and may be a continuum. Cardioprotective modalities effective against acute injury may therefore provide prolonged benefit. Hypoxic Preconditioning (HP), i.e., subjecting cardiomyocytes to sub-lethal hypoxia and reoxygenation before a prolonged lethal ischaemic insult, protects cardiomyocytes by activating the pro-survival Reperfusion Injury Salvage Kinase (RISK) pathway. We examined the hypothesis that HP can protect cardiomyocytes against toxicity of the ANTC compound Doxorubicin (Dox).

Methods: A toxic concentration of Dox was identified in an *in vitro* model of cardiotoxicity established in isolated adult rat ventricular myocytes (ARVM), using Propidium iodide (PI) permeability and altered morphology including cell-membrane blebbing as markers of cell-death. An *in vitro* hypoxic preconditioning (HP) protocol was characterised, and the effect of this HP-stimulus on cell-death with subsequent Dox-treatment was assessed. Induction of the RISK pathway by HP was investigated by pre-inhibiting the Phosphoinositide 3-kinase (PI3K)/Akt cascade and the Mitogen Activated Protein Kinase (MAPK) Extracellular signal-regulated Kinase (ERK) 1/2 pathway with 10µM LY294002 (LY) and 30µM PD98059 (PD) respectively. The role of oxidative stress in Dox-toxicity was probed using N-acetyl cysteine, a known Reactive Oxygen Species (ROS)-scavenger. Fluorescence of 30 nM Tetramethylrhodamine methyl ester (TMRM) was used to assess the mitochondrial transmembrane potential ($\Delta\Psi_m$). Laser-induced ROS generation with 3 µM TMRM was used to assess mitochondrial permeability transmembrane pore (mPTP) induction after Dox-treatment, with 1µM Ciclosporine A (CsA) as a positive-protective control against mPTP induction. Dox-induced cell-death was also reassessed as an agent to protect against mPTP induction.

Results and Discussion: 7.5 µM Dox resulted in significant increase in cell-death ($p<0.05$) after 18h (44.2 ± 4.7% Dox vs 18.7 ± 1.5 % Control). HP protected cardiomyocytes from Dox (35.4 ± 1.7% Dox; 14.7 ± 1.5% Dox HP). LY, but not PD, abrogated this HP-induced protection (Dox HP: 16.9 + 1.5%; Dox HP LY: 38.5 + 3.3%; Dox HP PD: 15.9 + 1.3%). ROS-scavenging failed to rescue cardiomyocytes from Dox-toxicity. Dox failed to alter $\Delta\Psi_m$ or mPTP-induction. However, although the protective effect of presence of CsA on mPTP-induction was abrogated in cells pre-treated with Dox, concomitant treatment with dox and CsA could not protect ARVMs from dox-toxicity.

Conclusions and future directions: HP protects cardiomyocytes against cell-death due to Dox. Cell-death data suggest this protection is mediated via the PI3K/Akt pathway. The role of MAPK ERK 1/2 against Dox-toxicity *in vitro* is unclear. Dox-toxicity appears to be independent of oxidative stress, variations in $\Delta\Psi_m$, or vulnerability of the mPTP-induction. Further work to delineate mechanisms of toxicity, and the downstream components of HP-induced protection is necessary.

Abbreviations.

ACE- Angiotensin Converting Enzyme.

ACEi- Angiotensin Converting Enzyme II inhibitor.

ALL- Acute Lymphoblastic Leukaemia

AML-Acute Myeloid Leukaemia.

AMPK- Adenosine Monophosphate activated Kinase.

ANTC- Anthracyclines.

APAF- Apoptosis Protease Activating Factor.

ARC- Apoptosis Repressor with Caspase recruitment domain.

ATP- Adenosine triphosphate.

BAD- Bcl-2-Associated Death promoter.

BAK- BCL-2 homologous antagonist killer.

BAX- BCL-2 associated death X protein.

BID- BH3 interacting-domain death agonist.

BNP- Brain Natriuretic Peptide.

BRDU- bromodeoxyuridine.

CAD- Coronary artery diseae.

CI- Confidence interval.

CAMKII- Calcium/Calmodulin regulated Kinase II.

CCF- Congestive Cardiac Failure.

cGMP- Cyclic Guanosine Monophosphate.

cMRI- Cardiac Magnetic Resonance Imaging.

CPC- Cardiac Progenitor Cells.

CREB- Camp Responsive Element Binding Protein.

CsA- Ciclosporine A.

CTn- Cardiac Troponin.

cTnI- Cardiac Troponin I.

cTnT- Cardiac Troponin T.

Cyp D- Cyclophilin D.

DAG- Diacyl Glycerol.

DAPI- 4′,6′-diamidino-2-phenylindole.

DCM- Dilated Cardiomyopathy.

DIABLO- Direct IAP Binding Protein with Low pI.

DISC- Death Inducing Signalling Complex.

DMSO- Dimethyl Sulfoxide.

DNR-Daunorubicin.

DNM- Daunomycin.

Dox- Doxorubicin.

DRP1- Dynamin Related Protein-1.

dsRNA- Double stranded ribonucleic acid

DXZ- Dexrazoxane.

ECM- Extracellular matrix.

eNOS- Endothelium Derived Nitric Oxide.

Epi- Epirubicin.

Epo- Erythropoietin.

ERK- Extracellular signal Regulated Kinase.

ESC- European Society of Cardiology.

FADD- Fas associated Death Domain.

FASL- Fas Ligand.

GAPDH- Glyceraldehyde-3-phosphate dehydrogenase

GSK-3β- Glycogen Synthase Kinase 3 beta.

HDAC- Histone Deacetylases.

HF-ABP- Heart-type fatty acid binding protein.

HMGB1- High Mobility Group Box Protein 1.

HO-1- Haem oxygenase 1.

HP-Hypoxic Preconditioning.

HR- Hazard ratio.

HTRA2- High-Temperature Requirement 2.

IAP- Inhibitors of apoptosis proteins.

Ida-Idarubicin.

IL- Interleukin

IL-1- Interleukin-1.

IL-1β- Interleukin 1β

IL-1R- Interleukin 1 Receptor.

IL-1R- Interleukin 1 Receptor Antagonist.

IL-6- Interleukin 6.

IL-33- Interleukin 33.

IκB- Inhibitor of NFκB.

IKK- IκB Kinase.

iNOS- Inducible Nitric Oxide.

IP3- Inositol trisphosphate.

IPC-Ischaemic Preconditioning.

Ipsc- Induced pluripotential stem cells.

LCI- Myosin Light Chain I.

LCII- Myosin Light Chain II.

LTCC- L-type Calcium Channel.

LV- Left Ventricle.

LVEF- Left Ventricular Ejection Fraction.

LVESV- Left Ventricular End Systolic Volume.

MAPK- Mitogen Activated Protein Kinases.

MHC-Myosin Heavy Chain.

MI- Myocardial Infarction.

MM- Multiple myeloma.

MMP-2- Matrix Metalloproteinase-2.

MMP-9- Matrix Metalloproteinase-9.

MnSOD- Manganese-dependent Superoxide Dismutase.

mPTP- Mitochondrial Permeability Transition Pore.

MS-Multiple Sclerosis.

NAD- Nicotinamide Adenine Dinucleotide.

NAD(P)H- Nicotinamide Adenine Dinucleotide Phosphate.

NCX- Sodium-Calcium Exchange channel.

NFKB-Nuclear Factor Kappa B.

NHE- Sodium-Hydrogen Exchange channel.

NHL- Non Hodgkin's lymphoma.

NO- Nitric Oxide.

NTproBNP- N-terminal pro B-type Natriuretic Peptide.

PEG-Polyethylene glycol.

PGC- PPARγ Co-activator.

PI- Propidium Iodide.

PiC- Inorganic Phosphate carrier.

PKA- Protein Kinase A.

PKG- Protein Kinase G.

PI3K- Phosphoinositide 3 Kinase.

PIP2- Phosphoinositol bisphosphate.

PIP3- Phosphoinositol trisphosphate.

PTEN- Phosphatase and Tensin homologue.

PLC-Phospholipase C.

PIP2- Phosphoinositol bisphosphate.

PIP3-Phosphoinositol triphosphate.

PTEN-Phosphatase and Tensin homologue.

PPARγ- Peroxisome Proliferator-activated Receptor gamma.

RIP- Receptor Interacting Protein.

RISK- Reperfusion Injury Salvage Kinases.

ROS- Reactive Oxygen Species.

RNS- Reactive Nitrosative Species.

RYR- Ryanodine Receptor.

SDS- Sodium Dodecyl SulPhate.

SDS-PAGE- sodium Dodecyl Sulphate Polyacrylamide Gel Electrophoresis.

SERCA2A- Sarcoplasmic Reticulum Ca^{2+}-ATPase.

Smac- Second Mitochondria-derived Activator of Caspases.

SI- Simulated Ischaemia.

sIR- Simulated Ischaemia Reperfusion.

SR-Simulated Reperfusion.

SOD- Superoxide Dismutase.

sST-2- Soluble Suppression of Tumorigenicity-2,

TLR-2- Toll Like Receptor-2.

TLR-4- Toll Like Receptor-4.

TNF- Tumour Necrosis Factor.

Top1-Topoisomerase 1.

Top2- Topoisomerase 2.

TRADD- TNF-alpha Receptor Associated Death Domain.

TRAF- TNF Receptor Associated Factor.

TRAIL- TNF-Related Apoptosis-inducing Ligand.

TUNEL- Terminal deoxynucleotidyl transferase dUTP nick End Labelling.

UPS- Ubiquitin Proteasomal Pathway.

VDAC- Voltage-Dependent Anion Channel.

Chapter 1. Introduction.

Anthracyclines (ANTC) are a group of anthracenedione antibiotics that form integral part of chemotherapeutic protocols against a multitude of cancers, including solid organ tumours (e.g. Breast Cancer, Renal Cancer); soft tissue malignancies (e.g. Sarcomas); childhood cancers e.g., Acute Myeloid Leukaemia (AML), Acute Lymphoid Leukaemia (ALL); as well as haematological malignancies, e.g., Non-Hodgkin's Lymphoma (NHL), Multiple Myeloma (MM) (Minotti et al, 2004). Unfortunately their use is significantly limited by cardiotoxicity, which includes acute as well as chronic toxic effects. Acute ANTC-cardiotoxicity may manifest as inflammatory heart diseases (such as myocarditis or pericarditis), conduction abnormalities, and altered myocardial repolarisation. However, dilated cardiomyopathy (DCM) and refractory congestive cardiac failure (CCF) remains the most common and poorly understood manifestation of the chronic cardiotoxic effects of ANTC treatment (Schwartz et al, 1987; Gianni et al, 2008).

1.1. Anthracyclines.

Initially developed as antibiotics in late 1960s, ANTCs share a tetracyclic aglycone structure (see Fig.1.1) of four cyclohexane chains with a Daunosamine sugar moiety at Carbon C7 of ring A; adjacent quinone-hydroquinone groups in rings C and B; a methoxy substituent carbon C4 in ring D; a carbonyl group at C13; and a short side chain in C9. Doxorubicin (Dox) and Daunorubicin (DNR) were the first isolated ANTC, differing in the short side chains in C9 of ring D. In Dox this is a primary alcohol, while in DNR this side chain is a methyl group. Epirubicin (Epi) is a stereoisomer of Dox derived through axial-to-equitorial epimerisation of a hydroxyl group in the Daunosamine moiety, which leads to an increased volume of distribution and

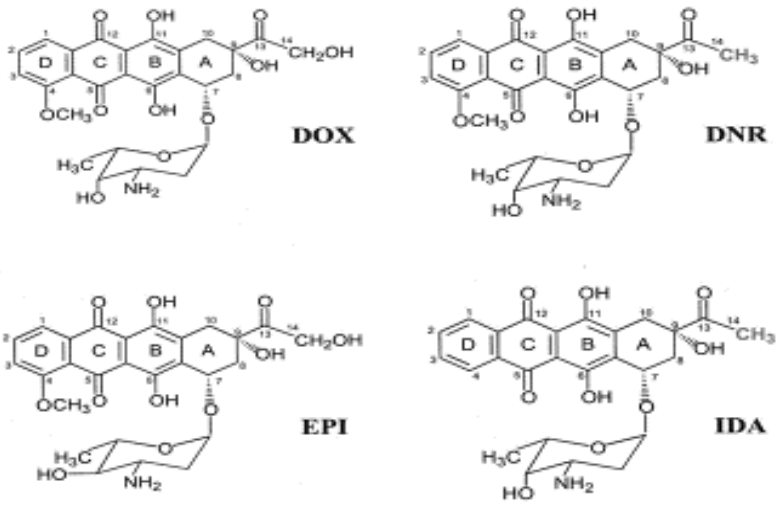

Fig.1.1. Molecular structure of Anthracyclines. The core tetracyclic aglycone structure of anthracyclines contain four cyclohexane chains with a sugar moiety at Carbon C7 of ring A; adjacent quinone-hydroquinone groups in rings C and B; and in ring D a methoxy substituent carbon C4 (DNR and Dox), a carbonyl group at C13 and a short side chain in C9 (Abbreviations: Dox-Doxorubicin, DNR- Daunorubicin, EPI-Epirubicin, IDA-Idarubicin).

shorter half-life. Idarubicin (Ida) is a derivative of DNR obtained by removing the 4-methoxy group in ring D. It has greater lipophilicity, higher cellular uptake, and a broader spectrum of activity against AML, MM, NHL, Breast cancer as well as multi drug resistant tumours. Other ANTC that have reached clinical practice include Pirarubicin, Aclarubicin and Mitoxantrone and find clinical use in disease as diverse as Systemic Sclerosis and Multiple Sclerosis (Minotti et al, 2004). The potential population vulnerable to cardiotoxicity of ANTCs is therefore not restricted to cancer-survivors only.

1.1.1. Manifestations and diagnosis of ANTC-Cardiotoxicity.

The cytotoxic potential of ANTC compounds rapidly found chemotherapeutic use in clinical setting, with DNR and Dox being used in chemotherapy regimen by early 1970s. The cardiotoxicity of ANTC, manifesting as heart failure, was soon apparent in clinical practice (von Hoff et al, 1979). Early observational data and retrospective study from symptomatic patient-cohorts led to a distinction between early (or, acute) cardiac complaints that manifested within hours to days, and the late onset toxicity of ANTC that manifested several months (and in many

cases years) after anthracycline treatment had been completed. Acute ANTC-associated injury that have been described include manifestations of myocarditis or pericarditis, transient arrhythmias, QT-prolongations, delayed ventricular repolarisation, and transient depression of Left ventricular (LV) ejection fraction (LVEF) (von Hoff et al, 1979; Gianni et al, 2008). These were considered reversible, and hence different in pathogenesis from the irreversible chronic heart-failure syndromes associated with ANTC-chemotherapy. In adults, the chief manifestations of chronic ANTC-cardiotoxicity, however, are in the forms of DCM and CCF. Irreversible cardiac-failure syndromes may manifest months to years following cessation of treatment (Zhai et al, 2010). For example, it has been noted that the risk of symptomatic CCF increases by 15-fold in childhood cancer survivors compared to age-matched controls (Lipshultz et al, 2013b), while the risk of cardiac-death in patients who have received ANTC-based chemotherapy is nearly 8-fold greater than in the background population (Khawaja et al, 2014). Despite these findings, and despite investigations into the pathogenesis of ANTC-cardiotoxicity for several years, the molecular mechanism and the underlying pathophysiology of this late manifestation of cardiac-injury remains poorly understood.

In recent years, however, considerable insights have been made into the problem of ANTC-cardiotoxicity, with the result that the understanding of this puzzling clinical problem is undergoing a paradigm shift. Increasing literature suggests that ANTC-mediated cardiotoxicity is a dynamic process. Acute-cardiotoxicity maybe the manifestation of a more progressive injury, with early changes remaining physiologically compensated, subclinical, asymptomatic, and only later manifesting as overt heart-failure (Ganz et al, 1993; Cardinale et al, 2015). For example, Cardinale et al (2015) followed a study-population of 2600 patients who received ANTC-based chemotherapy over a period of ten years. Echocardiographic monitoring in this study revealed a significant fall in LVEF, beginning as early as 3 months after ANTC chemotherapy in nearly 9% patients over the ten years of the study (Fig. 1.2). Similarly, Cove-

Smith et al (2014) found that in animal-models, rats subjected to weekly doses of Dox showed decline in cardiac function on cardiac magnetic resonance imaging (cMRI), and also demonstrated histological signs of cardiac-tissue injury, along with elevation of serum biomarkers e.g. cardiac Troponins (cTn) before symptomatic cardiac failure was noted. These data suggest that the functional decline seen in animal models and the subclinical decline observed in humans reflect a progressive injury. The toxicity of anthracyclines on the myocardium may therefore begin early, and acute cardiotoxicity may be the consequence of early exhaustion of compensatory mechanisms in a subpopulation, while in others the clinical manifestation may only be delayed by more prolonged compensation. Continuous but physiologically compensated asymptomatic decline in LVEF, therefore, may be the mechanism of ANTC-cardiotoxicity. Indeed, a 2016 position paper from the European Society for Cardiology (ESC) reflects this emerging consensus that ANTC cardiotoxicity is a phenomenon of continuous progressive decline in LVEF, with many patients initially remaining asymptomatic,

Kaplan–Meier curve showing the cumulative incidence of cardiotoxicity in the study population.

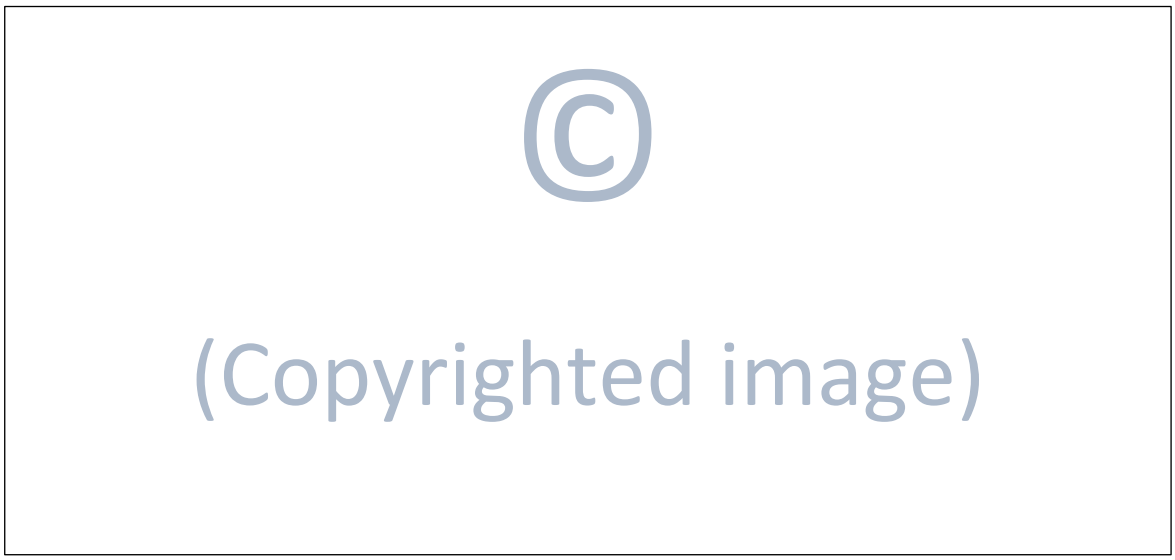

Fig.1.2. Incidence of heart-failure following ANTC-based chemotherapy over ten years, as determined by echocardiography-measured fall in ejection fraction. The cumulative incidence was 9% over ten years. In overwhelming majority, this manifested within 1 year (Cardinale et al, 2015).

but later presenting with heart failure in the context of a secondary trigger which may precipitate exhaustion of compensatory mechanisms (Zamorano et al, 2016). This physiological compensatory capacity of the heart may, in fact, be a factor in the lack of clarity of ANTC-cardiac injury, since CCF itself is considered a clinical diagnosis of a syndrome of physiological decompensation, with overall absolute LVEF value being a part of interpretation of the clinical picture. Further, the most commonly used investigation to determine LV systolic function (LVSF)- echocardiography- holds considerable variability between user. Various different approaches have been taken therefore to classify and characterise ANTC-cardiotoxicity in efforts to better define and address this poorly understood clinical problem. However, despite emerging evidences of early changes to the myocardium, optimum modality of investigation, ideal time for investigating, and ideal window for intervention is debated in clinical practice. As early as the later part of 1970s, Bristow et al (1978) tried to classify ANTC-cardiotoxicity histologically. Schwartz et al (1987) subsequently attempted a classification based on LVEF, while Stoddard et al (1992) described decline in isovolumetric relaxation time measured by Doppler-ultrasound. Indeed, in association with subclinical LVEF decline, LV end systolic volume (LVESV) and pulse wave velocity show an increase within 6 months of ANTC-based chemotherapy, suggesting increase in ventricular strain (Drafts et al, 2013). However, a uniform consensus diagnosis of ANTC-cardiotoxicity still remains elusive, owing to the varied morphological manifestations and the unpredictable temporal sequence associated with it. In general, a significant decrease in LVEF by 10-20% from baseline, or a decline in LVEF in association with signs and symptoms of CCF may be considered consistent with cardiotoxicity associated with ANTC treatment, even if absolute LVEF remains above what is considered normal (Khawaja et al, 2014). However, efforts to identify patients at risk, and to identify early ANTC-cardiotoxicity has so far failed to reach definitive consensus translating into clinical practice. Among other investigations, circulating serum cardiac biomarkers have been explored

in efforts to identify and predict patients at risk of ANTC-cardiotoxicity. Cardiac troponin T (cTnT) and cardiac troponin I (cTnI) levels correlate to a high degree of specificity with cardiomyocyte injury. cTns are therefore among the first-line cardiac investigations used to detect myocyte necrosis and risk stratify patients suspected of suffering from acute myocardial infarction. cTn is also useful in other cinical contexts, e.g., pulmonary embolism, sepsis, stroke etc (Agewall and Giannitsis, 2014) where information on cardiac strain offer guide clinical anagement. Indeed, with ANTC-treatment, early rise and persistent elevation in cTnI in the first month after chemotherapy have been reported to correlate with decline in LVEF confirmed by echocardiography in patients receiving chemotherapy with high dose anthracyclines (Cardinale et al, 2000). However, it ought to be recognised that the large-volume troponin release detected during, e.g., myocardial ischaemia arises from thin filament necrosis, reflecting irreversible myocyte death (Anaya and Moliterno, 2013). By comparison, smaller volumes of troponin may be detected by newer high sensitivity assays in a number of different clinical contexts including stroke, sepsis, and even vigorous exercise. The source of this troponin is believed to be the cytosolic compartment of cardiomyocytes, and not necessarily reflect cardiomyocyte necrosis. The clinical significance of such rise is therefore unclear (Agewall and Giannitsis, 2014). Indeed, studies investigating cTn rise in chemotherapy-induced cardiotoxicity have found a less clear role for these biomarkers in prediction and prognostication of cardiotoxicity, particularly in moderate and low dose ANTC chemotherapy-protocols where cumulative doses are less than 300mg/m^2 (Ky et al, 2014; Tian et al, 2014). Further, studies exploring cTn levels after ANTC-chemotherapy have failed to detect significant circulating levels late after chemotherapy in order of months, highlighting the difficulty in identifying asymptomatic individuals at risk of cardiotoxicity (Feola et al, 2011; Armenian et al, 2014). Other serum markers of cardiomyocyte-stress have been investigated to detect ANTC-cardiotoxicity, including the natriuretic peptide Brain-Natriuretic peptide (BNP) and its N-

teminal propeptide NT-proBNP. Both BNP and NT-proBNP are used in clinical practice in investigation of cardiac failure. However, rise in NT-proBNP has been observed after ANTC-chemotherapy with stable LVEF (Romano et al, 2011) and, as with cTn, their value in predicting ANTC-cardiotoxicity has been questioned in subsequent larger studies (Ky et al, 2014). More novel serum biomarkers to predict and identify ANTC-cardiotoxicity have been investigated, including Galectin-3, Myeloperoxidase, soluble suppression of tumorigenicity-2 (sST-2), Heart-type fatty acid binding protein (HF-ABP). However, the data remain preliminary and none have translated into routine use in clinical practice (Moazeni et al, 2017).

The effort to identify patients at risk of ANTC-induced cardiotoxicity, and to detect early cardiotoxicity arises from the observations suggesting that ANTC-associated cardiac dysfunction, if detected early, may be amenable to treatment. For example in the study by Cardinale et al (2015), a significant proportion of patient who were identified to have asymptomatic decline in LVEF showed recovery towards baseline values when they were treated in line with current medical practice guidelines, with Angiotensin convertase enzyme II (ACE)-inhibition or β-adrenergic blockade (β-blockade) after decline in ejection fraction was identified (Fig. 1.3). Similarly, treatment with high dose hydroxymethylglutaryl-Coenzyme A (HMG-CoA) reductase inhibitors ("statins") to inhibit cholesterol biosynthesis may have a beneficial role in protecting the at-risk myocardium from ANTC-cardiotoxicity (Henninger and Fritz, 2017). Indeed, although large scale prospective trial remains awaited to evaluate the role of statins in ANTC-cardiotoxicity, a meta-analysis of fourteen studies conducted by Kalam et al (2013) found a significant association between the administration of statins, and reduction in occurrence of cardiovascular events in patients who had received ANTC and/or Trastuzumab.

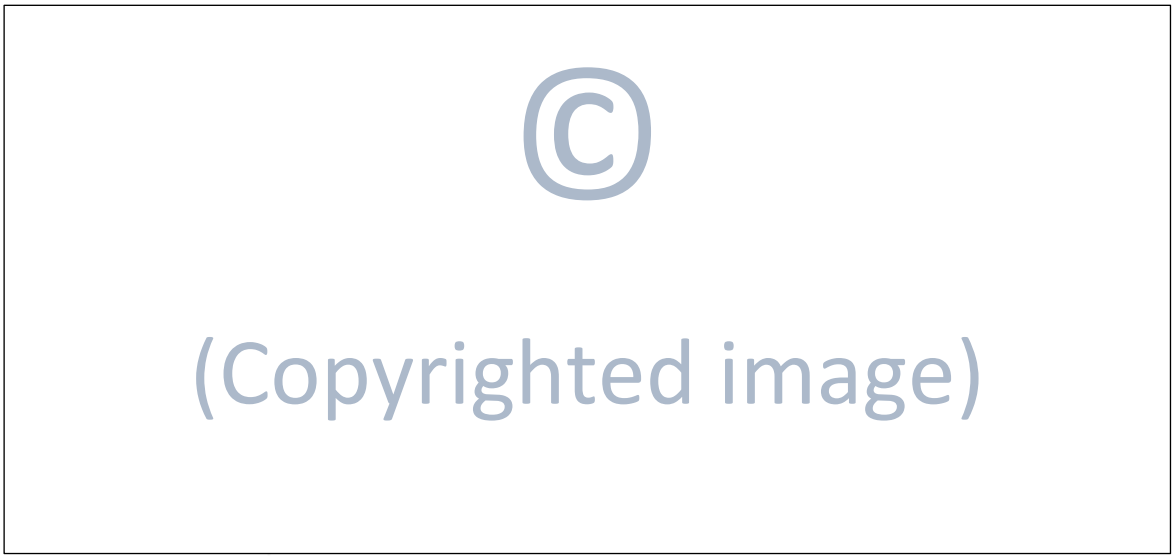

Fig. 1.3. The influence of early intervention against anthracycline-induced cardiotoxicity. The left ventricular ejection fraction (LVEF) in 82% of patients with echocardiogram-defined heart-failure improved when they were treated with optimum combinations of Angotensin II convertase enzyme (ACE)-inhibition and/or β-adrenergic blockade (Cardinale et al, 2015) (Abbreviations: CT=Chemotherapy, HF=Heart failure, LVEF=Left Ventricular Ejection Fraction).

The protective effect was similar to those observed with β-blockade, ACE-inhibition, as well as administration of the iron chelating agent Dexrazoxane (DXZ). DXZ was previously investigated as a protective agent against ANTC-induced cardiotoxicity in children receiving ANTC-chemotherapy (Lipshultz et al, 2012). Using NT-proBNP rise as a marker of cardiac injury, Lipshultz et al (2012) observed a significant decrease in cardiac strain in the group receiving DXZ. However, the clinical use of DXZ is limited given a small but significant concern regarding long-term potential for causing secondary malignancies (Lipshultz et al, 2012). Other measures explored against ANTC-cardiac injury include dietary supplementation of, e.g., Coenzyme Q10, α-tocopherol, etc, but analysis of experimental data fail to support definitive evidence of protection with these measures (van Dalen et al, 2011). Lifestyle factors, including smoking-cessation and physical exercise are recognised as important aspects in primary interventions against ANTC-cardiotoxicity. Interestingly, data from small animal models supports the advice that life-style modification to include exercise may have beneficial effects in protecting the myocardium against ANTC-cardiac injury. In particular, a role is suggested for aerobic exercise

in preventing ANTC-induced cardiac injury. Haywards group, for example, observed a beneficial effect against ANTC-cardiotoxicity in a rodent model of exercise-training three times per week, compared to sedentary rats (Chicco et al 2006a). The authors noted a protective effect against LV dysfunction when Dox (2.5mg/kg) was administered after exercise, as well as a protective effect against caspase-3 induction as a marker of apoptosis, compared to rats with sedentary regime subjected to Dox. Further, the authors noted reduced levels of lipid peroxidation and increased levels of glutathione peroxidase in rats subjected to regular exercise along with Dox treatment, compared to rats treated with Dox alone. Other groups have reported observation that preconditioning with short acute bouts of exercise before Dox administration protects against subsequent measured decline in cardiac function (Wonders et al, 2008, Hydock et al, 2008). Indeed, this importance of lifestyle measures is reflected in the current recommendations in clinical practice, where the ESC supports primary preventative life-style measures including modifying risk factors such as smoking-cessation, addressing obesity, and adequate exercise, in addition to secondary measures including pharmacotherapy (Zamorano et al, 2016).

1.1.2. Risk factors of ANTC-cardiotoxicity.

Currently known clinical variables poorly predict the risk and onset of ANTC-cardiotoxicity (Khawaja et al, 2014). Risk of cardiac-failure due to ANTC has been postulated to depend primarily on the cumulative-dose of ANTC administered during the chemotherapy regimen. Doses up to 300 mg/m^2 Dox (and equivalent-doses of other ANTCs) are considered relatively safe, with an incidence of CCF reaching up to 2%. By contrast, the mortality from symptomatic heart failure secondary to DCM approaches 60% within 2 years in patients who have received high dose ANTC of 450 to 600 mg/m^2 Dox or equivalent (Suter et al, 2013). However, even lower doses of ANTC may trigger injury resulting in asymptomatic decline in cardiac function that does not manifest in overt, clinically decompensated cardiac failure. For example, the incidence of

cardiotoxicity in patients receiving the highest limits of safe recommended dose is approximately 5%. However in childhood cancer survivors, reduced fractional shortening and increased afterload (compared to age matched controls) has been demonstrated beginning from doses approximating 100 mg/m^2, with a noticeable 4.5-fold increase noted at doses in excess of 270 mg/m^2 (Hudson et al, 2007). In survivors of childhood lymphoma who received ANTC-based treatment (with or without mediastinal irradiation), echocardiographic measurements demonstrated a higher prevalence of diastolic dysfunction at median doses equivalent to 160 mg/m^2 Dox, more than 10 years after completion of treatment (Christiansen et al, 2014). Further, in adult populations, asymptomatic deterioration in LVEF, LV end systolic diameter (LVESD) and increased LV strain has been demonstrated within 6 months of initiating ANTC-based chemotherapy (Drafts et al, 2013). Underlying cardiopulmonary disorders, metabolic disorders, and increasing age are recognised to increase the risk of ANTC-toxicity. For example for ANTC-induced heart failure, Pinder et al (2007) reported a hazard ratio (HR) of 1.58 with a 95% confidence interval (CI) of 1.39 to 1.79 in patients with concomitant coronary artery disease (CAD), with diabetes a HR of 1.74 (95% CI 1.66 to 1.83), and with increasing age risk a HR of 1.79 per 10 years (95% CI 1.66 to 1.93). Some authors estimate an approximate doubling of risk of ANTC-cardiotoxicity with each additional 10 years increase in age (Harbeck et al, 2011).

Amongst other risk factors associated with ANTC-cardiotoxicity, chromosomal factors and genetic determinants have been identified as influences (Lipshultz et al, 2013b). The female sex is associated with a higher incidence of cardiotoxicity, which may be related to higher percentage of body fat allowing greater cardiac-accumulation of the lipophobic ANTC-compound. Genetic determinants associated with altered incidence of LV dysfunction after ANTC therapy include, e.g., the hereditary hemochromatosis associated gene allele HFE C282Y, which confers a 9-fold increase in risk of myocardial damage, and may reflect concomitant

toxicities of iron-loading and of ANTC-chemotherapy (Lipshultz et al, 2013a). The CBR3 G allele homozygosity for the carbonyl reductase 3 enzyme confers an increased risk of approximately 5-fold compared to the GA/AA genotype (Lipshultz et al, 2013b). Similarly, gene-variants of proteins involved in cellular redox pathways, e.g., the NAD(P)H: quinone oxidoreductase 1 gene NQO1 (Blanco et al 2008) and the Glutathione GSTP1p.I105V variant (Dasgupta et al, 2003) have been identified to confer increased risk. This may be a reflection of oxidative-stress postulated to be induced by ANTC group of drugs. Gene alleles of the Dox efflux transporter ABCC2 have also been suggested to confer increased risk, possibly by influencing drug-efflux from sub-cellular organelles (Armenian et al, 2013). Survivors with trisomy 21, even when the congenital cardiovascular abnormalities are excluded, have an increased risk of cardiotoxicity, while Afro-Caribbean race is considered to confer increased risk (Grenier and Lipshultz, 1998). Additionally, comorbid conditions such as cardiovascular disease, endocrinopathies, inflammatory conditions, obesity, as well as traditional life style factors including smoking and sedentary lifestyle are known to be associated with increase in incidence of cardiotoxicity following ANTC chemotherapy (Lipshultz et al, 2013a; Lipshultz et al 2013b Lipshultz et al, 2014).

Therefore, the risk of ANTC-cardiotoxicity is very likely a composite of the insult on the myocardium due to the cumulative drug-dose; factors that affect the distribution; metabolism and transport of the drug; along with individual hereditary and acquired factors that increase the vulnerability of the myocardium to drug-induced injury.

1.1.3. Pathology of ANTC-mediated cardiac injury.

The exact mechanism of chronic cardiotoxicity of ANTC still remains debated, but an inflammatory response and compensatory adaptations have been noted in the ANTC-insulted myocardial tissue in humans (Bristow et al, 1978), as well as in animal models (Cove-Smith et

al, 2014). Human autopsy studies show that ANTC distributes widely within the body, accumulating in the liver, heart and the brain (Berthiaume e al, 2007). Histologically, animal models show that repeated administrations of Dox leads to delayed chronic active myocarditis, lymphocytic infiltration, cardiomyocyte degeneration, compensatory hypertrophy, oedema, fibroblast proliferation and, over a longer period of time, collagen deposition and fibrosis. For example, in the animal model study by Cove-Smith et al (2014) cited above, chronic low-dose administration of Dox in a rat-model was reported to lead to myocardial necrosis, oedema, lymphocytic infiltration and loss of myofibrillar architecture (Fig.1.4). This suggests a chronic inflammatory injury and consequent repair and remodelling response may be a component of ANTC-injury.

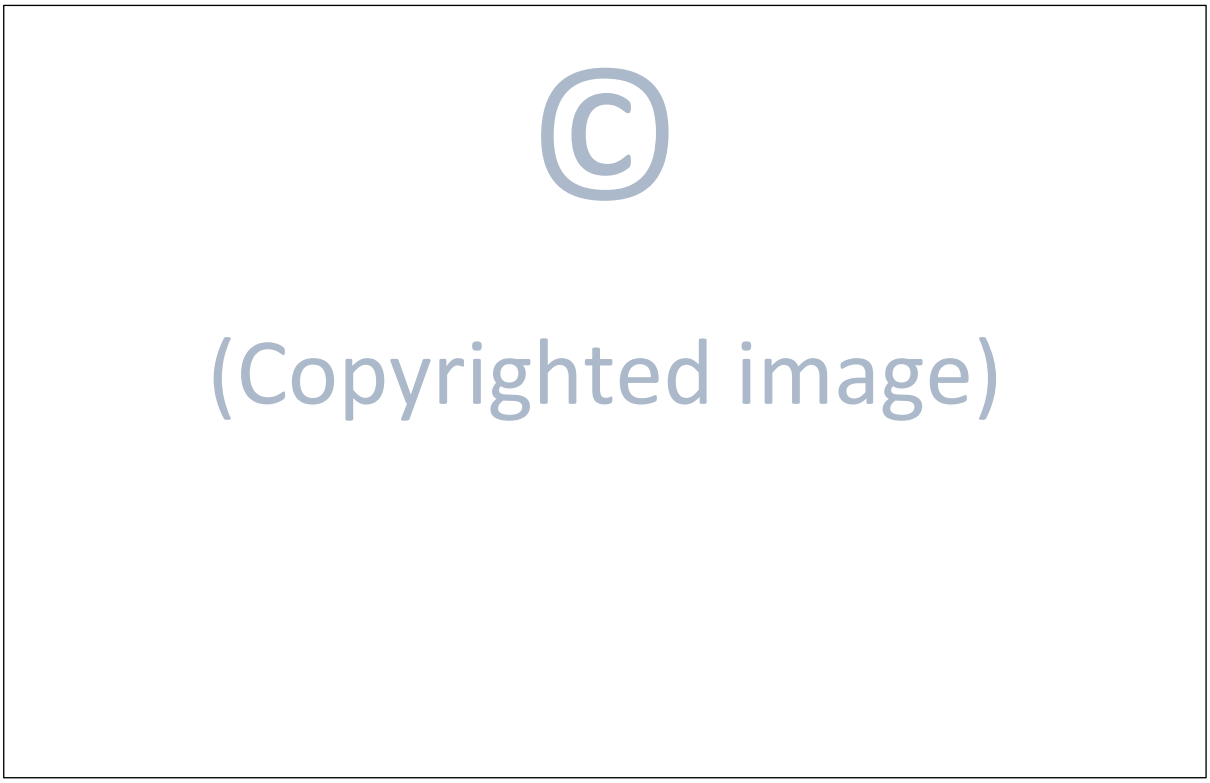

Fig. 1.4. Histological features of cardiotoxicity of Anthracyclines in an animal model. Multi-focal and well-demarcated intracellular vacuolation of cardiomyocytes (dashed arrows); lymphoplasmacytic inflammation (solid arrow); and a degenerate cardiomyocyte (bent arrow) in rat atria seven weeks after beginning a once-weekly Doxorubicin treatment protocol (Cove-smith et al, 2014).

1.1.4. Molecular pathology of ANTC-mediated cardiac damage.

In bio-molecular aetiology, evidence supports a multi-factorial process in ANTC-induced cardiac dysfunction, which includes an immune-system mediated response against cardiomyocytes and extracellular matrix degradation. This may lead to altered signalling between the basement membrane and the cardiomyocyte, e.g., through alterations of laminin-integrin interactions and consequent attenuation of integrin-linked small G-protein coupled signalling (Ross and Ross, 2001). Further, degradations of structural components of the cardiomyocyte contractile apparatus and disruption of the cellular bioenergetic pathway may attenuate the pumping function and efficiency through the cardiac cycle, reducing cardiac output. Decreased viability of potential stem-cell pools may also mediate an altered and inefficient repair response (Zhang et al, 2009).

Supporting a role for activation of cardiomyocyte death pathways, proteomic analysis of hearts from rabbits subjected to a chronic dosing regimen of DNR-induced cardiomyopathy demonstrated an increase in calpain protease, along with an increase in caspase-6 activity (Stěrba et al, 2011). The authors in this experiment further demonstrated a decrease in myoglobin and Heart-type fatty Acid Binding Protein (HFABP) abundance, suggesting alterations in myocardial energy storage and metabolism. Additionally, they identified a number of sarcomeric-structural changes including increased desmin expression, diminished localisation of desmin to the cardiomyocyte Z-disk, decreased expression of myosin light chain isoforms 1 and 2, and attenuated beta isoform of myosin heavy chain protein. Similarly, using transmission electron microscopy, Cove-Smith et al (2014) observed a temporal disruption of myofibrillar architecture and Z-line distortion. These observations may partly explain contractile dysfunction observed in ANTC-toxicity. Desmin is known to form a link between the Z-disk and basement membrane proteins, e.g., Laminin, and alterations have been noted to

lead to disrupted signalling in some forms of inherited cardiomyopathies (Mavroidis et al, 2008).

In addition to intracellular structural alterations, animal models of Dox-toxicity utilising both bolus dosing as well as interrupted chronic dosing regimen exhibit changes associated with extracellular remodelling. This includes increased matrix metalloproteinase (MMP)-2 and MMP-9 expression, decreased density of fibronectin distribution, and decreased contents of tubulin, fibronectin, kinase-related protein (or telokin), and smooth muscle/nonmuscle myosin light-chain kinase (Stěrba et al, 2011). Further, increased Collagen IV α-chain expression and an increase in vimentin (expressed from activated fibroblasts, endothelial cells and smooth muscle cells) has been reported in small animal models of ANTC-toxicity (Lenčová-Popelová et al, 2014). Importantly, Collagen IV is known to be elevated in the inflammatory peri-infarct zones post- myocardial infarction (MI) (Morishita et al, 1996). In other organ systems e.g. lung, kidney, and liver, collagen IV isoform expressions have been associated with fibrotic diseases (Sand et al, 2013). This suggests extracellular matrix remodelling and alteration of the basement membrane molecular structure is a component of the ANTC-injury to the heart.

ANTC have also been demonstrated to deplete the human cardiac progenitor stem cell (CPC) pool through induction of premature senescence, inhibition of growth, and induction of cell-death. In rat models of cardiotoxicity, Dox decreases the viability of clonogenic c-kit positive CPCs *in vitro* (De Angelis et al, 2010). Further, in mice, knock-out of the cardiac senescence marker protein SMP 30 leads to increased Dox-induced cardiomyocyte apoptosis compared to wild type controls (Miyata et al, 2013). Transplantation of induced pluripotential stem cells (iPSCs) and embryonic cells post-MI in Dox stressed murine heart has been demonstrated to improve fractional shortening and ejection fraction *in-vivo*, along with lower levels of cardiomyocyte apoptosis *in vitro* (Merino et al, 2014). The improvement in cardiac function and

cardiomyocyte apoptosis was associated with reduced MMP-9 activity, along with attenuation of interstitial and vascular fibrosis compared to control animals which did not receive similar cell-transplants. This suggests depletion of CPC population and attenuation of progenitor cell function may have a role in induction and/or exacerbation of myocardial injury due to ANTC.

These data highlight that anthracycline-induced cardiac injury is likely to be the result of a complex multifactorial process, which includes inflammation and extracellular matrix (ECM) degradation, alterations to structural and contractile proteins, as well as increased collagen deposition and impaired repair processes.

1.2. Mechanism of ANTC-mediated cardiomyocyte death.

Given that ANTC are chemotherapy agents, it is not surprising that they are cellular toxins and inhibit survival-related signalling cascades. In dividing cells, ANTC exert their cytotoxic effect through intercalation with DNA, forming a stable ternary complex with the DNA-Topoisomerase II structure during DNA replication. This leads to inhibition of DNA replication, arrest of cell cycle in G1 and G2, and induction of programmed cell-death (Zhang et al, 2012). However, since cardiomyocytes are terminally differentiated cells, the mechanism of ANTC-mediated cardiomyocyte death is less well understood, but postulated to involve a number of different mechanisms, including inhibition of pro-survival signalling, induction of apoptosis, necrosis, protein misfolding, alterations of autophagic flux, as well as disruption of cellular and mitochondrial metabolomics and mitochondrial biogenesis pathways (Lenčová-Popelová et al, 2014; Khiati et al, 2014).

1.2.1. ANTCs modulate pro-survival signalling cascades.

ANTC compounds have been shown experimentally to modulate a number of protein-signalling cascades in the myocardium, although the exact contributions of these changes on the observed cardiotoxicity of anthracyclines remains far from clear. Altered induction or

inhibitions of specific signalling cascades may, however, explain the pathological responses of the intact myocardium culminating in cardiomyocyte injury, cell-death, and altered myocardial structure and function. For example in cultured H9C2 cardiomyoblast-derived cell lines, Dox has been reported previously to induce phosphorylation of Akt/Protein Kinase B (PKB), a downstream mediator of Phosphoinositide3-Kinase (PI3K) (Merten et al, 2006). In this report, the authors noted a cellular-hypertrophic response as a consequence of Dox treatment, which was specific to the induction of the PI3K/Akt pathway, distinct from additional activation of calcineurin signalling. Further, the authors were able to demonstrate sustained Akt phosphorylation for upto 360 minutes following exposure to Dox. Interestingly, in *ex vivo* models, Deres et al (2005) had previously demonstrated phosphorylation of Akt when isolated rat hearts were perfused with a supraphysiological concentration (100 µM) of Dox for 60 minutes in a Langendorff-apparatus. Further of interest, in *in vivo* models, Ichihara et al (2007) observed a phosphorylation response of Akt with high-dose bolus injection in a murine model of Dox-toxicity. Free oxide radical generation (discussed in section 1.3.1) may have a role in this PI3K/Akt phosphorylation induction, since reactive oxygen species (ROS)-species may accumulate in cardiomyocytes consequent to Dox-tretment, and secondarily lead to accumulation of reactive nitrative and nitrosative species. Nitration of tyrosine residues of receptor tyrosine kinases secondary to this accumulation of reactive oxygen and nitrative species has been hyposthesised to activate PI3K/Akt pathways (Deres et al, 2005). Supporting their hypothesis, Deres et al noted that Akt phosphorylation could be abrogated by concomitant perfusion with the antioxidant compound dihydrolipoamide at 200 µM, while Ichihara et al (2007) could inhibit PI3K/Akt induction with concurrent administration of super oxide dismutase (SOD). Moreover, PI3K/Akt phosphorylation-induction may serve an adaptive stress response, since activation of this pathway has been observed to prevent induction of death pathways by modulating mitochondrial morphology in response to pathological stress,

e.g., ischaemia-reperfusion injury (Ong et al, 2015). Gharanei et al (2013b), for example, noted an upregulation of Akt phosphorylation after perfusing rat hearts with Dox in an *ex vivo* Langendorff models, which the authors noted to increase further when the mitochondrial division inhibitor mdivi-1 was coperfused with Dox. In contrast to this, Dox has also been observed to promote the degradation of PI3K/Akt pathway by protein phosphatases (Fan et al, 2008). This may secondarily allow activation of the pro-apoptotic proteins, e.g. BCL-2 associated death promoter (BAD). Conversely, potentiaing the pathway of PI3K signalling has been reported to offer a protective effect against ANTC-toxicity. Kitamura et al (2014), for example, observed that deleting ARIA (apoptosis regulator through modulating IAP expression), a plasma-membrane recruiter for the PI3K-phosphatase Phosphatase and tensin homologue (pTEN) protein in rat models ameliorated Dox-induced Cardiomyopathy *in vivo* (Kitamura et al, 2014). Moreover, a number of agents e.g. Erythropoietin (Epo) (Kim et al, 2008), Propranolol (Yano et al, 2008), Propofol (Sun et al, 2014) etc. that show a cytoprotective effect against ANTC-cardiotoxicity do so, at least in part, by potentiation of PI3K/Akt pathway (Jia et al, 2014).

Induction, attenuation, and inhibition responses of other pro-survival kinases have further been noted in experimental models of ANTC-cardiotoxicity. For example, using Terminal Deoxynucleotidyl Transferase-Mediated dUTP Nick End-Labeling (TUNEL) assays to measure apoptosis, Zhu et al (1999) observed an increase in cardiomyocyte apoptosis in cultured neonatal rat cardiomyocytes upon treatment with the anthracycline Daunomycin (DNM). In their report, the authors demonstrated activation of the Mitogen activated protein kinases (MAPK) p38 MAPK, Jun N-terminal Kinase (JNK) and Extracellular signalling regulated kinase (ERK) 1 and ERK 2 (collectively, ERK 1/2) in response to DNM treatment. Interestingly however, selective inhibition of ERK 1/2 with 50 μM of the inhibitor PD98059 was noted to exacerbate DNM toxicity, while inhibition of p38 MAPK with 10 μM SB203580 in this experiment was associated with a suppression in DNM-induced apoptosis. Similarly, in a chronic dosing model

in rats, Lou et al (2005) observed a rise in p38 MAPK phosphorylation over a three-week period following Dox treatment. This was associated with an increased phosphorylation of c-JNK-protein over the same time. However, the authors noted a biphasic response of ERK 1/2 phosphorylation, with a rise in phosphorylated protein over hours, followed by a decrease in phosphorylation over 3 weeks after the final Dox dosage. These changes in protein-phosphorylation levels were accompanied by a fall in mRNA expression levels of ERK 1/2, and the animals were found to be in heart failure with depressed LV end-diastolic pressure (LVEDP), symptomatic dyspnoea, and displayed increased mortality by 3 weeks. Potentiating the ERK signaling pathway has been suggested to be a possible mechanism of the protective effect, e.g., of the fatty acid Oleylethanolamide in *in vivo* protection against Dox-toxicity (Su et al, 2006). Interestingly, the phosphorylation-induction of MAPK ERK 1/2 following anthracycline treatment has previously been reported to be deleterious. For example, Liu et al in their 2008 report noted an increase in apoptosis of H9C2 cardiomyoblasts following Dox-treatment, which was associated with an increase in MAPK ERK 1/2 phosphorylation, but not p38 or JNK. Their data suggested this increase in apoptosis was mediated by phosphorylation of pro-apoptotic proteins BCL-2 associated death X protein (BAX) and BAD by the ERK kinases, in conjunction with p53 phosphorylation induction by activated ERK 1/2 (Liu et al 2008). Inhibition of ERK 1/2 MAPK pathway using the inhibitor U0126 was noted to limit this phosphorylation and nuclear translocation of both MAPK ERK 1/2 and p53, and attenuated Dox-induced increases in the levels of BAX, of p53 upregulated modulator of apoptosis (PUMA)-α, of cleaved caspase-9, and activated caspase-3. Similarly, Gharanei et al (2013b) noted an increased phosphorylation of ERK 1/2 proteins when Dox was perfused in isolated Langendorff-perfused rat heart model, while phosphorylated p53 levels in isolated adult rat ventricular myocytes were also noted to be increased following Dox treatment. In their report, the authors noted that the mitochondrial divison inhibitor mdivi-1 was able to prevent upregulation of ERK 1/2 phosphorylation, as well

as the phosphorylation induction responses observed for p53 and the mitochondrial pro-fission protein dynamin related protein-1 (DRP-1). These data suggest that phosphorylation induction, activation, or attenuation of MAPK cascades, including MAP ERK 1/2, p38 MAPK, and the JNK pathway may have a role in the toxicity observed as a consequence of ANTC exposure, including through induction of mitochondrial stress-responses, induction of cell-death pathways, and through altering the balance of proteins involved in cell-death .

1.2.2. ANTCs modulate Topoisomerase-enzymes and alter mitochondrial metabolomics.

In addition to altering pro-survival signalling cascades, in cancer cells ANTC inhibit DNA-repair mechanisms, triggering cell-death mechanisms secondary to DNA-damage pathways. In this regard, the roles of topoisomerase enzyme isoforms have come under particular focus in mediating cardiomyocyte toxicity (Nitiss and Nitiss, 2014).

Supporting the hypothesis of cardiotoxicity secondary to topoisomerase enzyme modulation, Dox is known to stabilise a ternary cleavage-complex formed Topoisomerase II (Top2) and DNA during DNA-replication, leading to double stranded DNA breaks that can induce cell cycle arrest and death. In adult vertebrates, Top2 exists in two isoforms - α and β. Top2α-DNA complex stabilisation is thought to be a molecular mechanism of cytotoxicity of ANTC against cancer cells. However, only the β isoform (Top2β) is expressed in cardiomyocytes. ANTC-induced Top2β activation in cardiomyocytes has been suggested to be the underlying mechanism of altered expression seen in the mitochondrial-genome encoded proteins, including proteins involved in the respiratory chain, the mitochondrial biogenesis pathway, and further, for activation of proteins involved in the cell-death pathways. In a mouse-model of Dox-toxicity, Zhang et al (2012) demonstrated the downregulation of transcript-levels of proteins involved in mitochondrial biogenesis, including PPARγ co-activator (PGC) 1α and PGC 1β. Transcript and protein levels of PGC-regulated proteins involved in bioreductive pathways and ATP

biosynthesis were also downregulated, including Ndufa3 (which encodes subcomplex-3 of NADH dehydrogenase 1α), SDHA (encoding subunit A of Succinate dehydrogenase complex II) and Atp5a1 (encoding ATP synthase subunit α or Atp5a). Importantly, the authors showed that cardiomyocyte-specific deletion of Top2β protected the mice from Dox-induced progressive heart-failure seen in wild-type control animals.

In addition to the above findings, investigations into the role of topoisomerase in ANTC-cardiotoxicity also reveal a role for other isoforms of the enzyme. Adult vertebrate mitochondria express two further topoisomerases- Topoisomerase 3α (Top3α) and Topoisomerase 1-mitochondrial isoform (Top1(mt)). Top1(mt) functions solely within the mitochondria, while Top3α is also found to have a role in nuclear DNA-replication (Wang et al, 2002). In 2014, Khiati et al demonstrated that the protein levels of mitochondrial respiration complexes III and IV (which are encoded in both nucleus and mitochondria-dependent manner) are reduced in a cardiac specific manner in mice receiving Dox-treatment, and this down-regulation was accentuated in mice lacking Top1(mt). This stands in contrast to the protective role of Top2β deletion observed by Zhang et al and, taken together, indicates ANTC-cardiotoxicity may be the result of alterations in a complex interplay of mitochondria-targeted and mitochondria-derived protein expression secondary to topoisomerase poisoning, resulting in altered mitochondrial function and biogenesis.

1.2.3. ANTCs alter mitochondrial structure and function.

At a subcellular level, the chief sites of ANTC accumulation are the mitochondria, the nucleus, and the endoplasmic reticulum (Solem et al, 1994; Berthiaume and Wallace, 2007). The accumulation within the mitochondria may partly be a result of affinity of ANTC for cardiolipin, a lipid located on the inner mitochondrial membrane. In addition to the alterations in

mitochondrial biogenesis and function, ANTC have been shown to alter the structure and the transmembrane potential ($\Delta\Psi_m$) of cardiac mitochondria.

Early after ANTC administration, the mitochondria show swelling, membrane disruption and loss of membrane integrity (Cove-smith et al, 2014). Further, acute Dox-stress has been shown to upregulate the mitochondrial division protein DRP-1 (Dynamin related protein-1). Inhibition of mitochondrial division attenuated contractile dysfunction and infarct size seen in rat hearts perfused with Dox in the reperfusion stage of a Langendorff ischaemia-reperfusion model of Dox stress (Gharanei et al, 2013a). Khiati et al (2014) demonstrated that Top1(mt) knockout mice suffered extensive mitochondrial fragmentation, swelling, altered cristae structure, and an attenuated increase in mitochondrial numbers in response to Dox treatment. This suggests ANTC induce a direct mitochondrial structural damage, and additionally mitochondria attempt increased division in response to Dox.

ANTC may also alter mitochondrial energetic state by altering the function of mitochondrial respiratory complex proteins, leading to loss of the proton-motive force that drives the ATP generation. For example, in a rat-model of ANTC-induced cardiomyopathy, Lebrecht et al (2010) demonstrated a reduced activity of mitochondrial genome-encoded components of respiratory chain. Further, ANTCs have been shown to inhibit the reduced form of mitochondrial Nicotinamide Adenine Dinculeotide dehydrogenase (NADH) and Succinate dehydrogenase protein, as well as the function of the Magnesium (Mg^{2+})-dependent F_1F_0-ATPase in the mitochondria (Berthiaume et al, 2007). The $\Delta\Psi_m$ in cardiomyocytes has been demonstrated to fall within 60 minutes of perfusing isolated rat hearts with Dox (Montaigne et al, 2010). Similarly, a reduction in $\Delta\Psi_m$ in murine cardiomyocytes is observed 72 hours following a bolus 25mg/kg of Dox (Zhang et al, 2012). Uncoupling of electrons from the respiratory chain leads to depletion of high energy adenine nucleotides, and such uncoupling has been

demonstrated in both *in vitro* as well as *in vivo* models of ANTC-toxicity (Doroshow et al 1986; Lebrecht et al, 2010).

Interestingly, this collapse of $\Delta\Psi_m$ in response to ANTC is prevented by specifically inhibiting the mitochondrial permeability transition pore (mPTP), independent of the calcium (Ca^{2+}) uptake uniporter and the Sodium(Na^+)-Ca^{2+} exchanger (NCX) (Solem et al, 1993). The mPTP is a mitochondrial membrane associated multi-protein complex which is implicated in induction of necrotic cell death (Halestrap and Richardson, 2015; Kwong and Molkentin, 2015). Historically it has been postulated to be a multimeric channel spanning the outer mitochondrial membrane (OMM) and the inner mitochondrial membrane (IMM). The mPTP is a non-selective channel which has been noted to have a role in maintaining the permeability barrier of the IMM. In the "pore-closed" state, the mitochondrial inner matrix is impermeable to most solutes and ions, including Ca^{2+} and hydrated inorganic ions (Crompton,1999). A number of factors, including excessive oxidative stress in the form of accumulation of ROS-species, low pH, Ca^{2+}, as well as accumulation of phosphate ions leads to a transition of the pore to an irreversible permeabilization of the mPTP, cycling the complex from the "pore-closed" to a "pore-open" state. This transition to "pore-open" state is accompanied by uncoupling of oxidative phosphorylation and reversal of the activity of the The F_1F_0-ATP synthase to mediate ATP-hydrolysis (Halestrap et al, 2004). Further, transition to the "open" state is accompanied by increase in permeability and free passage of solutes, allowing diffusion of molecules below 1.5kDa size (Halestrap et al, 2004; Giorgio et al, 2009). This secondarily increases inner-mitochondrial osmotic pressure, inducing mitochondrial matrix swelling, unfolding of cristae, and outer membrane rupture with consequent nonspecific release of intermembrane-space proteins into the cytosol, including Cytochrome C leading to induction of necrotic cell-death (Kinally et al, 2011). The exact structure of the mPTP remains to be determined, but considerable evidences have emerged in the recent decade shedding light on the identitiy of

the molecular components that form this molecular entitiy. Historically, the mPTP was postulated to be composed of at least five proteins suggested to form the core component of the mPTP. These were Creatine Kinase (CK, initially postulated to exist in the cytosolic aspect), Voltage dependent anion channel (VDAC, located in mitochondrial outer membrane), translocator protein (outer membrane), Adenine Nucleotide Translocase (ANT, located in the inner membrane) and Cyclophilin D (Cyp D, located in the mitochondrial matrix). However, emerging data challenge this view. Evidence indicate that the pore is formed in the IMM, since mPTP can be formed in mitochondriae where the outer membrane has been removed, i.e., mitoplasts (Silekyte et al, 2011). Current evidence supports a model where ANT, the inorganic phosphate carrier (PiC), and the the F_1F_0-ATPase complex interact to form a core component of the mPTP, with Cyp D acting as a regulator of pore formation in the IMM (Halestrap and Richardson, 2015; Kwong and Molkentin, 2015). Reguation of mPTP opening by Cyp D maybe dependent on the interactions of this molecule with F_1F_0 ATP synthase through the lateral stalk of the latter complex. VDAC and the inner membrane component of Cyp D have been postulated in the past to recruit apoptotic proteins such as the BH3-domain pro-apoptotic protein BAX at site of intermembranal interactions where junctional complexes are formed (Crompton, 1999 and 2003). A role is now suggested for CK as an intermembrane space protein, along with VDAC in the OMM and the protein Hexokinase, in stabilising junction sites in interaction with ANT in the IMM (Halestrap and Richardson, 2015). However, an essential role for VDAC has been called into question, since murine mitochondriae in which all VDAC isoforms are knocked out retain an unaltered capability for mPTP transition (Baines et al, 2007). Furthermore, evidence indicate that proteins BAX and BAK (BCL-2 homologous antagonist killer) in the outer mitochondrial membrane interact with the core mPTP when the transition complex assembles, and may have a role progression of mPTP opening (Karch et al, 2013),

independent of the oligomerisation-dependent action of BAX in opening the OMM to release cytochrome C in induction of apoptosis.

The mPTP has been demonstrated to be involved in the induction of cardiomyocyte death following ischaemia-reperfusion injury as well as in in heart failure (Elrod et al, 2010). Since the collapse of $\Delta\Psi_m$ in response to ANTC-treatment is correlated specifically to induction of the mPTP (Solem et al, 1993), it may be hypothesised that inhibiting the mPTP induction, along with stabilising the mitochondrial transmembrane potential may have a protective influence against ANTC-toxicity on cardiomyocytes.

1.2.4. ANTCs induce cell-death via necrosis, apoptosis, and autophagy.

Although cardiomyocyte death is believed to be a key component of ANTC-cardiotoxicity, investigating the exact mechanism of cell-death offers conflicting explanations. Myocardial tissue in Dox-treated animal models exhibits histological signs of necrosis, but biomolecular analyses suggest other mechanisms, including programmed cell-death or apoptosis, may also be involved. Necrosis, or "unprogrammed" cell-death is characterised by cell-swelling, vacuolation, organellar rupture and non-specific karyolysis. These features were considered to delineate it as a death-response to non-specific toxic and lethal insults, distinct from the ordered or "programmed" cell-death of apoptosis which is induced by specific death-signalling and is dependent on ATP-hydrolysis. Apoptotic cell-death was considered "clean", characterised by cell-shrinkage, pyknosis, karyorrhexis, externalisation of plasmalemmal phosphatidylserine residues, protein-crosslinking, and phagocytosis of apoptotic debris (Levin et al,1999). However, it is recognised now that necrosis and apoptosis may utilise similar biomolecular pathways, including induction of similar caspases, and in execution of the final death pathway. It is increasingly recognised that a continuum exists whereby, e.g., early apoptosis and mPTP-induction may transform into a necrotic pathway in conditions such as

ATP-starvation, culminating in activation of the final activator Caspase-3 (Zeiss,2003; Martel et al, 2012).

Both necrotic and apoptotic cell-death has been described in ANTC-cardiotoxicity models, including in *in vivo* (e.g., Zhang S, et al, 2012) as well as *in vitro* (e.g., Zhang H et al, 2013). At a biomolecular level, necrotic cardiomyocyte-death may be secondary to the effects of ANTC on the mitochondria, especially on the mPTP. Mitochondria from rats treated with Dox show an increased sensitivity to induction of mPTP opening (Ascensão et al, 2010; Gharanei et al, 2013a). As described in the above section, In the induced, open, state, there is unrestricted movement of molecules smaller than 1.5 kDa accros the mPTP, which dissipates the transmembrane potential, inducing mitochondrial swelling, outer membrane rupture, and release of Cytochrome C. Caspase-3 activation resulting from Cytochrome C release can stimulate mPTP induction, which may act as a feed-forward mechanism for further Cytochrome C release. Deletion of mitochondrial Cyp D protects cardiomyocytes from known pore-induction stimuli, e.g. Ca^{2+} overload and oxidative stress, but sensitivity of cells to apoptotic-death stimuli is preserved (Baines et al, 2005). Mitochondrial Cyp D gene deletion in mice has been shown by Nakayama et al (2007) to protect from histological changes of necrosis and from physiological decline in cardiac function observed in control animals two weeks following a single large dose of Dox. Importantly, both oxidative stress and Ca^{2+} overload are hypothesised to be components of ANTC-mediated cardiotoxicity. Interestingly, ANTC-induced induction of the pro-inflammatory interleukin (IL) cytokine interleukin-1 (IL-1) β isoform (IL-1β) has been previously observed to rise in a dose-dependent manner in murine models of Dox-toxicity, with levels of serum IL-1β, IL-1 receptor antagonist (IL-1RA), and cardiomyocyte levels of IL-1 receptor I (IL-1RI) correlating with degree of myocardial tissue fibrosis, myocyte vacuolisation, and degeneration (Zhu et al, 2011). The necrotic cell-death pathway, therefore, maybe a target to explore in protecting against ANTC-cardiotoxicity.

In addition to necrosis, however, considerable evidence indicates apoptotic cell-death machinery to be involved in cardiomyocyte death in ANTC-toxicity. Apoptosis is an evolutionarily conserved active-death mechanism described as mediated via two canonical modes- the extrinsic pathway and the intrinsic pathway. The intrinsic pathway is initiated by intracellular or mitochondrial signals, and may be triggered by a diverse array of factors including non-receptor signalling induced by cellular stress, e.g., withdrawal of pro-survival signalling or intracellular stress-responders, e.g., reactive oxygen and nitrite species (ROS and RNS respectively), culminating in loss of suppression against apoptosis (Elmore et al, 2007; Yao et al, 2017). Early chages induced by activation of the intrinsic pathway results in a shift in the cell-death program, normally regulated by a balance of the anti-apoptotic molecules BCL-2, BCL-X_L, and Mcl-1 and of pro-apoptotic proteins e.g. BAD, BH3 interacting-domain death agonist (BID), Bnip3 and Nix. Loss of mitochondrial transmembrane potential and opening of the mPTP further allows the release of mitochondrial IMM-sequestered proteins, e.g., high-temperature requirement 2 (HTRA2)/Omi and direct IAP binding protein with low pI (DIABLO)/ second mitochondria-derived activator of caspases (SMAC), inhibiting the activity of the inhibitor of apoptosis proteins (IAP) (van Loo et al, 2002) and activate Cytochrome C (Zhang et al, 2009). Induction of pro-apoptotic BCL-2 family molecules by cellular-stress stimuli leads to translocation of pro-apoptotic molecules e.g. BAX and BAK to the OMM and reinforces activation of Cytochrome C, which is able to recruit the Apoptosis protease activating factor-1 (Apaf-1) and procaspase 9, triggering the apoptosome formation, feed forward auto-activation of caspase 9, and subsequently activates procaspase 3. Contrasted with this non-receptor signalling that triggers the intrinsic apoptotic pathway, the extrinsic pathway is considered to be activated by cell surface death ligands, resulting in activation of cell-surface “death-receptors” which are characterised by the conserved 80 amino-acid “death-domain” in the intracellular aspect and a cysteine-rich extracellular domain (Elmore, 2007). Ligand binding,

e.g., by Tumour necrosis factor (TNF), TNF receptor associated factor (TRAF), FAS llgand (FASL), TNF-related apoptosis-inducing ligand (TRAIL) etc. results in trimerization of these cell-surface death-receptors allowing recruitment of adaptor proteins, e.g., FAS associated death domain (FADD), TNF receptor associated death domain (TRADD) etc., and ultimately activate caspase-8 to induce the Death Inducing Signalling Complex (DISC), culminating in the activation of procaspase-3.

Increasing evidence indicates that "cross-talk" exists between various different pathways of cell-death. Caspase-8 has also been noted to activate BID, BAX and BAK (Gustafsson and Gottlieb, 2003), which may be an example of cross-talk between the canonical extrinsic and the intrinsic pathways. Caspase-8 induced BID-cleavage results in mitochondrial translocation of cytosolic BID and induction of subsequent Cytochrome C release, independent of caspase activity (Li et al,1998). Further, emerging evidence indicate that necrotic cell-death may be triggered by the same cell-surface receptors (e.g., TNF-α) that trigger apoptosis, e.g., by differential energetic states as a result of, e.g., ATP-depletion (Li and Beg, 2000; Lin et al 2004). *In vitro*, TNF-α and TRAIL-induced "programmed necrosis" death pathways have been described in cell-lines, which is noted to involve inhibition of Caspase-8 induced cleavage of receptor-interacting proteins (RIP) (Chan et al, 2003). This highlights that avenues exist whereby necrosis, necroptosis and apoptosis may variably contribute or cross-talk in ANTC-mediated cardiomyocyte death.

ANTCs may directly activate promoters of apoptotic pathway. Dox has been shown to induce an early upregulation of the p53-pathway and upregulate apoptotic proteins including Apaf-1, Fas, MDM2, as well as the p53 inducible gene *Trp53inp1* (Zhang et al, 2012). Moreover, ANTC are capable of activating the innate immune receptors TLRs-2 and 4 in the myocardium (Ma et al, 2012). TLR-4 activation by ANTC inhibits GATA-4, a transcriptional activator of BCL-X_L.

Notably, TLR-4 deficiency attenuated GATA-4 downregulation, reduced cardiomyocyte apoptosis as measured by TUNEL-assay, and reduced myocardial functional decline in a mice model of Dox-induced cardiomyopathy (Riad et al, 2008). In animal models of ANTC-toxicity, enhanced degradation, e.g. through the ubiquitin-mediated system, of survival factors (e.g., apoptosis repressor with caspase recruitment domain, or ARC) and of antagonists of apoptosis a (e.g., BCL-2) have been described (Ranek et al, 2009). Further, in *in vivo* models, mice subjected to Dox-treatment has been reported to show an increased level of the pro-inflammatory cytokine IL-6, and an increased level of BAX/BCL-2 ratio (Westermann et al, 2008). Interestingly, the IL-1 family cytokine interleukin-33 (IL-33) was recently reported to attenuate Dox-induced apoptosis in a murine model of ANTC-cardiotoxicity. IL-33, the ligand for the receptor sST-2, was previously reported to suppress cardiomyocyte apoptosis and Caspase-3 activation and increased activation of IAP (Inhibitors of Apoptosis Proteins) homologues in pressure-overload models of heart failure (Seki et al, 2009). This indicates that the inflammatory innate cellular response as well as the paracrine effects of the inflammatory milieu elicited by ANTC-chemotherapy may have a role in cardiomyocyte death. Moreover, ANTC may alter the transcription of proteins in cardiomyocytes to the advantage of the pro-apoptotic proteins. DNR has been shown to inhibit the binding of the transcription factor CBF/NF-y to a CCAAT-region in the promoter box of GATA-4 in a p53-dependent manner, inhibiting the transcription of GATA-4 mRNA (Park et al, 2011). Similarly, Kawamura et al (2004) demonstrated reduced mRNA levels of the transcriptional co-activator p300 in a murine model of Dox-toxicity. In this experiment, transgenic mice overexpressing p300 displayed increased anti-apoptotic BCL-2 and MDM-2 levels, and were protected against Dox induced DNA-cleavage and caspase-3 induction (Kawamura et al, 2004).

In addition to the intrinsic apoptotic pathways, ANTC-toxicity on cardiomyocytes has also been demonstrated to involve the induction of extrinsic pathway of apoptosis. In rat-models of

ANTC-cardiotoxicity, activation of the transcription factor NFkB has been shown to directly activate pro-apoptotic genes, including Fas ligand (FASL), Fas, c-Myc and p53 (Li et al, 2007; Zhang et al, 2009). Dox has been shown to activate NFkB in neonatal rat ventricular myocytes in a TLR-2 dependent mechanism, while TLR-2 knock-out attenuates NFkB activation and lowers cardiomyocyte apoptosis in mice treated with Dox (Nozaki et al, 2002). Further, Kalivendi et al (2005) observed activation of the transcription factor NFAT4 and an increased FASL expression in H9C2 cardiomyoblasts secondary to Dox treatment. Similarly, in *in vivo* experiments, Nakamura et al administered once-weekly doses of Dox (2mg/kg) and observed an increase in FAS-mediated cardiomyocytes apoptosis. This could be prevented by the administration of a neutralising Anti-FasL-antibody (Nakamura et al, 2000). Further supporting the role of Fas-mediated death pathway in ANTC-cardiotoxicity, cardiomyocyte-targeted overexpression of soluble (s)Fas, a competitive inhibitor of FasL, was shown by Niu et al (2009) to preserve cardiac function and reduce apoptotic indices in response to a low-dose Dox regimen in a murine model of Dox-toxicity.

Interestingly, work in animal models support the hypothesis that apoptosis and necrosis are part of a more complex explanation of the chronic course of ANTC-mediated injury. For example in rat-models, apoptosis peaks at 24-48 hours after bolus Dox-administration before declining to baseline levels seen in control animals (Arola et al, 2000). Among other mechanisms put forward to explain the chronic course of Dox-toxicity, the contributions of autophagy has been emphasised by some experiments. Autophagy is a physiological mechanism of bulk-degradation of short-lived organellar structures and proteins by the Ubiquitin-proteasomal pathway (UPS). Autophagy may co-exist with apoptosis in the metabolically stressed cardiomyocyte (Tacar et al, 2014). Increased protein misfolding; enhanced UPS-mediated degradation of key structural proteins, eg, β-catenin; degradation of survival factors, e.g., ARC (apoptosis repressor with caspase recruitment domain) and the

apoptosis antagonist BCL-2 have been noted in animal models of ANTC-toxicity (Ranek et al, 2009). In rabbits, the concentrations of poly-ubiquitinated proteins GrP75 and Hsc70, mediators of chaperone mediated autophagy, has been shown to be increased (Sterba et al, 2011). Further, cardiomyocytes from rats receiving high dose Dox have been demonstrated to have an increased myosin Light chain II (LCII) to Light chain I (LCI) ratio, an indicator of increased autophagic flux (Zhang Y, et al, 2011a). Similarly, inhibiting autophagy has been observed to limit autophagic-vacuole formation and mPTP induction, and further protect against decline in cardiac function (Ling et al, 2013). Furthermore, ANTC related cardiotoxicity has been shown to be exacerbated in mice transgenic for overexpression of Nrdp1, an E3-ligase enzyme that mediates ubiquitin-conjugation to target poly-ubiquitinated proteins for proteasomal degradation (Zhang et al, 2013). This indicates that autophagy-mediated degradation of key structural and functional components may be a component of ANTC-mediated cardiomyocyte injury.

Autophagic pathways, in additon to their role for turnover of cellular machinery, may moreover form a link in the cross-talk between apoptosis and necrosis death, and interact with and influence both pathway. For example, the ubiquitinylation state of the Receptor Interacting Protein (RIP) group of proteins RIP-1 and RIP-3 has been noted to influence the activation of the apoptotic pathways and NFkB induction, and proteolysis of de-ubiquitinated RIP-3 by Caspase-8 in the Death Inducing Signalling Complex (DISC) has been noted as important in apoptotic-caspase induction in response to TNF-α as well as Fas mediated apoptosis (He et al, 2009). In the absence of Caspase-8, TNFR1 activation leads to programmed activation of necrosis, or necroptosis. Interestingly, Zhang et al (2016) observed a reduced burden of necrotic cardiomyocyte-death as observed by Evans blue staining when RIP-3 null mice were subjected to bolus doxorubicin-insult intraperitoneally. This highlights that interplay between canonical cell-death pathways and the machinery of molecular turnover may play a significant

role in cardiomyocyte-death secondary to ANTC. Targeting key mediators of the necrotic and apoptotic pathway, as well as the cellular autophagic flux needs to be explored further in delineating the mode of ANTC-Cardiotoxicity. However, given the role of ANTC as chemotherapy agents, differentiating between death-pathways in malignant cells and in cardiomyocytes is necessary before translational interventions may be explored.

1.3. Mediators of ANTC-cardiotoxicity.

Although considerable insights have been made into the mechanisms of ANTC-cardiotoxicity, the identity of the trigger(s) that initiate this cardiomyocyte injury remains elusive. Evidence have been offered in support of a number of different mechanisms, including a role for reactive oxidative and nitrosative species-mediated injury (Weinstein et al, 2000), Ca^{2+} overload-mediated cell-death (Doroshow et al, 1986; Solem et al, 1994), and excess iron accumulation in the cytosol (Ichikawa et al, 2014). The exact mechanism may be an interaction of a number of different key mediators in the metabolically stressed cardiomyocyte, inducing a final common pathway of cell-death.

1.3.1 Reactive oxygen and Nitrogen species.

The hypothesis of oxidative stress and consequent cellular apoptosis/necrosis was, for a considerable amount time, considered the strongest explanation of the mechanisms of cardiomyocyte dysfunction/death in ANTC-cardiotoxicity (Minotti et al, 2004; Berthiaume et al, 2007). Futile redox-cycling of the quinone moieties of the core ANTC-structure (Fig. 1.5) may generate excess superoxide anion, hydrogen peroxide, and hydroxyl radicals (collectively referred to as Reactive Oxygen Species, or ROS), which saturate the catalase and the glutathione (GSH)-mediated ROS-detoxification system. The quinone-semiquinone redox-cycling may also sustain ROS levels by increasing free cellular iron and potentiating ferrous-ferric cycling of molecular iron (Childs et al, 2002; Ichikawa et al, 2012). Since cardiomyocytes

are rich in mitochondria and relatively deficient in endoplasmic reticulum-associated cytochrome p450 enzymes, substantial burden falls on the mitochondria for bio-reduction of ANTC. Excess ROS may allow dissipation of the mitochondrial transmembrane potential. *In vivo* Dox-treated mice show evidence of elevated lipid peroxidation compared to control animals (Childs et al, 2002), while free radical scavengers e.g. probucol, and use of DXZ as an iron-chelator demonstrates a protective effect against Dox-toxicity in *in vivo* animal models (Konig et al, 1991; Kumar et al, 2001). Further, superoxide ROS ions may generate peroxynitrite species (or Reactive nitrite species, RNS) through reactions with nitric oxide (Beckman et al, 1996). RNS are selectively oxidant, reacting slowly with most biological molecules including amino acids, and thereby inducing nitrosative stress. In a murine model of Dox-toxicity, depression of cardiac function with high dose intraperitoneal injection of Dox has been shown by to correlate significantly with nitrotyrosine products (Weinstein et al, 2000; Mihm et al, 2001; Mihm et al, 2002). Further, promoting peroxynitrite catalysis improves survival and attenuates Dox-induced fall in cardiac function in murine models of Dox-toxicity (Pacher et al,

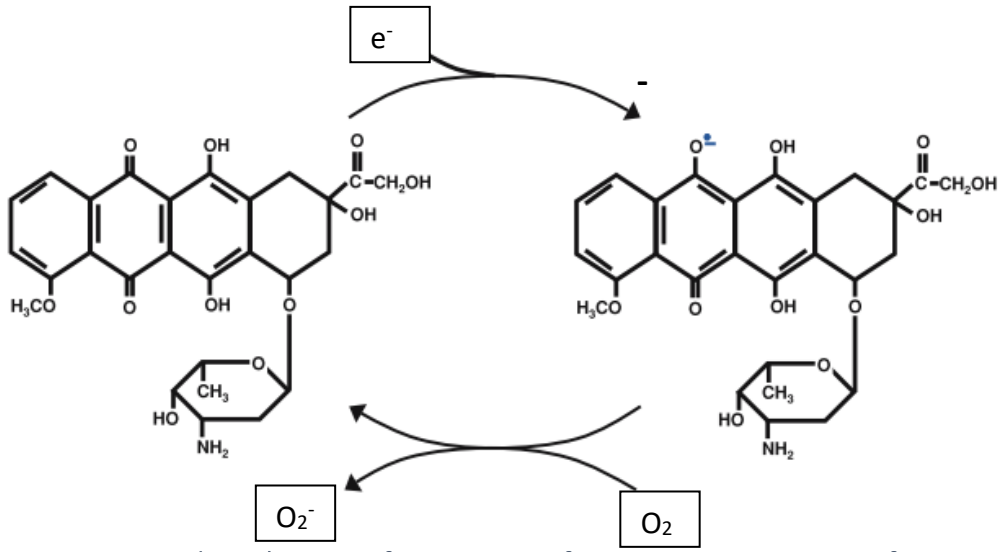

Fig.1.5. Proposed mechanism of generation of reactive oxygen species from ANTC compounds. The quinone group in C_{12} (ring C) may be capable of undergoing univalent reduction to semiquinone radical. In presence of molecular oxygen, the semiquinone auto-oxidises to generate the parent anthracycline along with superoxide anion (Modified from; Wallace and Berthiaume, 2007).

2003). In clinical practice, however, benefits of ROS-quenching remains unclear. A 2011 Cochrane review concluded that the use of N-acetyl cysteine (NAC) to restore GSH-reductive capacity and reduce ROS-burden shows no significant cardioprotective effect (van Dalen et al, 2011). Similarly, iron-chelation with DXZ was not observed in this review to offer any excess survival benefits compared to control groups. This raises the question whether oxidative and nitrosative stress may be the trigger of injury, or a pathological mediator of a separate underlying injury mechanism.

1.3.2. Calcium signalling in ANTC-cardiotoxicity.

Although Ca^{2+} is crucial to the contractile function of cardiomyocytes, abnormal Ca^{2+} cycling and altered Ca^{2+} signalling has been noted in human heart failure. For example, L-type calcium channel (LTCC) activity increases in the failing human heart (Luo and Anderson, 2013; Glukov et al, 2015). ANTC have been demonstrated in both *in vitro* as well as in chronic *in vivo* models to increase mitochondrial membrane permeabilisation and allow Ca^{2+} release from mitochondria (Solem et al, 1994). Cardiac mitochondria from rats subjected to weekly treatments of Dox (2mg/kg for 13 weeks) display increased mitochondrial Ca^{2+} accumulation (Solem et al, 1994). Further, mitochondria from Dox-treated animals show increased Ca^{2+}-induced depolarisation of transmembrane potential. Furthermore, the suspected triggers of ANTC-toxicity may also initiate pathological Ca^{2+} signalling. ROS, for example can activate calmodulin dependent kinase II (CAMKII) (Sag et al, 2011). CAMKII has a role in phosphorylation and regulation of Ca^{2+} regulatory proteins including ryanodine receptor 2 (RyR2), Sarcoplasmic Reticulum Ca^{2+}-ATPase (SERCA2A), phospholamban, and LTCC (Sag et al, 2011; Luo and Anderson, 2013). Excess Ca^{2+} within the cytosol can activate a number of signalling cascades including protein kinase A (PKA), CAMKII and adenosine monophosphate regulated kinase (AMPK) (Koval et al, 2011). Abnormal CAMKII activation has been linked to the contractile dysfunction in ANTC-induced heart failure secondary to altered sarcoplasmic reticulum Ca^{2+}

release, elevated diastolic Ca^{2+} content in the sarcoplasmic reticulum, and reduced transient Ca^{2+} amplitude (Olson et al, 2005).

In addition to aberrant activation of Ca^{2+}-regulated signalling cascades, ANTC may mediate cardiomyocyte dysfunction through direct actions on specific Ca^{2+} regulatory proteins. For example, both isoforms of Ryanodine receptor (RyR) are modified by ANTC (Feng et al, 1999; Hanna et al, 2011), possibly as a consequence of modification of thiol groups in these proteins, or due to drug-protein interaction. The Ca^{2+} binding capacity of Calsequestrin, for example, is decreased in the presence of DNR (Charlier et al, 2005). In rabbit-models of chronic DNR-toxicity, protein levels as well as gene expressions of SERCA2A and 2B, RYR2, Calsequestrin, and NCX have been shown to be significantly downregulated (Stěrba et al, 2011). Moreover, mRNA levels of RYR2, and ryanodine- binding kinetics of the RYR2 protein has been shown to be significantly downregulated in response to DNR, particularly in the left ventricle (Lenčová-Popelová et al, 2014).

These observations suggest ANTC-cardiotoxicity is very likely a multi-factorial process (Fig.1.6). Diverse factors such as altered mitochondrial respiratory function, mitochondrial biogenetic pathways, excess oxidative and metabolic stress, altered Ca^{2+} homeostasis, as well inhibition of pro-survival factors and excess of cellular death signals contribute to the final manifestation of the ANTC-injured failing heart.

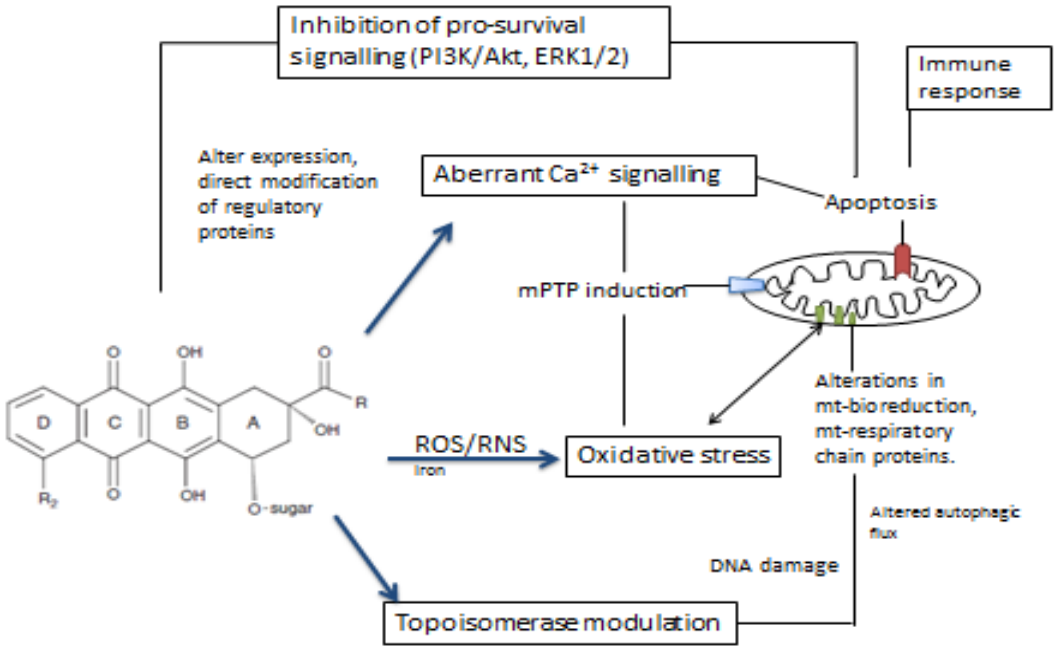

Fig 1.6. Postulated mechanisms involved in ANTC-cardiotoxicity. Iron overload and/or futile recycling of the quinone moieties of ANTC may lead to generation of ROS/RNS species, which directly lead to mPTP induction and necrotic cell-death. Oxidative stress and direct toxic effects on Ca^{2+} regulatory proteins may secondarily lead to aberrant Ca^{2+} signalling, resulting in contractile dysfunction and/or secondarily inducing the mPTP transition. DNA damage and Topoisomerase modulation by ANTC may lead to alterations of mitochondrial biogenesis and the mitochondrial respiratory chain. Inhibitions of pro-survival signalling and alterations of autophagic fluxes may further alter the balance of apoptosis in favour of pro-apoptotic factors, while mitochondrial protein degradations may be responsible for inhibited respiration (Abbreviations: ERK=Extracellular signalling related kinase, Ca^{2+}= Calcium, mPTP=Mitochondrial permeability transition pore, mt=Mitochondria, PI3K= Phosphoinositide 3-kinase, ROS=Reactive Oxygen Species, RNS=Reactive nitrosative species) (Illustration by author).

1.4. Reperfusion injury.

It is interesting to note that the cardiomyocyte injury caused by ANTC shares aspects that are similar to the mechanism(s) associated with "ischaemia-reperfusion injury". This includes the involvement of ROS, RNS, Ca^{2+} overload, altered autophagic flux, as well as altered metabolic state secondary to modulation of mitochondrial function.

1.4.1 What is reperfusion injury.

During myocardial infarction, cardiomyocytes deprived of oxygen due to the absence of blood-flow undergo cell-death. The gold-standard treatment for an acute-MI is therefore restoration of coronary flow by Percutaneous Coronary Intervention (PCI) or by pharmacological

thrombolysis. However, even after restoration of blood flow to the ischaemic myocardium, further cardiomyocyte injury occurs in the ensuing 24 to 48 hours. Early studies in dogs showed coronary occlusion for periods as short as 30-minutes led to histological changes of necrosis comparable to permanent ligation of a coronary artery for 24 hours (Reimer et al, 1977). The final infarct size may therefore be much larger than what would be predicted for the duration of ischaemia. It is estimated that this reperfusion-related injury accounts for nearly 50% of the final infarct size (Marber et al, 1993; Hausenloy and Yellon, 2003). A number of explanations have been put forward for this paradoxical finding of cardiomyocyte-death despite the relief of ischaemia, including postulated roles for injurious triggers, e.g., ROS, RNS, aberrant Ca^{2+} signalling and other mediators that are also hypothesised to play a role in ANTC-cardiotoxicity.

1.4.2. ROS and RNS in reperfusion injury.

ROS and RNS have been implicated as a key mediator of ischaemia-reperfusion injury. In the oxygen-deprived state of ischaemia, oxidative phosphorylation is inhibited. Re-initiation of oxidative phosphorylation at the onset of reperfusion, however, has been noted to be accompanied by the generation of ROS. For example, xanthine dehydrogenase, which converts Nicotinamide Adenine Dinucleotide (NAD) to its reduced form of NADH, has been suggested to undergo proteolytic cleavage during ischaemia to form Xanthine oxidase, which may be responsible for generation of reactive superoxide radicals in the post-ischaemic cardiomyocytes (Thompson-Gorman et al, 1993; Xia et al 1995). As with its putative role in the aetiology of ANTC-cardiotoxicity, excessive ROS may lead to mitochondrial matrix swelling, collapse of $\Delta\Psi_m$, and induction of transition of the mPTP to the open state. Further, ROS may also cause phosphorylation and degradation of anti-apoptotic proteins e.g. BCL-2 (Juhaszova et al, 2004). Furthermore, mPTP induction by ROS may in turn be caused by inhibition of the respiratory chain, and allow further ROS formation by the mitochondria. This phenomenon of ROS-induced ROS release has been suggested to function as a feed forward loop that may

exacerbate the process of reperfusion injury (Zorov et al, 2000; Halestrap and Pasdoi, 2009). Supporting a role for ROS-species in reperfusion-injury, application of antioxidants, e.g., N-acetyl cysteine in chick cardiomyocyte model of ischaemia-reperfusion protects against cell-death (Levraut et al, 2002). Therefore, similar to the proposed mechanism of Reactive-species mediated ANTC-cardiotoxicity, ROS and RNS species may mediate reperfusion-injury through induction of the mPTP, and/or by potentiating the induction of the apoptotic pathway which may ultimately lead to cardiomyocyte death.

1.4.3. Calcium signalling in reperfusion injury.

In addition to reactive radicals, aberrant Ca^{2+} signalling has been strongly suggested to be involved in the molecular pathology of reperfusion-injury. While alterations in levels and function of Ca^{2+}-regulating proteins may lead to excess mitochondrial Ca^{2+} accumulation in ANTC-toxicity, the mechanism of Ca^{2+}-mediated toxicity in reperfusion injury that has been described share similarities as well as differences. The loss of oxidative phosphorylation during ischaemia leads to lactate accumulation, leading to an excess cumulative proton (H^+) burden during ischaemia and an excess intracellular Na^+ ($[Na^+]_i$) accumulation as a consequence of increase in the Na^+-H^+ exchanger (NHE) activity (Murphy and Eisner, 2009). The increase in $[Na^+]_i$ may secondarily stimulate NCX, which leads to intracellular Ca^{2+} accumulation at reperfusion (Garciarena et al, 2013). NCX has been shown to be capable of activating Ca^{2+} related CAMKII cascade (Villa-Petroff et al, 2007). Further, Ca^{2+} entry via sarcolemmal L-type Ca^{2+} channels (LTCC) and deficient import of cytosolic Ca^{2+} into the sarcoplasmic reticulum (SR) by SERCA2A promotes Ca^{2+} overload in the cardiomyocyte. Intracellular Ca^{2+} ($[Ca^{2+}]_i$) is therefore elevated during reperfusion— either as a consequence of reversal of the NCX, or secondary to activation of the LTCC during ischaemia (Zhang H et al, 2013).

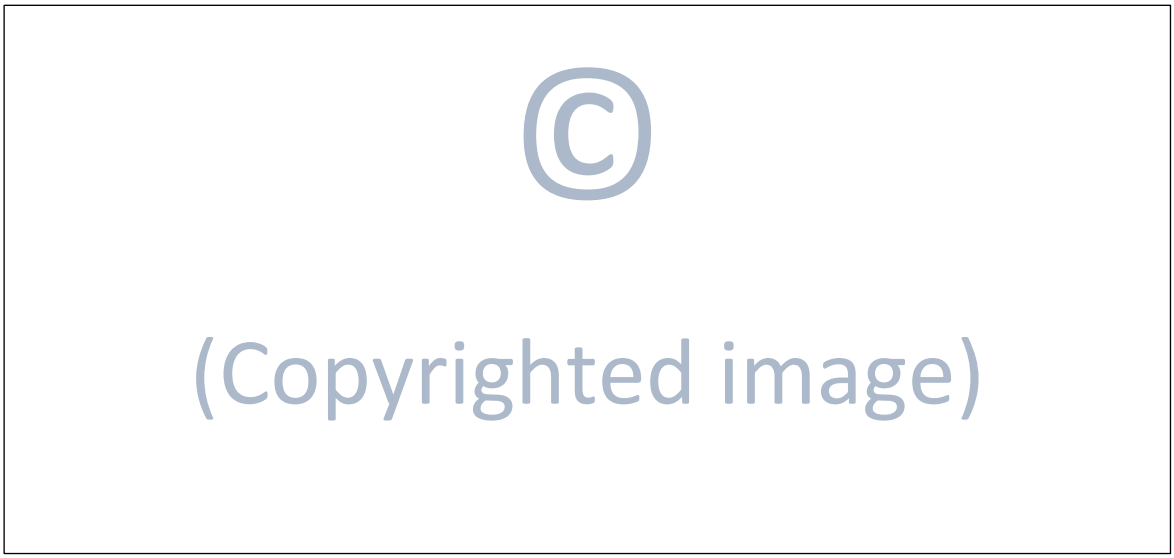

Fig.1.7. Postulated mechanisms of Reperfusion-mediated injury to cardiomyocytes. Calcium and ROS species are among key mediators considered to be mediators of ischaemia-reperfusion (IR)-injury. Generation of Xanthine Oxidase during ischaemia is a postulated mechanism of generation of ROS species during reperfusion. ROS species are capable of inducing mPTP transition, e.g., through molecular switches like GSK-3β. Similarly, intracellular calcium overload may occur due to LTCC activation during ischaemia. Alternatively, lactate build up maybe capable of activating the NHE, and build up Na^+, leading to secondary activation of the NCX. This excess calcium may lead to loss of mitochondrial transmembrane potential, or directly lead to transition of the mPTP. Alternatively, aberrant signalling due to ROS and/or calcium may also lead to induction of apoptotic signals. (Abbreviations. $\Delta\Psi_m$=Mitochondrial transmembrane potential, $[Ca^{2+}]_i$ = Intracellular calcium, LTCC= L-type Calcium Channel, $[Na+]_i$ = Intracellular Sodium Concentration, mPTP= Mitochondrial permeability transition pore, NCX=Sodium Calcium Exchanger, NHE= Sodium Hydrogen Exchanger, ROS=Reactive Oxygen species, XO=Xanthine Oxidase) (Murphy et al, 2009).

Furthermore, reduced Ca^{2+} uptake by the SR, reduced Ca^{2+} release, and reduced activity of the Ryanodine receptor (RyR) has been observed in isolated Langendorff-perfused heart models of IR injury, along with reduced mRNA and protein levels of SERCA2A and RyR (Temshah et al, 1999). In these experiments, the authors were able to demonstrate partial rescue against the decrease of mRNA and protein-levels by perfusing with superoxide dismutase and with catalase, suggesting a causal role for ROS-species in the alterations of Ca^{2+} regulatory proteins during reperfusion injury. Therefore, pathological role for deleterious Ca^{2+} signalling and ROS species may be interlinked. Further supporting a role for aberrant Ca^{2+}-signalling in reperfusion injury, Ca^{2+}-induced signalling cascades, e.g., CAMKII have been shown to be capable of inducing cardiomyocyte death (Said et al, 2011). Inhibiting these cascades improves cardiac

contractile function and reduces markers of necrosis, e.g., Cytochrome C levels, as well as apoptosis, e.g., BAX/BCL-2 ratio, in *ex vivo* animal models (Salas et al 2010). Specifically, the delta subunit of CAMKII has been suggested to activate NFkB through phosphorylation and inhibition of IkB (Ling et al, 2013; Zhang XQ et al, 2013). Ca^{2+}-related signalling, e.g., Calcineurin cascade and AMPK signalling may also be capable of inhibiting autophagy, which has been suggested to have a role in reperfusion injury (Huang et al, 2010, He et al 2014). Inhibiting aberrant calcium-mediated signalling therefore has been a target in mitigating reperfusion injury.

In summary, the mechanisms postulated to lead to the altered cardiomyocyte survival in ANTC toxicity share key mediators that appear to have a role in the toxicity in ischaemia-reperfusion injury. This includes ROS/RNS species and altered Ca^{2+} signalling, which may secondarily activate cell-death mechanisms, including by mPTP induction and by activation of the apoptosome and of necrosis. Interventions directed at limiting ischaemia-reperfusion injury may therefore offer also offer a protective-effect against ANTC toxicity.

1.5. Ischaemic preconditioning.

Ischaemic preconditioning (IPC), i.e., subjecting a target organ to brief periods of hypoxia/ischaemia followed by reperfusion, is another paradoxical aspect of the puzzle of reperfusion injury and its salvage. Murry et al (1986) described what is considered the first published evidence that preconditioning a canine heart with short periods of ischaemia offers a protective effect against a subsequent prolonged ischaemic insult by limiting infarct size. Since then, the IPC phenomenon has been confirmed to exist in different species, including in porcine heart, rat heart, murine heart and bovine myocardium (Iliodromitis et al, 2007). Circumstantial evidence further points to an IPC effect existing in humans, since pre-infarction

angina has been reported to be associated with smaller infarct sizes and more rapid revascularisation following thrombolysis (Andreotti et al, 1996; Kloner et al, 1995a; Kloner et al, 1995b).

1.5.1. IPC-mediated cardioprotection.

In order of cardioprotective potential, IPC is described by some authors as weaker only to myocardial revascularisation (Yellon and Baxter 1995). It offers a strong protection against progression of the ischaemic wave front and limits infarct size (Yellon and Baxter 1995; Downey et al, 2007). The initial protection offered by IPC was observed to be immediate but transient, lasting between 2 and 4 hours before subsiding. However a second window of protection, albeit less robust, was subsequently identified in the research investigating the mechanism of protection mediated by IPC, which reappears after 12-24 hours and persists for nearly 72 hours (Marber et al, 1993; Yellon and Baxter 1995; Kis et al, 2003). A number of preconditioning mimetics have been identified which offer similar protection against ischaemia-reperfusion injury as seen with IPC. These include diverse insults such as heat stress, hypothermia, sepsis, myocardial stretch etc., as well as various pharmacological agents e.g. volatile anaesthetics, opioids, nitrates (Cohen et al, 2001; Downey et al, 2007, Illiodromitis et al, 2007).

1.5.2. Signalling pathways in IPC.

Multiple, redundant, cell-surface receptors have been identified as triggers of IPC. This includes Adenosine $A_{1,}$ A_{2B} and A_3 receptors, Bradykinin receptors, Cannabinoid CB2 receptors, delta-opioid receptors, muscarinic receptors, natriuretic peptides receptors etc. (Cohen et al 2001; Solenkova et al, 2006). These triggers activate a complex network of pro-survival signalling cascades, and protects the cardiomyocyte from death-stimuli during the reperfusion phase of a subsequent prolonged ischaemic episode (Hausenloy et al, 2005). G-protein coupled receptor (GPCR)-linked signalling, as well as receptor tyrosine kinase mediated signalling arising from

these receptors have been identified as the most common trigger which serve to initiate a protective signalling cascade (Cohen et al 2000).

1.5.3. The "RISK" pathway.

Evidence to date implicates a complex signalling cascade involving PI3 Kinase (PI3K), Protein Kinase C (PKC), and MAP kinase pathways, e.g., MAPK ERK 1/2 as mediators of IPC-induced protection (Hausenloy, 2013). Identified by the Yellon group in 2002 (Schulman et al, 2002) and collectively termed the "Reperfusion Injury Salvage Kinase" (or "RISK") pathway, these cascades interact at multiple levels.

PI3K, for example, is known to be activated by a number of preconditioning triggers. Class I_A PI3Ks (which includes the PI3K α, β and δ isoforms) can be activated by receptor tyrosine kinases and by cytokine receptors, while GPCRs have been shown to activate Class I_B isoforms (e, PI3K γ) (Oudit et al, 2004). Inositol trisphosphate (IP3), generated by PI3K, is the activator of a diverse and complex array of downstream cascades which includes PDK1, Akt/PKB isoforms, as well as monomeric G-protein regulated signalling (Datta et al, 1999). For example PDK-1, after binding to PI3K, activates Akt/PKB, p70S6K and glucocorticoid-regulated kinase-1 (SGK1) (Biondi et al, 2001; McManus et al, 2004). Further, Akt can subsequently activate ERK. The targets of these cascades include Glycogen Synthase Kinase (GSK)-3β, the mammalian target of Rapamycin (mTOR) C1 pathway, eNOS, as well as specific caspases (Oudit et al, 2004). PI3K inhibition, e.g., by Wortmannin, has been shown to abrogate IPC-mediated protection (Tong et al, 2000; Hausenloy et al, 2005). Similarly, P70S6K was shown to have an essential role in the delayed phase of protection offered by preconditioning (Kis et al, 2003).

Furthermore, signalling cascades downstream of PI3K, as well as phosphoinositoltrisphosphate (PIP3) derivatives like Diacylglycerol (DAG), PIP2 and Phosphatidylcholine etc. can activate additional downstream cascades implicated in IPC-mediated protection. PKC, for example, has

been shown to be a downstream mediator of PI3K-mediated protection (Tong et al, 2000), while both p38 MAPK and ERK 1/2 have been shown to be a part of the signalling cascades mediating early as well as delayed protection offered by IPC (Fryer et al, 2001).

These data show that the RISK pathway of IPC-mediated protection involves a complex network of signalling cascades. PI3K plays a central role as the initial activator, and subsequently activates further downstream kinases, e.g., ERK 1/2 and PKC which form an interacting complex of pro-survival signalling cascades in protecting against reperfusion injury.

1.5.4. Mechanisms of IPC-mediated protection.

The exact mechanism(s) of the protection offered by the activation of pro-survival signalling cascades is yet to be clearly defined, but appear to converge on stabilisation of the mitochondrial transmembrane potential, preventing induction of the mPTP, preventing apoptosis, and improved mitochondrial stress response (Maulik et al, 1999; Fryer et al, 2001; Lacerda et al, 2009).

IPC has been shown to preserve mitochondrial transmembrane potential, preserve Cytochrome C levels, and prevent pathological induction of the mPTP in ischaemia-reperfusion (Costa et al 2008; Hausenloy and Yellon, 2003; Illiodromitis et al, 2007). This preservation may be secondary to limiting Ca^{2+} overload during reperfusion. In isolated Langendorff-perfused hearts, IPC has been observed to attenuate the ischaemia-induced decline in Ca^{2+} content in the SR, improve SR Ca^{2+} release and uptake, as well as preserve protein content of SERCA and Phospholamban (Osada et al, 1998, Temshah et al, 2002). Moreover, IPC has been shown to modulate the transcription and synthesis of proteins involved in the apoptotic pathway. IPC limits nuclear translocation of NFκB, and upregulates BCL-2 in rat models of ischaemia-reperfusion injury (Maulik et al, 1999). Of particular note, GSK-3β is a phosphorylation-target of key IPC-induced signalling cascades including PI3K. GSK-3β inhibition has been shown to

protect against the induction of the mPTP in ischaemic preconditioning (Tong et al, 2002). Similarly, STAT3 may mediate protection by phosphorylating and inhibiting GSK-3β, which has been suggested to be independent of the DNA binding activity of this transcription factor (Pedretti and Raddatz, 2011). STAT3 has also been shown to upregulate transcription of anti-apoptotic BCL-2 and downregulate BAX (Hattori et al, 2001), while STAT3-dependent phosphorylation may be a mechanism of inhibition of the pro-apoptotic factor BAD (Lecour et al, 2005). Further, STAT3 has been suggested to protect the mPTP induction directly, which maybe a consequence of its interactions with Cyp D (Boengler et al, 2010).

The known pathways triggered by IPC have also been shown to be initiators of the delayed protection observed with preconditioning. Increases in the expression of anti-oxidant pathways, e.g., Manganese superoxide dismutase (MnSOD), glutathione peroxidase and catalase has been noted with IPC (Das et al, 1993), which may hold particular relevance to protection against the postulated mechanism of toxicity of anthracyclines on cardiomyocytes. MnSOD and Haem oxygenase 1 (HO-1) are among factors suggested to be mediators of this delayed protective effect (Hausenloy and Yellon, 2010). STAT3, for example, activates MnSOD (Lecour et al, 2011). Further, MnSOD is also upregulated by a number of cytokines including IL-1β and TNF-α (Yamashita et al, 2000). Inhibiting MnSOD transcription has previously been shown to abrogate delayed IPC-mediated protection in rat cardiomyocytes (Yamashita et al, 1994). Similarly, siRNA mediated inhibition of HO-1 has also been shown to block delayed protection conferred by simulated IPC as well as by pharmacological preconditioning agents (Jancsó et al, 2007).

In addition to altering the balance of death-signalling pathways, end-effectors of IPC may protect mitochondrial function and alter autophagic flux. For example, IPC has been shown to improve mitochondrial H^+ leak in response to ischaemia-reperfusion (Quarrie et al, 2011).

Further, mitochondrial high energy phosphate content and oxidative phosphorylation pathway is preserved in the preconditioned myocardium (Kobara et al, 1996). Delayed ischaemic preconditioning has been shown to activate the expression of nucleus-encoded components of the electron transfer chain (McLeod et al, 2004), which results in improved ADP-sensitive respiration and electron transfer chain activity. Furthermore, IPC has been demonstrated to increase transcript levels PGC-1 and Nrf1– both components of nuclear encoded regulators of mitochondrial biogenesis (McLeod et al, 2004). IPC also improves autophagic flux, while Beclin 1 inhibition by BCL-2 has been demonstrated in rat models of limiting reperfusion injury with IPC (Peng et al, 2013).

1.6. Summary.

ANTC-induced cardiomyocyte injury remains incompletely understood, but many postulated aspects of the biomolecular pathology are similar to the injury inflicted during reperfusion following an ischaemic insult. This includes aspects of toxicity associated with highly reactive species e.g. ROS and RNS, the mechanisms initiated by pathological Ca^{2+} overload, alterations of mitochondrial transmembrane potential ($\Delta\Psi m$), and induction of cell-death by apoptosis and necrosis through, e.g., induction of mitochondrial permeability transition pore (mPTP) or through induction of the apoptosome. Similarly, alterations are also noted in the metabolic pathway in the cardiomyocyte including inhibitions of the respiratory complexes, and of alteration to autophagic flux. However, multiple interventions including ROS-scavenging with N-acetyl cysteine (NAC) or iron-chelation with Dexrazoxane have failed to translate clinically to providing meaningful protection against cardiotoxicity caused by Dox (an anthracycline compound) (van Dalen et al, 2011). Moreover, Dox has been shown to modulate a number of pro-survival signalling cascades. For example, phosphorylation induction of PI3K/Akt and MAPK/ ERK 1/2 has been observed in response to doxorubicin-insult in ischaemia-reperfusion

stressed myocardium (Ghanaranei et al, 2013a), while other groups have reported dephosphorylation of PI3-Kinase (PI3K)/Akt after Dox exposure which may lead to activation of apoptotic pathways (Fan et al, 2008). Induction of PI3K signalling, e.g. by decreasing the recruitment of the phosphatase PTEN to the plasma membrane, has been demonstrated to ameliorate doxorubicin-induced cardiomyopathy *in vivo* (Kitamura et al, 2014). Other experiments have implicated the MAPK ERK 1/2 pathway in protection against Dox-induced cardiotoxicity (Lou et al, 2005; Zhu et al, 1999; Su et al, 2006).

A protective effect against lethal ischaemic injury is observed at cellular and organ levels when cardiomyocytes are subjected to brief non-lethal hypoxic insults followed by short periods of reperfusion before lethal ischaemia is inflicted. This powerful protective phenomenon, termed hypoxic preconditioning (HP) or ischaemic preconditioning (IPC), protects cardiomyocytes against hypoxia-reperfusion injury and subsequent cell-death by activating potent pro-survival signalling pathways. A complex of signalling cascades, collectively termed the Reperfusion Injury Salvage Kinase (RISK)-pathway has been implicated in the protection observed with HP (Yellon et al, 2015; Davidson et al 2006). Interestingly, the RISK pathway involves the same signalling cascades that are observed to be modulated by anthracycline treatment, e.g., PI3-Kinase (PI3K), Protein Kinase C (PKC), and MAP kinase pathways, and the end-effect of these cascades are postulated to act on similar molecular mediators, e.g., ROS and RNS species and further protect organellar structures, e.g., mPTP, that are modulated in the pathogenesis of anthracycline cardiotoxicity. We therefore explored the hypothesis that HP may offer protection against the toxicity of anthracyclines on cardiomyocytes.

Chapter 2. Hypotheses and objectives.

2.1. Hypotheses.

The overall research hypothesis of the work presented in this thesis explored whether hypoxic preconditioning (HP) can protect cardiomyocytes against anthracycline-mediated injury. Doxorubicin was used as a representative anthracycline, and the hypothesis was explored using isolated adult rat ventricular myocytes (ARVM) model.

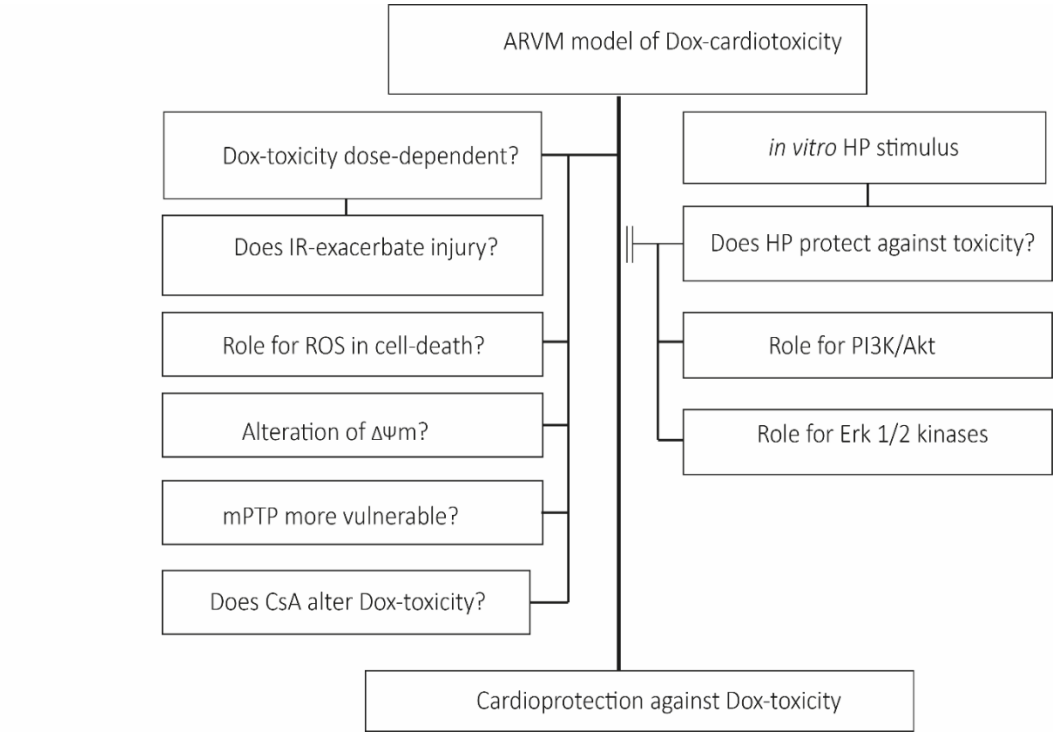

Fig.2.1. Main research hypotheses explored in the presented work. In an Adult Rat Ventricular Myocyte (ARVM) model, we explored the toxicity of doxorubicin, using cell-death as a marker of injury. On doxorubicin-stressed cells we explored the effect of iscahemia-reperfusion injury (IR-injury), the role of N-acetyl cycsteine (a known ROS-scavenger),and alterations of mitochondrial transmembrane potential (ΔΨm). To explore the role of mitochondrial permeability transition pore (mPTP) on doxorubicin-induced injury, we investigated mPTP-induction and cell-death in presence of Ciclosporine A (CsA), since CsA is known to increase the stimulus-threshold required for induction of the mPTP. To probe if hypoxic preconditioning (HP) was protective against doxorubicin-injury, we characterised an *in vitro* HP stimulus, and investigated if a preceding HP stimulus could protect against subsequent doxorubicin-toxicity. We further explored the role of the signalling pathways induced by the Reperfusion injury salvage kinases (RISK) in their potential to protect against doxorubicin-mediated cardiomyocyte death in this model.

As explained in introduction, there is a lack of clarity and consensus on the mechanism of anthracycline cardiotoxicity. Cell models offer the advantage that the toxicity of the compound on isolated cardiomyocytes can be studied, independent of the effect on other cell-types and any compounding physiological variables. We therefore aimed to establish a consistent reproducible model of toxicity of Dox *in vitro*, and investigate the possible mechanisms of cardiomyocyte-death in anthracycline-mediated cardiomyocyte injury. This model will further allow us to explore the protective potential of HP and the pathways of protection, if any. The hypotheses can therefore be broken down into two individual lines of investigation (Fig. 2.1).

2.2. Objectives

2.2.1. Objective 1. To investigate mechanisms of anthracycline-cardiotoxicity in an isolated ARVM cell model.

Our first objective is to explore the mechanisms cardiomyocyte- injury due to Dox, using cell-death as a reflection of anthracycline-injury. The involvement of mediators, e.g., oxidative stress, Ca^{2+}, etc, as well as cell-death pathways, e.g., mitochondrial pore transition will be explored.

2.2.2. Objective 2: Hypoxic preconditioning protects cardiomyocytes against toxicity of doxorubicin.

Our second objective is to evaluate whether hypoxic preconditioning may offer protection against anthracycline-cardiotoxicity. Further, we aim to explore the phosphorylation status of PI3K/Akt and MAPK ERK 1/2 and the respective changes in response to Dox and to HP independently and in combination. Since Dox modulates signalling cascades including PI3K/Akt and MAPK ERK 1/2 that form the the RISK pathway induced by HP, differentially inhibiting the respective cascades with LY294002 and PD98059 and re-examining the influence on cell-death due to Dox will offer potential insights into the role of these kinases in protection or pathogenesis of anthracycline cardiotoxicity.

Chapter 3. Materials and Methods.

3.1. Materials.

3.1.1. Animals.

Male adult Sprague-Dawley rats (150g-450g weight) were obtained from the UCL biological Services Unit for use in this experiment. All animals were housed in a temperature, humidity and light cycle controlled environment. All animal experiments were carried out in accordance with the UK Home Office Guide on the Operation of Animal (Scientific Procedures) Act of 1986 under home office licence PPL 70-8556

3.1.2. Cell culture medium.

Medium 199 with Earle's salt and L-glut (Invitrogen Catalogue number: 31150-030) was supplemented with Creatine (5 mM), Carnitine (2 mM) and Taurine (5 mM). 5 ml of 100x Penicillin/Streptomycin solution (Sigma CAS: P4333) was added directly to the final supplemented solution.

3.1.3. Ciclosporine A.

Ciclosporine A (CsA) from *Tolypocladium inflatum* (Merck Millipore, CAS No. CAS 59865-13-3) was dissolved in DMSO per manufacturer's instructions. Further dilution was carried out in medium 199 for use in cell-survival experiments, or in Tyrode's solution (137 mM NaCl, 2.7 mM KCl, 1 mM $MgCl_2$, 1.8 mM $CaCl_2$, 0.2 mM Na_2HPO_4, 12 mM $NaHCO_3$, 5.5 mM D-glucose, pH 7.4) with or without 3 µM Tetramethyl rhodamine methyl ester (TMRM) for use in mPTP induction assays. Final concentration of CsA used was 1 µM.

3.1.4. Doxorubicin.

Doxorubicin hydrochloride (Sigma Aldrich, catalogue no. D1515) was dissolved in DMSO per manufacturer's instructions. This was further diluted in medium 199 to the indicated concentrations and used immediately.

3.1.5. Hydrogen peroxide.

30% Hydrogen peroxide (H_2O_2) solution in deionised H_2O (Sigma-Aldrich, CAS Number 7722-84-1) was further dissolved in medium 199 to 100 µM, 50 µM and 1 µM solutions and used immediately. 1 µM H_2O_2 solution was used with or without dissolved N-acetyl cysteine (NAC) as indicated.

3.1.6. Hypoxic buffer.

A buffer was prepared containing 127.8 mM NaCl, 14.8 mM KCl, 1.2 mM KH_2PO_4, 1.2 mM $MgSO_4$, 2.2 mM $NaHCO_3$, 1.0 mM $CaCl_2$, 10 mM Sodium-lactate in deionised water as previously described (hypoxic buffer, Ong et al, 2010). The buffer was gassed with 95% N_2-5% CO_2 (N_2-CO_2) immediately before use and pH was adjusted to 6.4 at 37 °C. Fresh buffer was prepared on the day of use.

3.1.7. Insulin.

Insulin is a known inducer of the RISK kinases, and was therefore used as a positive control to induce PI3K/Akt ohosphorylation and MAPK/ ERK 1/2 phosphorylation. Human insulin (Invitrogen, Paisley, UK) was dissolved in medium 199 to obtain a final concentration of 275 u/ml and used immediately.

3.1.8. LY294002.

LY294002 is a selective PI3K/Akt inhibitor. LY294002 hydrochloride (Sigma Aldrich, CAS 934389-88-5) was dissolved in DMSO per manufacturer's instructions before final dilution in medium 199 or in normoxic buffer, as appropriate respectively, to obtain a final concentration of 10 µM.

3.1.9. N-acetyl cysteine.

N-acetyl cycsteine (NAC) (Thermo Fisher Scientific, CAS No. 616911) was dissolved in DMSO per manufacturer's instructions. This was further dissolved in medium 199 to obtain a final concentration of 250 µM NAC.

3.1.10. Normoxic buffer.

Normoxic buffer was prepared by dissolving 10 mM Glucose, 118 mM NaCl, 1.2 mM KH_2PO_4, 1.2 mM $MgSO_4$, 22 mM $NaHCO_3$, 1.0 mM $CaCl_2$, in deionised water. The solution was gassed with carbogen and pH adjusted at 37 °C to pH 7.4 before use.

3.1.11. PD98059.

PD98059 is a MAPK ERK 1/2 inhibitor. PD98059 (Sigma Aldrich, CAS No. 167869-21-8) was dissolved in DMSO per manufacturer's instructions, before final dilution in medium 199 or in normoxic buffer as appropriate respectively to obtain a final concentration of 30 µM.

3.1.12. Propidium iodide.

Propidium Iodide (PI) crosses the depolarised cellular and nuclear membrane and intercalates with doubles stranded nucleic acid, staining DNA in dead cells which can be identified by its fluorescence. PI (1 mg/ml) (Thermo Fisher. Catalogue No. P3566) was used at a final concentration of 5 µg/ml.

3.1.13. Tetramethyl rhodamine methyl ester.

Tetramethyl rhodamine methyl ester (TMRM) perchlorate (Thermo Fisher Catalogue no. T-668) was dissolved in DMSO per manufacturer's instructions. Further dilution in Tyrode's solution yielded a final concentration of 30 nM TMRM solution to estimate mitochondrial transmembrane potential, or a 3µM TMRM solution used in mPTP-induction assay.

3.1.14. Antibodies.

Primary antibodies to Total-Ak (t-Akt), Phospho-Akt (Ser 473) (p-Akt), Total ERK p44/42 (t-ERK) and Phospho-ERK p44/42 (Thr202/Tyr204) (p-ERK) were obtained from Cell Signalling Technologies and used at a dilution of 1:1000. Antibodies to Glyceraldehyde 3-Phosphodehdrogenase (GAPDH) and α-tubulin were obtained from Abcam and used at a dilution of 1:1000.

3.2. Methods.

3.2.1. Isolation of ventricular cariomyocytes and assessment of cell-death

3.2.1.1. Isolation of adult rat ventricular cardiomyocytes.

Adult male Sprague-Dawley rats (150-450g weight) were administered terminal anaesthesia with 65 mg/kg Pentobarbital injected intraperitoneally. The anaesthetised rats were monitored till cessation of peripheral and central nervous system reflexes but before cardiac arrest. The thoracic cavity was opened by clamshell thoracotomy and the pericardial sac opened to access the heart and ascending aorta. The heart was stabilised by the base with index and second finger and incised immediately below the aortic arch. The heart was then immersed in ice-cold isolation buffer. The aortic trunk was identified and cannulated rapidly (<3 mins excision to cannulation) and placed on a modified Langendorff apparatus maintained at 37 ˚C, and retrogradely perfused with myocyte isolation buffer containing 0.75 M Ca^{2+} (Solution 1, appendix a) delivered at a constant rate of 10 ml/ min to clear the heart of blood. This was followed by chelation of Ca^{2+} and sinus arrest with 100 µM EGTA-buffered solution (Solution 2) perfused at the same rate, before introduction of collagenase solution containing 100 mM Ca^{2+}. The extracellular matrix was subjected to digestion for 10-12 minutes till visually estimated alteration of solution viscosity and/or ventricular pallor. The ventricles were then excised, dissected into smaller pieces, and gently bathed in collagenase solution until a colloidal suspension of cardiomyocytes was obtained. The cells were subsequently allowed to precipitate into a pellet by standing. The supernatant was discarded, and the pellet re-suspended in myocyte buffer containing increasing concentrations of Ca^{2+} (solutions 4 and 5, final Ca^{2+} concentration 1 M) before re-suspending in supplemented cell culture medium (M199).

The cells were seeded onto laminin coated cell-culture dishes and left to adhere undisturbed for 60 minutes. Excess, non-adherent cells were washed away with 1 ml medium per well, and

the wells replenished with 2 ml medium 199. These were allowed to rest for a further one hour before any further experiments were carried out. Cell isolations yielding an excess of 20% death under basal conditions at the end of experimental protocols were excluded from experiment and interpretation.

3.2.1.2. Assessment of cell-death.

Each experiment was set-up in duplicate. Cell-death analysis was carried out in a blinded fashion. Each treatment group in an experiment was randomised to a numerical value with the aid of a publicly available, free-to-use, list-randomisation service provided by Randomness and Integrity services Ltd (https://www.random.org/lists/). A key to this randomised list was maintained in Microsoft excel software. Analysis of cell-death in ImageJ software was carried out in numerical order, before de-randomisation according to the key.

At the end of cell-survival experiments, PI was introduced into cell-culture plate and allowed to incubate for at least 30 s before microscopic analysis. Representative images were recorded using a Nikon Eclipse TE200 microscope, and analysed using ImageJ. Cells were considered dead according to the following criteria (Goto et al, 2009) (representative image shown in fig.3.11):

a. Evidence of staining of nuclei with propidium iodide.

b. Morphological changes, including evidence of membrane blebbing in the presence or absence of PI uptake.

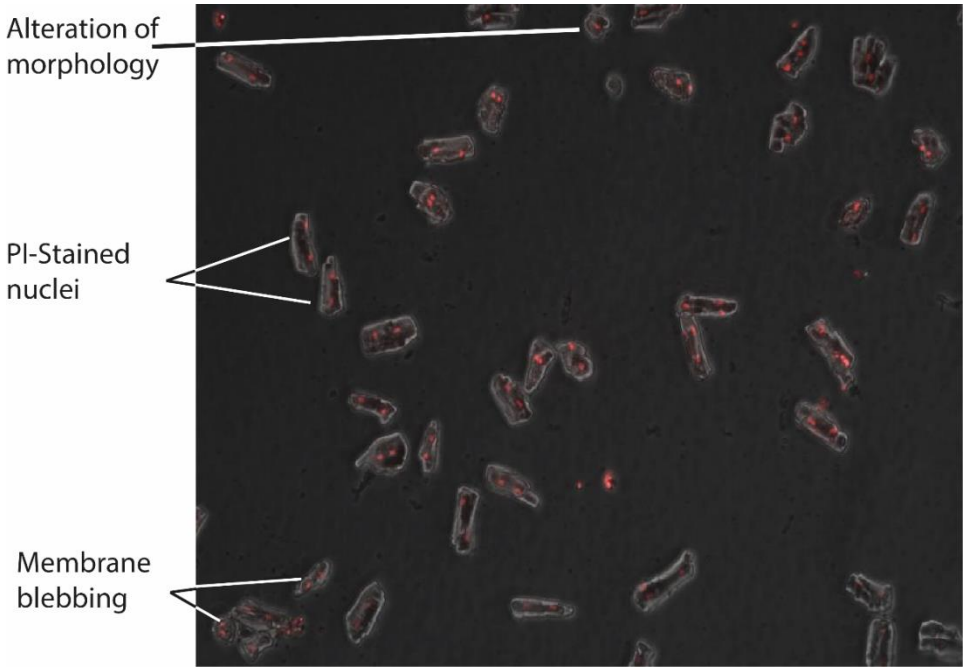

Fig.3.1. Evaluation of cell-death. Cardiomyocytes were considered as dead on the basis of nuclear staining with propidium iodide (PI), on observation of morphological changes including membrane blebbing and alterations of the cellular architecture. Example photomicrograph shows evidence of these features in different cells upon analysis in imageJ.

3.2.2. Investigation of *in vitro* toxicity of increasing doxorubicin-concentrations on isolated cardiomyocytes.

Isolated cardiomyocytes were transferred from medium 199, unless otherwise specified, to a medium containing Dox. The toxicity was evaluated for two different exposure-times. Cells were treated with 0.5 µM, 1 µM, 2 µM, and 5 µM, 7.5 µM, 10 µM, 15 µM and 20 µM Dox and cell-death evaluated after 4 hours. In a second experiment, cardiomyocytes were incubated with 1 µM, 2 µM, and 5 µM, 7.5 µM, 10 µM, 15 µM and 20 µM and cell-death evaluated after 18 hours (Fig. 3.2). As control, basal cell-death was evaluated from cardiomyocytes incubated in medium 199 for matched incubation periods.

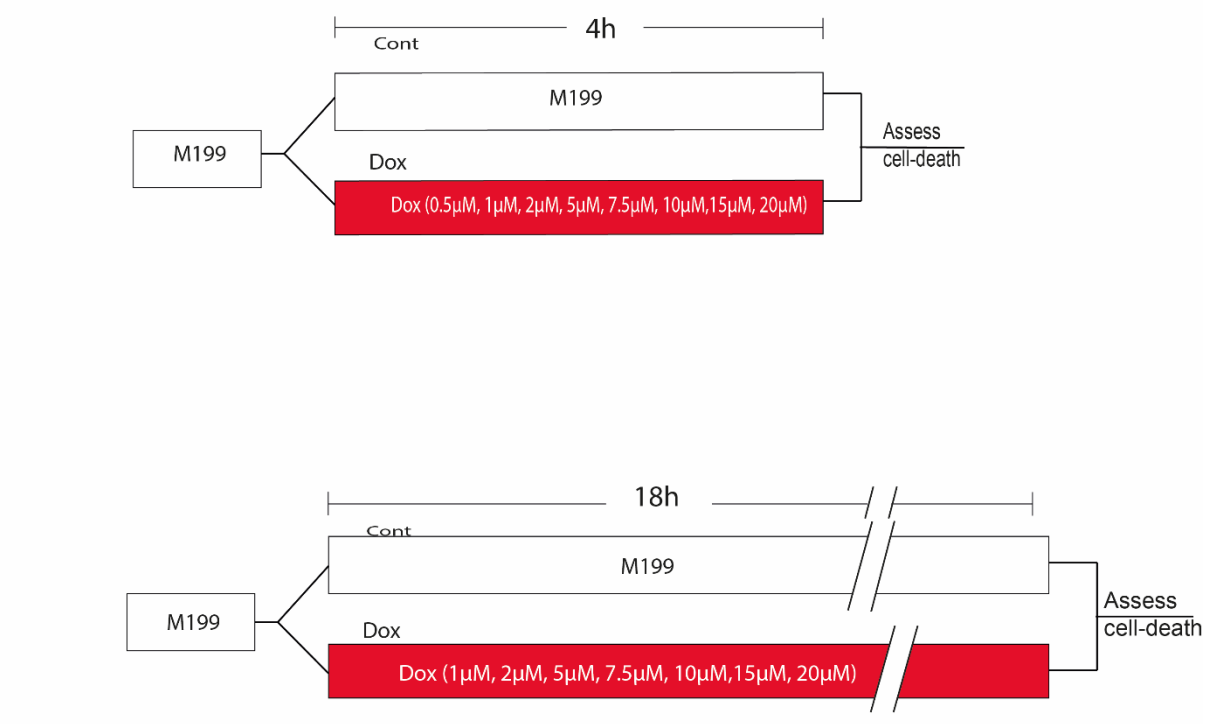

Fig. 3.2. Protocols for model of doxorubicin-induced cell-death. Cardiomyocytes were subjected to increasing concentrations of doxorubicin over 4 hours and 18 hours, and cell-death evaluated. Basal cell-death was evaluated in cardiomyocytes maintained in cell-culture medium for identical incubation periods.

3.2.3. Evaluating the effect of concomitant ischaemia-reperfusion and doxorubicin-injury on isolated cardiomyocytes.

3.2.3.1. Characterisation of a model of *in vitro* ischaemia-reperfusion injury in isolated cardiomyocytes.

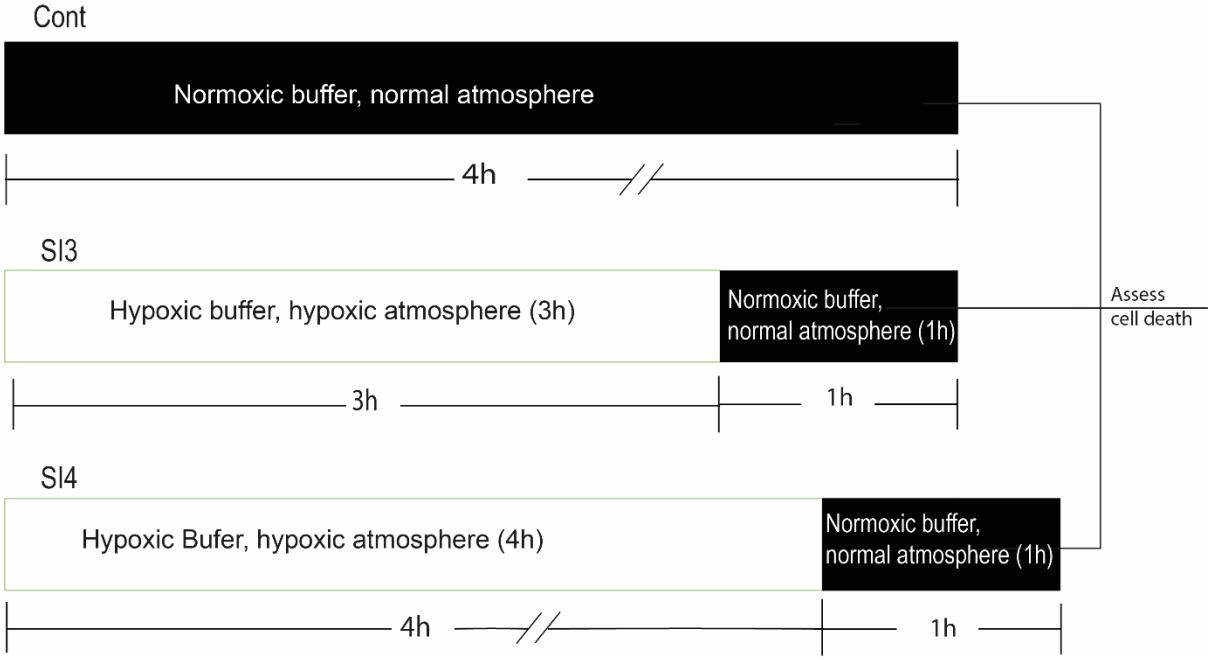

Fig. 3.3. Schematic diagram of protocols tested for ischaemia-reperfusion injury *in vitro*. Cardiomyocytes were subjected to hypoxia (simulated ischaemia, SI) in a hypoxic buffer for 3 hours (SI3) or 4 hours (SI4). Reoxygenation was carried out in normal environment in a normoxic buffer for 1 hour in both protocols. The control (Cont) was incubated in normal atmosphere in a normoxic buffer.

To explore the hypothesis that ischaemia-reperfusion (IR) injury may exacerbate the injury inflicted by exposure to Dox-treatment, we first developed a protocol to simulate IR-injury *in vitro*. Cardiomyocytes were transferred from medium 199 to a hypoxic buffer and subjected to hypoxia for 3 hours (SI3) or 4 hours (SI4) before transferring to normoxic buffer and normal environment for 1 hour to initate reoxygenation for both groups. Control cardiomyocytes were subjected to normoxic buffer in normal environment for 4 hours (Fig. 3.3).

3.2.3.2. Investigation of the effect of ischaemia-reperfusion injury on doxorubicin-stressed cardiomyocytes.

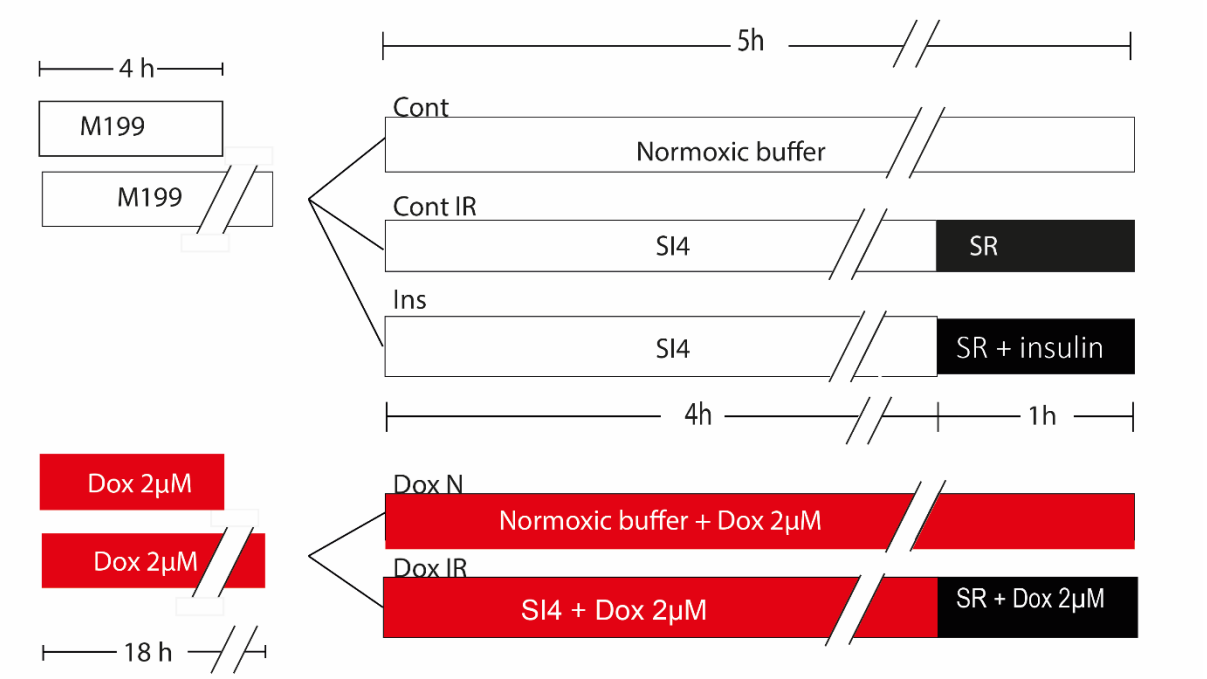

Fig.3.4. Experimental layout for evaluating the effect of ischaemia-reperfusion injury in cardiomyocytes treated with doxorubicin. Cells were incubated in 2 µM doxorubicin for 4 hours or 18 hours, before subjecting these in the presence of doxorubicin to 4 hours hypoxia (similualted ischaemia, or SI) followed by 1 hour reoxygenation (denoted simulated reperfusion, or SR) (Dox IR). Doxorubicin pre-treated normoxic controls (Dox N) were transferred to normoxic buffer in presence of doxorubicin, and incubated for 5 hours. In untreated controls, cardiomyocytes were incubated in medium 199 and transferred to normoxic buffer alone for 5 hours (Cont); subjected to IR (Cont-IR); or evaluated in a positive control experiment by subjecting to 4 hours hypoxia followed by reoxygenation in normoxic buffer with insulin (Ins).

Cardiomyocytes were incubated for 4 hours or 18 hours in 2 µM Dox, then transferred to hypoxic buffer with 2 µM Dox and subjected to hypoxia for 4 hours (Dox IR) (Fig 3.4). Cells were then transferred to normoxic buffer with 2 µM Dox to initiate reoxygenation, and incubated for 1 hour in a normoxic environment. Pre-treated normoxic controls (Dox N) were transferred to normoxic buffer containing 2 µM Dox, and incubated for 5 hours.

Untreated controls were incubated in medium 199 alone for 4 or 18 hours, then transferred to normoxic buffer for 5 hours (Cont), or subjected to IR-injury (Cont IR). As a positive protective agent against IR-injury, insulin (275u/ml) was used. A control group was established in

untreated cells subjected to SI4, which where transferred to normoxic environment in normoxic buffer with dissolved insulin (Ins) after hypoxia.

3.2.4. Investigating the effect of co-incubation with NAC on doxorubicin-induced cardiomyocyte-toxicity.

3.2.4.1. Estimation of cardiomyocyte toxicity in response to increasing H_2O_2 concentrations over time.

To investigate the effect of increasing concentrations of H_2O_2 on cell-death, cardiomyocytes were transferred from medium 199 to a solution of medium 199 containing H_2O_2 at concentrations of 1 µM, 50 µM and 100 µM H_2O_2. These were incubated for 4 or 18 hours. Incubation in cell culture medium alone served as control. Cell-death was evaluated at the end of incubation (Fig. 3.5).

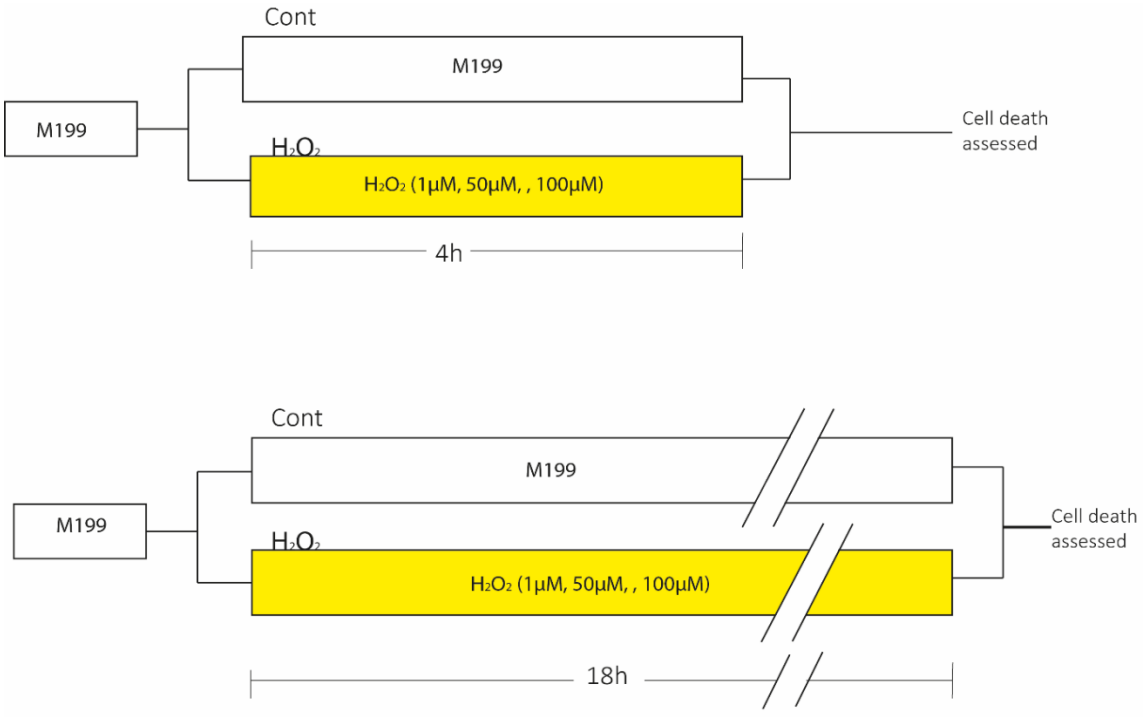

Fig. 3.5. Schematic diagram of experimental design for estimating H_2O_2 induced cell-death. H_2O_2 in medium 199 at the indicated concentrations were used to incubate cardiomyocytes for 4 or for 18 hours. Cell-death was evaluated at the end of this incubation period.

3.2.4.2. Evaluating the effect of co-incubation with NAC on doxorubicin toxicity.

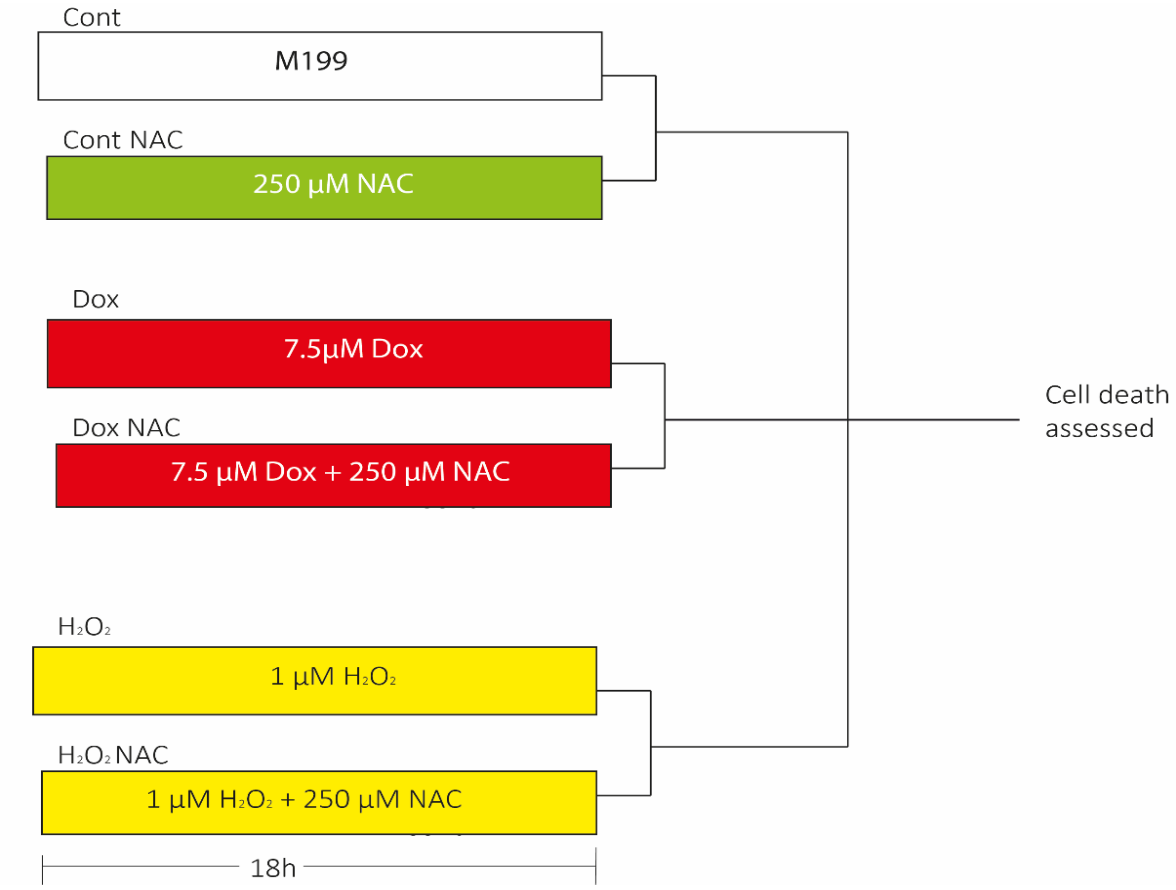

Fig. 3.6. Experimental layout for investigating the effect of N-acetyl cysteine on doxorubicin toxicity. Cardiomyocytes were transferred into medium 199 with 1 µM H_2O_2 alone (H_2O_2), 7.5 µM doxorubicin alone (Dox), doxorubicin with 250 µM NAC (Dox NAC), or 1 µM H_2O_2 with NAC (H_2O_2 NAC). As control, cardiomyocytes were incubated with medium 199 alone (Cont) or with 250 µM NAC (Cont NAC).

To probe the effect of potential ROS-scavenging on Dox-induced cardiomyocyte injury, we evaluated cell-death in cardiomyocytes incubated for 18 hours in 7.5 µM Dox alone (Dox), or with 250 µM NAC (Dox NAC), since NAC is known to be a potent ROS-scavenger. As positive control, cardiomyocytes were incubated with 1 µM H_2O_2 alone (H_2O_2) or with 250 µM NAC (H_2O_2 NAC) dissolved in medium 199. As a third control, cardiomyocytes were incubated with 250 µM NAC (Cont NAC) dissolved in medium 199 alone. Basal cell-death was evaluated in cells incubated in medium 199 alone (Cont). Cell-death was evaluated after 18 hours incubation (Fig.3.6).

3.2.5. Investigation of effect of doxorubicin treatment on mitochondrial transmembrane potential.

3.2.4.1. Investigation of collapse of mitochondrial transmembrane potential in response to FCCP.

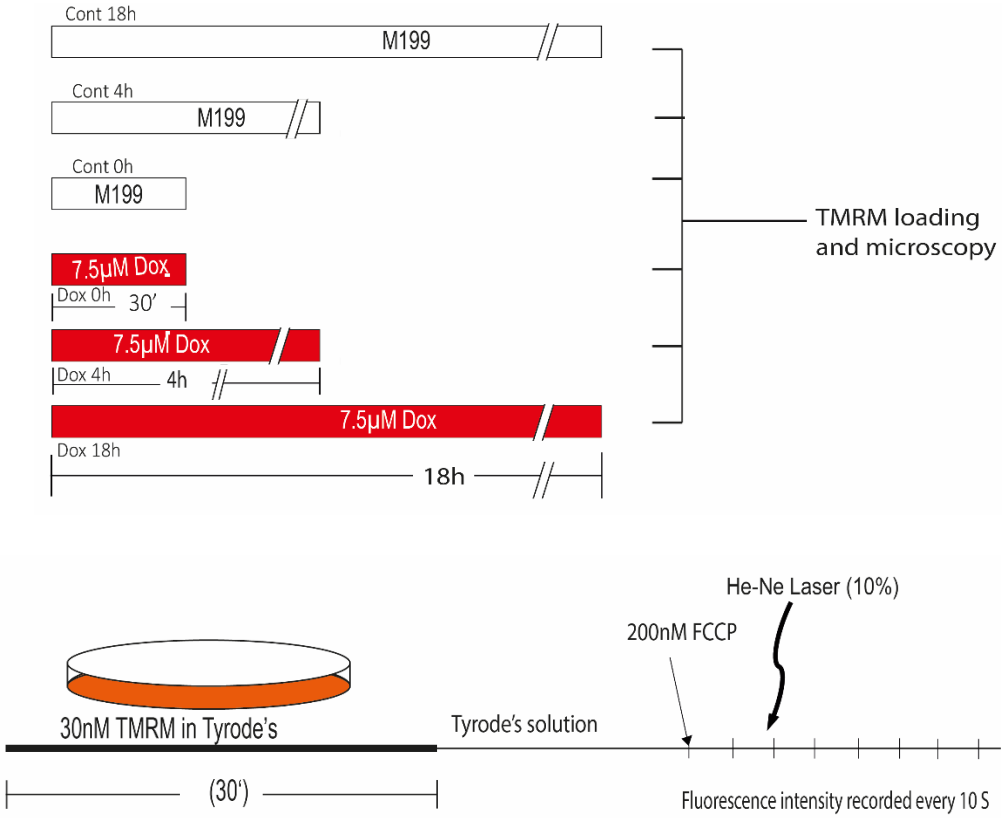

Fig. 3.7. Experimental layout for assessment of $\Delta\Psi_m$ collapse with FCCP. Cardiomyocytes were incubated in the indicated treatment for 18 hours. TMRM loading was achieved by incubating for 30 minutes in Tyrode's solution with dissolved 30 nM TMRM. Imaging was performed on the platform of a Leica SP5 confocal microscope. Mitochondrial respiration was arrested using 200 nM FCCP, and TMRM fluorescence recorded every 10 seconds using 10% He-Ne laser for 80 seconds or till complete loss of fluorescence signal.

To investigate the mitochondrial transmembrane potential ($\Delta\Psi_m$), temporal collapse and the residual fluorescence of TMRM was evaluated after arresting mitochondrial respiration with the uncoupling agent FCCP at a concentration of 200nM. Cardiomyocytes were plated in a 32 mm glass-bottomed cell-culture plate and incubated with 7.5 µM Dox in medium 199 for 30 minutes (Dox 0h), 4 hour (Dox 4h) and 18 hours (Dox 18h). Corresponding controls were incubated in medium 199 alone (Cont 0h, Cont 4h and Cont 18h respectively, Fig. 3.7). At the end of treatment period, incubating solution was discarded and cells were loaded with TMRM

by incubating in 30 nM TMRM dissolved in Tyrode's solution for 30 minutes. Excess dye was discarded, and the cells were washed with 1ml TMRM-free Tyrode's solution three times. The wells were then replenished with Tyrode's solution and the plates mounted on the stage of a Leica SP5 confocal microscope (Leica, Wetzlar, Germany) equipped with ×40 oil immersion objective lens (numerical aperture 1.0). Baseline $\Delta\Psi_m$ was estimated by measuring the fluorescence of TMRM using an incident He-Ne laser at 543 nm (10% maximum intensity) as a light source. The intensity of emitted light was recorded between 580-596nm (line average of 2 scans). FCCP was then introduced to the solution at a final concentration of 200 nM, and images obtained every 10 seconds for 80 seconds or till complete loss of fluorescence. The images were deconstructed to red, green, and blue channels in ImageJ software and intensity of emitted light in the red channel was measured. Optical fluorescence was plotted against time after introduction of FCCP (in seconds) to assess temporal variation, and analysed for statistical significance.

3.2.4.2. Estimation of $\Delta\Psi_m$ variation in response to doxorubicin treatment.

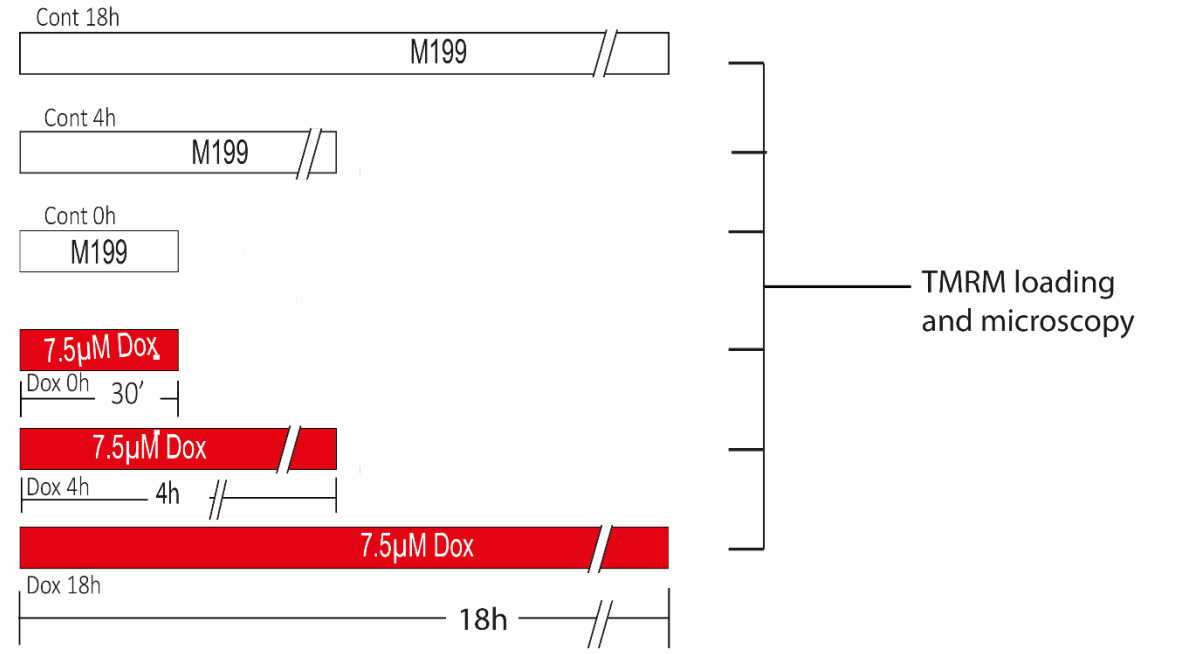

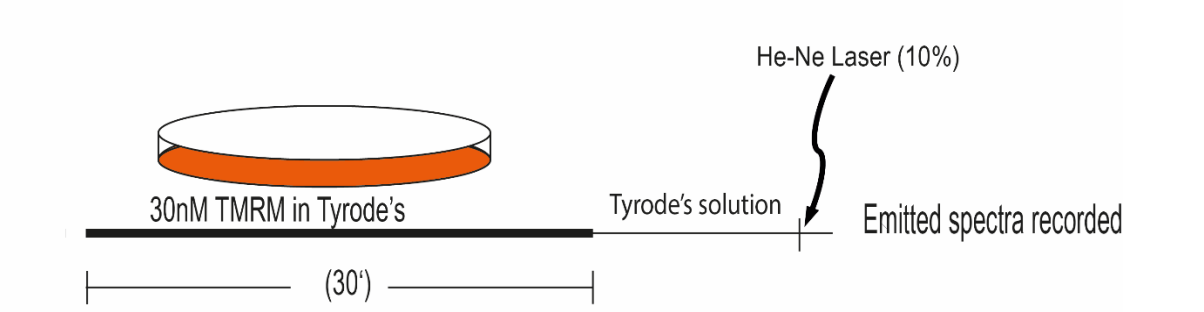

Fig 3.8. Experimental layout for assessment of $\Delta\Psi_m$. Cardiomyocytes were incubated in the indicated treatment for 18 hours. Medium 199 was exchanged for Tyrode's solution with 30 nM TMRM and allowed to incubate for 30 minutes before exchanging for dye-free Tyrode's solution. Imaging was performed on the platform of a Leica SP5 confocal microscope and images recorded of the fluorescence intensity of TMRM using 10% He-Ne laser incident laser.

To evaluate $\Delta\Psi_m$ variation, cardiomyocytes from treatment groups Dox 0h, Dox 4h and Dox 18h (section 3.2.4.1.) were loaded with 30 nM TMRM as above, and the emited fluorescence recorded at 580-596 nm after focussing 543 nm 10% He-Ne laser on the stage of a Leica SP5 confocal microscope (×40 oil immersion objective lens, numerical aperture 1.0) (Fig. 3.8). Corresponding controls (Cont 0h, Cont 4h and Cont 18h respectively) were incubated in medium 199 alone. Images were deconstructed to red, green, and blue channels in ImageJ

software and intensity of emitted light in the red channel was measured. This approach to $\Delta\Psi_m$ measurement has been described previously both form our own lab (Sidall et al, 2010) as well as by other groups (Juhaszova et al, 2004).

3.2.6. Investigation of the role of the mitochondrial permeability transition pore in doxorubicin toxicity.

3.2.5.1. Measurement of time taken to mitochondrial permeability pore induction following doxorubicin treatment.

To assess the influence of Dox treatment on the transition of the mitochondrial transition permeability pore (mPTP), cardiomyocytes were incubated with 7.5 µM Dox for 18 hours (Dox).

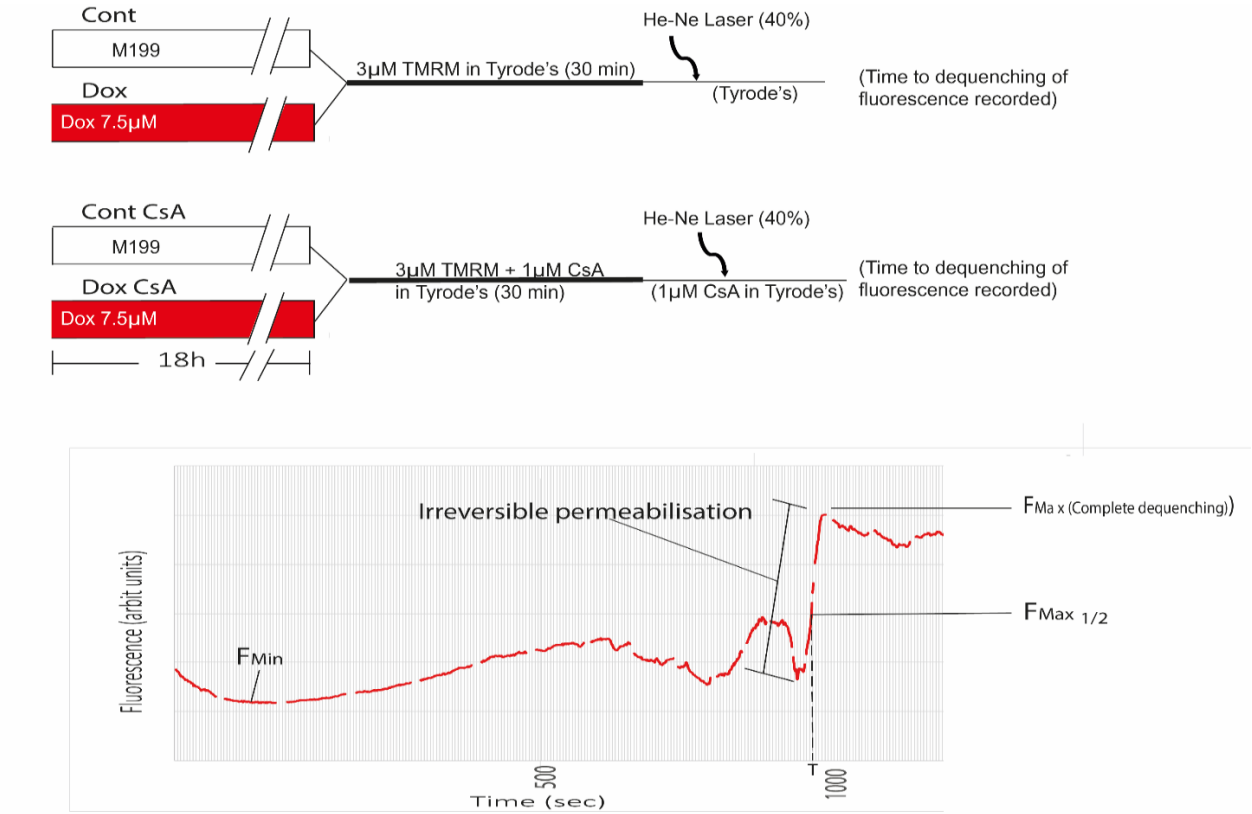

Fig. 3.9. Experimental layout for estimating time taken to mPTP induction. Cardiomyocytes were incubated in the indicated treatment for 18 hours. Medium 199 was exchanged for Tyrode's solution with 3 µM TMRM, and allowed to incubate for 30 minutes. Cells were then subjected to 40% intensity incident He-Ne laser with continuous recording of the emission spectra at 580 nM-596 nM. Time taken to reach half of maximum fluorescence-intensity was recorded as time taken to mPTP induction (T). 1 µM CsA was used a positive control, and loaded with TMRM and subsequently maintained in Tyrode's solution.

Cells were loaded with a higher concentration of 3 µM TMRM, using a similar protocol as above. Plates were subjected to 40% intensity incident He-Ne laser on the imaging platform of a Leica SP5 confocal microscope, and continuous recording of the emission spectra at 580 nM-596 nM was undertaken (Fig. 3.9). Time taken to complete de-quenching of TMRM fluorescence from mitochondria to cytosol was taken as complete transition of the mitochondrial pore. Time taken for fluorescence in each cardiomyocyte to reach half of maximum intensity was recorded as time taken to mPTP induction (Fig.3.9, T). Control (Cont) cardiomyocytes were incubated with medium 199 only. Ciclosporine A (CsA) is a compound that increases the threshold of induction-stimulus required for mPTP-transition to "open" state, which is detected as an increase in the time taken to mPTP induction. Therefore, 1 µM CsA was used as positive control in this experiment, and loaded in Tyrode's solution with TMRM after Dox treatment (Dox CsA), or after incubation in medium 199 alone (Cont CsA). For these positive controls, imaging was carried out in Tyrode's solution with dissolved 1 µM CsA.

3.2.5.2. Investigating the effect of CsA co-treatment on doxorubicin-toxicity.

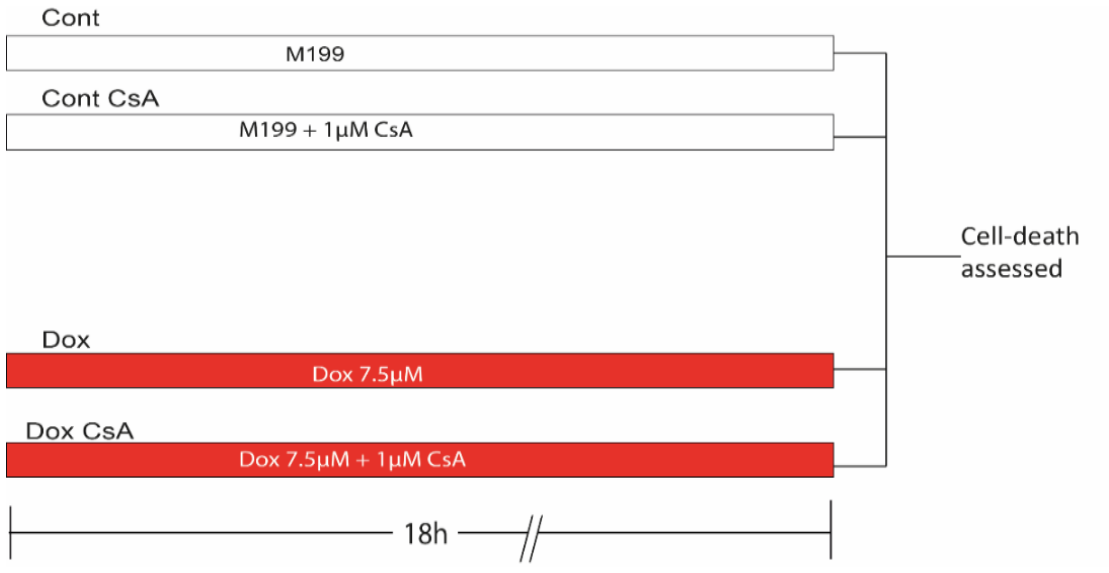

Fig. 3.10. Experimental design for investigating the effect of CsA on doxorubicin-induced cell-death. Cardiomyocytes were incubated with 7.5 µM doxorubicin alone or with 1 µM CsA for 18 hours and cell-death assessed. As control, cardiomyocytes were incubated in medium 199 alone or with dissolved 1 µM CsA for 18 hours.

Cardiomyocytes were incubated in 7.5 µM Dox alone (Dox) or co-incubated with Dox and 1 µM CsA (Dox CsA) for 18 hours before assessment of cell-death. Control cardiomyocytes were incubated in medium 199 alone (Cont) or with 1 µM CsA (Cont CsA) for 18 hours (Fig.3.10).

3.2.7. Investigation of the effect of hypoxic preconditioning on doxorubicin-induced cell-death.

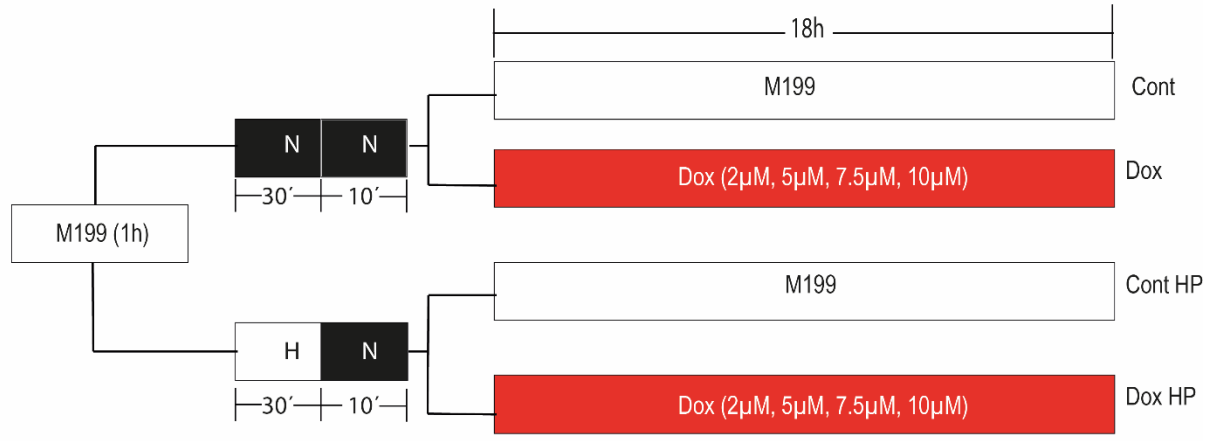

Fig. 3.11. Protocol for evaluating the influence of hypoxic preconditioning on doxorubicin-induced toxicity. Cardiomyocytes were subjected to 30 minutes hypoxia followed by 10 minutes reoxygenation, then transferred to medium 199 with dissolved doxorubicin (concentrations indicated) for 18 hours. As control, cells were subjected to a control protocol and incubated with the indicated concentrations of doxorubicin for 18 hours. (Abbreviations Dox= Doxorubicin, H=Hypoxic buffer, N=Normoxic buffer).

To investigate the effect of hypoxic preconditioning (HP) on Dox mediated cell-death, cardiomyocytes were maintained in medium 199 for 1 hour, then transferred to hypoxic buffer in a hypoxic airtight chamber at 37 °C, and incubated for 30 minutes before exchanging into normoxic buffer in normal atmosphere at 37 °C for 10 minutes. Cells were then transferred into medium 199 alone (Cont HP, Fig, 3.11) or with Dox at concentrations 2 µM, 5 µM, 7.5 µM, and 10 µM (Dox HP) and incubated for 18 hours. Normoxic controls were established by incubating cardiomyocytes in normoxic buffer alone for 40 minutes, then transferred to medium 199 alone (Cont) or into respective Dox concentrations (Dox, Fig, 3.11).

3.2.8. Investigation of the reperfusion injury salvage kinase components involved in hypoxic preconditioning mediated protection against doxorubicin-toxicity.

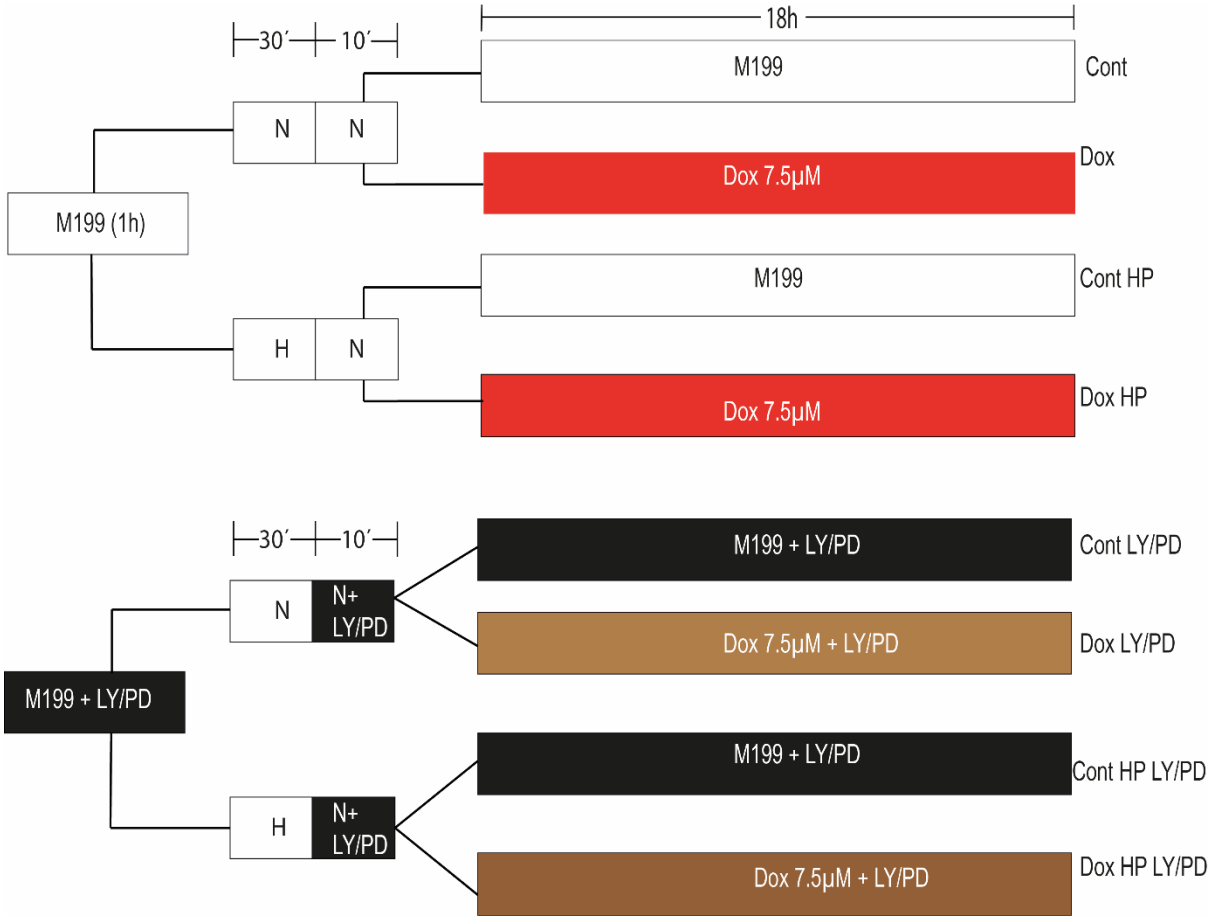

Fig. 3.12. Experimental set-up for inhibition of PI3K/Akt and of MAPK ERK 1/2 respectively. Cells were pre-incubated with 10μM LY294002 to inhibit PI3K/Akt, or with 30μM PD98059 to inhibit MAPK ERK 1/2. Hypoxic stimulus was delivered *in vitro* and the inhibitors reintroduced at reoxygenation. Cells were incubated in a bathing media with dissolved doxorubicin and LY294002 or PD98059 as appropriate respectively (Abbreviations: Dox= Doxorubicin, H=Hypoxic buffer, LY=LY294002, N=Normoxic buffer, PD=PD98059).

To delineate the involvement of the reperfusion injury salvage kinase (RISK) pathway HP-mediated protection, cardiomyocytes were pre-incubated in medium 199 for one hour with 10 μM LY294002 to inhibit induction of PI3K/Akt, or with 30 μM PD98059 to inhibit MAPK ERK 1/2 respectively. Cells were then subjected to hypoxia for 30 minutes in an inhibitor-free hypoxic buffer. LY294002 and PD98059, as appropriate, were reintroduced in normoxic buffer and cells incubated for 10 minutes in normal atmosphere before exchange into the respective inhibitors dissolved in medium 199 alone (Cont HP LY and Cont HP PD respectively), or with 7.5 μM Dox

(Dox HP LY and Dox HP PD respectively, Fig. 3.12) and incubated for 18 hours. Preconditioned controls were established by incubating cardiomyocytes in inhibitor-free medium 199 alone, then eliciting hypoxic preconditioning with 30 minutes hypoxia in hypoxic buffer followed by reoxygenation for 10 minutes in normoxic buffer in a normal atmosphere. Cells were then transferred to medium 199 alone (Cont HP) or 7.5 µM Dox (Dox HP, Fig. 3.12) and incubated for 18 hours. As normoxic controls for inhibitor-treatment, cardiomyocytes pre-incubated with LY294002 and PD98059 as above were transferred to inhibitor-free normoxic buffer in normal atmosphere and incubated for 30 minutes, then exchanged into normoxic buffer with dissolved LY294002 or PD98059 as appropriate and incubated for 10 minutes. Cells were then transferred in presence of the respective inhibitors to medium 199 alone (Cont LY and Cont PD), or into 7.5µM Dox (Dox LY and Dox PD, Fig. 3.12) and incubated for 18 hours. Basal cell-death was evaluated after incubating cells in normoxic buffer in normal atmosphere for 40 minutes, then transferring to medium 199 alone for 18 hours (Cont). Reference Dox-toxicity was established by incubating cells in 7.5 µM Dox for 18 hours after 40 minutes incubation in normoxic buffer (Dox, Fig. 3.12).

3.2.9. Western blot analysis

3.2.9.1. Analysis of induction of phospho-Akt and phospho-ERK in response to hypoxic preconditioning.

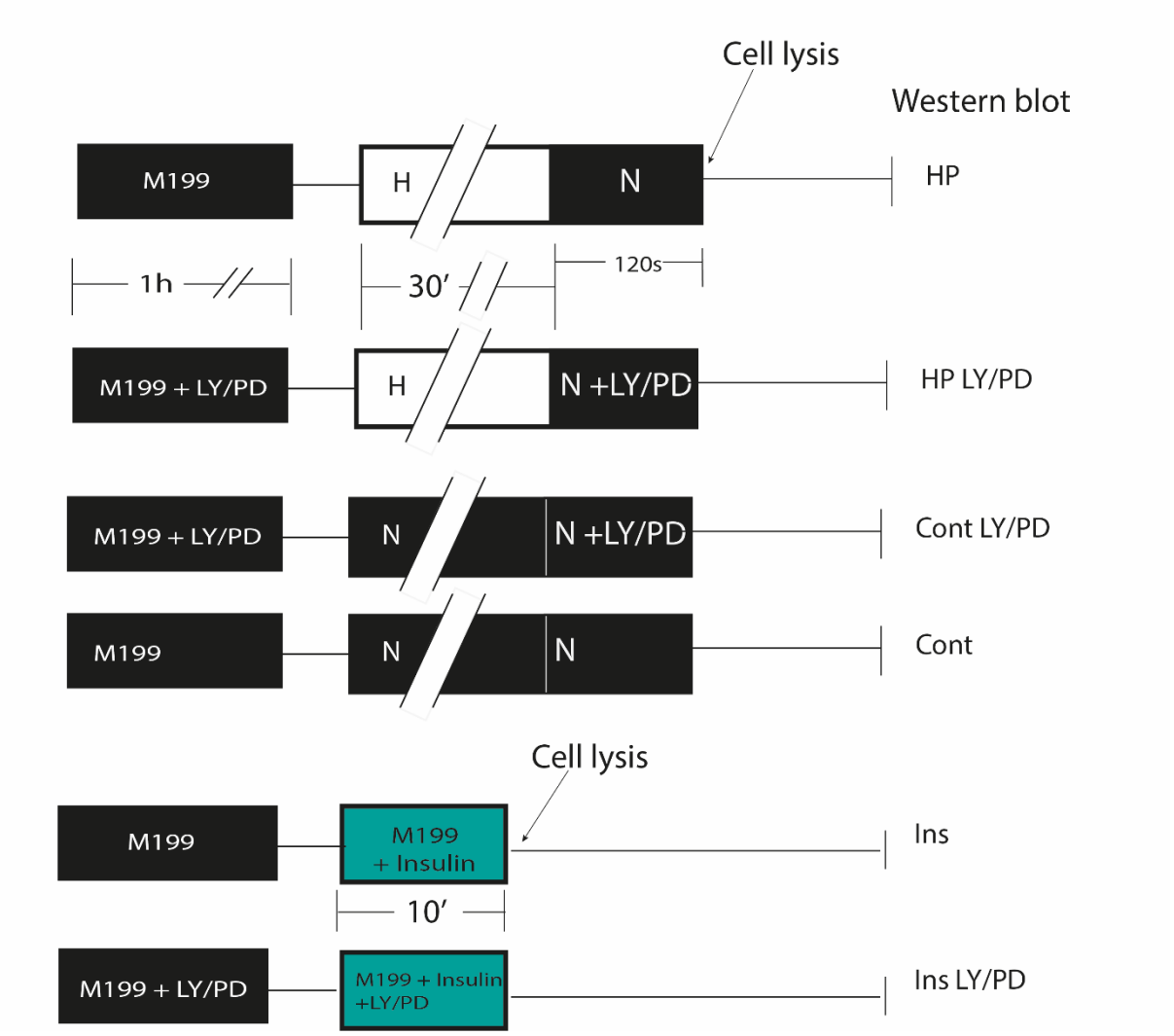

Fig.3.13. Protocol for collection of Western blot sample to analyse protein kinase induction following preconditioning. Cardiomyocytes were pre-incubated with 10 µM LY294002 (LY) or with 30µM PD98059 (PD) then subjected to 30 minutes hypoxia before transfer to reoxygenation buffer in normoxic environment. Samples were collected by lysing cells 120s after completion of hypoxic phase of preconditioning, within the time zone of simulated reperfusion. Insulin treatment was used as a positive inducer of phospho-Akt and phospho-ERK 1/2, and in positive controls, cells were lysed after 10 minutes of insulin (275u/ml) treatment, following 1 hour of treatment with the inhibitors LY294002 or PD98059, as appropriate.

The activation of PI3K/Akt pathway and MAPK ERK 1/2 by HP was analysed by Western blot analyses following characterisation (Chapter 4, section 4.3). Cardiomyocytes were pre-incubated for one hour in medium 199, then provided a hypoxic stimulus by incubating in a hypoxic buffer in hypoxic atmosphere for 30 minutes. These were then transferred into a

normoxic buffer in normal atmosphere, and cells lysed at 120 seconds after hypoxia (HP, Fig. 3.13). Pre-incubation in 10 µM LY294002 or 30µM PD98059 was used to inhibit PI3K/Akt and MAPK ERK 1/2 respectively before inducing hypoxic-stimulus in an inhibitor-free hypoxic buffer in hypoxic atmosphere for 30 minutes. Cells were then transferred into normoxic buffer with 10 µM LY294002 (HP(LY)), or with 30µM PD98059 (HP(PD)) respectively and reoxygenated for 120 seconds before cell lysis. As non-preconditioned inhibitor-treated controls, cardiomyocytes were incubated in medium 199 with the respective inhibitors, then transferred into normoxic buffer in a normal atmosphere for 30 minutes. These were then transferred to normoxic buffer with dissolved inhibitors and lysed at 120 seconds as above (Cont(LY) and Cont(PD) respectively, Fig. 3.13). Phosphorylation of both PI3K/Akt and MAPK ERK 1/2 under basal conditions was evaluated in cells incubated in normoxic buffer alone for 30 minutes, then lysed after an additional 120 seconds (Cont, Fig.3.13).

As positive control, cardiomyocytes were treated to medium 199 with 275u/ml insulin in medium 199 for 10 minutes to induce the RISK kinases, and samples lysed as described below. Insulin-induced RISK kinase induction was inhibited by pretreating cardiomyocytes to medium 199 with LY294002 or with PD8059 for one hour, then transferred to medium with insulin and the respective inhibitors.

Cell lysis was carried out with boiling 1x SDS-PAGE sample loading buffer, and harvesting of the lysate carried out using a cell-scraper. The samples were boiled at 100˚C for two minutes to inhibit protein phosphatases. Samples were resolved by standard SDS-PAGE and transferred to a nitrocellulose membrane using standard Western blotting protocol. The membrane was blocked with 5% Bovine serum albumin for one hour before incubating with respective primary antibodies, and allowed to adhere overnight. Primary antibodies were then discarded and membrane washed and loaded with respective species-specific secondary antibodies using

standard Western blot protocol. The membranes were then recorded using Li-COR Odyssey® imaging system and software, before further analysis using imageJ. The protein content for each treatment group were evaluated using standard imageJ Western blot analysis approach.

To evaluate PI3K/Akt phosphorylation induction, phosphorylated and non-phosphorylated protein levels (p-Akt and t-Akt levels) was determined for each sample group. Both p-Akt and t-Akt were normalised to the respective levels of the housekeeping protein Glyceraldehyde 3-phosphate dehydrogenase (GAPDH) in each well, i.e., p-Akt:GAPDH and t-Akt:GAPDH ratios were identified. Phosphorylation induction in the respective groups were then determined as the ratio of p-Akt:GAPDH to t-Akt: GAPDH. Similarly, to evaluate phosphorylation of MAPK ERK 1/2, phosphorylated and non-phosphorylated protein content of ERK 1/2 were normalised to the content of the housekeeping protein α-tubulin in each well (p-ERK: α-tubulin and t-ERK: α-tubulin respectively) and the ratio of p-ERK: α-tubulin to t-ERK: α-tubulin evaluated.

3.2.9.2. Analysis of PI3K/Akt and MAPK ERK 1/2 induction in response to doxorubicin treatment.

To analyse the induction PI3K/Akt and MAPK ERK 1/2 in response to Dox-treatment, cells were subjected 7.5 µM Dox for 15 minutes, 4 hours or 18 hours (Dox 0h, Dox 4h and Dox 18h, Fig.3.14). Control cardiomyocytes were incubated in medium 199 alone (Cont 0h, Cont 4h and Cont 18h). Cells were lysed with boiling SDS-PAGE and probed using standard Western blotting protocol, before recording in Li-COR® odyssey as described above. Blots were analysed using ImageJ as above.

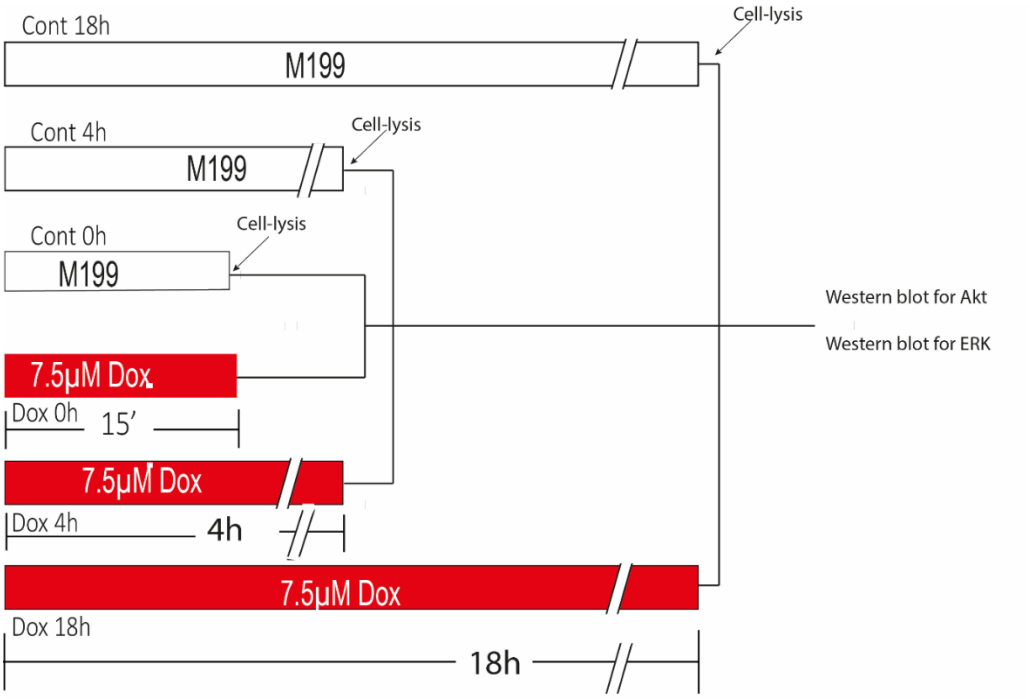

Fig.3.14. Experimental layout for protein collection and analysis of phosphorylation-induction of Akt and ERK 1/2 following doxorubicin treatment. Cardiomyocytes were incubated with 7.5µM doxorubicin for 15 minutes, 4 hours or 18 hours. Control Cardiomyocytes were incubated in medium 199 alone. Cells were lysed with boiling SDS-PAGE and analysed by standard western blotting protocol.

3.2.10. Statistical analysis.

All data were analysed using Graphpad prism (version 5.0). Values are expressed as mean ± Standard error of the mean (SEM). Analysis of statistical significance where carried out with multiple Students t-test where samples where small to the order of n=2, or using Repeated-measures ANOVA where sample sizes were larger. Where F achieved $P<0.05$ for ANOVA table, Tukey's post-hoc comparison test was carried out and differences were considered significant if p-values were determined to be $p<0.05$.

Chapter 4. Characterisation and development of models and protocols.

4.1. Model of doxorubicin toxicity.

4.1.1. *In vitro* model of doxorubicin toxicity.

Although anthracycline cardiotoxicity has been investigated in *in vivo*, *in vitro*, as well as in *ex vivo* models, a number of different hypotheses are offered to explain the aetiology of cardiomyocyte injury. The various different models in which investigations into anthracycline-injury has been described, along with the varying modes, models and time-periods to elicit significant injury, makes investigating the toxicity of these compounds challenging using any single reproducible model of toxicity. Different animal models as well as cell systems have been used to investigate the cardiotoxicity of anthracyclines (Stěrba et al, 2011). Reports from *in vivo* as well as *in vitro* models reveal a dose-dependent effect in the toxicity of doxorubicin, and a high concentration of anthracyclines may induce cardiac dysfunction where low dose concentrations show no apparent effect. For example, Edwards et al (2016) failed to observe any significant cardiac dysfunction in a murine model with 1-15 mg/kg intraperitoneal Dox after 6 to 8 months, but achieved cardiac failure in mice injected with higher concentrations of up to 45 mg/kg doxorubicin. Similarly, reports from *in vivo* models have shown large single bolus doses of anthracyclines achieve symptomatic heart failure within a short span of time, typically in the order of 72 hours (Zhang et al, 2012, Chatterjee et al, 2010). Other investigators have reported data from small animal models using low dose, interrupted dosing, mimicking human chemotherapy protocols which demonstrate evidence of early structural changes before overt heart failure symptoms manifests. In a Dox-induced model of toxicity in rats, for example, evidence of histological and organellar changes along with myofibrillar disarray were noted within a period of six weeks, before evidence of cardiac failure were noted (Cove-Smith et al,

2014). Similarly, proteomic analysis in a rabbit model of daunorubicin toxicity similarly showed evidence of altered gene expression and mRNA translation of cardiac structural proteins immediately after cessation of an interrupted dosing regimen (Lenčová-Popelová et al, 2014). An early increase in apoptotic proteins was previously reported in a very similar model (Stěrba et al, 2011). Furthermore, emerging data in human subjects show early evidence of asymptomatic- and therefore subclinical- cardiac dysfunction within weeks to months of cessation of anthracycline chemotherapy, which in some cases may improve spontaneously (Cardinale et al, 2015). Of particular note however, anthracyclines are retained within cardiomyocytes more than in other cells (Johnson et al, 1986). Reports using *in vitro* models of Dox toxicity reveal a dose-response effect on cell-death and in cellular injury, e.g., in the cardiomyocyte-toxicity of anthracyclines in human induced pluripotential stem cells (Zhao and Zhang, 2017). Importantly, cardiomyocyte injury in response to Dox begins early under experimental conditions and may precede induction of cell-death. Even very low concentrations of Dox may have early effect on physiological pathways, e.g., cellular respiratory pathways (Darrabie et al, 2012), while in isolated adult rat cardiomyocyte models, degradation and proteolysis of intracellular structural proteins may begin as early as one hour, before cell-death induction takes place (Lim et al, 2004). This suggests that anthracycline toxicity may be a dynamic process that begins early and is sustained in the cardiomyocyte, which is likely to be more vulnerable due to preferential accumulation of the compound. In this context, for our experimental aims *ex vivo* models, e.g., human atrial muscle models, were considered less appropriate, since anthracyclines show greater accumulation within the ventricle (Lencova-Poppelova et al, 2014) and, further, the limited extracorporeal viability of tissues such as the human atrial muscle or rodent isolated Langendorff perfused heart limited the time-period for which the tissue may be exposed to anthracyclines. We therefore chose an *in vitro* cell model

to investigate the toxicity of anthracyclines. We used Dox as a representative anthracycline compound, with cell-death as a representative marker of cardiomyocyte injury.

4.1.2. Adult rat ventricular myocytes.

We used freshly isolated primary adult rat ventricular myocytes as the *in vitro* cellular model as they are the most appropriate model for these studies. This model offers a highly pure system, with low numbers of contaminating cells. The cells are non-dividing terminally differentiated cells like the adult human heart, and, further, it is a relatively inexpensive and efficient model that offered high throughput for reproducing experiments (Fearon et al, 2013). In contrast, neonatal rat ventricular myocytes are a mixed isolate containing fibroblasts, and continue to undergo some proliferation after isolation; cardiomyocytes derived from induced pluripotential stem cells (iPSCs-CM) have an immature phenotype; and cardiomyoblast tumour-derived cell lines are dedifferentiated and rapidly dividing cell models. We therefore reasoned that adult cardiomyocytes reproduced a mature cardiomyocyte at risk of doxorubicin-injury more accurately. Further, this cellular model offered a potential for continuum in developing future *ex vivo* and *in vivo* models in which this work may be further explored.

4.1.3. Concentrations of doxorubicin investigated during characterisation experiments.

Peak plasma concentration of Dox is typically in the range of 5 µM in humans (Minotti et al, 2001), and falls to a steady-state concentration of 1 µM to 500 nM Dox over 48 hours. Some basal cell-death is observed in the *in vitro* ARVM model due to the isolation process. We therefore tested a range of Dox concentrations for their effect on cell-death in this model in order to identify the minimum toxic dose that manifested a significant rise in cell-death relative to basal cell-death. Specifically, we tested from 0.5 µM up to the peak 24 hour concentration observed in humans (5 µM). We also incubated cardiomyocytes with supraphysiological concentrations of Dox (7.5 µM, 10 µM, 15 µM and 20 µM) in order to maximize the possible effect on survival within a relatively short culture period.

4.1.4. Overall cell-death as an index of doxorubicin toxicity.

Dox has been described variously as capable of inflicting necrotic as well as apoptotic cardiomyocyte-death (Zhang et al, 2009). The individual contributions of necrosis and apoptosis to doxorubicin-induced cardiomyocyte death is unclear, and both types of cell-death have been reported in adult rat ventricular myocytes (Delpy et al, 1999; Lim et al, 2004). Furthermore, in cultured endothelial cells, a transition from apoptosis to necrosis has been reported as Dox concentration increases above 5 µM (Kotamraju et al, 2000). Certain apoptotic assays, e.g., TUNEL staining may overestimate proportion of cardiomyocytes undergoing apoptotic death (Tokarska-Schlattner et al, 2006). Therefore, we assessed the overall cardiomyocyte-death using two different modalities. We assessed irreversible permeabilization of cell membrane by using propidium iodide (PI) staining. We further used morphological changes including cell-membrane blebbing as a marker of cell-death (Goto et al, 2009).

4.1.5. Characterisation of a model of doxorubicin-induced toxicity.

Initial experiments were designed to establish a model of injury where the toxicity of Dox on isolated adult rat ventricular myocytes could be reproduced. This is discussed in detail in subsequent sections.

4.1.5.1. Toxicity of doxorubicin on cardiomyocytes after 4 hours of treatment.

We first investigated the effect of increasing concentrations of Dox on cardiomyocyte death after a treatment period of eight hours, as described section 3.2.2. and Fig. 3.2.

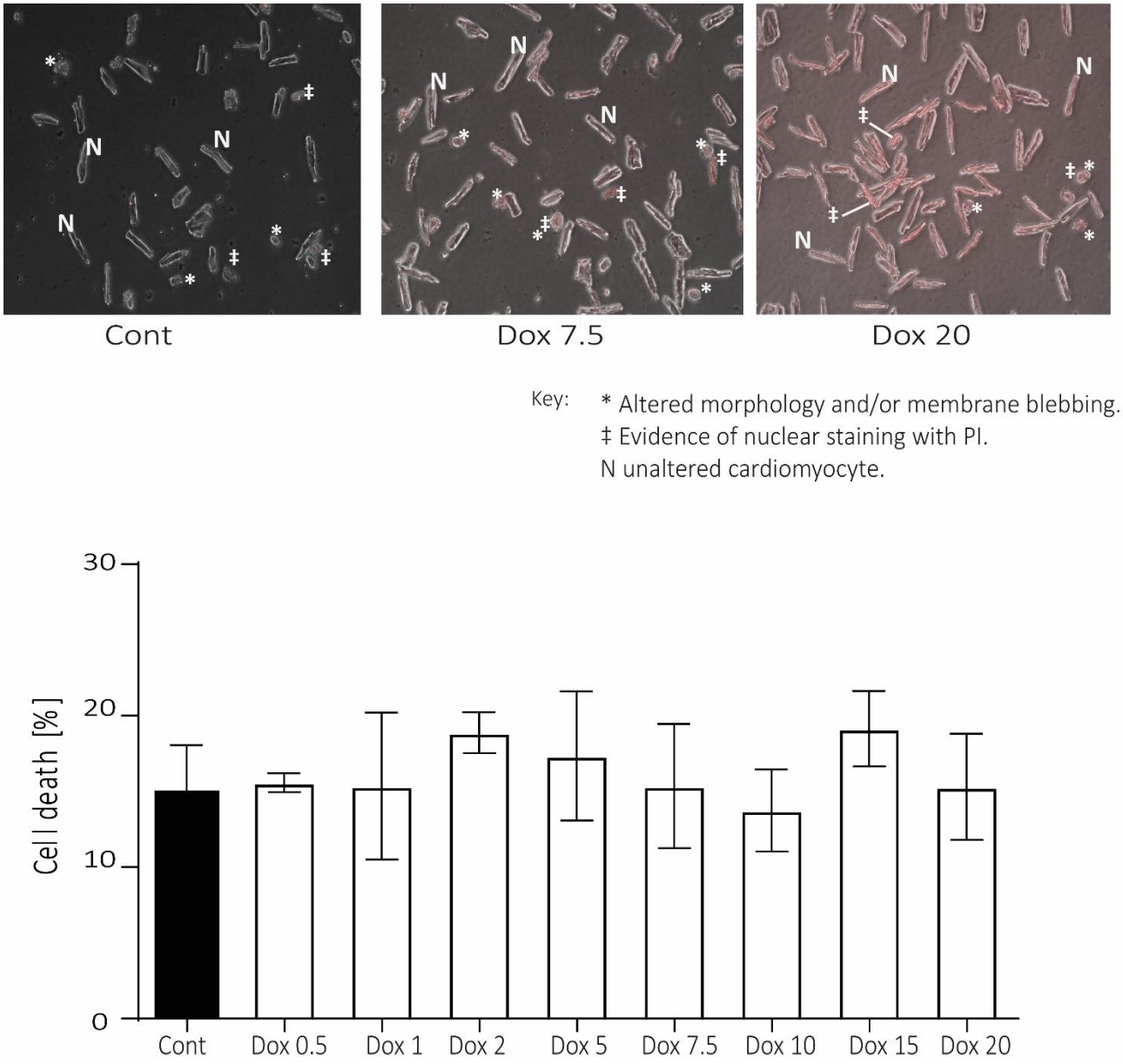

Fig. 4.1. Toxicity of doxorubicin over 4 h. No significant differences were identified with any concentration of doxorubicin (indicated in Arabic numerals) compared to the basal cell-death (Cont). Mean cell-death remained below in each treatment remained below 20% (*n*=2 for Dox 0.5, Dox 7.5, Dox 15 and Dox 20. *n*=4 for all other treatments, p>0.05) (representative photograph of cell-death in top panel, see also Appendix B, Fig. I).

Fig. 4.1 shows the results of these experiments. The basal level of cell-death remained below the exclusion criterion of 20% (Cont, mean cell-death 15.0 $\pm$ 2.9 %). No significant differences were identified between Cont and any of the concentrations of Dox to which cardiomyocytes were exposed (ANOVA p>0.05).

4.1.5.2. Toxicity of doxorubicin on cardiomyocytes in the presence of an additional insult of ischaemia-reperfusion injury.

Ischaemia-reperfusion injury (IR) has been postulated to share some common mechanisms of toxicity with anthracycline-mediated cardiomyocyte injury, as explained in introduction. This includes injury secondary to generation of ROS-species, alterations of the Ca^{2+} signalling pathways and Ca^{2+} sensitive channels, alterations of the mitochondrial respiratory pathways, and activation of cell-death mechanisms regulated at the level of the mitochondrial inner and outer membranes. Since the toxicity of anthracyclines on cardiomyocytes are slow, inflicting IR-injury on cardiomyocytes stressed by concomitant non-toxic concentration of Dox may uncover latent or subthreshold injury due to anthracyclines. Since we did not observe any significant differences in doxorubicin-induced cell-death after 4 hours, we investigated if Dox might cause a subthreshold injury that would be revealed after a "second hit", i.e., additional injury in tne form of IR.

4.1.5.2.1. Ischaemia-reperfusion injury model.

We first evaluated and characterised an *in vitro* model of cell-death due to IR with two different hypoxia times of 3 hours (SI3) and 4 hours (SI4), comparing the cell-death to basal-levels observed in cardiomyoytes incubated in m199 alone (Cont). Fig.4.2 shows the results of these experiments. Only a protocol with 4 hours hypoxia (SI4) and 1 hour reoxygenation resulted in a statistically significant injury (mean cell-death 36.3 $\pm$ 4.1%) compared to basal cell-death (Cont, 19.5 $\pm$ 1.2%; $p<0.05$ Cont vs SI4, $n=5$) (Fig. 4.2). The data we obtained in these characterisation experiments are consistent with results described by our lab using the same model previously (Smith et al, 2010). We therefore considered these results robust and reproducible, and adopted this protocol of 4 hours hypoxia and 1 hour reperfusion (SI4 protocol) to inflict IR-injury in subsequent experiments.

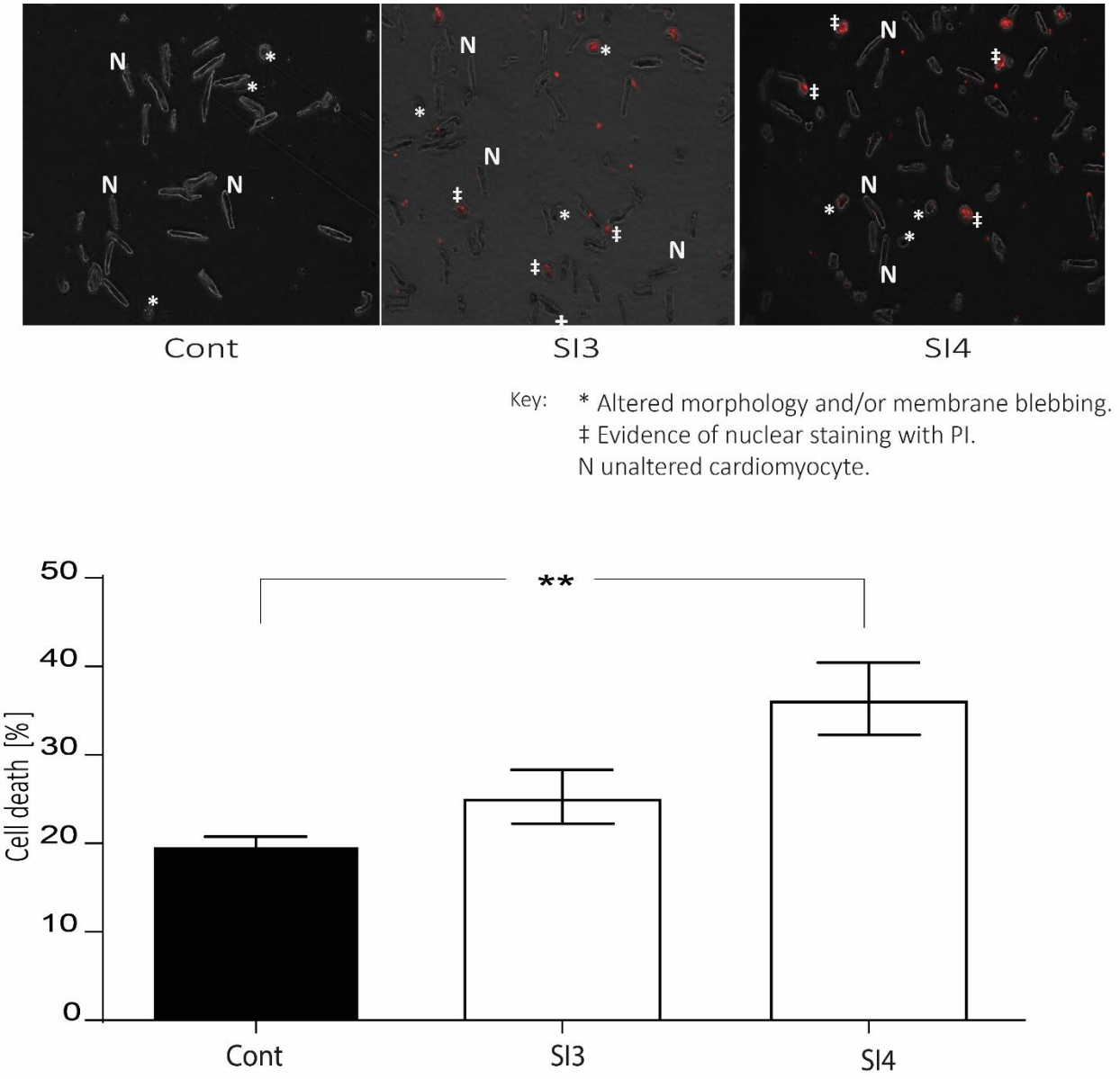

Fig. 4.2. Cell-death with increasing time of hypoxia with a maintained period of reoxygenation in ischaemia-reperfusion. With reoxygenation period maintained at 1 hour, SI4 (4 hours hypoxia) but not SI3 (3 hours hypoxia) showed a statistically significant increased cell-death compared to Cont ($p<0.05$, $n=5$) (Abbreviations: SI= simulated ischaemia) (representative photograph of cell-death in top panel).

4.1.5.2.2. Effect of addition of ischaemia-reperfusion injury on cell-death subjected to doxorubicin treatment for 4 hours.

Having identified 4 hours hypoxia as an optimum insult for significant injury, we next investigated the effect of inflicting this additional insult on cardiomyocytes subjected to Dox treatment (Fig. 3.4). We therefore subjected cells to IR after pre-treating them with 2 µM Dox for 4 hours, as described in section 3.2.3 (Fig. 3.4). The pre-treatment period was incorporated

to allow for accumulation of the drug or its potential metabolites within the cardiomyocytes, and alterations to metabolic or cell-survival pathways, if any, to be initiated (Olson et al, 1988; Charlier et al, 2005). Further, this protocol mimicked the situation where the myocardium that has been stressed by anthracyclines may subsequently be subjected to an additional insult such as ischaemia and reperfusion that occurs as the result of myocardial infarction. We used a concentration of 2 μM Dox since this is close to half peak plasma levels, and may therefore potentially induce a subthreshold injury that would be revealed by this "second hit" in the form of IR-injury.

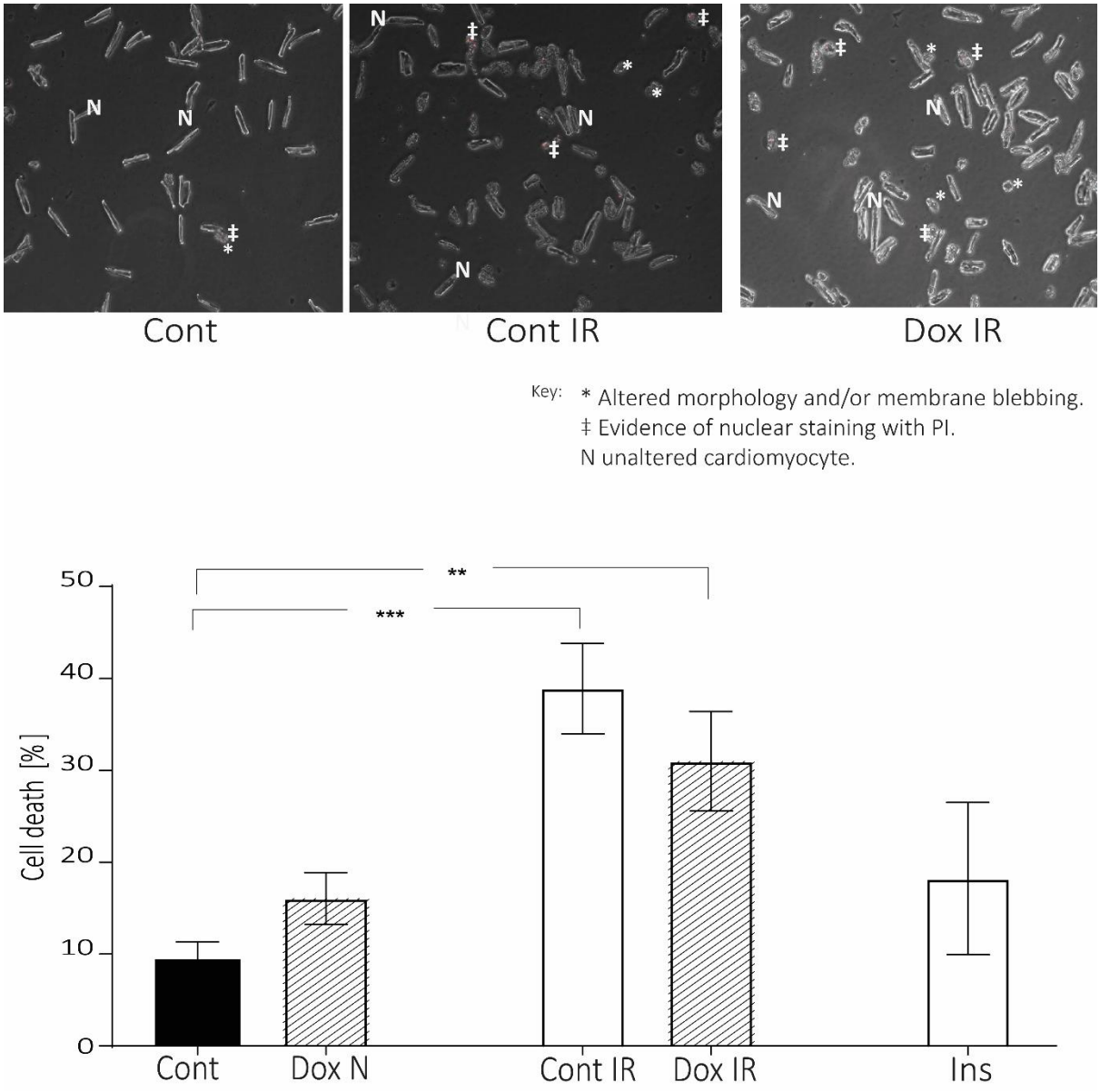

Fig. 4.3. Effect of ischaemia-reperfusion injury on cardiomyocytes after 4 h doxorubicin treatment. Compared to ischaemia-reperfusion in untreated cells (Cont IR), 2µM doxorubicin pre-treatment resulted in no significant difference in cell-death (Dox IR). The presence of the positive control insulin (Ins) rescued untreated cardiomyocytes from IR-injury, and no significant differences were noted between basal cell-death (Cont) and Ins (ANOVA $p<0.05$, $n=3$) (representative photograph of cell-death in top panel, see also Appendix B, Fig. III).

Fig. 4.3 shows the results of these experiments. Analysis of cell-death revealed that IR alone (Cont IR, mean cell-death 38.9 $\pm$ 2.8%) and IR after Dox pre-treatment (Dox-IR, 30.9 $\pm$ 3.1%) resulted in no significant differences. Both treatments resulted in significantly greater toxicity compared to basal cell-death (Cont, 9.4 $\pm$ 1.0%) (Fig 4.3). For comparison, untreated controls

reoxygenated with the positive control insulin after hypoxia were protected (Ins, mean cell-death 18.2 ± 4.7%), and no significant differences were identified compared to control. 2 µM Dox alone (Dox N, 16.0 ±1.6%) did not exhibit any significant toxicity. The results presented are a mean of three different repeat experiments (*n*=3). We concluded with reasonable confidence therefore that Dox at the concentration(s) and incubation periods we explored, did not inflict any significant overt or subthreshold injury.

4.1.5.3. Toxicity of doxorubicin over 18 hours.

Our experiments suggested that 4 hours may not be an appropriate time in which any potential pathways for cardiomyocyte toxicity could manifest in this model. Therefore, we explored if prolonging the time of exposure to Dox to 18 hours would result in any increase in cardiomyocyte death. This incubation period was chosen partly due to methodological limitations. Beyond this, primary adult rat ventricular myocytes begin to reach the limits of viability *in vitro* and display dedifferentiation, and therefore may yield inappropriate and inconsistent conclusions if significantly prolonged (Louch et al, 2011). Since cell-death was minimal at the lowest concentration, we excluded 0.5 µM Dox in subsequent experiments (section 3.2.2, Fig. 3.2).

Fig. 4.4 shows the results of these experiments. A significant rise in cell-death was identified after incubation with 7.5 µM Dox (Dox 7.5, mean cell-death 37.0 ± 4.9%), 10µM Dox (Dox 10, 43.1 ± 4.7%), 15 µM Dox (Dox 15, 56.7 ± 7.3%) and 20 µM Dox (Dox 20, 49.7 ± 4.1%). Compared to basal cell- death (Cont, mean cell-death 15.6 ± 1.2%), 1 µM Dox (Dox 1, 14.6 ± 2.8%), 2 µM Dox (Dox 2, 16.2 ± 1.8%) and 5 µM Dox (Dox 5, 30.9 ± 2.9%) showed no significant difference in cell-death following incubation for 18 hours (ANOVA $p<0.05$, *n*=7) (Fig. 4.4)).

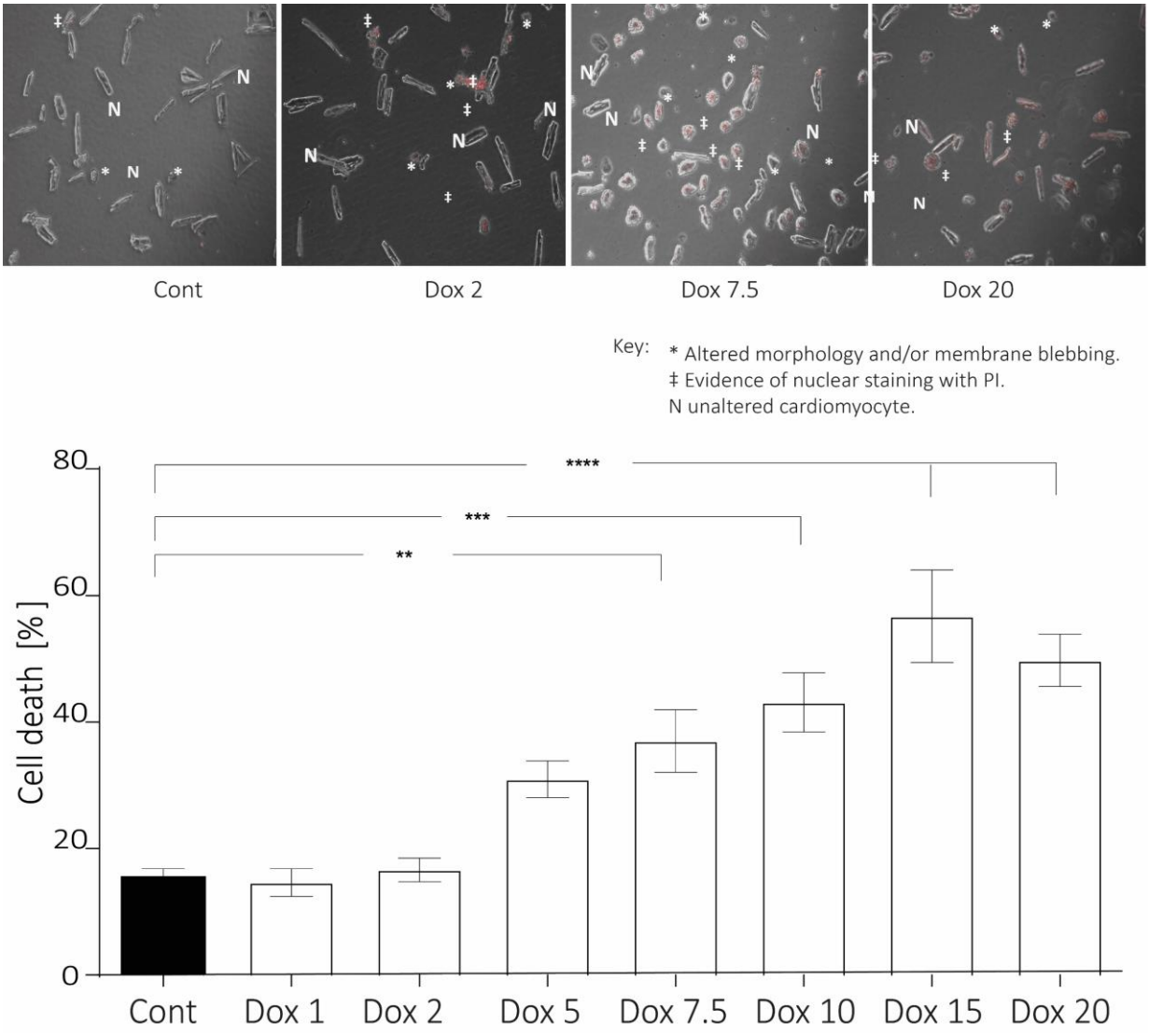

Fig. 4.4. Mean cell-death after 18 h incubation with various concentrations of doxorubicin. A trend in increase in cell-death was noted with doses excess of 5 µm doxorubicin (Dox 5), but only reached statistical significance with 7.5 µM (Dox 7.5) and higher concentrations. 1 µM doxorubicin (Dox 1) and 2 µM doxorubicin (Dox 2) exposure showed no difference compared to basal cell-death (Cont) (ANOVA $p<0.05$, $n=7$) (representative photograph of cell-death in top panel, also see Appendix B, Fig. II).

We considered the possibility that the lack of difference in cell-death with 1-5 µM Dox may be explained by wash-off of detached, dead cells during introduction of PI and consequent agitation of cell culture wells. To assess this, we counted the total number of cells in each treatment group (i.e., both live and non-viable cells), normalized to the number of cells in the control group (Cont) (Fig 4.9). This revealed no significant differences or variations in the final

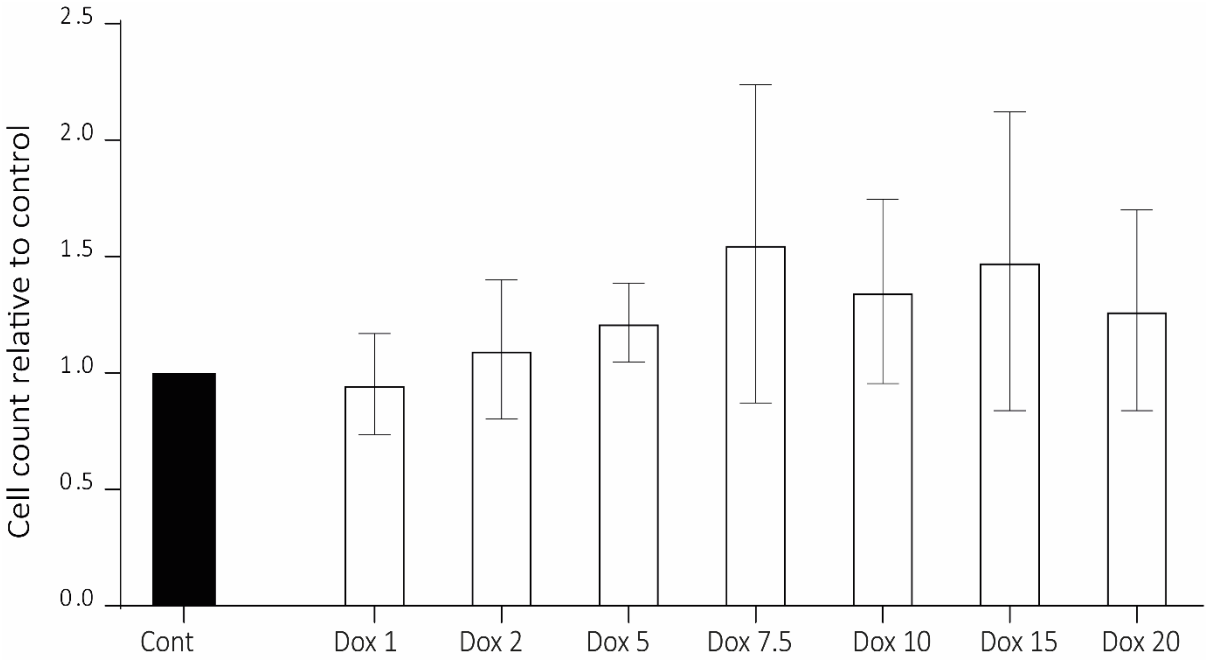

Fig. 4.5. Variations in total cell-count with increasing doxorubicin at the end of 18 h, normalised to control. Total cumulative counts of live and non-viable cells were calculated for each treatment group and expressed as ratio to control (Cont). No significant differences were identified on statistical analyses of the variations (ANOVA $p>0.05$, $n=7$).

cell-count relative to control (ANOVA $p > 0.05$, $n=7$) (Fig. 4.5), suggesting that differential wash-off did not contribute to the different survival observed.

4.1.5.4. Effect of ischaemia-reperfusion on cardiomyocytes after 18 hours doxorubicin pre-treatment.

Since we did not observe any evidence of toxicity below 5 µM (peak physiological plasma concentration), we re-explored the hypothesis that a latent subthreshold injury may exist with lower concentrations of doxorubicin. For reasons described above, we pre-treated isolated cardiomyocytes with 2 µM Dox for 18 hours, before subjecting these cells to IR- injury using the protocol described in section 3.2.3.2 (Fig. 3.2)

Fig. 4.6 shows the results of these experiments. IR alone (Cont IR, mean cell-death 48.5 $\pm$ 1.9%), and after Dox pre-treatment (Dox IR, 48.1 $\pm$ 1.8%) both resulted in comparable cell-deaths, significantly higher than basal cell-death (Cont, 16.3 $\pm$ 1.6%) (Fig. 4.6). In the positive

control experiment, insulin protected untreated cardiomyocytes from IR-injury (Ins, 20.6 ± 0.9%), with no significant differences observed compared to Cont. Dox alone was not toxic to cardiomyocytes (Dox N, 12.9 ± 1.7%) (ANOVA $p<0.05$, $n=3$).

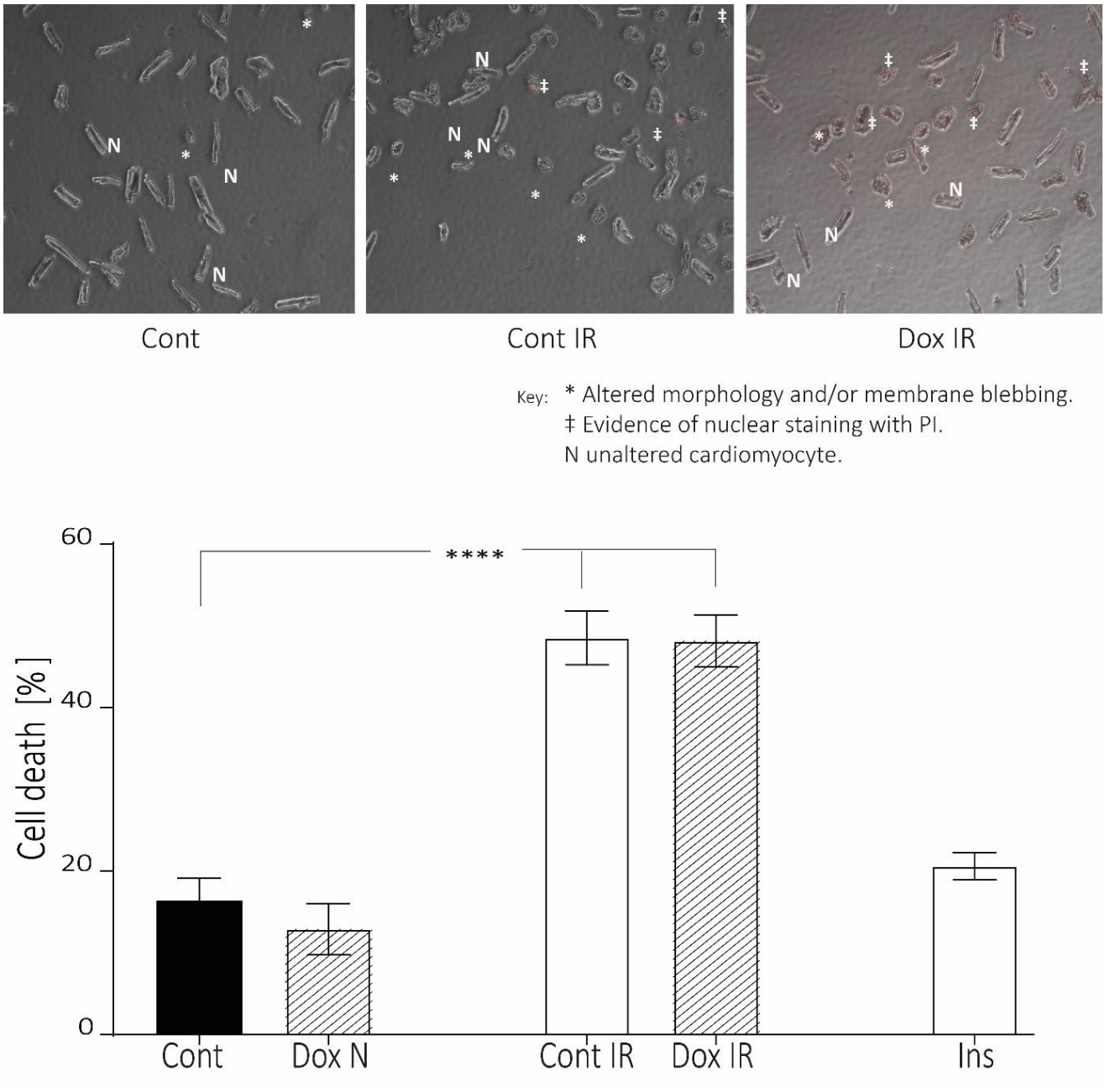

Fig. 4.6. Effect of IR after 18h pre-treatment with doxorubicin. Cell-death after IR showed no difference between untreated cardiomyocytes (Cont IR) and after 2µM doxorubicin pre-treatment (Dox IR). In the positive control experiment, 275u/ml insulin (Ins) protected untreated cells from IR-injury, and no differences were identified compared to basal basal cell-death (Cont) (ANOVA $p<0.05$, $n=3$) (representative photograph of cell-death in top panel, see also Appendix B, Fig. IV).

4.1.6. Final protocol of model of doxorubicin-induced cardiomyocyte toxicity.

Our experiments described above showed that in this *in vitro* ARVM model, Dox inflicted a significant injury only when cardiomyocytes were incubated with a minimum of 7.5 µM concentration, over a period of 18 hours. Additional insults in the form of IR-injury failed to uncover any latent toxicity in cells pre-treated for both 4 hours and over 18 hours with a lower concentration of 2 µM doxorubicin. Based on these data, unless otherwise indicated in the experiments, we used the toxicity of a concentration of 7.5 µM Dox on cardiomyocytes incubated over a period of 18 hours as the standardised model of doxorubicin-cardiotoxicity.

4.2. Characterisation and development of protocol for hypoxic preconditioning.

In subsequent chapters, we explore the potential protective effect of *in vitro* preconditioning against Dox-induced cardiomyocyte death. For these experiments, we characterised and standardised an *in vitro* protocol for hypoxic preconditioning (HP) that could protect cardiomyocytes against IR-injury. We therefore characterised the protocols by evaluating their capacity to protect against IR-injury in the SI4 model we had developed earlier (Fig 4.3). We evaluated two different protocols of *in vitro* HP, as described below.

4.2.1. Choice of hypoxic preconditioning stimulus.

A number of different methods have been described for preconditioning isolated cardiomyocytes *in vitro*. This includes, for example, use of pharmacological agents e.g. Adenosine receptor agonists (Liu et al, 1991), α1-adrenergic receptor agonists (Bannerjee et al, 1993), Bradykinin B2 receptor agonists (Brew et al, 1995) etc. Previous reports from *in vitro* models of IR-injury, e.g. human atrial trabecular models, suggest ischaemic/hypoxic preconditioning confers a stronger protection and greater recovery from reperfusion injury compared to preconditioning by pharmacological agents alone (Cleveland et al, 1997). This may be a consequence of the activation of multiple redundant pathways that HP initiates, compared

to initiation of unitary cascades by activation of receptor-linked signalling. Similarly, work in *in vivo* and *ex vivo* models show ischaemic preconditioning offers greater protection against reperfusion injury compared to known preconditioning stimuli such as hypothermia (van den Doel et al, 1998) or LPS (Rowland et al, 1997). Ischaemic/hypoxic preconditioning has therefore been considered one of the most powerful cardioprotective factors (Illiodromitis et al, 2007), and was considered the preferable preconditioning stimulus for our experimental purposes.

A number of different preconditioning protocols have been described, which confer protection by simulating the metabolic conditions and/or the physiological insult of ischaemia/hypoxia. These protocols differ in the species of cardiomyocytes used, mode of delivering hypoxia, hypoxic protocol-length etc (Wu, 1999; Marber 2000; Diaz and Wilson, 2006). For example Armstrong and Ganote (1994) compacted freshly isolated adult rabbit cardiomyocytes by centrifugation and subjected these to substrate deprivation and hypoxia by discarding excess supernatant and introducing an oil-layer as barrier to gaseous exchange. Similarly, Rakhit et al (2001) subjected neonatal rat ventricular myocytes to 90 minutes hypoxia (95% argon-5% CO_2 atmosphere with <1% O_2) in a buffer with high lactate, low pH and high potassium (K^+) to precondition these cells before replacing this "hypoxic buffer" with normal cell-culture medium. In our own lab, Hausenloy et al (2010) bathed isolated murine cardiomyocytes in a low pH buffer (pH 6.2) with high lactate and high K^+, and subjected these cells to 10 minutes hypoxia in an airtight chamber before replacing the buffer with normal cell-culture medium. These differences in protocols and modalities highlighted the need to construct a HP-protocol specific to the cell-model that we were using, i.e. isolated adult rat ventricular cardiomyocyte model. We therefore chose a model for HP where cardiomyocytes were incubated in a hypoxic environment, using a buffer with low pO_2 (<10.0 kPa), no glucose, high lactate, high K^+ and low pH to simulate the hypoxic environment as a preconditioning stimulus. This was followed by incubation in a normoxic buffer with normal glucose and normal pH to simulate reperfusion.

This model of hypoxic preconditioning has been used in this lab as an HP-stimulus against IR-injury (Hausenloy et al, 2010).

4.2.2. Protocols 1 and 2 for hypoxic preconditioning.

The two protocols for HP that we evaluated differed in the time-period that cardiomyocytes were subjected to hypoxia during the preconditioning phase (Fig. 4.7). To simulate hypoxia, the cardiomyocytes subjected to preconditioning (samples designated HP Protocol 1 and HP Protocol 2, Fig. 4.7) were incubated in hypoxic buffer, placed in an airtight hypoxic chamber, and normal residual-atmosphere was expelled by flushing the chamber with N_2-CO_2 gas.

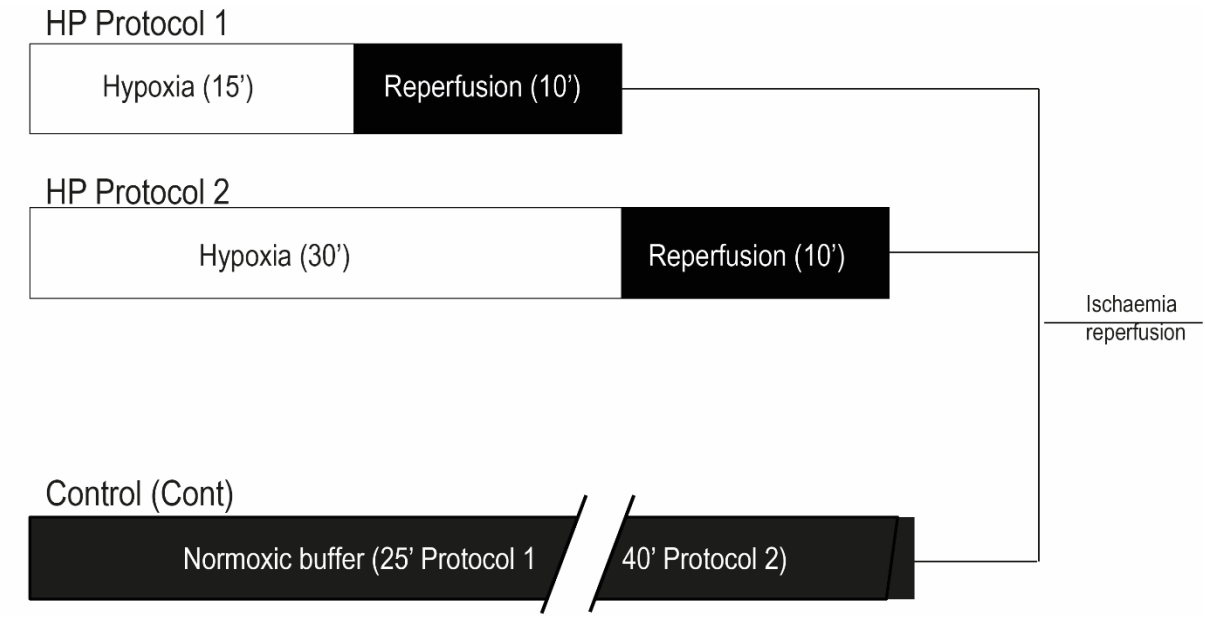

Fig. 4.7. Experimental layout for Protocol 1 and Protocol 2 for hypoxic preconditioning. Cardiomyocytes were subjected to hypoxia for 15 minutes in hypoxic buffer in a sealed hypoxic environment in Protocol 1 (Protocol 1), followed by transfer to a normoxic buffer in normal atmosphere for 10 minutes. Cardiomyocytes in Protocol 2 (Protocol 2) were subjected to hypoxia incubated in hypoxic buffer for 30 minutes, followed by transfer to normoxic buffer in a normal atmosphere for 10 minutes. Controls were incubated in normoxic buffer for 25 minutes (Protocol 1) or 40 minutes (Protocol 2). Cells were transferred to medium 199 after both protocols, and left undisturbed for 18 hours before further experiments.

In the first protocol we tested (Protocol 1), the cardiomyocytes were incubated in this simulated hypoxic environment for a total of 15 minutes, then transferred to normoxic buffer

and incubated in normoxic atmosphere at 37 °C for 10 minutes to simulate the reperfusion phase. In the second protocol (Protocol 2), the cardiomyocytes were subjected to simulated hypoxia for 30 minutes, before transferring to normoxic buffer in normal atmosphere at 37 °C for 10 minutes as for Protocol 1. For each protocol, controls (designated Cont) were incubated in normoxic buffer, in normoxic atmosphere, for the respective matched time, i.e., 25 minutes for Protocol 1 and 40 minutes for Protocol 2. Preconditioned cells and controls were transferred to medium 199 and incubated for 18 hours (Fig. 4.7).

4.2.3. Evaluation of hypoxic preconditioning protocols in protecting cardiomyocytes against ischaemia-reperfusion-injury.

As shown in Fig.4.8, 18 hours after preconditioning, cardiomyocytes death due to IR was evaluated using the SI4 model previously developed. Preconditioned cells were subjected to

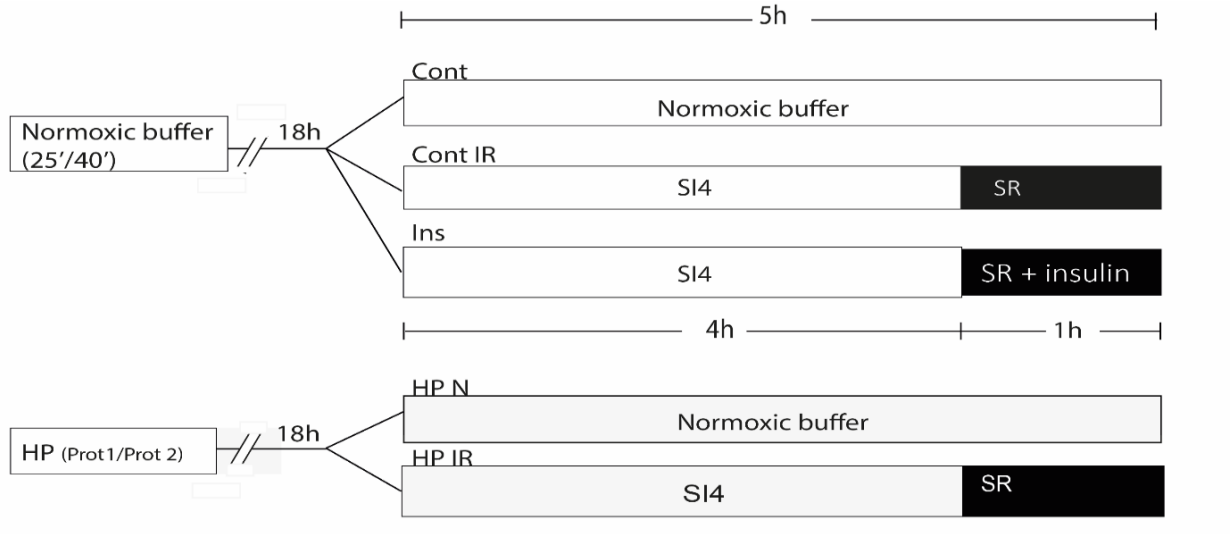

Fig. 4.8. Schematic diagram depicting evaluation of the protective potential of hypoxic preconditioning protocols 1 and 2. Cells were preconditioned (HP) using Protocol 1 or Protocol 2. Control cardiomyocytes (Cont) were treated with normoxic buffer in a normoxic environment for matched times. 18 hours after preconditioning, both HP and Cont were subjected to 4 hours hypoxia (SI) followed by 1 hour reperfusion (SR). As positive control, insulin was introduced at reoxygenation (Ins) in a subgroup of control non-preconditioned cells (Abbreviations: HP=Hypoxic-preconditioned, Cont=Control, Prot 1= Protocol 1, Prot 2= Protocol 2, SI=Simulated ischaemia, SR=Simulated reperfusion).

IR-injury (HP-IR) or incubated for 5 hours in normoxic buffer in normal atmosphere (HP-N). Non-preconditioned controls were subjected similarly to IR-injury (Cont-IR), or incubated in

normoxic buffer in normal atmosphere for 5 hours (Cont). As a positive control against reperfusion injury, a further subgroup from non-preconditioned control (Ins) was subjected to 4 hours hypoxia, but reoxygenation was carried out in normoxic buffer with dissolved insulin (Fig. 4.8).

4.2.3.1. Protocol 1 does not protect cardiomyocytes from ischaemia-reperfusion injury.

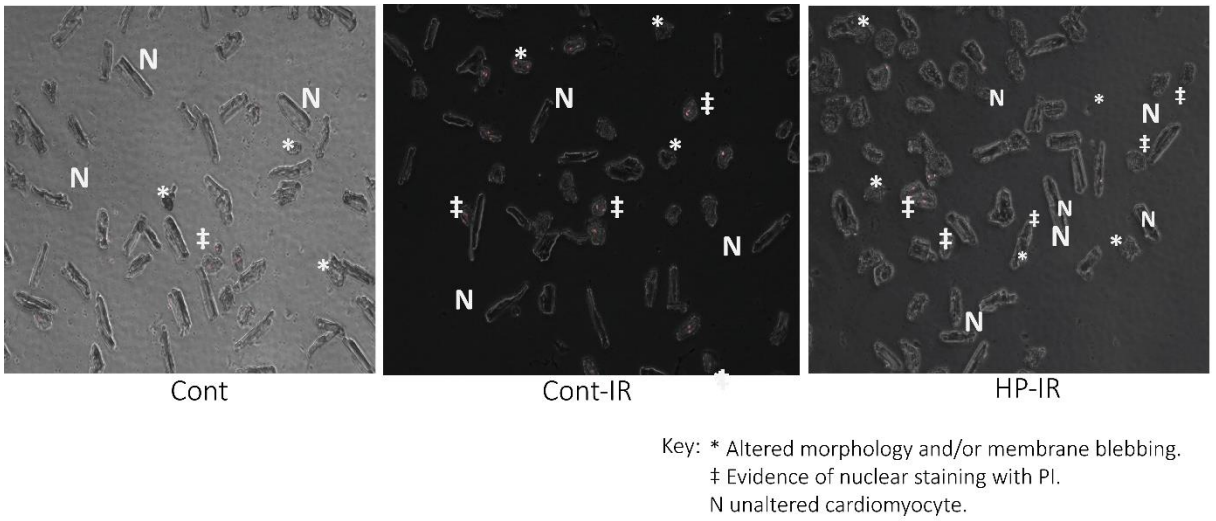

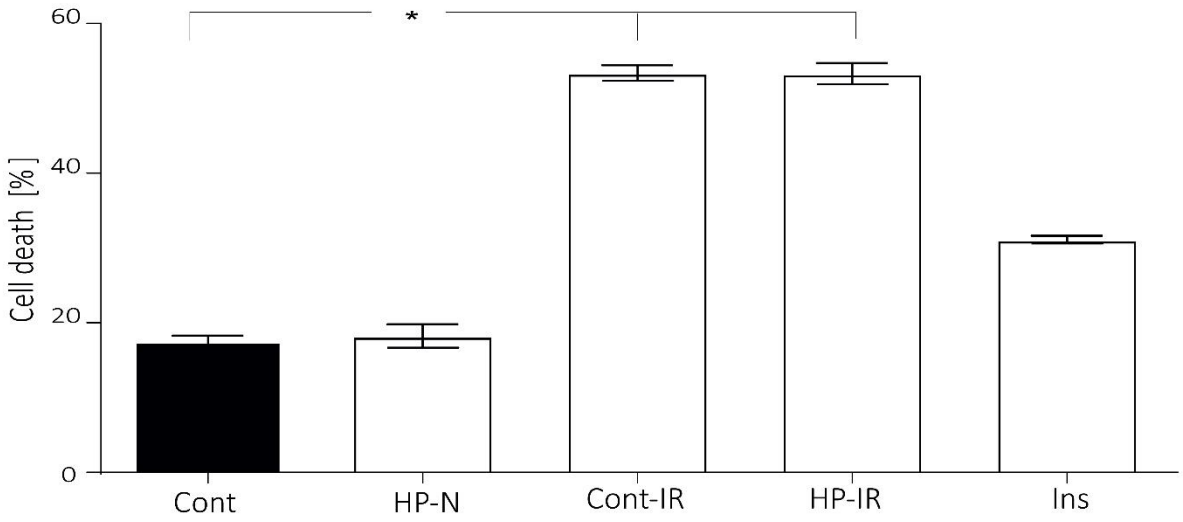

Fig. 4.9. Protocol 1 fails to protect cardiomyocytes from ischaemia-reperfusion injury. Cell-death after ischaemia-reperfusion (IR) was similar in cells subjected to both Protocol 1 (HP-IR) and control protocol (Cont-IR), and significantly higher that basal cell-death (Cont). By contrast, the positive control insulin (Ins) protected non-preconditioned cardiomyocytes from IR (Multiple t-Test $p<0.05$ Cont vs Cont-IR and Cont vs HP-IR, $n=2$) (representative photograph of cell-death in top panel, see also Appendix B, Fig.V).

Fig.4.9 shows the results of these experiments. Subjecting cardiomyocytes to IR-injury after protocol 1 showed a significantly higher cell-death in both preconditioned cells (HP-IR, mean

cell-death 53.3 ± 1%) and non-preconditioned controls (Cont-IR, 53.3 ± 1.4%) compared to normoxic control (Cont, 17.2 ± 1%) (Fig. 4.9). No significant differences existed between the Cont-IR and HP-IR groups. By comparison, presence of insulin protected non-preconditioned control cardiomyocytes from IR-injury (Ins, mean cell-death 31.1 ± 0.5%.). Preconditioned cardiomyocytes incubated in normal atmosphere did not show any significant differences compared to control (HP-N, mean cell-death 18.2 ± 1.5%). The cell-death observed for both Cont-IR and HP-IR differed significantly from basal cell-death and insulin control upon multiple t-tests ($p<0.05$, $n=2$).

The results described are observation of two repeat experiments ($n=2$). Although this is a small sample size, the data showed very close consistency between the experiments and, moreover, we observed a very high consistency in cell-death observed with the positive control insulin, allowing us a measure of confidence to conclude that Protocol 1 did not hold an appropriate protective potential, at least in a window 18 hour after preconditioning. We therefore proceeded to evaluate protection offered by Protocol 2.

4.2.3.2. Protocol 2 protects cardiomyocytes from ischaemia-reperfusion injury.

When Protocol 2 was used as a preconditioning stimulus (Fig. 4.10), IR-insult after 18 hours resulted in a significant rise in cell-death in control cardiomyocytes only (Cont-IR, mean cell-death 41.2 ±6%) but not preconditioned cells (HP-IR, 20.2 ± 5%, $p<0.05$ Cont-IR vs HP-IR). HP-IR showed no significant differences compared to basal cell-death (Cont, mean cell-death 18.1 ± 3.1%), or to cell-death observed in non-preconditioned cells subjected to the positive control agent insulin during reoxyegnation (Ins, mean cell-death 31.1 ± 0.5%, $p<0.05$ Cont-IR vs Ins). HP alone did not inflict any significant injury (HP-N, mean cell-death 10.5 ± 1.7%). The results are the mean of three repeat experiment ($n=3$) (ANOVA $p<0.05$, $n=3$) (Fig. 4.10). This

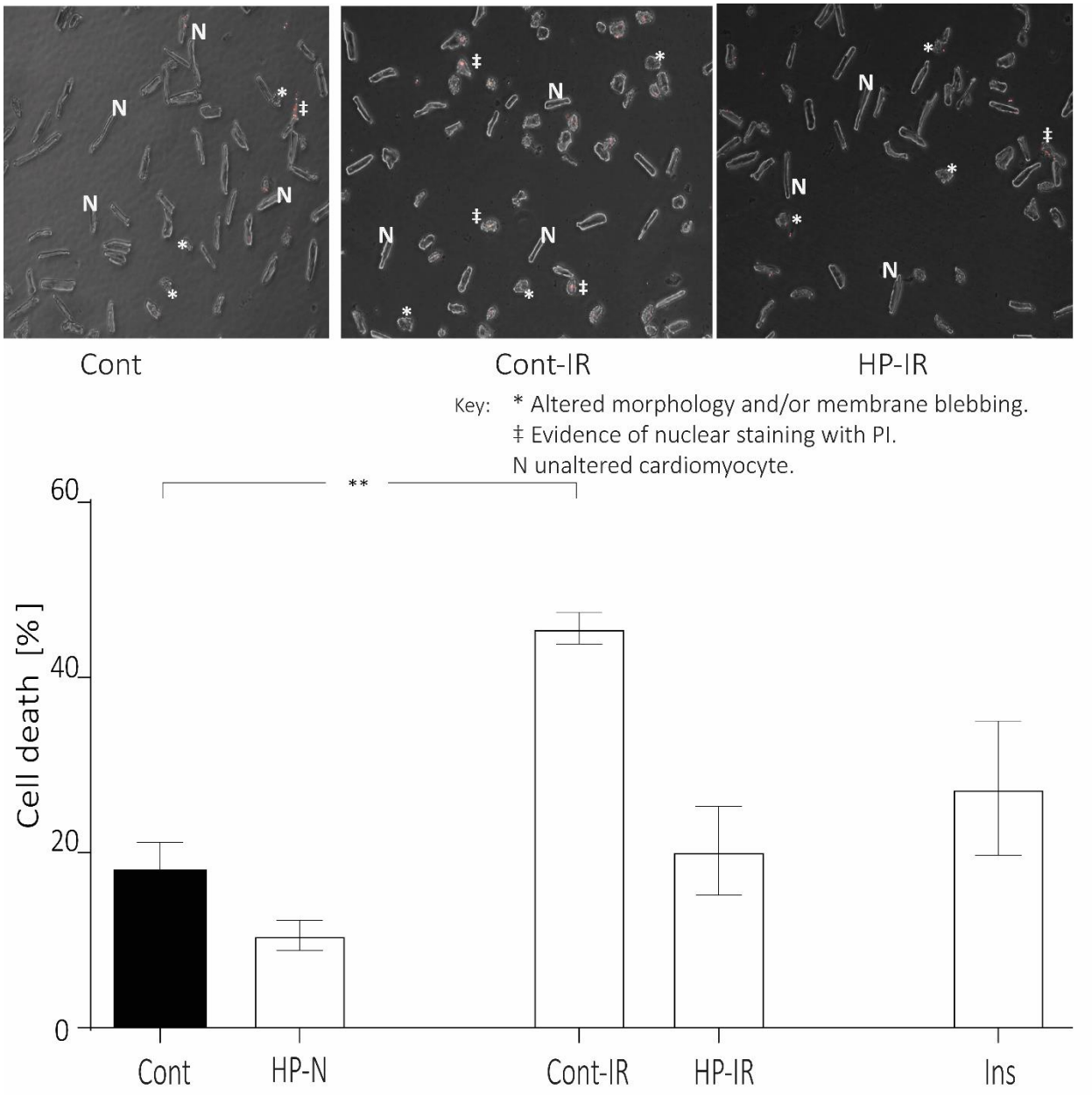

Fig. 4.10. Protocol 2 protects cardiomyocytes from ischaemia-reperfusion injury 18 h after preconditioning. Ischaemia-reperfusion (IR)-injury 18 hours after preconditioning (HP) induced a significant injury in non-preconditioned cardiomyocytes (Cont-IR), but not in cardiomyocytes subjected to Protocol 2 (HP-IR). No differences were identified between basal cell-death (Cont), HP-IR and the levels of cell-death observed in non-preconditioned cells when the protective agent insulin was introduced at reoxygenation (Ins) (ANOVA $p<0.05$, $n=3$) (representative photograph of cell-death in top panel. See also Appendix B, Fig. VI).

experiment confirmed that Protocol 2 was an appropriate stimulus for hypoxic preconditioning that could confer protection against IR-injury in a window 18 hour after HP.

4.2.3.3. Protocol 2 also confers protection against ischaemia-reperfusion within a shorter window after preconditioning.

Ischaemic preconditioning confers a biphasic protection against IR-injury with an initial protective effect that is initiated immediately, and lasts between 8 hours to 12 hours. This is followed by a second peak in protective effect that is noted 18 to 24 hours, and may last for up to 48 to 72 hours (Kis et al, 2003). The above experiments were carried out during the window typically associated with this latter second window. In the next experiment, therefore, we wanted to confirm whether Protocol 2 could protect against IR-injury within the first window. Therefore, 4 hours after preconditioning with Protocol 2, cell-death following IR-injury was evaluated using the SI4 model. Preconditioned cells were subjected to IR (HP-IR), or incubated in normoxic buffer in normal atmosphere (HP-N) for 5 hours. Non-preconditioned controls

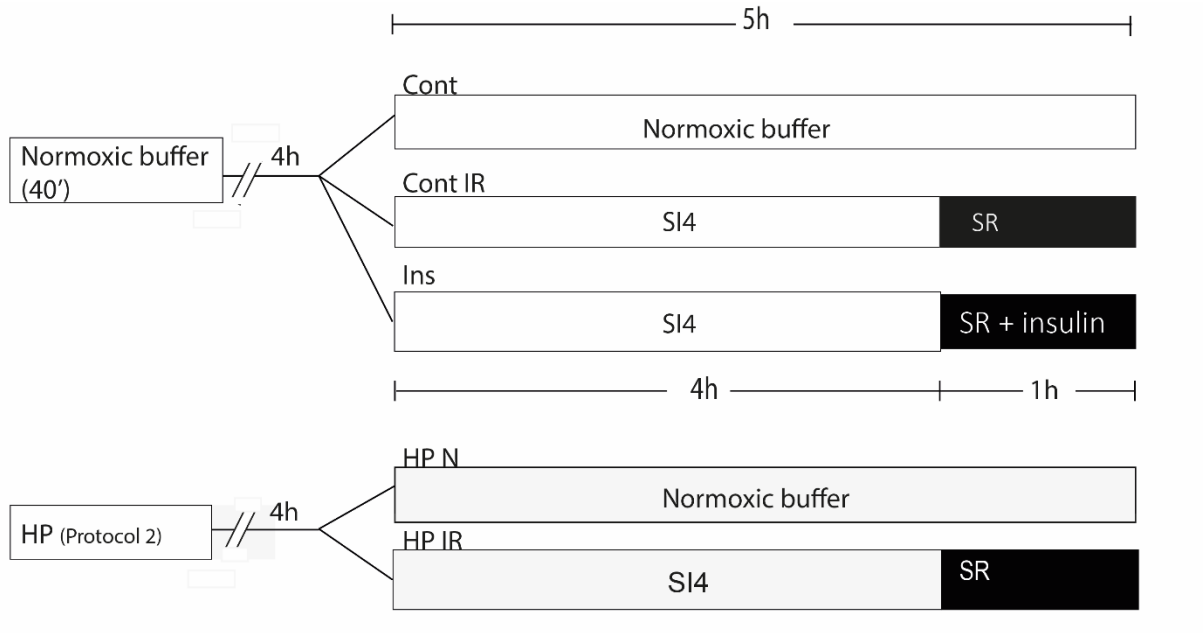

Fig.4.11. Schematic diagram of experimental setup for validation of Protocol 2 in the "classical" window of preconditioning. Cardiomyocytes preconditioned with Protocol 2 were subjected to IR-injury 4 hours after hypoxic preconditioning (HP) to confirm that classical HP-mediated protection is preserved.

were subjected to IR (Cont-IR), or incubated in normoxic buffer in normal atmosphere for 5 hours (Cont) to evaluate basal cell-death. We used insulin as positive control in these experiment as described in the preceding experiment. Therefore, a subgroup from control (Ins)

was subjected to 4 hours hypoxia of the SI4 protocol, but reoxygenation was carried out in normoxic buffer containing dissolved insulin (Fig. 4.11).

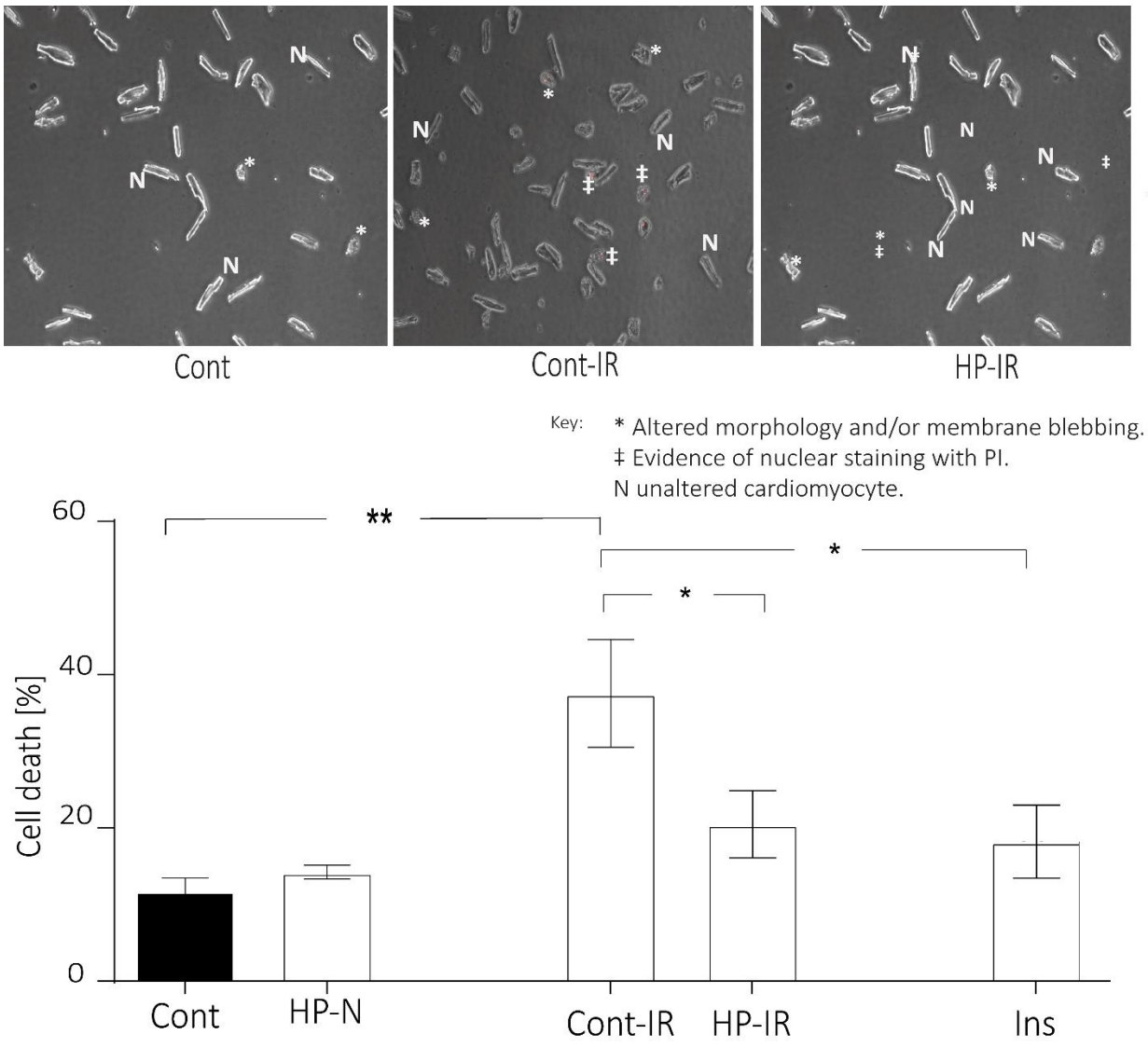

Fig. 4.12. Protocol 2 protects cardiomyocytes against ischaemia-reperfusion injury in the acute window. 4 hours after preconditioning (HP), ischaemia-reperfusion (IR) inflicted a significant injury in non-preconditioned control cells (Cont-IR) only. Cells subjected to Protocol 2 were protected from ischaemia-reperfusion injury (HP-IR), with no differences identified between basal cell-death (Cont), HP-IR and non-preconditioned controls protected by insulin (Ins) (ANOVA $p<0.05$, $n=4$) (representative photograph of cell-death in top panel. Also see Appendix B Fig.VI).

Fig. 4.12 shows the results of these experiments. Only non-preconditioned control group displayed evidence of significant rise in cell-death with IR (Cont-IR, mean cell-death 37.5 $\pm$ 7%). Preconditioned cardiomyocytes were however protected (HP-IR, mean cell-death 20.5 $\pm$ 4.4%), and showed no evidence of significant injury ($p<0.05$ Cont-IR vs HP-IR, $n=4$) (Fig. 4.12). No

significant differences were identified between HP-IR and basal cardiomyocyte death (Cont, mean cell-death 11.4 ± 2%, *n*=4). Insulin protected non-preconditioned controls from IR-injury, and no differences were identified between HP-IR, Cont and Ins (Ins, *n*=3, mean cell-death 18.2 ± 4.8%, p<0.05 Cont-IR vs Ins) (ANOVA p<0.05) (Fig. 4.12).

4.2.4. Final protocol for Hypoxic preconditioning.

Based on the above experiments we adopted Protocol 2 as the stimulus for HP. Therefore, where cardiomyocytes were preconditioned in subsequent experiments, we subjected the cells to 30 minutes hypoxia, followed by 10 minutes reoxygenation.

4.3 Characterisation of Western blot protocol.

In the subsequent chapter (section 5.2) we describe the results of inhibition of PI3K/Akt and MAPK ERK 1/2 on the effect of hypoxic preconditioning on Dox-induced cell-death. We consolidated these data by exploring the phosphorylation state of Akt (p-Akt) and of ERK 1/2 (p-ERK) as described in section 5.2.3. However, achieving optimum Western blotting conditions from the *in vitro* cell culture experiments were difficult, necessitating a characterisation approach before we obtained any clear signal indicating protein content. In our initial Western blots, cell-cultures were established in 32 mm culture dishes. We explored the content of p-Akt in these preliminary experiments. Cells were subjected to HP, and 7.5 µM Dox introduced after reoxygenation. Cells were lysed 5 minutes after completion of reoxygenation and introduction of Dox (15 minutes after completing the hypoxia phase of preconditioning) (Dox HP, Fig.4.13).

As untreated controls, cells were transferred into medium 199 after HP (Cont HP) before lysis. PI3K/Akt was inhibited by preincubating cells for 1 hour in 10 µM LY294002. Cells were then subjected to hypoxia in inhibitor-free hypoxic buffer for 30 minutes, followed by reoxygenation in the presence of 10 µM LY294002 in normoxic buffer.

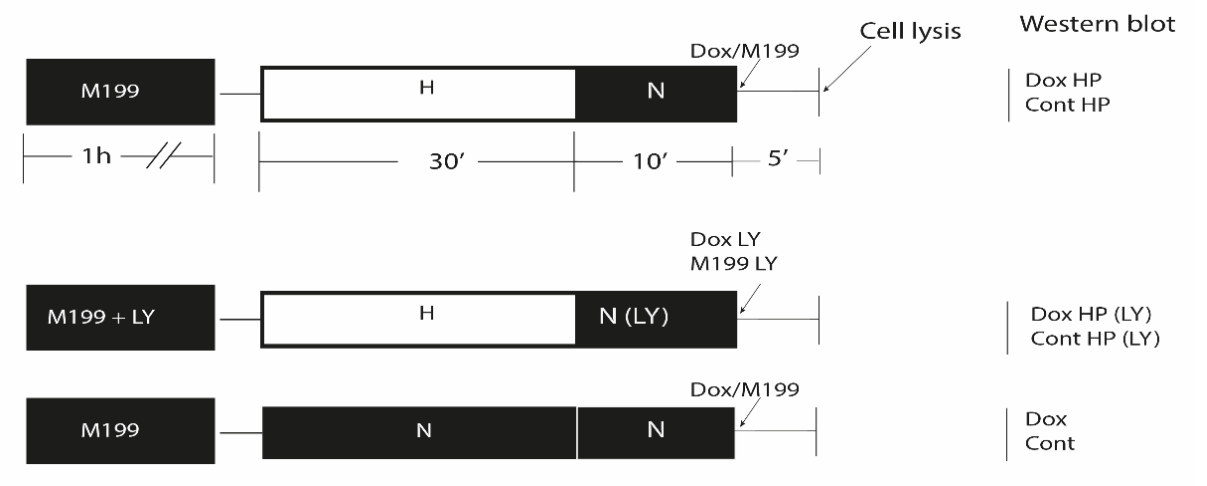

Fig. 4.13. Experimental setup for Western blot analysis sample collection. Cardiomyocytes were incubated in medium 199 alone, or with the kinase inhibitors 10 µM LY294002 to pre-inhibit PI3K/Akt. These were then subjected hypoxic preconditioning by incubating in inhibitor-free hypoxic buffer, before transferring to normoxic buffer with or without LY294002. Cells were subjected to 7.5µM Dox treatment alone or with the LY294002 at the end of reoxygenation phase of preconditioning. Control cardiomyocytes were incubated in medium 199 alone or with LY294002 after HP and lysed 5 minutes after starting Dox treatment.

After reoxygenation, inhibitor was maintained along with Dox (Dox (LY)), or medium 199 (Cont (LY), Fig.4.13). Akt phosphorylation in non-preconditioned cells, in the presence of Dox and under basal conditions, were probed by incubating cardiomyocytes in normoxic buffer alone for 40 minutes, then transferring to 7.5 µM Dox (Dox), or medium 199 (Cont). Protein levels were probed using standard Western blot conditions, and Glyceraldehyde 3-phosphate dehydrogenase (GAPDH) levels probed as loading control.

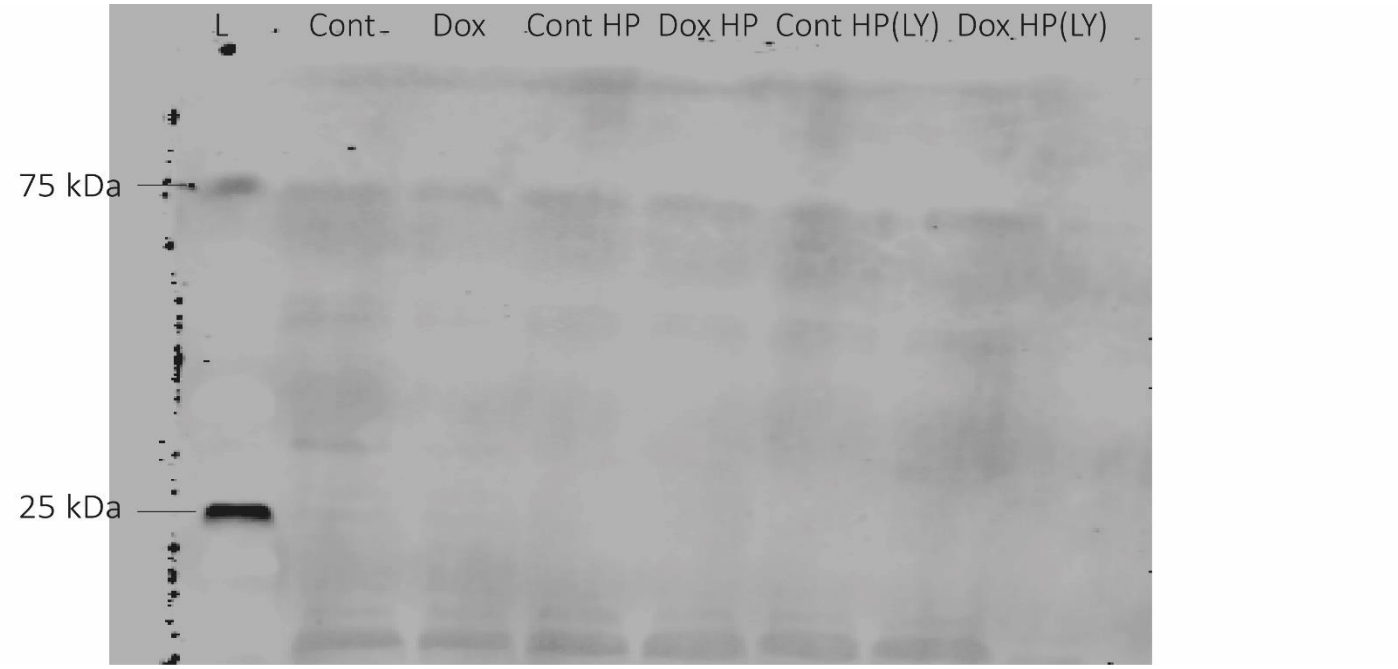

Fig. 4.14. Result of protein-collection from 32mm cell-culture dish. Example western blot is shown exploring induction of p-Akt and GAPDH after sample lysis in 32mm cell-culture dishes 5 minutes following Dox treatment. No individual signal for either the p-Akt, nor the housekeeping gene GAPDH could be identified.

Fig. 4.14 shows an example blot from this experimental set-up. We failed to identify any discernible signals for either p-Akt, or of GAPDH housekeeping protein, in these experiments. Indicating the sample collected during cell lysis contained no significant protein content of either the protein of interest (p-Akt) or of the loading control.

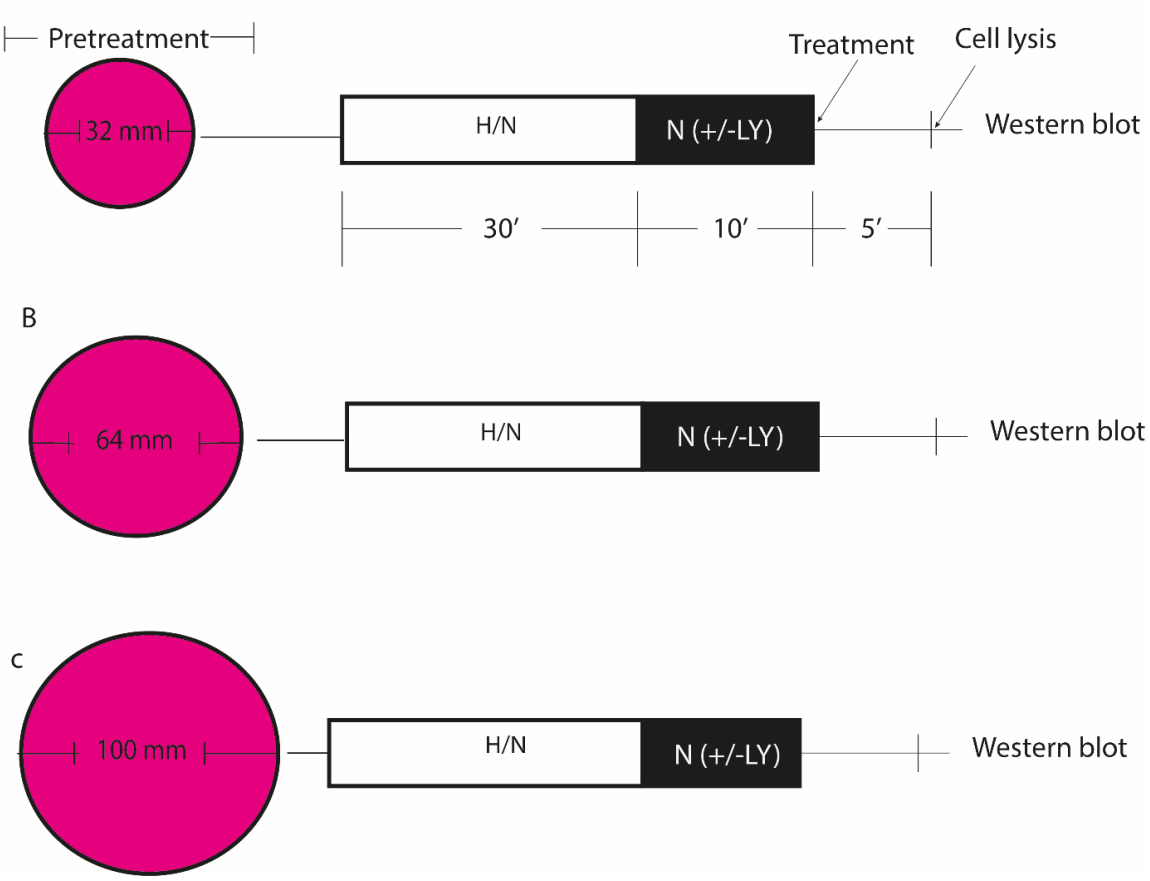

Fig. 4.15. Different cell-culture volumes explored to obtain suitable protein yield during Western blot characterisation. Following yield of very low concentration of proteins from 32-mm dishes (Panel A), experiments were set-up in 64 mm-dish (Panel B) and subsequently 100mm cell-culture dish (Panel C). In each experimental set-up, cells were lysed 15 minutes after end of hypoxia, corresponding to a time point 5 minutes after completion of simulated reperfusion and 5 minutes after the time point Dox is added as an insult.

Since these initial western blot experiments were setup using 32 mm cell-culture dishes (Fig. 4.15 A), we hypothesised that the lack of any significant signals for proteins may be due to low protein-content and yield obtained from the cultures established in a small volume cell-culture dish. We therefore established the ARVM primary cultures for the respective treatments in larger diameter dishes of 64 mm and 100 mm to obtain greater volume, and therefore higher protein content (Fig. 4.15 B and 4.15 C) and re-explored the content p-Akt and GAPDH.

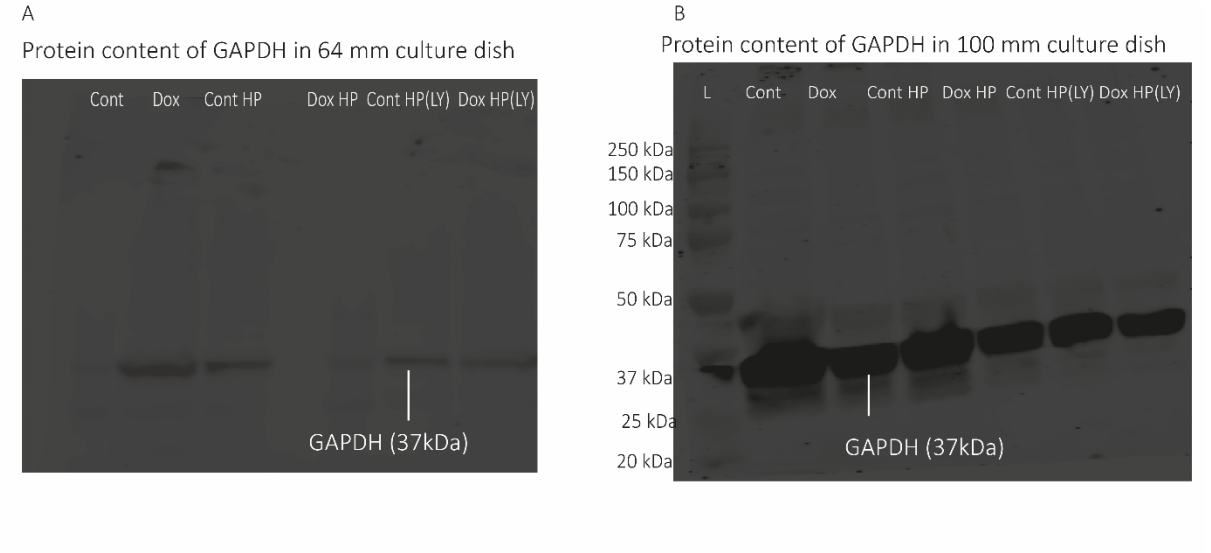

Fig. 4.16. Western blot highlighting differences in protein content between different volumes of cell-culture dishes. A. Western blots exploring the content of p-Akt and GAPDH after collecting lysate from cells incubated in 64 mm cell-culture plates. A faint signal for GAPDH is observed but no clear signal for p-Akt is noted. B. Western blot exploring the content of p-Akt and GAPDH in lysates from cell-culture established in 100 mm cell-culture dishes. A prominent signal for GAPDH was noted. No clear signal for p-Akt could be identified.

Fig. 4.16 shows the result of this Western blot. Lysing cells in 64mm culture dish showed a faint signal for the housekeeping gene GAPDH, but no signal was observed for p-Akt. However, lysing the cells following incubation in 100mm cell culture dishes yielded a robust signal for the housekeeping gene GAPDH. Despite this prominent signal for the loading control, however, we failed to observe any significant signal for the p-Akt protein. These experiments did, however, indicate that the ideal volume for obtaining an appropriate protein yield to detect by Western blot required a 100 mm cell-culture plate.

In subsequent Western blots, therefore, all treatment groups were established in 100 mm culture dishes. However, in light of persisting absence of any signal for p-Akt in response to HP, we hypothesised that the phosphorylation response may occur early after preconditioning, much earlier than the time point at which we were lysing the cell-culture for protein collection. We therefore conducted a time course experiment, where cells were subjected to hypoxic phase of HP, followed by cell-lysis through specific time-intervals of 60 seconds through the

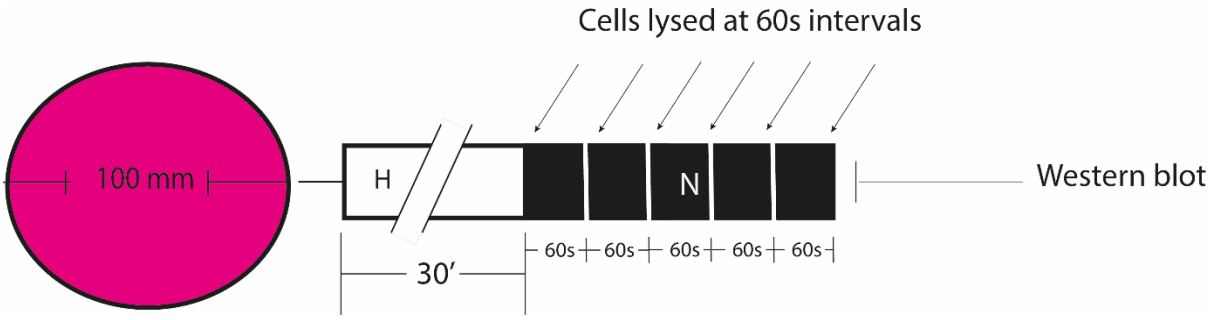

Fig.4.17. Harvestation of protein samples through different time-points to analyse Akt content. Cells were lysed immediately after completing hypoxia, and subsequently at 60 second intervals up to 300 seconds. Protein lysates were probed with Western blot for housekeeping genes GAPDH and t-Akt and p-Akt.

reoxygenation phase, upto 5 minutes. These samples were then probed to assess the p-Akt content at each time-point (Fig. 4.17). The total Akt protein (t-Akt) content was also explored in these samples, and the ratio of total and phosphorylated Akt respectively were normalised to GAPDH content in each sample, i.e., t-Akt:GAPDH and p-Akt:GAPDH ratio evaluated. Phosphorylation response of Akt at each time point was then evaluated as the ratio p-Akt:GAPDH ratio to t-Akt:GAPDH.

Fig. 4.18 shows the result of this experiment. The ratio of phosphorylated protein normalised to GAPDH rose to approximately 1.8 times that of total Akt, peaking at 120 seconds before declining towards baseline at 300 seconds. This experiment showed that the peak in p-Akt content after HP occurred before the conclusion of reoxygenation phase (10 minutes reoxygenation) of our experimental protocol of hypoxic preconditioning, and therefore before Dox had been introduced to preconditioned cells. Therefore as final protocol, in further Western blots where the phosphorylation induction of Akt and MAPK ERK 1/2 in response to HP were explored, cell lysis was carried out at 2 minutes (120 seconds) after completing hypoxic phase, as shown in Fig. 3.13. In subsequent experiments, we used insulin as a positive control,

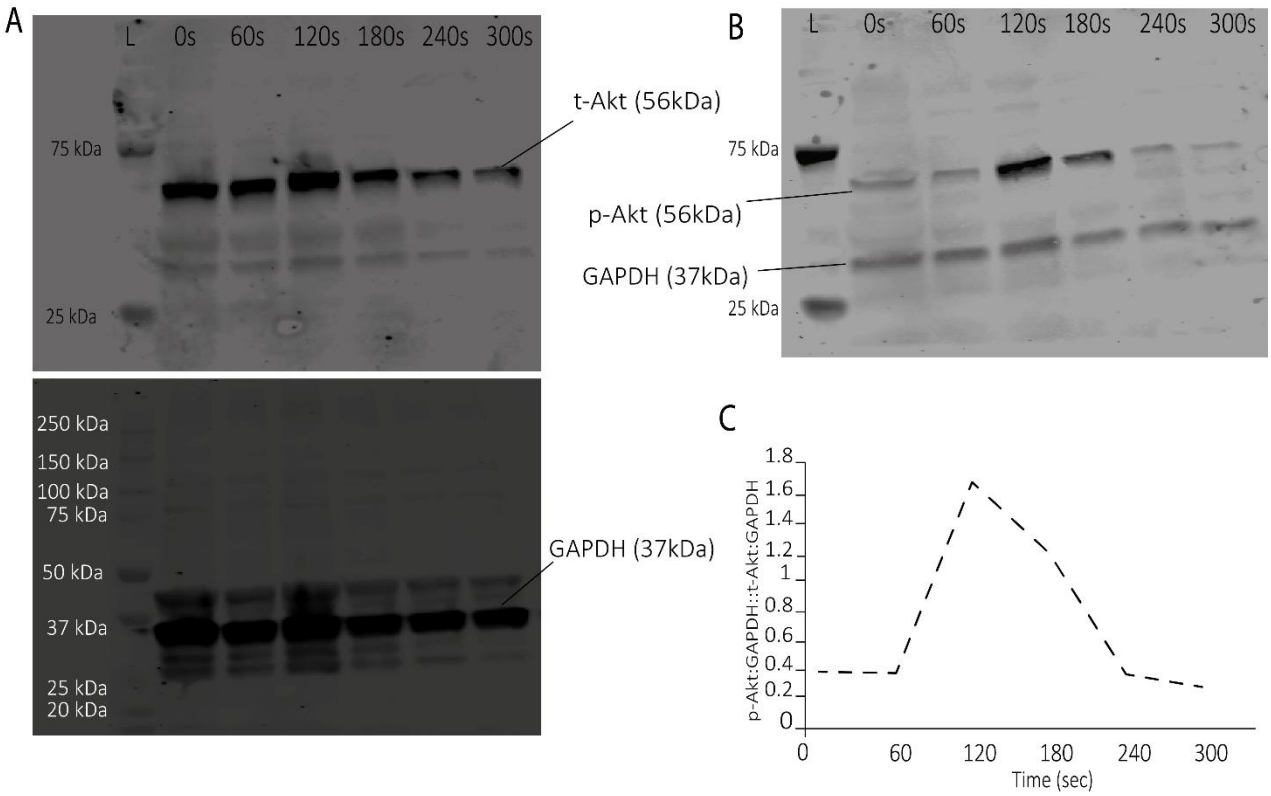

Fig.4.18. Western blot analysis of phosphorylation induction of Akt over time following hypoxia phase of preconditioning. Total Akt protein content (normalised to GAPDH, panel A) and phosphorylated protein content (normalised to GAPDH, panel B) both showed an increase noted to be peak at 120 seconds after end of hypoxia, before declining in the following 180 seconds.

since it is a known inducer of the reperfusion injury salvage kinase (RISK) pathway. Cells were incubated with insulin (275u/ml) for ten minutes before they were lysed and prepared for gel-loading using similar method to other samples, as described in section 3.2.9.2.

4.4. Discussion.

4.4.1. Characterisation of doxorubicin toxicity on cardiomyocytes.

In developing an *in vitro* model of Dox-induced cell-death, we observed a dose-dependent and time-dependent rise in the cytotoxic potential of doxorubicin, which is consistent with the results reported by other groups in various different *in vitro* cardiomyocyte models including adult rat ventricular myocytes (Lim et al, 2004), Neonatal rat ventricular myocytes (e.g., Ichikawa et al, 2014) as well as human induced pluripotential stem cells (Maillet et al, 2016). We observed no significant toxicity in cardiomyocytes subjected to any of the Dox concentrations we tested up to 4 hours (Fig. 4.1). It ought to be mentioned that the sample size from which we drew this conclusion varied from 2 to 4, and therefore statistical power was low for the higher concentrations of Dox. Therefore, in subsequent experiment we re-explored cell-death with similar concentrations of doxorubicin, but after prolonging the exposure time to 18 hours.

In this second group of experiments, we observed statistical significance in cell-death at and above 7.5 µM doxorubicin. The data shown here represent a sample size of seven repeat experiments (n=7), which may be considered an adequately large sample size for an *in vitro* experiment to draw confident conclusions. Moreover, the results are consistent with toxicity observed in other *in vitro* systems which report similar dose-dependent rise in cardiomyocyte-death. For example, Zhang and Zhao (2017) observed a rise in cell-death with increasing Dox concentrations in human induced pluripotential stem cells (iPSCs) after incubating these cells for 48 hours, with IC_{50} of 3.5 µM. In the same experiment, assessment of cardiac troponin as a marker of cell-injury showed some damage at low concentrations up to 1.2 µM but further significant injury above 2.5 µM doxorubicin. Similarly, Yan et al (2015) found a dose-dependent fall in cell viability and an increase in the apoptotic index of TUNEL-staining after incubating of H9C2 cardiomyoblasts with 1-20 µM doxorubicin. Criticisms have been made of *in vitro* and *in*

vivo models of anthracycline toxicity where very high concentrations of anthracyclines, many times higher than peak physiological values, have been used (Stěrba et al, 2011). For example Chatterjee et al (2008) reported significant rise in cell-death in an *in vitro* murine cardiomyocyte model with 26 µM to 36 µM doxorubicin. Similarly, Zhang et al (2012) induced cardiotoxicity in their *in vivo* murine model using a bolus dose of 25 mg/kg in an *in vivo* murine model. Therefore, it is important to highlight that the toxicity we see in this model manifests at a concentration close to and immediately above peak plasma concentrations of doxorubicin, which is typically around 5 µM. We were therefore satisfied that this model allowed close and adequate *in vitro* replication of the postulated toxic effects of anthracyclines on cardiomyocytes.

4.4.2. Ischaemia-reperfusion injury in doxorubicin stressed cells.

Our initial experiments failed to display significant rise in cell-death with concentrations of Dox lower than peak plasma values. This result was consistent after both 4 hours, and after 18 hours incubation. We considered the possibility that a latent injury process may exist with lower concentrations below 5 µM doxorubicin, which was not sufficient to manifest in excess cell-death, and therefore used IR-injury as a "second hit", or an additional insult, to test this hypothesis. We used a concentration of 2 µM doxorubicin. This is a concentration immediately below half the peak-plasma concentration of Dox in humans. Since Dox accumulates in the cardiomyocyte, and since the toxicity is a long-term process, it has been argued that accumulation of Dox or its metabolites, e.g., the alcohol derivative doxorubicinol, may hold a pathological role in mediating the long-term toxicity of anthracyclines (Bertihaume et al, 2007). Moreover, long-term concentration of Dox in the plasma and in the myocardium will, logically, be below the peak plasma concentration. Furthermore, previous reports exploring doxorubicin-toxicity have noted an injurious toxic effect with concentrations as low as 1 µM Dox (Gharanei et al, 2013b; Montaigne et al,2010). In our initial characterisation experiments, we observed no significant toxicity at similar concetrations of Dox alone over incubation periods of 4 hours

and of 18 hours. We therefore chose 2 μM Dox as a concentration below peak plasma concentration, but higher than that reported in literature, e.g., by Montaigne et al and Gharanei et al, in order to probe any latent sub-threshold injury. The pre-treatment period was incorporated to allow for accumulation of the drug or its potential metabolites within the cardiomyocytes, and alterations to metabolic or cell-survival pathways, if any, to be initiated (Olson et al, 1988; Charlier et al, 2005). Further, this protocol mimicked the situation where the myocardium that has been stressed by anthracyclines may subsequently be subjected to an additional insult such as ischaemia and reperfusion that occurs as the result of myocardial infarction, which may reflect the increased risk of anthracycline-induced heart-failure in patients with underlying ischaemic heat disease (Curigliano et al, 2016). However, we failed to observe any significant rise in IR-induced cardiomyocyte death when cells were pre-treated with doxorubicin. This observation was consistent after a pre-treatment period of 4 hours, and after a pre-treatment period of 18 hours. The results for each incubation period are collated data from three repeat experiments (n=3). This sample size is relatively small, and this may be considered a limitation of these experiment. However, in these same experiments, we were consistently able to reproduce robust and significant protection against IR-injury using the positive control insulin, allowing further confidence in the results of these experiments.

The lack of any significant increase in IR-injury on Dox pre-treated cells may be interpreted in two different ways. One possibility is that in this *in vitro* model, Dox does not trigger cell-death pathways in common with IR-injury and, therefore, any subthreshold toxicity due to Dox is not revealed due to the added stress in the form of IR. However, an alternative hypothesis may also be considered. The complex intracellular interactions initiated by Dox pre-treatment may compensate or alter potential pathways of cell-injury due to IR. For example, Dox increases autophagic flux *in vivo* (Zhang et al, 2011a), while autophagy may be beneficial against IR-injury (Yitzhaki et al, 2010). Similarly, doxorubicin-induced degradation of survival factors e.g. BCL-2

noted in *in vitro* models (An et al, 2009) may attenuate the inhibition of pathways deleterious in IR-injury, e.g., those initiated by Beclin 1 (Peng et al, 2013). This highlights that competing pathways may compensate and alter the sensitivity of cardiomyocytes to cell-death when both anthracycline and IR-injury is present.

Our results and experimental set-up ought to be contrasted with the approach taken by other groups who have observed an exacerbation of IR-injury in the presence of Dox. Gharanei et al (2013b) for example, observed an increase in infarct size in the intact myocardium in an isolated and perfused rodent heart model when Dox was introduced during 120 minutes of reperfusion after a preceding of 35 minutes of ischaemia, compared to infarct sizes due to ischaemia and reperfusion alone. For comparison, in our protocol IR-injury was inflicted on isolated cells as an after-treatment, following a preceding period of doxorubicin-pretreatment. Wether this difference in protocol and timing of doxorubicin-insult with relation to reperfusion injury may be a factor in the differences in the results would require further analysis. Interesingly, pre-existing coronary artery disease is recognised as a risk factor for development of heart failure after ANTC-chemotherapy (Pinder et al, 2007; Harbeck et al, 2011). However, Moser et al (2006) analysed the risk of cardiovascular disease in a Danish and Belgian population based registry of 476 patients with aggressive Non-Hodgkins Lymphoma who received ANTC-based chemotherapy with or without radiotherapy between 1980 and 2000. They concluded the risk of coronary artery disease after ANTC-treatment in this group of patients was similar to the population risk of coronary artery disease over a followup period up to 20 years. The risk associated predominantly to ANTC-chemotherapy was, however, of chronic heart failure. It may therefore be hypothesised that the ischaemia-stressed myocardium is more vulnerable to Dox-injury, although Dox (and indeed anthracyclines) may not increase the risk of ischaemic heart disease. Clarification of this hypothesis with further work, and alteration of treatment protocols may be explored in future works to explore similar hypotheses.

4.4.3. Limitations of *in vitro* model of doxorubicin toxicity used.

Our model maybe criticised in light of the fact that we have used cell-death alone to assess injury. Further, the assessment of cell-death was made on the basis of nuclear staining with propidium iodide (PI), along with morphological changes previously described as associated with apoptosis in cardiomyocytes (Gotto et al, 2008). it ought to be noted that the permeabilization of the plasma membrane and the nucleolemma that is demonstrated by propidium iodide intercalation with nucleic acid and staining of the nuclei is a feature of necrosis or a very late feature of apoptosis (Cummings et al, 2004; Riccardi and Nicoletti, 2006), while structural and morphological changes are also late features of necrotic cell-death associated with ATP depletion and disruption of cytoskeleton (Cummings et al, 2004). Since PI intercalates with helical double-stranded (ds) nucleic acid, staining of dsRNA in the cytoplasmic compartment may, moreover, yield false-positive results. By the estimates of some authors this false positive may be as high as 40% false events reported in published ltierature (Rieger et al, 2010). However, this artefactual result as a consequence of dsRNA staining is particularly a problem in proliferating cells and cells with a large nucleus-to-cytoplasmic ratio (characterised as nucleus:cytoplasm ratio <0.5) and was a factor, in association with available technology ad expertise, in guiding us to adult rat ventricular myocytes in preference over neonatal rat ventricular myocytes in establishing our model.

In establishing the model of toxicity, the contributions of apoptosis and of necrosis due to Dox were not delineated in detail in the model. As explained earlier in introduction (section 1.2.4), ANTC may induce necrotic as well as apoptotic cell-death. Apoptosis is typically described as caspase-dependent, or caspase-independent. Caspase-independent programmed cell-death may, further, be cathepsin-dependent, or cathepsin-independent but calpain-dependent (Nicoletopolou et al, 2013). Necrosis is typically deemed to be ATP-independent. Concomitant probing for Annexin V and PI may shed some light into the time course of apoptosis in the

model we developed and describe above. Early apoptotic cells are typically observed to be positive for Annexin V but not PI, while late apoptotic cells as well as primary necrotic cells are dually positive for both PI and Annexin V (Brauchle et al, 2014). Other approaches to characterising apoptosis (early or late) and necrosis may also have been adopted. For example, concomitant and time-course analysis of other markers of apoptosis, e.g., analysis of nuclear membrane integrity with 4′,6′-diamidino-2-phenylindole (DAPI) (Cummings et al, 2004), apoptosis measurement with Caspase-3 assay, or TUNEL staining (indicating Karyorrhexis), or investigation of karrhyyorrhexis with, e.g., bromodeoxuridine assays (Darzynkiewicz and Zhao, 2011) may have allowed us to shed more light on the course, mechanism and contribution of apoptosis in this model. Similarly, correlation of PI staining with a second-dye, e.g., Evans-blue, or estimation of levels, e.g., Lactate dehydrogenase (LDH) release or estimation of high-mobillity group box 1 protein (HMGB1) levels may have allowed further clarity and more sensitive quantification particularly of cumulative primary necrotic cell-death (Marshal et al, 2014). This would have allowed consolidation of the observations recorded on cell-death, and shed some light on the predominant mode of cell-death and the relative induction of these pathways in the model described above. This is a limitation of our experiments, and ought to be addressed in future course of work.

The lack of clarification of the mode(s), or co-existence of modes of any of the cell-death pathways in the model we describe above limits any further deductions or insights into the possible mechanisms of ANTC-toxicity in the model. Further of note, changes observed with low concentrations of Dox may occur without induction of cell-death mechanism, and include degradation of structural and functional proteins and alterations in metabolic pathways including cellular respiration which may occur independent of induction of cell-death pathways observed with higher concentrations. It is possible to, e.g., identify titin degradation products (T2) after incubating with Dox in this model for the above experiments.

However, the overall hypothesis of the work presented in this report was to explore the protective potential of preconditioning against doxorubicin-induced injury, and cell-death offered a sensitive marker for both the injury process and HP-mediated protection. We therefore considered detailed exploration of the metabolic effect of Dox to be beyond the scope of our work at this stage. It ought to be noted however that Dox possesses intrinsic auto-fluorescence characteristics, which is quenched by binding to DNA. When excited by incident light in visible range, a concentration dependent increase is noted in the intensity of emitted fluorescence peaking between 540 and 680nM (Gnapareddy et al, 2015), which may interfere with absorbance-based assays which utilise absorbances around this wavelength.

4.4.4. *In* vitro hypoxic preconditioning protocol.

HP is well characterised as a protective modality against IR-injury (Hausenloy et al, 2005). However, the experiments we describe explored the protective potential of HP against a different trigger of injury, i.e., drug-induced injury. Further, characterisation of the Dox-toxicity model indicated that the time-scale a protective stimulus was required to last was in the order of 18 hours, which is typically associated with what is termed the second window of preconditioning (SWOP) (Yellon and Baxter, 1995). Therefore, we first evaluated and characterised a specific protocol for HP that could protect cardiomyocytes against IR-injury in this second window, before evaluating the potential for this stimulus to protect against Dox-toxicity.

We evaluated two different hypoxic preconditioning protocols for their potential to protect cardiomyocytes against IR-injury. In these experiments, we used insulin as a positive control to protect against reperfusion injury, which is well described in our own lab (Davidson et al, 2006) as well as by other groups (Aikawa et al, 2000). This therefore allowed us to standardise the HP-protocol to a known cardioprotective agent. The first protocol we tested, namely 15 minutes hypoxia followed by 10 minutes reoxygenation, failed to show any protection against IR-injury

inflicted 18 hours after preconditioning. This observation in two repeat experiments (*n*=2) led us to alter the protocol and extend the hypoxia time. Although *n*=2 is a small sample size, the data showed very close consistency between the experiments and, moreover, we observed a highly consistent protection from cell-death with the positive control, allowing us a measure of confidence to conclude that Protocol 1 did not hold an appropriate protective potential. For comparison Protocol 2, which had an extended hypoxia time of 30 minutes, showed a consistent and reproducible protection from IR-injury 18 hours after preconditioning, and matched the positive control insulin in protecting from IR-induced cardiomyocyte death. This data was obtained from a sample size of three (*n*=3), and allowed us to conclude with confidence that protocol 2 conffered a suitable protective stimulus in the second window of preconditioning. In the next experiment, we confirmed that Protocol 2 could protect against IR-injury within the shorter or first window time-period, associated with the conventional observations of immediate protective effect of HP. We repeated this experiment for four different isolations (*n*=4), which allowed us to conclude confidently that the stimulus offered "classical" first window preconditioning stimulus.

Our experiments show that there exists a threshold injury, below which the hypoxia stimulus does not offer any protective potential at 18 hours. This is likely to be a manifestation of what is called the threshold phenomenon (Faircloth et al, 2004; Diaz and Wilson, 2006). For example, Hale and Kloner (1999) had previously observed that preconditioning with two cycles of 7 minutes ischaemic preconditioning reduced infarct size due to prolonged coronary artery occlusion in an *in vivo* rabbit model, whereas one cycle of 5 minute ischaemic preconditioning did not. A corollary conclusion that may be drawn is that activation of pro-survival signalling is absent or insufficient below a threshold level, and is therefore incapable of protecting cardiomyocytes from IR-injury. A similar conclusion maybe drawn from previous observations in animal models of ischaemic preconditioning which have investigated the early window of

preconditioning. For example, Tsuchida et al had previously observed that a short ischaemic preconditioning stimulus of 2 minutes, along with concomitant activation of Adenosine A1 receptors with acadesine, limited infarct size in rabbit hearts *in vivo* in an infarct delivered immediately after preconditioning. Neither acadesine alone, nor 2 minutes ischaemic preconditioning alone could limit infarct size in this report (Tsuchida et al, 1993). Similarly, Sandhu et al (1997) reported a lower protective potential with one cycle IPC, compared to three cycles before an IR-injury was inflicted in a rabbit model (Sandhu et al, 1997). Bell and Yellon had shown that in a murine model, four cycles IPC protected eNOS knockout ($eNOS^{KO}$) mice to similar extent to wild type, but this protection was abrogated in $eNOS^{KO}$ mice when less than four cycles of IPC was used (Bell and Yellon, 2001). We did not examine whether prolonging the hypoxia time in the preconditioning phase offered similar protection or was deleterious, since this was beyond the scope of the experiments described. However, this may be investigated in future work for further characterisation of the second window of preconditioning (SWOP).

4.4.5. Western blot.

Our experiments characterising a Western blot protocol to explore the levels of proteins of interest demonstrate, understandably, that the volume of protein in the lysate is dependent on the volume used to establish the initial cell-culture. Of note, initial cell-seeding concentrations and volume were established using an estimated confluency from the concentration of cells observed in the final suspension of cardiomyocytes during the isolation procedure, and not calculated or quantified. This may be considered a limitation of the work described in these experiments. Since ARVMs are a monoculture, a level of confidence could be adopted regarding the expression levels of housekeeping genes. Normalisation of protein levels to housekeeping gene-product is an established method of estimating protein content in Western blot protocols (Lo et al, 2015), although varied differences, e.g., differences in conditions of lysis, sample preparation, loading, antibody-affinity, as well as variations in

conditions of blotting and analysis can all affect the final result. It is therefore necessary to optimise the conditions under which sample collection and Western blotting is carried out, and the observations from our experiments reinforces this. The initial Western blot using a small volume cell-culture dish (32 mm) showed diffuse non-specific signals when probed for protein content. However, by progressively increasing cell-culture volumes using larger culture plates (64 mm and 100 mm), we were able to obtain more robust signals for the housekeeping proteins GAPDH. GAPDH was used in blots exploring Akt phosphorylation since the molecular weight of GAPDH (37 kDa) is distinct from that of Akt (56 kDa) and in well resolved SDS-PAGE blot would be expected to appear as a distinct signal with greater migration distance than Akt. GAPDH is known to be expressed abundantly in adult rat ventricular myocytes, perform housekeeping roles (Diez and Simm, 1998), and has been probed in reports from our lab previously (Hausenloy et al, 2005, Davidson et al, 2006). It ought to be highlighted that we did not attempt to quantify the protein content from the different cell-culture dish volumes against a known standard, which may be considered a limitation of our experiment. However, cell-seeding density may vary between experiments, and further the final volume of cell lysate obtained after introduction of boiling SDS-PAGE buffer may differ by factors of microliters, even with strict optimisation. We therefore correlated both total and phospho-protein content of Akt to the loading control GAPDH as a common reference value. In light of robust signal for GAPDH, we were satisfied that the initial characterisation experiments optimised the volume as well as sample preparation conditions to probe the expression of the proteins of interest. Future work may address the question of protein content, but this would require further characterisation beyong the scope of the work described in the current report.

Chapter 5. Results.

5.1. Investigation of the mechanism of doxorubicin-induced cardiomyocyte toxicity.

5.1.1. Cardiomyocyte-death increases with H_2O_2 concentrations and increase in incubation-time.

Having established a reproducible model of Dox-toxicity, we first probed the potential role of reactive oxygen species in Dox-toxicity in this model by exploring the effect of co-incubation with N-acetyl cysteine (NAC), which is a known potent ROS-scavenger. We used H_2O_2 as a positive control in these experiments.

We first sought to identify a concentration of H_2O_2 that closely mimicked the toxic effect of 7.5 µM Dox. We therefore investigated the effects of 1 µM H_2O_2, 50 µM H_2O_2 and 100 µM H_2O_2 on cardiomyocyte death (Fig.5.1). After incubating cells for 4 hours (Fig. 5.1 A), a significant rise in cell-death was observed only with 50 µM H_2O_2 (mean cell-death 83.3 $\pm$ 11.0%) and 100 µM H_2O_2 (91.6 $\pm$ 4.1%). However, 1 µM H_2O_2 (mean cell-death 20.2 $\pm$ 2.0%) showed no significant difference from basal cell-death (Cont, 13.1 $\pm$ 2.3%) (ANOVA $p<0.05$, $n=3$). Incubating with the same three concentrations over 18 hours (Fig. 5.1B), however, resulted in a significant rise in cell-death with all concentrations of H_2O_2. Incubation with 1 µM H_2O_2 resulted in a rise in mean cell-death to 42.6 $\pm$ 1.1%, significantly higher than basal cardiomyocyte death (Cont, 15.5 $\pm$ 2.1%) and comparable to levels previously observed with 7.5 µM Dox during initial characterisation experiments. 50 µM H_2O_2 (cell death 99.3 $\pm$ 0.6%) and 100 µM H_2O_2 (cell death 96.8 $\pm$ 3.1%) both resulted in very high levels of toxicity (ANOVA $p<0.05$, $n=3$).

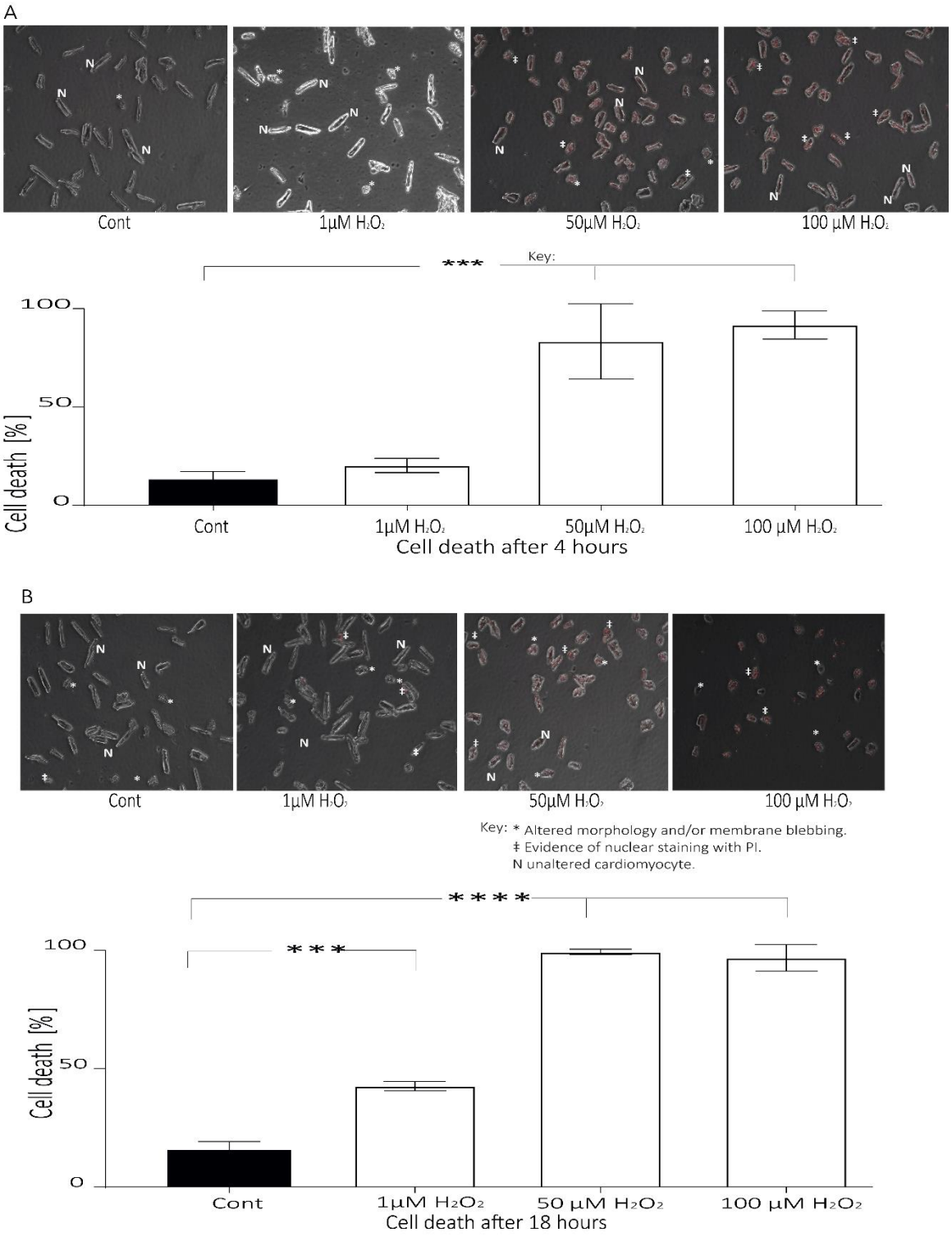

Fig. 5.1. Cardiomyocyte death induced by different concentrations of H_2O_2 over two different incubation periods. (A) Cell-death over 4 hours following treatment with 1 μM, 50 μM and 100 μM H_2O_2. Both 50 μM H_2O_2 and 100 μM H_2O_2 resulted in significant rise in cell-death (ANOVA $p<0.05$, $n=3$). For comparison, 1 μM H_2O_2 did not differ significantly from basal cell-death (Cont). (B) Cell-death over 18 hours with same concentration of H_2O_2. All three concentrations resulted in a significant rise in cell-death. Toxicity of 1 μM H_2O_2 was lower than 50 μM H_2O_2 or 100 μM H_2O_2, and was comparable to levels previously observed with 7.5 μM doxorubicin (ANOVA $p<0.05$, $n=3$) (representative photographs of cell-death displayed in top panels).

5.1.2. Effect of co-treatment with N-acetyl cycsteine on Dox-toxicity.

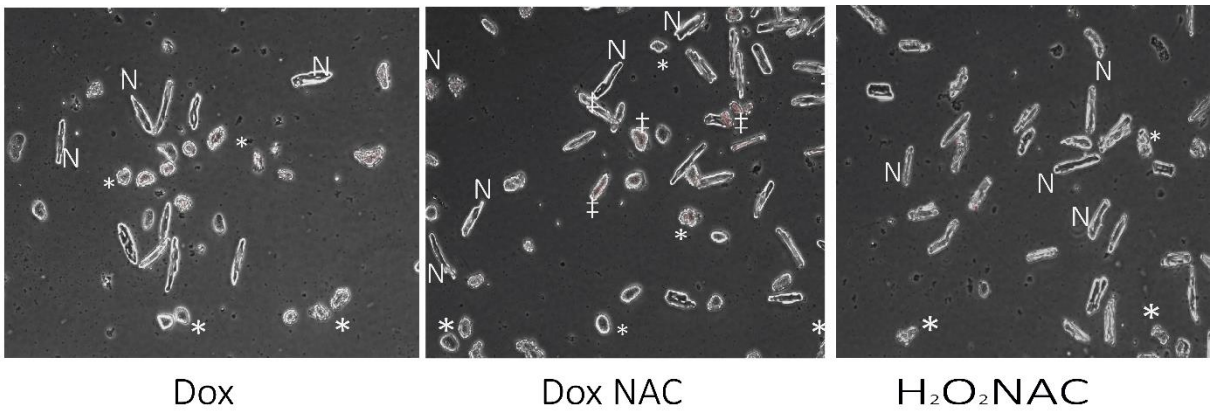

Key: * Altered morphology and/or membrane blebbing.
‡ Evidence of nuclear staining with PI.
N unaltered cardiomyocyte.

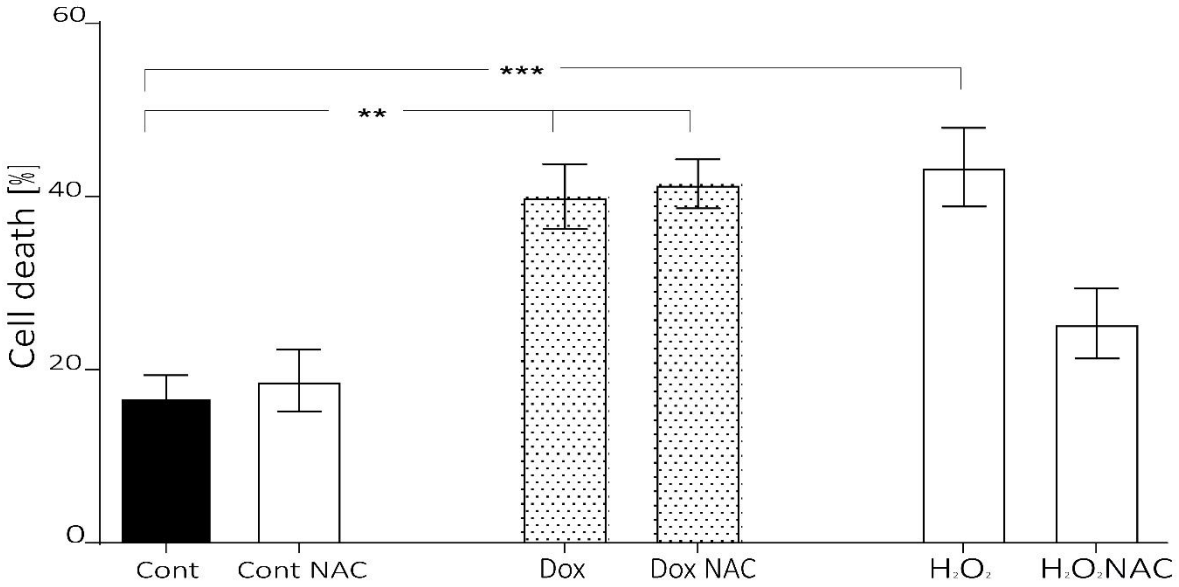

Fig. 5.2. Effect of presence of N-acetyl cysteine on doxorubicin-induced toxicity. Treatment with 7.5µM doxorubicin alone (Dox) and in the presence of 250 µM NAC (Dox NAC) both resulted in significant rise in cell-death after 18 hours. For comparison, 1 µM H_2O_2 alone (H_2O_2) resulted in a significant rise in mean cell-death compared to basal cell-death (Cont), but the presence of NAC rescued cardiomyocytes from H_2O_2-induced cell-death (H_2O_2 NAC) ($p<0.05$, $n=4$) (example photographs of cell-death displayed in top panels, see also Appendix B, Fig. VIII).

We next investigated the effect of co-incubation with N-acetyl cycsteine (NAC) on Dox toxicity after an 18 hours exposure (Fig. 5.2). Based on the previous experiment, 1 µM H_2O_2 was used as a positive control. In these experiments, Dox alone (Dox, mean cell-death 40.0 $\pm$ 3.7%) and presence of NAC during Dox-treatment (Dox NAC, 41.4 $\pm$ 2.8%) both resulted in significant rise

in cell-death compared to basal cell-death (Cont, 16.6 ± 2.7%) (Fig.5.2). No statistical significance was identified in the difference between Dox and Dox NAC. For comparison, the toxicity of 1 µM H_2O_2 (H_2O_2, 43.4 ± 4.5%) was abrogated in the presence of NAC (H_2O_2 NAC, mean cell-death 25.3 ± 4%; $p<0.05$ H_2O_2 vs H_2O_2 NAC, $n=4$) (ANOVA $p<0.05$, $n=4$).

These experiments indicated that presence of NAC did not offer any protective effect against the toxicity of Dox on cardiomyocytes.

5.1.3. Effect of doxorubicin on cardiomyocyte mitochondrial transmembrane potential ($\Delta\Psi_m$).

Alterations of mitochondrial transmembrane potential ($\Delta\Psi_m$) has been hypothesised to be a potential process involved in mediating cardiotoxicity due to Dox treatment. We therefore investigated the state of the mitochondrial transmembrane potential in this model after subjecting cardiomyocytes to Dox pre-treatment for 30 minutes, 4 hours and 18 hours. The rhodamine ester tetramethyl rhodamine methyl ester (TMRM) crosses the mitochondrial membrane proportional to the $\Delta\Psi_m$, and at nanomolar concentrations aggregates in the mitochondria. Measurement of fluorescence of TMRM in response to incident light, therefore, allows an estimation of the $\Delta\Psi_m$. We therefore imaged cardiomyocytes with 10% He-Ne incident laser after loading with 30 nM TMRM and recorded the intensity of the emitted light. This approach to evaluate the $\Delta\Psi_m$ has been reported previously from our lab (Sidall et al, 2013) as well as by other groups (Juhaszova et al, 2004).

5.1.3.1. TMRM loading in cardiomyocyte mitochondria is not influenced by doxorubicin treatment.

To ensure TMRM accumulation in the mitochondria and fluorescence intensity of the emitted light was not altered by the presence of Dox, we first evaluated the temporal collapse of fluorescence of 30 nM TMRM in control cells (Cont) and in doxorubicin-treated cardiomyocytes (Dox) after introducing 200 nM of the mitochondrial uncoupling compound FCCP (Fig. 5.3). The

fluorescence was recorded for 80 seconds after introducing the uncoupling agent. The experiment was repeated in cells subjected to 7.5 µM Dox for 30 minutes (Fig. 5.3A, Cont T0 and Dox T0), 4 hours (Fig.5.3B, Cont T4 and Dox T4) and 18 hours (Fig.5.3C, Cont T18 and Dox T18).

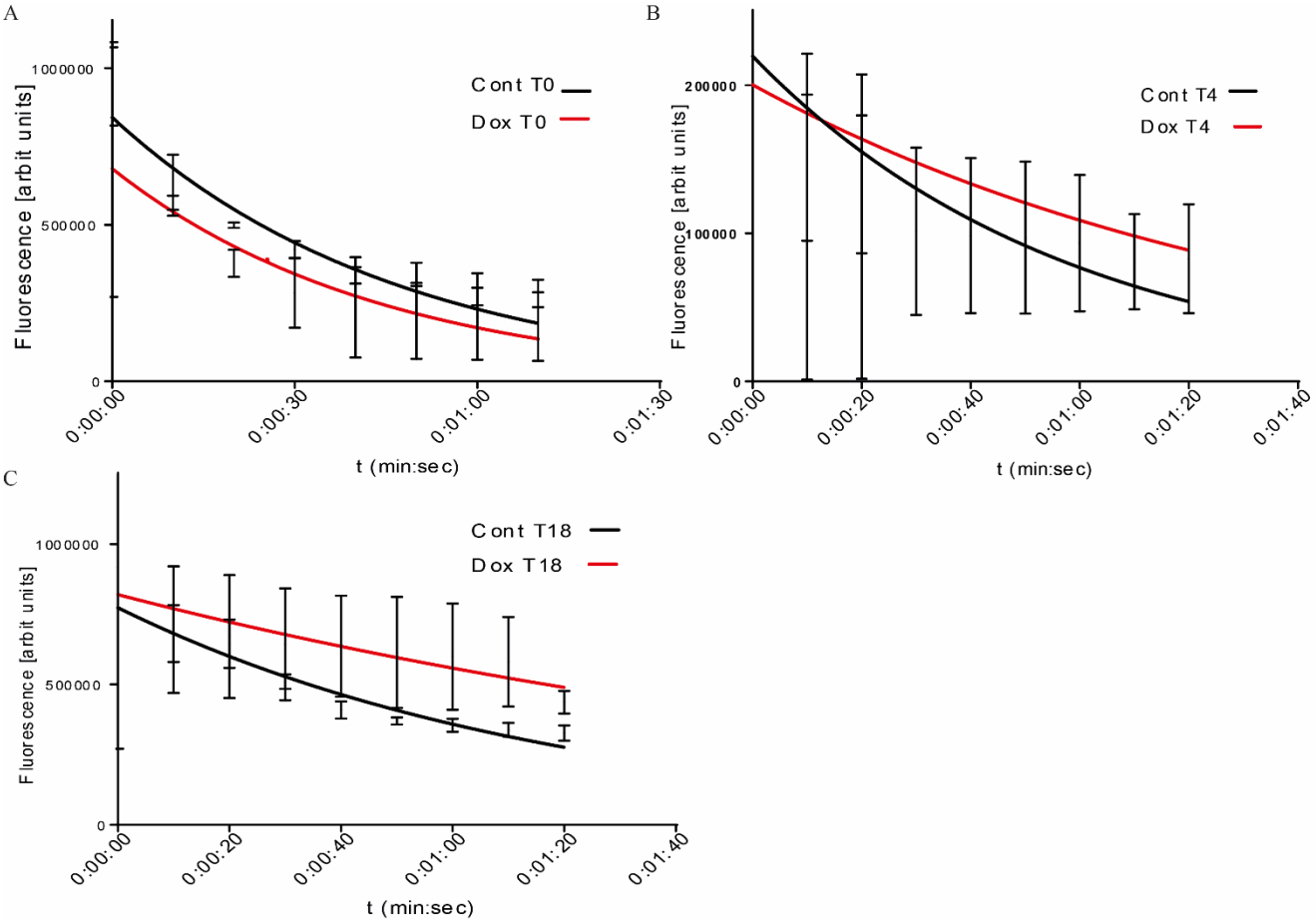

Fig 5.3. TMRM fluorescence does not vary after mitochondrial uncoupling between control cells and cells subjected to doxorubicin treatment. Fluorescence of 30nM TMRM in control cardiomyocytes and cells subjected to 7.5µM doxorubicin after treatment with 200 nM FCCP showed no variation in the presence and absence of doxorubicin. This was consistent with doxorubicin exposure over 30 minutes (Fig. 5.3A, Cont T0 and Dox T0), 4 hours (5.3B, Cont T4 and Dox T4) and 18 hours (5.3C, Cont T18 and Dox T18).

For each treatment period, statistical analysis failed to reveal any significant differences in TMRM fluorescence between control and doxorubicin-treated cardiomyocytes at the recorded time intervals, indicating Dox treatment did not alter accumulation or fluorescence intensity of

TMRM (ANOVA, p>0.05, *n* =2). Therefore, TMRM can be reliably used to measure mitochondrial membrane potential in these cells even in the presence of doxorubicin.

5.1.3.2. Resting $\Delta\Psi_m$ does not vary in response to doxorubicin treatment over time.

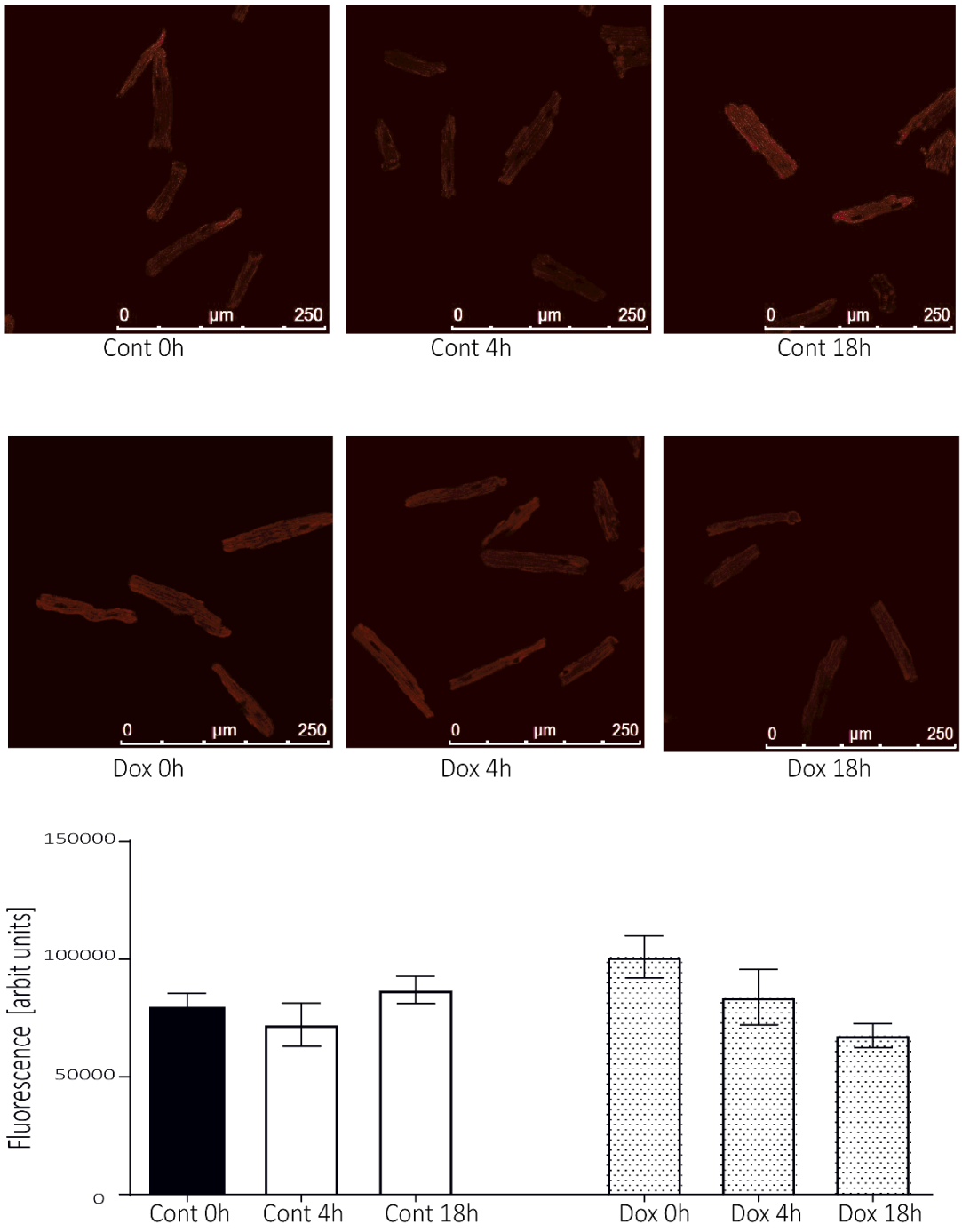

Fig. 5.4. Mitochondrial transmembrane potential variation over time with doxorubicin treatment. $\Delta\Psi_m$ after treatment with 7.5 µM doxorubicin for 30 minutes (Dox 0h), 4 hours (Dox 4h) and 18 hours (Dox 18h) and $\Delta\Psi_m$ in time-controlled basal cardiomyocytes (Cont 0h, Cont 4h and Cont 18h) showed no significant variation. (ANOVA p=0.1, *n*=6) (example photographs of fluorescense after TMRM staining displayed in top panels).

We next investigated variation in baseline $\Delta\Psi_m$ by measuring fluorescence intensity of TMRM after Dox-treatment (Fig. 5.4). No variation was noted in $\Delta\Psi_m$ over time, as measured by TMRM fluorescence (in arbitrary fluorescence units) after Dox-exposure for 30 minutes (Dox 0h, 101055 $\pm$ 8979), for 4 hours (Dox 4h, 83864 $\pm$ 11754) and 18 hours (Dox 18h, 67562 $\pm$ 5143). Similarly, in control cells, fluorescence at baseline (Cont 0h, 79719 $\pm$ 5812), after 4 hours (Cont 4h, 72169 $\pm$ 9236) and after 18 hours (Cont 18h, 86962 $\pm$ 5877) did not exhibit any significant variations. Treatment and control groups showed no statistical variations (ANOVA P=0.1, *n*=6). This suggested that in this *in vitro* model, 7.5 µM Dox did not induce significant $\Delta\Psi_m$ variations.

5.1.4. Time taken to mitochondrial permeability transition pore opening does not alter with doxorubicin treatment.

Having ruled out any significant alterations in the $\Delta\Psi_m$ over time as a consequence of Dox exposure, we explored the role of mitochondrial permeability pore (mPTP) transition in induction of the cell-death due to Dox in this model. A positive control, Ciclosporine A (CsA), was used in these experiments at 1 µM concentration, since CsA is known to raise the threshold of stimulus required for induction of mPTP transition, which reflects as a significantly prolonged time taken for mPTP transition when CsA is present. We used 3 µM TMRM in these experiments. TMRM acts as a photosensitiser for ROS. At micromolar concentrations, TMRM quenches in the mitochondria. Progressive ROS accumulation consequent to phototreatment leads to mPTP opening associated with depolarisation of the mitochondrial transmembrane potential and free passage of ions across the mPTP. This is detected by rapid dequenching of TMRM fluorescence as the probe is released into the larger volume of the cytosol. Therefore, subjecting cardiomyocytes to a high intensity laser allows a real-time measurement of the temporal induction of the mPTP. This approach to evaluation of mPTP vulnerability has been reported from this lab before (Davidson et al, 2006). We therefore measured the time taken to mPTP induction after Dox exposure for 18 hours. In positive control experiments, 1 µM CsA

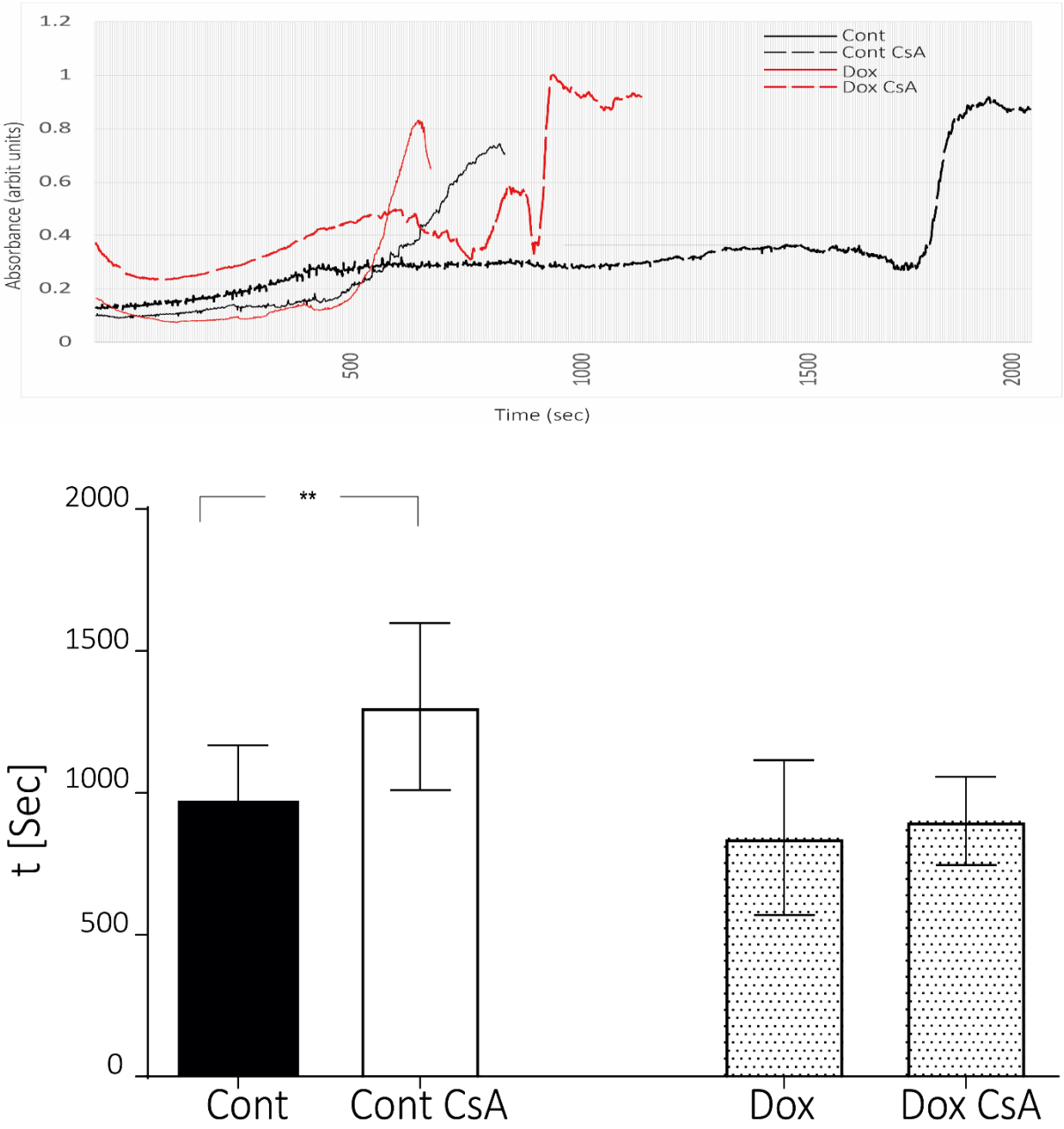

Fig. 5.5. Doxorubicin does not influence mPTP transition in vitro. Time taken to mPTP induction in cells treated with 7.5µM doxorubicin (Dox) failed to show any significant differences compared to control (Cont). Presence of 1µM Ciclosporine A (CsA) prolonged time taken for mPTP-transition in control cardiomyocytes (Cont CsA), but not in cells pre-treated with doxorubicin (Dox CsA) ($p<0.05$, $n=7$) (representative trends to fluorescence-dequenching shown in top panel).

was introduced during TMRM probe loading, and maintained in solution during the generation of oxidative stress leading to mPTP induction.Fig. 5.5 shows the results of these experiments. Dox pre-treated cardiomyocytes did not undergo mPTP transition with any significant

difference (Dox, mean time to mPTP induction 842.1 ± 103 s) compared to control (Cont, 972.1 ± 74 s) (Fig. 5.5). The positive control CsA prolonged time taken to mPTP induction in basal cardiomyocytes only (Cont CsA, 1304 ± 111.4s). Surprisingly, this protective effect was abrogated in cells subjected to Dox pre-treatment (Dox CsA, mean time to mPTP transition 901 ± 58.7s; $p<0.05$, Cont CsA vs Dox CsA) (ANOVA $p<0.05$, $n=7$). These experiments indicated vulnerability of the mPTP to transition to the open state was not increased due to Dox-treatment in this model.

5.1.5. Presence of Ciclosporine A does not alter doxorubicin-induced cardiomyocyte death *in vitro.*

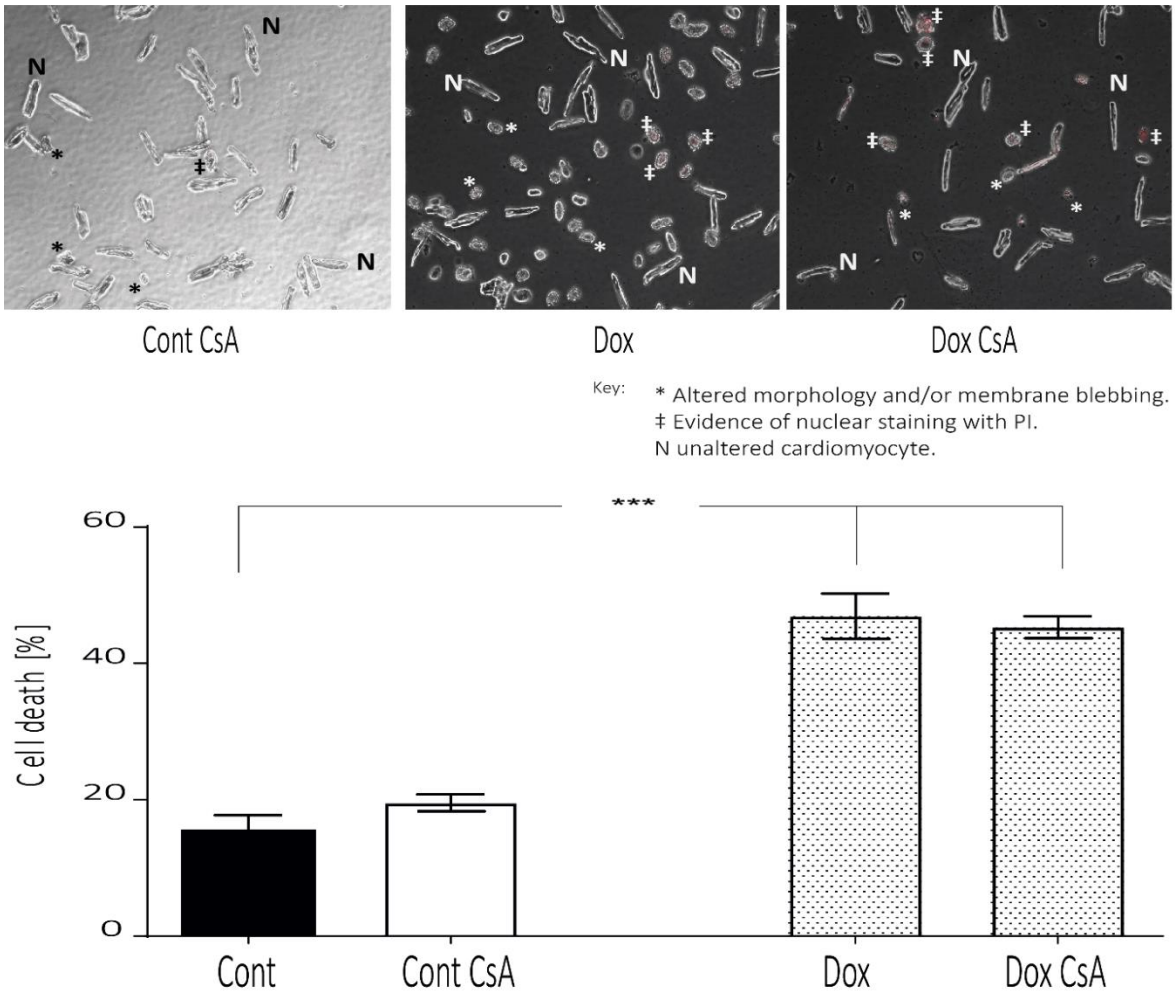

Fig. 5.6 Doxorubicin-induced cell-death in the presence of Ciclosporine A. Treatment with 7.5µM doxorubicin alone (Dox) and in the presence of 1 µM Ciclocsporine A (Dox CsA) both resulted in similar levels of cardiomyocyte-death. Compared to basal cell-death (Cont), presence of CsA alone (Cont CsA) showed no significant difference in cell-death after 18 hours (ANOVA $p<0.05$, $n=7$) (representative photographs of cell-death displayed in top panels. See also Appendix B. Fig. IX).

Since CsA-mediated mPTP-protection was abrogated in cells pre-treated with doxorubicin, we investigated the effect of co-treatment with 1 µM CsA on Dox-toxicity and on untreated cardiomyocytes. The results are shown in fig. 5.6. Analysis of cell-death showed a similar and significant rise in cell-death in cells exposed to Dox alone (Dox, mean cell-death 46.9 $\pm$ 3.3%), and in cells subjected to Dox in the presence of CsA (Dox CsA, 45.3 $\pm$ 1.6%). CsA alone (Cont CsA, 19.5 + 1.2%) was not toxic and displayed no significant differences in survival compared to control (Cont, 15.6 $\pm$ 2.1%) (ANOVA $p<0.05$, $n=7$). This showed presence of CsA could not protect against nor exacerbate Dox-toxicity, but CsA alone was not toxic at the concentrations used.

5.2. Effect of hypoxic preconditioning on doxorubicin-mediated cardiomyocyte death.

Having explored the potential mechanisms leading to cell-death, we investigated hypoxic preconditioning (HP) as a mechanism of protection against doxorubicin-induced injury in this model of *in vitro* toxicity. We had previously characterised a protocol to deliver an *in vitro* HP stimulus that protected cardiomyocytes against IR-injury (Chapter 4, section 4.2.3). We therefore used this protocol, and investigated cell-death after incubating cardiomyocytes with different concentrations of Dox after this preconditioning HP stimulus. As control for HP, cardiomyocytes were incubated in normoxic buffer for 40 minutes and subjected to identical Dox concentrations over the same time-period.

5.2.1. Hypoxic preconditioning protects cardiomyocytes from doxorubicin-toxicity.

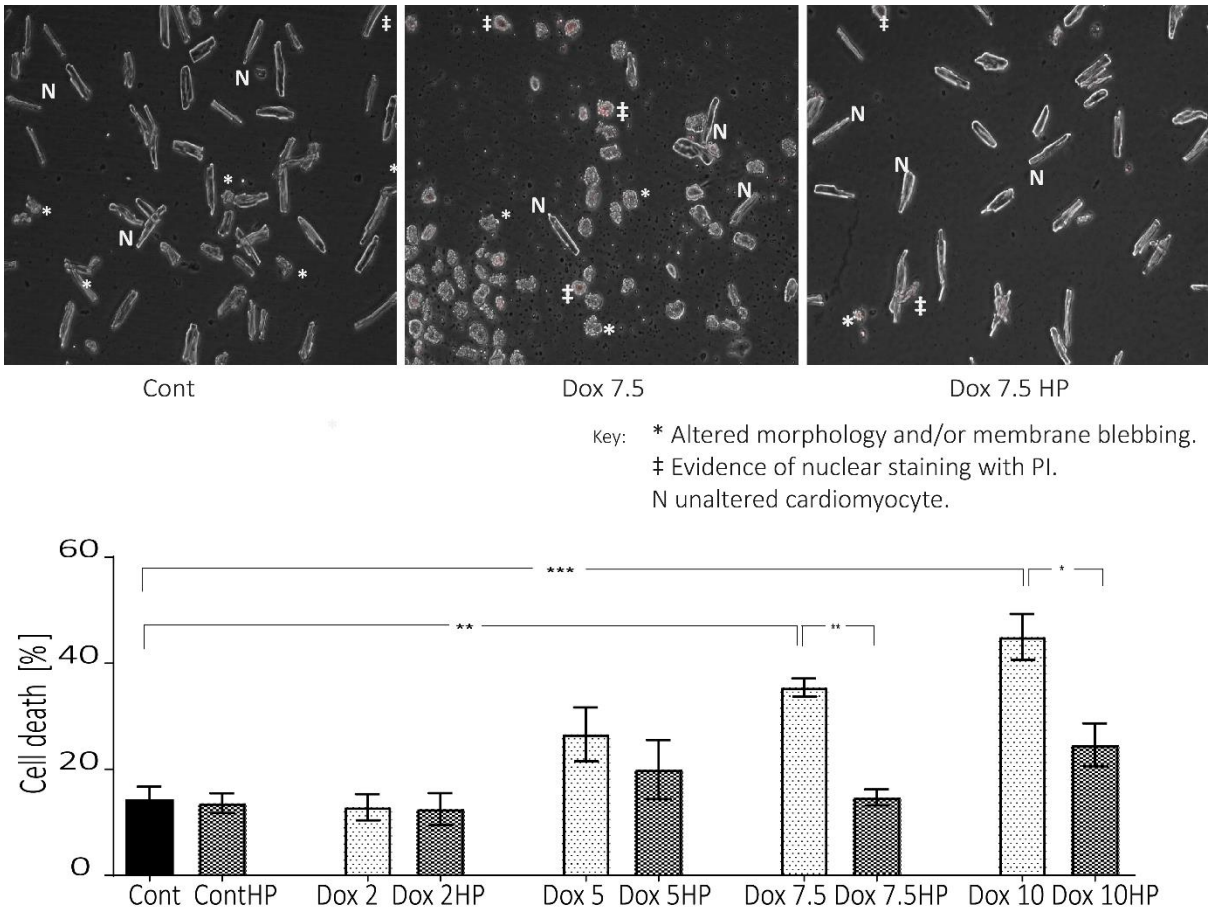

Fig. 5.7. Effect of hypoxic preconditioning on subsequent doxorubicin-mediated cardiomyocyte toxicity. In non-preconditioned cells, a dose dependent rise in cell-death was observed with doxorubicin treatment, which achieved statistical significance with 7.5µM doxorubicin (Dox 7.5) and 10µM doxorubicin (Dox 10). For comparison, preconditioned cardiomyocytes were protected across all doxorubicin concentrations, with no difference in cell-death compared to control (ANOVA $p<0.05$, $n=5$) (representative photographs of cell-death displayed in top panels. See also, Appendix B Fig. X).

In non-preconditioned controls cell-death was noted to be significantly high, but only with concentrations of 7.5 µM Dox (Dox 7.5, 35.4 $\pm$ 1.7%) and 10 µM Dox (Dox 10, 44.9 $\pm$ 4.3%) (Fig. 5.7). HP protected against the toxicity of both Dox 7.5 µM (Dox 7.5 HP, 14.7 $\pm$ 10.5%) and 10 µM (Dox 10 HP, 24.6 $\pm$ 4.0%), and no differences were observed when compared to basal cell-death (Cont, 14.3 $\pm$ 5.3%). HP alone did not influence cell-death in basal cardiomyocytes (Cont HP, 13.6 $\pm$ 1.8%) (ANOVA $p<0.05$, $n=5$).

5.2.2. Protection against doxorubicin-injury due to hypoxic preconditioning is dependent on PI3K/Akt cascade, but independent of MAPK-ERK.

In light of the above results, we investigated the role of the RISK pathway in the protective effect of HP observed against toxic concentrations of doxorubicin. Pre-treatment with the reversible inhibitor 10 µM LY294002 was used to inhibit the PI3K/Akt pathway, while MAPK

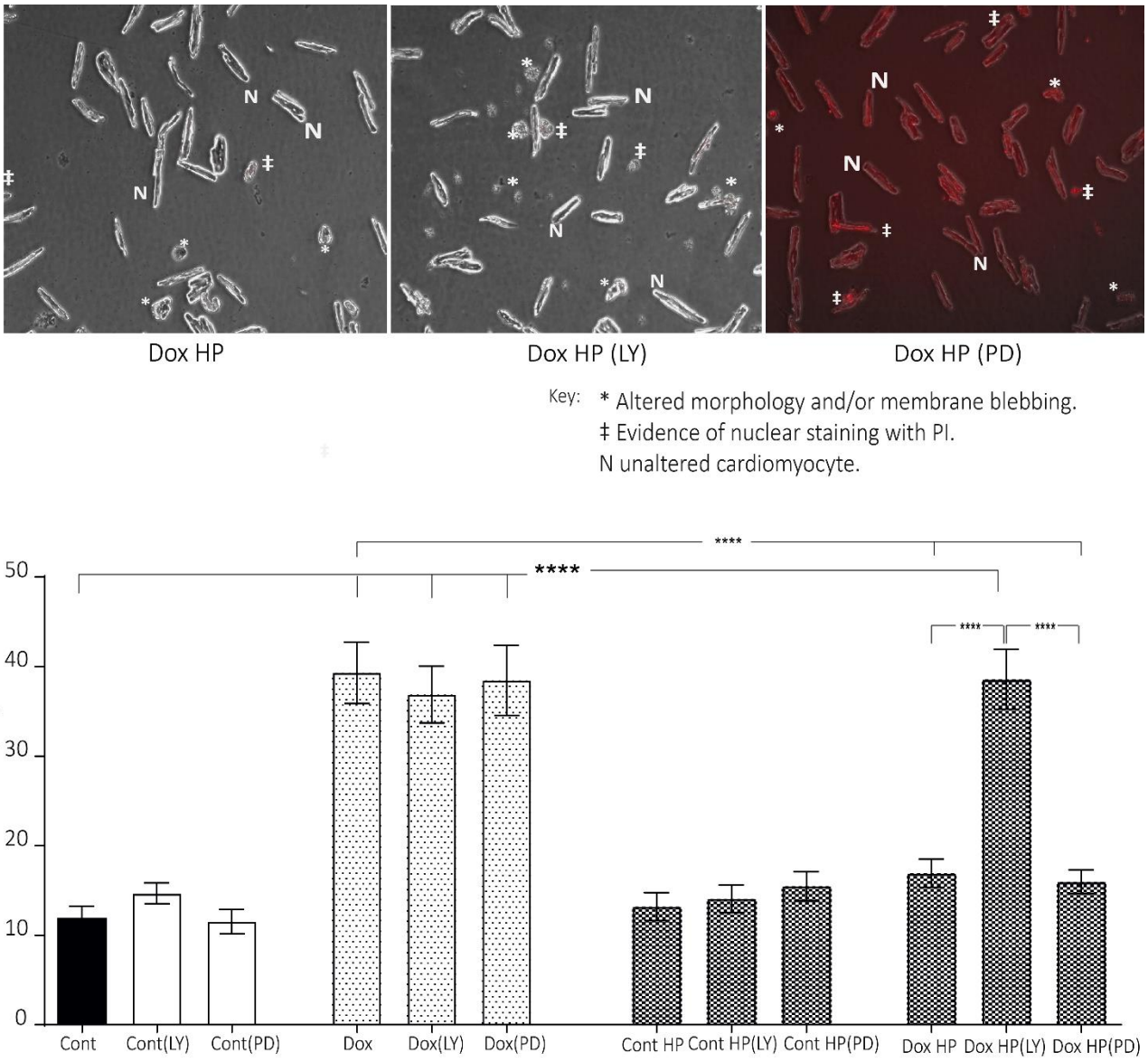

Fig. 5.8. Effect of inhibiting PI3K/Akt pathway and MAPK ERK 1/2 on preconditioning-mediated protection against Doxorubicin-induced cell-death. Excess cell-death due to treatment with 7.5µM doxorubicin (Dox) did not manifest in cells subjected to a preceding hypoxic preconditioning (HP) stimulus (Dox HP). Pre-treatment with 10µM LY294002 before HP (Dox HP (LY)) abrogated this protective influence, but the protection persisted in Dox HP group pre-treated with 30µM PD98059 (Dox HP (PD)). LY294002 and PD98059 alone did not have any significant effects (ANOVA $p<0.05$, $n=5$) (representative photographs of cell-death displayed in top panels, see also Appendix B Fig. XI).

ERK 1/2 was inhibited using 30 µM PD98059 before subjecting cells to HP. The protective effect of preconditioning on cardiomyocytes was then re-explored using 7.5 µM Dox as a toxic anthracycline concentration. Fig. 5.8 shows the results of these experiments. Compared to basal cell-death (Cont, mean cell-death 11.2 ± 1.2%), Dox alone resulted in significant toxicity after 18 hours (Dox, 39.3± 3.4%), which was not observed in preconditioned cells (Dox HP, 16.9 ± 1.5%). However, this protective effect of HP was abrogated in cells pre-treated with 10µM LY294002 before preconditioning (Dox HP(LY), 38.5 ± 3.3%; $p<0.05$, Dox HP vs Dox HP(LY)), but not 30µM PD98059 (Dox HP (PD) 15.9 ± 1.3%; $p<0.05$, Dox HP(LY) vs Dox HP (PD)). Neither LY294002 alone (Dox (LY), mean cell-death 36.8 ± 3.1%), nor PD98059 alone (Dox (PD), 38.4 ± 3.1%) altered the toxicity of Dox significantly (ANOVA $p<0.05$, $n=5$).

5.2.3 Western blots.

Having observed the effect of differential inhibition of PI3K/Akt and MAPK ERK 1/2 on doxorubicin-toxicity following HP, we used Western blotting to confirm the induction of the respective kinases by HP, and their respective inhibitions with LY294002 and PD98059. Insulin was used as a positive control to induce the respective protein cascades in these experiments.

5.2.3.1. PI3K/Akt phosphorylation in response to hypoxic preconditioning.

Fig. 5.9 panel A shows a representative Western blot investigating the expression levels of phosphorylated Akt (p-Akt). An increase in phosphorylated protein content was noted in cells subjected to HP (HP, lane 6). A more prominent increase in levels of p-Akt with the positive control insulin (Ins, lane 4) was also noted. 10µM LY294002 pre-treatment inhibited the increase in p-Akt in response to HP (HP(LY), lane 7), and attenuated the phosphorylation induction in insulin-treated cells (Ins(LY), lane 5). No prominent signal for p-Akt was identified in control cells under basal conditions (Cont, lane 2) or after LY294002 treatment alone (Cont(LY), lane 3).

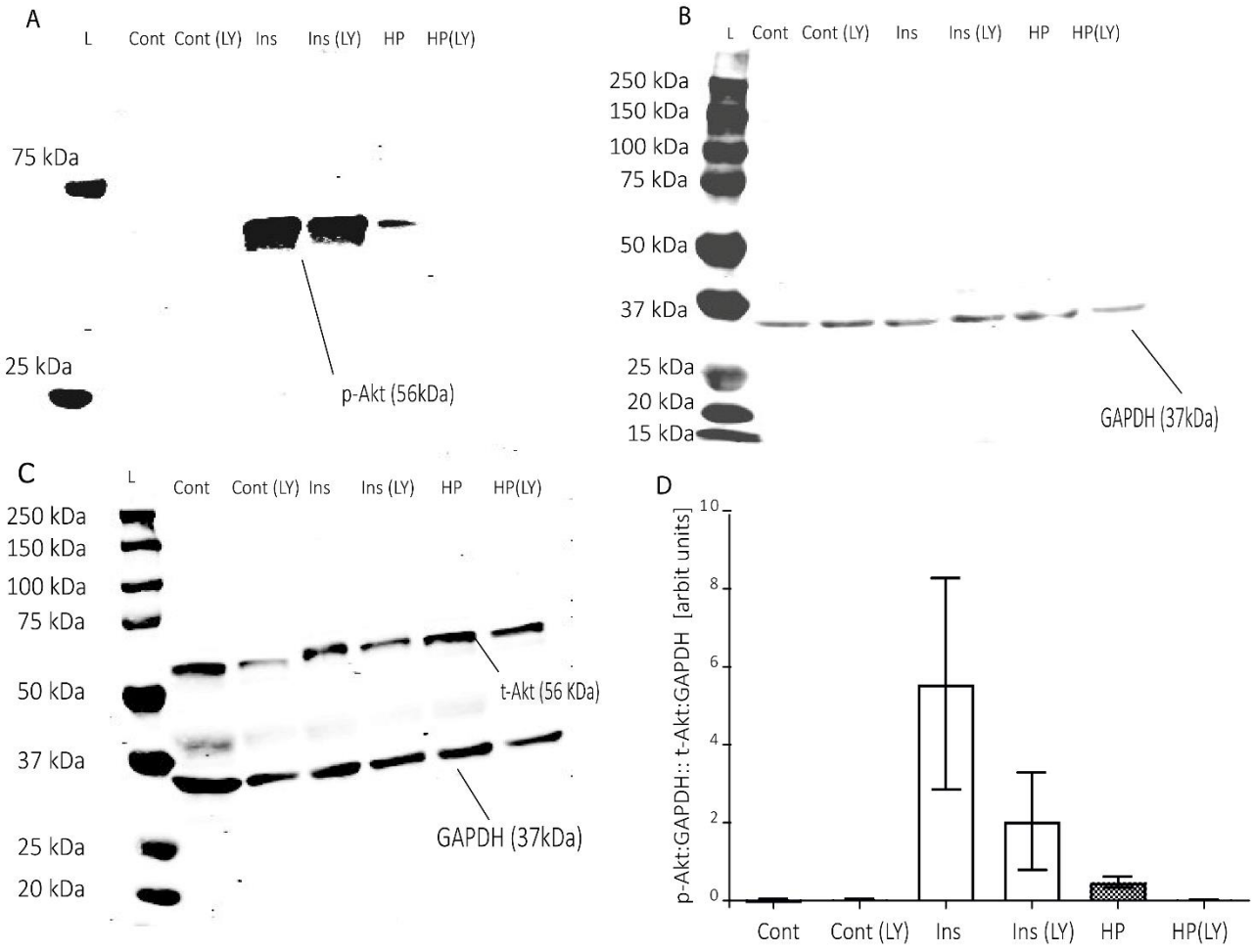

Fig. 5.9. Western blot analysis of hypoxic preconditioning-induced phosphorylation of Akt. (A) Representative blot showing expression of p-Akt induction. Both insulin (Ins) and hypoxic preconditioning (HP)-induced an increase in p-Akt, which was attenuated by 10µM LY294002 treatment. (B) Expression of the housekeeping gene GAPDH in the same blot as A. (C) Expression of t-Akt protein in the same samples as shown in panel A, run on a different Western blot membrane, along with the expression of GAPDH. (D) Mean p-Akt to t-Akt ratios obtained from Western blot analyses. Compared to resting state, HP resulted in an increased expression level of p-Akt that was inhibited by LY294002 pre-treatment. The positive control insulin showed a strong induction of p-Akt, which was also inhibited by LY294002 pre-treatment (*n*=3).

Fig.5.9 panel B shows the content of housekeeping gene GAPDH in the same samples as panel A. The GAPDH protein content was used as a loading control in these experiments, and a signal was identified across all samples. Fig. 5.9 panel C shows expression of total Akt (t-Akt) and GAPDH in the same samples shown in panel A, analysed on a separate Western blot. Prominent signals for both t-Akt and GAPDH were identified across all samples. To identify the ratio of p-Akt to t-Akt in each treatment group, p-Akt levels (Fig.5.9 panel A) were normalised to GAPDH

content (Fig. 5.9 panel B) in each sample well (i.e., expressed as p-Akt: GAPDH). Similarly, t-Akt levels were normalised to GAPDH (i.e., t-Akt: GAPDH ratio identified from Fig. 5.9 panel C). Fig. 5.9 panel D shows the ratio of p-Akt and t-Akt normalised to GAPDH (p-Akt: GAPDH :: t-Akt: GAPDH) in the respective treatment groups, as a mean of three different repeat experiments. HP resulted in a mean 17-fold increase in the ratio of p-Akt to t-Akt compared to resting expression levels (Cont). This induction response was attenuated when cells were pre-treated with LY294002 before preconditioning (HP(LY)). The positive control Insulin (Ins) resulted in a mean increase of 200-fold in p-Akt to t-Akt ratio compared to control, and LY294002 pre-treatment attenuated this to 75-fold of basal levels. However, statistical analysis failed to show significance in the differences observed in the ratios of p-Akt to t-Akt in the various treatment groups ($p>0.05$, $n=3$).

5.2.3.2 Phosphorylation induction of MAPK ERK 1/2 in response to hypoxic preconditioning.

We next explored the phosphorylation of the ERK 1/2 proteins in response to HP. Fig. 5.10 panel A shows a representative Western blot for phosphorylated ERK 1/2 (p-ERK) and the housekeeping gene α-tubulin. Prominent signal for p-ERK content was observed after HP (HP, lane 6), which was attenuated by pre-treatment with PD98059 (HP (PD), lane 7). Increase in p-ERK content was also observed after insulin-treatment (Ins, lane 4), and in protein isolate from resting cardiomyocytes (Cont, lane 2). PD98059 pre-treatment resulted in attenuated p-ERK levels in both groups (Cont (PD), lane 3; and Ins (PD), lane 5). Fig. 5.10 panel B shows expression levels of total ERK 1/2 (t-ERK) in the same samples shown in panel A, analysed in a separate western blot. Although the blot gave a weak signal, t-ERK signal was observed across all groups. Analysis on imageJ software showed a dual peak at the expected molecular weight range of 42/44 kDa in all samples.

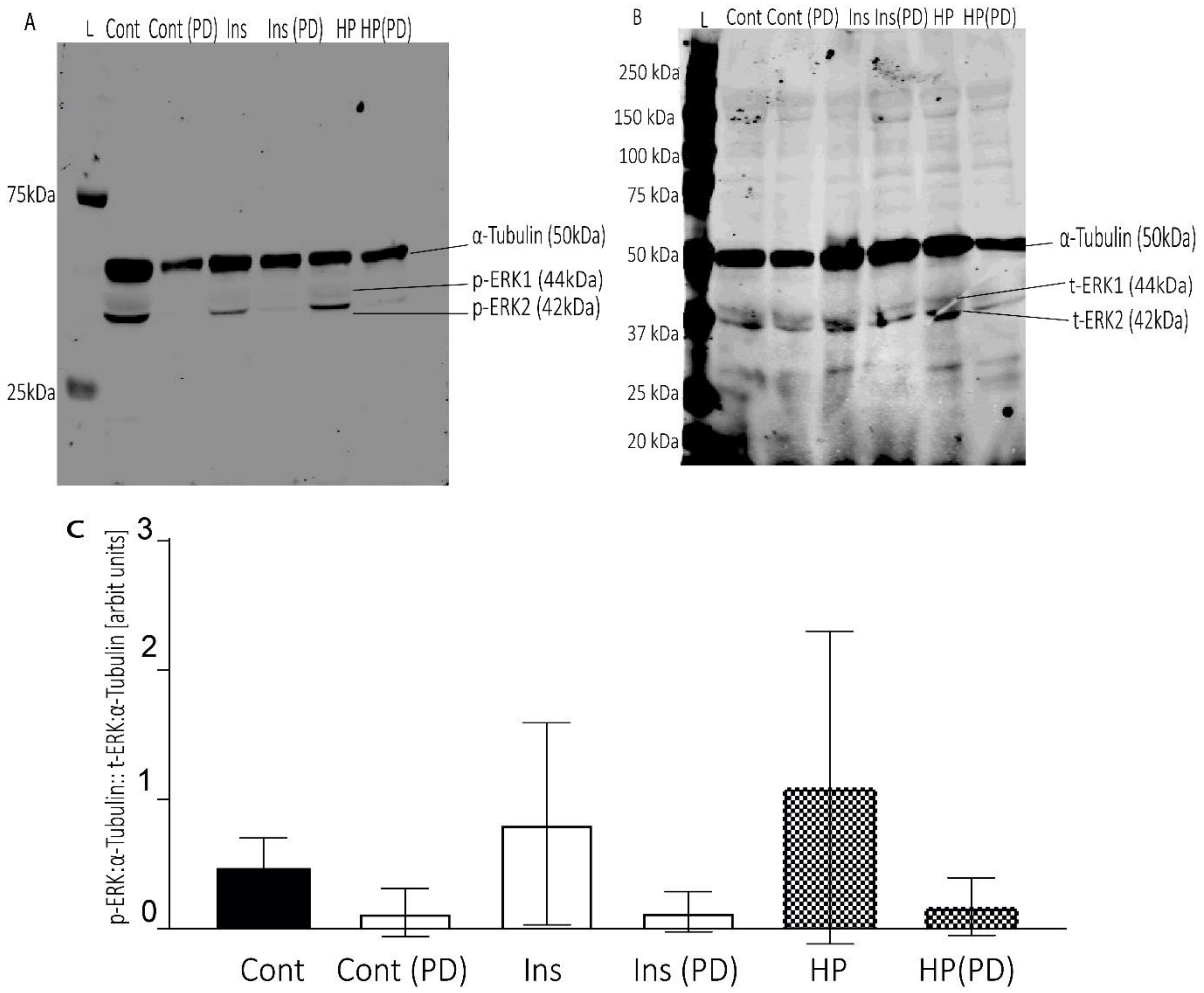

Fig. 5.10. Western blot analysis of hypoxic preconditioning induced phosphorylation induction of MAPK ERK 1/2. (A) Representative Western blot displaying expression levels of p-ERK and the housekeeping gene α-tubulin under basal conditions (Cont, lane 2), after pre-treatment with PD98059 alone (Cont(PD), lane 3), insulin treatment alone (Ins, lane 4), PD98059 pre-treatment with insulin (Ins(PD), lane 5), HP (lane 6), and cells pre-treated with PD98059 before HP (HP(PD), lane 7). (B) Western blot displaying expression levels of α-tubulin and t-ERK in the same samples as in Panel A. (C) Mean cumulative expression levels of p-ERK to t-ERK in three different experiments. HP showed a 2.7-fold elevation in p-ERK to t-ERK ratio compared to control, which was attenuated in the presence of PD98059. The positive control insulin 1.7-fold elevation of p-ERK to t-ERK ratio compared to control. PD98059 pre-treatment attenuated the p-ERK expression levels in all experimental groups (*n*=3).

The phosphorylation induction of MAPK ERK 1/2 was evaluated as relative ratios of p-ERK and t-ERK normalised to α-tubulin in each well. Therefore p-ERK: α-tubulin and t-ERK: α-tubulin ratios were identified for each individual treatment group, and the ratio p-ERK: α-tubulin:: t-ERK: α-tubulin evaluated. Fig. 5.10 panel C shows the results of these analyses in the respective groups, expressed as mean of three different experiments. A 2.7-fold increase was observed

after HP, compared to control. PD98059 pre-treatment attenuated this HP-induced phosphorylation induction to 0.36-fold of control (HP (PD)). Similarly, a 1.7-fold increase in p-ERK to t-ERK ratio was observed with the positive control agent insulin (Ins), which in PD98059 pre-treated cells was attenuated to 0.2-fold the ratio observed in control. PD98059 attenuated p-ERK levels in resting cells (Cont (PD)) to 0.3-fold the levels observed in control. However, statistical analysis failed to show significance in the differences in ratios of p-ERK to t-ERK in the between the various treatment groups ($p>0.05$, $n=3$).

5.2.3.3 Effect of doxorubicin treatment on PI3K/Akt and MAPK ERK 1/2 phosphorylation.

Having analysed the phosphorylation response of for PI3K/Akt and MAPK ERK 1/2 in response to HP, we briefly explored the induction of the respective kinases following Dox- treatment

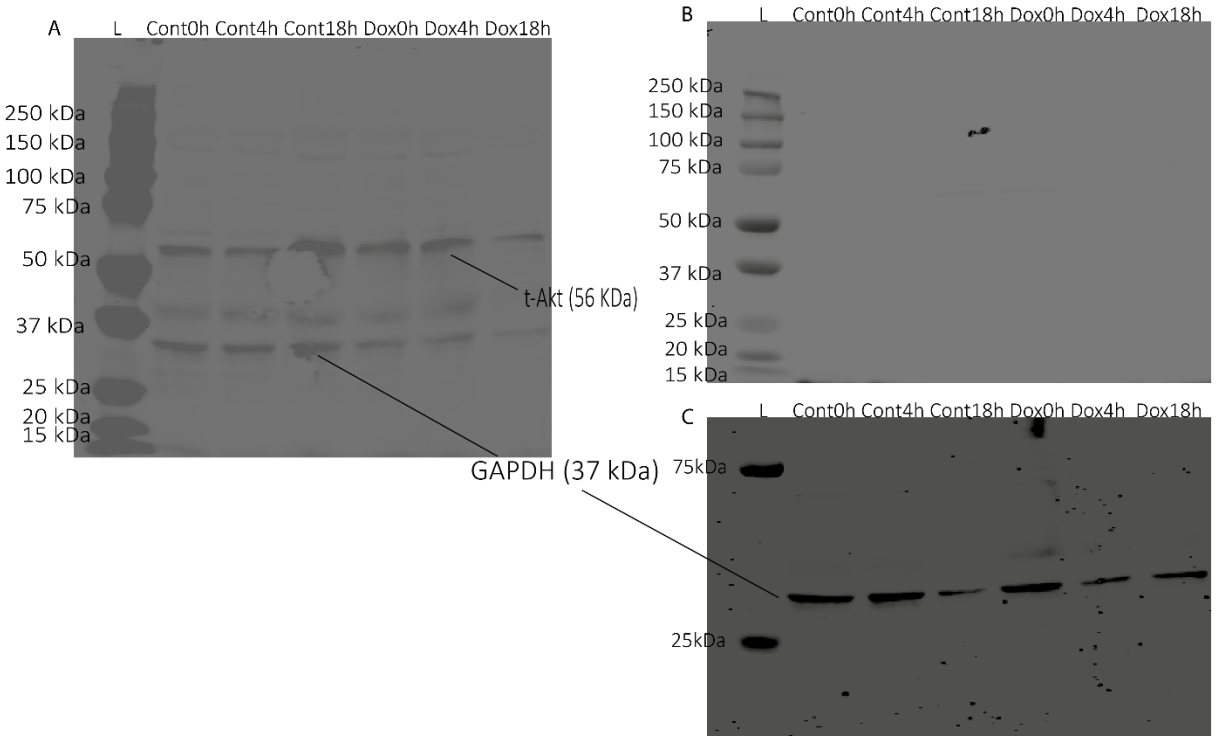

Fig. 5.11. Analysis of doxorubicin-induced phosphorylation of PI3K/Akt. A. A signal could be identified for t-Akt and the house keeping gene GAPDH at all time-points of treatment. B. No signal was identified for p-Akt. C. Analysis of GAPDH content showed a clear discernible signal in the same samples as shown in Panel B.

alone 15 minutes, 4 hours and 18 hours after initiation of drug-treatment. We explored the induction of PI3K/Akt and of MAPK ERK 1/2 (Fig.5.12) in two repeat experiments (*n*=2). Upon analysis of t-Akt and the housekeeping gene GAPDH, distinct signals were identified (Fig.5.11, panel A). However, no signal for p-Akt could be identified, although clear signal was evident for GAPDH in the respective samples (Fig.5.11, Panels B and C) on imageJ analysis. Similarly, on Western blot analysis for MAPK ERK 1/2, a bimodal signal corresponding to the molecular weight for ERK (42 and 44kDa) was identified upon probing for t-ERK, along with a robust signal for the housekeeping gene α-tubulin (Fig.512 panel A). Western blot for p-ERK however failed to show any clear evident signal, although a robust signal for the housekeeping gene α-tubulin was identified (Fig. 5.12 Panel B) in the respective samples. Statistical analysis was not carried out for the protein bands identified in these blots.

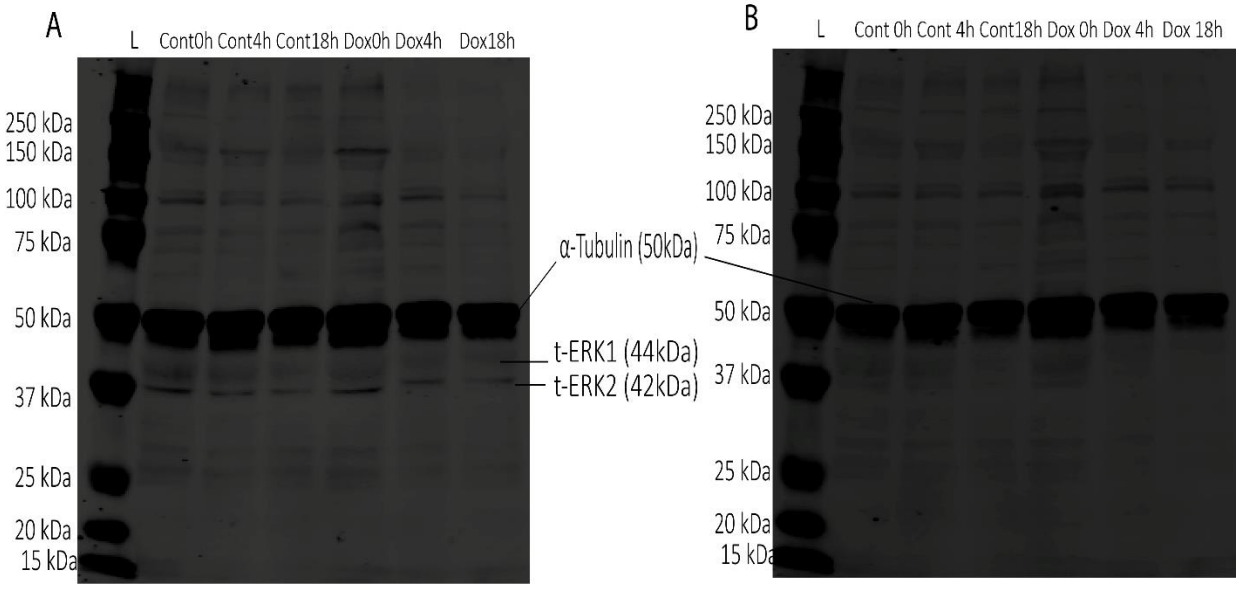

Fig. 5.12. Analysis of phosphorylation induction of MAPK ERK 1/2 in response to doxorubicin alone. A. A robust signal for the α-tubulin and weak but evident signal for the total isoform of ERK 1/2 were identified at all time points. B. Probing for phosphorylated ERK 1/2 (p-ERK) and α-tubulin revealed a robust signal for α-tubulin only, but no evident signal for the p-ERK.

5.3 Discussion.

5.3.1. Doxorubicin-toxicity is not altered by co-incubation with NAC.

The generation of ROS species has been postulated to be a mechanism mediating anthracycline-cardiotoxicity (Minotti et al, 2004; Berthiaume et al, 2007), which includes a proposed direct role for anthracyclines in generation of ROS and RNS species through futile cycling of the quinone-semiquinone moiety of the C-ring of the anthracycline core structure (Beckman et al, 1996; Weinstein et al, 2000; Mihm et al, 2001). An indirect role has also been proposed in generating ROS from enzymatic sources (Zhou et al, 2001). This enzymatic generation of ROS-species may be secondary to saturation of the cellular bioreduction pathways, or attenuation of the mitochondrial and cellular bioenergetic pathways including Complex I, NAD(P)H and NAD(P)H-dependent dehydrogenases, α-ketoglutarate dehydrogenase, etc. (Blanco et al, 2008). As a first step to identifying possible toxicity mechanisms of Dox in the model described, we explored if potential ROS scavenging could protect against *in vitro* cardiomyocyte death. We used N-acetyl cysteine (NAC) to probe our hypothesis, at a concentration of 250 µM. NAC is a direct acting antioxidant which is also a non-specific scavenger capable of scavenging several different ROS species including peroxide ions, ·hydroxide ions, and peroxynitrite ions (Day, 2008). These reactive species have been reported in literature as possible mediators of cardiomyocyte toxicity due to Dox (Pacher et al, 2003; Mihm et al, 2002). Further, NAC has been observed to exert ROS scavenging properties against ROS-species generated from respiratory complexes (Taddei et al, 2012) as well as from enzymatic sources (Peng et al, 2011). 250 µM is a high concentration of NAC, and has been reported previously to be capable of attenuating markers of ROS-expression, e.g. the levels of glycosylated subunit of NADPH ($gp91^{PHOX}$) (Peng et al, 2011). We used H_2O_2 as a positive control to generate oxidative stress in these experiments. The initial experiments showed 50 µM and 100 µM H_2O_2 resulted in cell death approaching or greater than 90% at both 4 hours and 18 hours. However, 1 µM H_2O_2 more closely replicated the toxicity of 7.5 µM doxorubicin, since

cardiomyocyte death failed to show any statistically significant difference at 4 hours, but approached levels observed with 7.5 µM Dox during initial characterisation of the model of doxorubicin-toxicity (Figs 5.1, 4.1 and 4.8). We therefore used 1 µM H_2O_2 as a positive control.

Our experiments suggest that in this *in vitro* model, ROS-species may not be the mediator of doxorubicin-toxicity. This differs from observations reported previously. For example, Deres et al (2005) had previously reported increased lipid peroxidation and protein oxidation in response to perfusion with Dox in an isolated Langendorff-perfused rat heart model. Similarly, Ichihahra et al (2007) noted an increase in lipid peroxidation in left ventricular tissue in an *in vivo* model where they injected mice intraperitoneally with doxorubicin, which correlated with cardiac dysfunction. The authors noted protection from both depressed cardiac function, as well as from increase in levels of lipid peroxidation products with polyethyleneglycated-Superoxide dismutase (PEGylated-SOD or PEG-SOD) as well as with fenofibrate. It ought to be highlighted that we did not directly visualise the generation of ROS-species in response to Dox treatment, instead using H_2O_2-induced cell-death as a positive control and surrogate marker for oxidative stress. Considering a second surrogate marker of oxidative stress, e.g., expression levels of proteins responsive to oxidative stress (for example $gp91^{PHOX}$) or direct visualisation of the content of ROS-species in response to H_2O_2 treatment, Dox-treatment, and the respective changes upon coincubation with NAC would have consolidated the results we observed and improved the robustness of the experimental design and the conclusions. This is a limitation of our experiment. Moreover, the sample size of these experiments was four (n=4). We did not pre-calculate the sample size for the experiments, which may be considered a limitation of the experiments. However, the protective role of NAC in the positive control experiment allows a substantial measure of confidence in the cell-survival data we observed. Supporting this observation, another investigator in our laboratory (Dr Piowtroska) observed no ROS-production following Dox treatment in cardiomyocytes. In her experiments, she used the dye

CM-H2DCFDA (DCF). DCF is a fluorescein diacetate probe sensitive to ROS-species (Kristiansen et al, 2009; King and Oh, 2004). In Dr Piowtrowska's experiments, cardiomyocytes were loaded with 8.5 µM DCF after incubating with 7.5 µM Dox for 4 hours or 18 hours, and DCF-fluorescence analysed using a 488 nm Argon laser in a Leica SP5 confocal microscope equipped with ×20 oil immersion objective lens (numerical aperture 1.0). As control, cardiomyocytes were incubated in medium 199 only. She observed no significant differences in the fluorescence of DCF after Dox treatment compared to control (Dr Piowtroska, personal communication). This supported the suggestion we draw from cell-death analyses that doxorubicin-mediated cardiomyocyte death in the particular model we explored was independent of ROS-species mediated toxicity.

In support of our observations, ROS-independent cell-death pathways have been implicated in Dox-toxicity. For example in H9C2 cardiomyoblasts, Ma et al (2013) observed doxorubicin-induced changes in p53-acetylation and histone deacetylases HDAC inhibition that were not affected by NAC treatment, despite reduction in DNA fragmentation and caspase 3 activation (Ma et al, 2013) in response to ROS-scavenging by NAC. p53-acetylation has been observed to promote apoptosis in previous reports (Zhang et al, 2011b; Yuan et al, 2011) This indicates that Dox could activate different cell-death pathways that maybe dependent and independent of ROS, and these may co-exist. This is important, since a number of *in vivo* models of Dox toxicity have utilised large bolus doses to induce cardiotoxicity (e.g., Zhang et al, 2012; Wang et al, 2012). As mentioned in an earlier section, necrotic or apoptotic pathways of cell-death may predominate depending on the concentration of Dox used, and it ought to be highlighted that apoptosis itself may lead to ROS generation (Montaigne et al, 2012). Further highlighting the ambiguity of the role of ROS-species, in *in vivo* rodent models, chronic dosing regimens of Dox has previously been reported to *increase* the myocardial antioxidant activity measured by total antioxidant performance (Ferreira et al, 2007), indicating that ROS generation due to

anthracycline treatment may be more complex than a causal effect of drug administration. Small scale observational studies in humans had previously reported acute *decrease* in cardiac lipid peroxidation in response to Dox infusion, as estimated by the levels of lipid conjugate di-enes (Minotti et al, 1996). Moreover, in clinical practice, the use of ROS-scavengers, e.g. NAC and alpha-Tocopherol, have failed to protect against the cardiotoxicity of anthracyclines (van Dalen et al, 2011). This highlights that the role for ROS-species as a critical mediator in Dox mediated cardiotoxicity is still unclear. In this context, the data described in this report indicates that ROS-independent death pathway may have a role in the model of Dox-toxicity we characterised. Reports investigating the cardiotoxicity of Dox may describe the presence of ROS-species in cardiomyocytes after Dox treatment as reflective of- or a marker- of a pathological process (Zhang et al, 2012). The results we observed suggest a requirement for caution in interpreting such data and in correlating the presence of ROS to cell-death levels.

5.3.2. Doxorubicin does not to alter resting mitochondrial transmembrane potential in cardiomyocytes *in vitro.*

Having established that ROS-scavenging did not rescue cardiomyocytes from doxorubicin-induced cell-death, we explored the role of other potential pathways in the cardiomyocyte-death due to Dox in the model of cell-death. Anthracyclines treatment in rodent models have been shown to alter the mitochondrial bioenergetic pathway, for example by reduced activity of the mitochondrial genome-encoded components of respiratory chain (Lebrecht et al, 2010), and by inhibition of the proteins that drive the proton-motive force and ATP generation, e.g., mitochondrial NADH and Succinate dehydrogenase protein, as well as the function of the Mg^{2+}-dependent F_1F_0-ATPase (Berthiaume et al, 2007). Dox therefore has been postulated to lead to loss of the proton-motive force that drives ATP generation. Rapid decline in the mitochondrial transmembrane potential ($\Delta\Psi_m$) has been reported in *ex vivo* models, e.g., within in 1 hour in

Langendorff-perfused rat hearts as observed by Montaigne et al (2010) in response to 1 µM Dox, or in murine cardiomyocytes within 72 hours after administering a bolus 25 mg/kg of dose of Dox *in vivo* (Zhang et al, 2012). $\Delta\Psi_m$ collapse may occur in response to a number of pathological mechanisms, including in particular Ca^{2+} overload and ROS-species generation. Collapse of $\Delta\Psi_m$ is a mechanism of induction of cell-death, e.g. by release of Cytochrome C. We therefore considered the hypothesis that fall in $\Delta\Psi_m$ may have a role in the toxicity we observed in response to Dox in this *in vitro* model of doxorubicin-toxicity.

In the experiments described, we used TMRM as an agent to report $\Delta\Psi_m$. A number of dyes have been used to investigate the transmembrane potential, which are as a class lipophilic and accumulate in the mitochondria according to the Nernst potential (Perry et al, 2011). This includes the compounds Rhod123, JC-1, Dioc6, TMRM and TMRE, each with its advantages and weaknesses. Rhod123 was considered unsuitable for our experimental aims, since dye aggregation and consequent quenching of fluorescence at higher probe concentrations holds the possibility of aberrant depolarization of $\Delta\Psi_m$. Further, Rhod123 has been previously shown to inhibit mitochondrial respiration more than TMRM (Scaduto and Grotyohann, 1999). Similarly, JC-1 reports $\Delta\Psi_m$ as a dual-colour, ratiometric assessment of the monomeric to the aggregate forms, but is highly sensitive to probe loading concentrations. Moreover, it is highly photosensitive, and in the aggregate form is slowly permeant, requiring time typically in the order of 90 minutes to reach equilibration in cardiomyocytes (Mathur et al, 2000), which we considered unsuitable for experimental purposes. DiOC6 was considered unsuitable since beyond extremely low concentrations in the order of 1 nM, the dye may be toxic to mitochondrial respiration and, moreover, may erroneously estimate transplasmalemmal potential rather than transmitochondrial potential (Rottenberg and Wu, 1998). The ethyl and methyl esters of tetramethylrhodamine (TMRE and TMRM respectively), for comparison, equilibrate rapidly across the cardiomyocyte in the order of 15 minutes, and was therefore

considered the most suitable probes. TMRM was used in preference to TMRE since it offered the lowest potential for inhibiting mitochondrial respiration when used at a concentration below 0.5 μM (Scaduto and Grotyohann, 1999). At nanomolar concentrations (1-30 nM), TMRM aggregates within the mitochondria, and consequent fluorescence provides an accurate assessment of the pre-existing $\Delta\Psi_m$ (Perry et al, 2011). We therefore used a low concentration (30 nM) TMRM and estimated the optical fluorescence using 10% intensity incident He-Ne laser to report the transmembrane potential.

As an initial characterisation experiment, we confirmed that 30 nM TMRM fluorescence decreased in both control and Dox treated cells in response to 200 nM FCCP. FCCP is a mitochondrial uncoupler and leads to loss of $\Delta\Psi_m$, with consequent decrease of the fluorescence of TMRM in the nanomolar concentrations we used (Joshi and Bakowska, 2011). This loss of fluorescence upon treatment with an uncoupler was used as a confirmation that TMRM fluorescence was dependent on mitochondrial accumulation, and therefore dependent on $\Delta\Psi_m$ in this model. Further, the fluorescence post-depolarisation was similar across all three treatment times in both Dox-treated cells and control, which allowed us to conclude that TMRM loading and optical fluorescence was not influenced by the presence of Dox itself. It ought to be highlighted that in cells treated with Dox for 4 hours (Dox 4 and corresponding control Cont 4), the initial mean 30 nM TMRM fluorescence was noted to be markedly lower in both Dox 4 h as well as control, compared to the cardiomyocytes treated for 30 minutes (Dox 0 and Cont 0), as well as 18 hours (Dox 18 and Cont 18). A wide variation was also noted in the baseline fluorescence, which persisted in the first 20 seconds beginning with introduction of 200nM FCCP (Fig. 5.3, panel B). The reason for this is unclear, but may reflect the low number of repeat experiments from which the data is collected (*n*=2), particularly given that this variation was not noted in the two other groups; the variation appeared to settle in the subsequent 60 seconds; and that fluorescence values later in the decaying trend approached

and reflected the values observed in the other two time groups. A larger sample size would have increased the robustness of this experiment, and ought to be considered in similar future experiments.

In subsequent experiments, we pre-treated cardiomyocytes with Dox for 30 minutes (Dox 0), 4 hours (Dox 4) and 18 hours (Dox 18) and analysed the differences in optical fluorescence of TMRM compared to control groups. However, these experiments did not detect any significant differences in the $\Delta\Psi_m$ amongst the different treatment groups. The results are collated from six repeat experiments (*n*=6) which, although not pre-calculated, was guided by acceptable sizes and commonly reported numbers in literature. Further, possible wash-off of dead cells from laminin attachments during the process of buffer exchanges during probe loading may yield artefactual false results. We had previously analysed differences in total cell-count after Dox treatment and PI introduction during the development and characterisation of the model of Dox toxicity (fig. 4.5.), and found no significant differences in cell count relative to control groups. This allowed us to conclude with confidence that Dox treatment did not influence $\Delta\Psi_m$ in this *in vitro* ARVM model.

$\Delta\Psi_m$ has been previously reported to fall in response to Dox by other authors. For example, Fisher et al reported a fall in $\Delta\Psi_m$ in cultured adult mouse ventricular myocytes using the JC-1 dye following 18 hours incubation with 1 µM Dox (Fisher et al 2005). Similarly, Dox-treatment in *ex-vivo* models in isolated, Langendorff-perfused, rat hearts (Montaigne et al, 2010) as well as cardiomyocytes isolated from mice following *in vivo* treatment with Dox (Zhang et al, 2012) showed a decline in resting $\Delta\Psi_m$. One explanation for these differences in observations may be the differences in experimental set ups. Montaigne et al used an *ex vivo* model, perfusing intact hearts in a Langendorff model. They used a lower concentration (1 µM doxorubicin) for a shorter time-period (1 hour), and measured the epicardial fluorescence of JC-1 dye aggregates

to estimate mitochondrial transmembrane potential semi-quantitatively. It is worth noting that at a similar dose-range in this isolated cardiomyocyte model, we do not observe any discernible differences in cell-death which led us to conclude that 1 µM Dox did not inflict any substantial injury. Similarly, Zhang et al (2012) isolated murine cardiomyocytes 72 hours after a large bolus dose of 25 mg/Kg intraperitoneally. They too used JC-1 dye, and observed a decrease in $\Delta\Psi_m$ (Zhang et al 2012). It is worth highlighting that the dose used by Zhang et al is several folds higher than what may be used physiologically in humans. Further, we used TMRM rather than JC-1 to measure $\Delta\Psi_m$. As explained above, aggregate (i.e., red) JC-1 equilibrates slowly across the cardiomyocyte and further the fluorescence is highly sensitive to probe loading concentrations and loading times. Furthermore, the fluorescence may change independently of $\Delta\Psi_m$ under some circumstances, e.g. by surface to volume ratio (Perry et al, 2011). These factors ought to be considered when analysing the differences of our findings compared to other groups. The results however indicate alterations of the mitochondrial transmembrane potential is not a mediating factor in induction of cell-death. It ought to be emphasised in this section however, that the data described do not allow any conclusions to be drawn regarding the mitochondrial energetic state, since $\Delta\Psi_m$ is influenced by the net gradient of ionic species across the mitochondrial membranes, but the proton gradient may be maintained or even increased without any changes in the $\Delta\Psi_m$, for example due to accumulation of cationic-species within the cytoplasm (Perry et al, 2011).

5.3.3. Influence of doxorubicin treatment on mPTP transition *in vitro.*

Our results described above indicated that dissipation of $\Delta\Psi_m$ was not involved in the cell-death we observed in this model, leading us to explore the role of other possible mechanisms of cell-death to explain cardiomyocyte toxicity observed. Opening of the mitochondrial permeability transition pore (mPTP) is considered a final event in induction of cellular death pathway, or the "point of no return" in cell-death. The mPTP had previously been reported to be involved in the

induction of cardiomyocyte death in heart failure in murine models of pressure overload (Elrod et al, 2010). Further, known pore-induction stimuli include Ca^{2+}-overload within the mitochondria, and doxorubicin-treatment has been shown to alter Ca^{2+} regulating proteins including SERCA2A and RyR. Furthermore, an increased sensitivity to induction of mPTP opening is noted in rats treated with Dox (Ascensão et al, 2010). We therefore hypothesised that an increased sensitivity to induction of mPTP could be a mechanism of cell-death in this model, which we explored in the subsequent experiment.

For reasons discussed above, TMRM was used as a reporting agent in this experiment exploring mPTP transition. We used a higher concentration of 3 µM of TMRM in these protocols. At these high concentrations TMRM is used in a dequenching mode, whereby accumulated dye within the mitochondria in the polarised state is released into the cytosol upon depolarisation, leading to unquenching of fluorescence. The collapse of the transmembrane potential which occurs on mPTP depolarisation is reflected by a non-linear increase in the fluorescence intensity of the probe. In the final state of the pore reaching a freely-permeant state, fluorescence intensity of TMRM plateaus as the probe is released into the cytosol. The added advantage of TMRM in experimental design was that at micromolar concentrations, TMRM further functions as a photosensitiser of ROS generation when subjected to high intensity laser, and therefore provides a source of oxidative stress that may induce the mPTP to reach the freely permeant "open" state. Measuring the fluorescent intensity versus time therefore provides a reflection of the rate of depolarisation, and therefore allows identification of increased vulnerability of the pore to reach the permanently open state by comparison of time taken to mPTP transition between different treatment groups. This experimental setup has been reported in our lab before (Hausenloy et al, 2003a; Davidson et al, 2006).

We used a higher intensity of 40% He-Ne laser to elicit TMRM fluorescence and generate oxidative stress. We used Ciclosporine A (CsA) as a positive control to inhibit the mPTP transition. CsA has been shown previously to bind to the Peptidyl Prolyl *cis-trans* isomerase Cyclophilin D (Cyp D) with high affinity, and is to date the most specific inhibitor of Cyp D known (Rao et al, 2014). CsA acts as a "desensitiser" of the pore transition, rather than blocking pore induction altogether (Bernardi et al, 2006; Halestrap and Richardson 2015), and mPTP transition in the presence of CsA requires higher levels of induction stimuli, e.g. Ca^{2+}. We used CsA at a 1 µM concentration, which has been reported previously to offer robust protection against pharmacological induction of mPTP in isolated ARVM models investigating heart failure (Xu et al, 2016).

5.3.3.1. Doxorubicin treatment does not increase increase time taken to mitochondrial permeability pore transition.

We identified no differences in the time to mPTP transition between Dox-treated cardiomyocytes and control. Surprisingly, CsA increased the time to pore induction in control cells only, but not in Dox-treated cardiomyocytes. The experiments were repeated to a total sample size of seven (*n*=7), which in the context of an *in vitro* experimental set up is a sample size large enough to draw very confident conclusions. The results are therefore interesting, since these observations are different from those reported by other groups in *in vitro* experiments (Gharanei et al, 2013a and 2013b), in *ex vivo* models (Montaigne et al, 2010), as well as in *in vivo* models (Marechal et al, 2011). For example, Marechal et al observed an increase in Ca^{2+}-induced mPTP transition *in vivo* with doxorubicin, administered both as a large-dose bolus as well as in an interrupted dosing models. The authors noted this response of mPTP induction to be abrogated by co-administration of 1mg/kg CsA. Similarly, Gharanei et al observed a protection from mPTP transition reported by 3 µM TMRM fluorescence dequenching when 0.2 µM CsA was used in conjunction with doxorubicin-treatment (Gharanei

et al, 2013a). Several explanations may be considered to account for these differences. The experimental set up we used differed in a number of ways from those used by other groups. For example, Gharanei et al (2013a) estimated mPTP induction using 3 µM TMRM, but they subjected primary adult rat cardiomyocytes to 10 mins of 1 µM Dox treatment after incubating cells overnight prior to transferring to laminin coated surface. The differences in timing of seeding to laminin plate and the consequent differences in cytoskeletal feedback signalling (Ross and Borg, 2001; Langenbach and Rando, 2002) maybe one explanation for the differences between the results we observed and those of Gharanei et al. Similarly, Montaigne et al (2010) measured the epicardial fluorescence of mitochondrial dye JC-1 following 60 min of 1 µM Dox infusion in isolated perfused rat hearts. As explained above, aggregate (i.e., red) JC-1 fluorescence is sensitive to probe loading concentrations and times, and may change independently of $\Delta\Psi_m$ under some circumstances. The findings we describe suggest it may be informative to re-explore the mPTP induction times with more than one reporting dye, e.g. Rhod123 in addition to TMRM, as this may allow greater clarity and more robust data on which to draw conclusions and reconcile the differences in these observations.

A further interesting result stands out from these experiments. The positive control CsA was able to desensitise the mPTP to induction stimulus in control cardiomyocytes only, but not in Dox treated cells. This is interesting, since this shows that the protective effect of CsA is abrogated in Dox-treated cells. We are not aware of similar observations having been reported before. Two hypotheses ought to be considered. We used 1 µM CsA, which has been used to evaluate mPTP induction by other groups before in *in vitro* in ARVM models of chronic drug-induced toxicity (Xu et al, 2016). This concentration offered robust protection from mPTP-induction assessed by Ca^{2+}-induced swelling. In our own lab 1 µM CsA has been used in *in vitro* experiments, estimating mPTP induction in murine cardiomyocytes, and identified robust protection (Dongworth et al, 2014). However, it ought to be highlighted that in *ex vivo* models

of IR-injury, protection against reperfusion injury is observed with 200 nM but not 1µM CsA (Griffiths and Halestrap, 1993). A narrow therapeutic window of 200-400 nM concentration has been reported in *in vitro* models of IR-injury using female SD rat ARVMs in the past (Nazareth et al, 1993). Moreover, CsA itself may cause toxicity in cardiomyocytes, which has been attributed to elevation of intracellular Ca^{2+} through the Ca^{2+} sensitive receptor (CsR), albeit at concentrations 3 to 8-times higher than those used in our experiments (Florio et al, 2003; Tang et al, 2011). Further, daunorubicin-treated rabbit models show altered intracellular Ca^{2+}-regulatory proteins, e.g. SERCA2A and 2B, RYR2 and Calsequestrin (Stěrba et al, 2011), which is likely to reflect a class-specific effect. Since Ca^{2+} is a known pore induction stimulus, and mitochondrial Ca^{2+} uptake through the Ca^{2+}-uniporter is dependent on the electrochemical gradient of Ca^{2+}, the hypothesis ought to be considered that the time taken to mPTP induction in the presence of CsA after Dox pre-treatment is a reflection of a compensation, where protection of the mPTP by CsA (as observed in control) is masked by a decrease in pore-induction time due to Ca^{2+} overload in the mitochondria. This hypothesis may be investigated further using Ca^{2+} sensitive dyes (eg, Fluo-4) to identify free cytosolic Ca^{2+}, e.g., after Dox treatment and after introducing CsA.

A second hypothesis that may explain the results we observed includes modification of the CsA-sensitive structure in the mitochondria. The mitochondrial receptor for CsA is Cyp D, which it binds with high affinity (K_D=13.4nM) (reviewed in Halestrap and Richardson, 2015; Gutiérrez-Aguila and Baines, 2015; Bernardi and Di Lisa, 2015). It is possible therefore that the attenuation of the protective effect of CsA in Dox pre-treated cells is due to alterations of Cyp D. Whether this alteration is at the level of gene expression, mRNA translation, protein degradation, or post-translational modification is impossible to deduce without further work. Estimation of gene expression and estimation of protein content may be carried out using widely used techniques, e.g. PCR and Western blotting respectively. However, interestingly, the structure

and function of Cyp D ought to be considered briefly when considering post-translational modifications that may explain these observations. In the suggested model of the mPTP induction, Cyp D has been suggested to interact with inorganic phosphate carrier (PiC) and adenine nucleotide translocase (ANT) in the assembled mPTP complex (Halestrap and Richardson, 2015), and interact with the lateral stalk of the F_1F_0-ATP synthase in the mPTP (Javadov and Kuznetsov, 2013) and inhibits the enzymatic activity of the complex. CsA binding to Cyp D leads to dissociation of Cyp D from ANT and PiC (Halestrap and Richardson, 2015), and further restores the enzymatic activity of the F_1F_0 complex (Giorgio et al, 2009). In the context of post-translational control of Cyp D function, it is worth highlighting that CsA binding site in Cyp D is a highly conserved α-helix, termed the CsA binding domain (CSBD). Analysis of Cyp D molecular structure reveals a lysine residue (K166) which lies stereochemically adjacent to the CSBD and is highly conserved from yeast to humans. K166 is deacetylated by the mitochondrial HDAC Sirtuin-3 (Sirt-3), and has been postulated to be a potential mechanism for regulating the mPTP protective function of Cyp D. Sirt-3 null mice show an increased vulnerability to Ca^{2+} induced swelling at 16 months, but not 3 or 6 months age (Haffner et al, 2010). For comparison, we used SD rat as a source of cardiomyocytes within a 150-450g weight range, which falls in a typical maximum age of 3 months (Brower et al, 2015). Interestingly, in cell-line models, Dox treatment has been observed to attenuate Sirt-3 expression in H9C2 cardiomyoblasts, which has been linked to dysfunction of the mitochondrial bioenergetic pathway (Cheung et al, 2015). Further, a role for Sirt-3 mediated deacetylation has been suggested for regulating a number of proteins of the mitochondrial ATP generating pathway including Acetyl CoA synthetase isoforms (ACeS2), Succinate dehydrogenase, Isocitrate dehydrogenase, NDUFAA9 (Pillai et al, 2010), many of which have been found to be attenuated at gene expression or protein expression levels in animal models of Dox toxicity (Khiati et al, 2014). Importantly, Dox treatment has further been described to directly deplete Sirt-3 both in *in vitro* as well as *in vivo*

models of Dox cardiomyopathy (Pillai et al, 2016). Therefore, a hypothesis ought to be considered that the results we observed may be explained by altered post-translational modification of cell-survival or of bioenergetic pathways as a consequence of Sirt-3 inhibition in this ARVM model. It may therefore be hypothesised that similar post-translational modification—specifically, acetylation of Cyp D— may be responsible for the abrogation of CsA-dependent mPTP protection that we observe in this ARVM model. This hypothesis maybe investigated by exploring the acetylation status of Cyp D, and indeed of other targets of Sirt-3-mediated deacetylation, after subjecting cardiomyocytes to Dox treatment as described in the model. Antibodies against acetylated-Lysine are commercially available, and this may be considered a potential future course of experiments.

5.3.3.2. Co-incubation with Ciclosporine A does not protect cardiomyocytes from doxorubicin-toxicity.

In light of the results discussed in the preceding section, we re-explored the cell-death in the model in the presence of both Dox and 1 µM CsA. In our previous experiment, the positive control CsA was introduced concomitantly with probe loading, *after* pre-treating cardiomyocytes with Dox for 18 hours. We considered the hypothesis that post-translational alterations to Cyp D leads to altered CsA binding, and explains the abrogation of CsA-mediated mPTP-protection in Dox pre-treated cells. Previous reports show post translational modifications of Cyp D, e.g. in sirt-3 knockout mice, renders the mPTP more prone to induction stimuli in aged rats, and the presence of CsA rescues the mPTP from this vulnerability (Haffner et al, 2010). Therefore we explored if the presence of CsA throughout the doxorubicin-exposure period reduced cell-death, which may indicate vulnerability of the pore as a factor in cell-death, and allow clarification of the data described above which suggested no excess vulnerability towards mPTP induction after doxorubicin-treatment. Conversely, to explain the abrogation of CsA-induced mPTP protection in Dox pre-treated cells, we further considered a hypothesis that

CsA may induce cytosolic and consequently mitochondrial Ca^{2+} overload in doxorubicin-stressed cells. Therefore, this experiment also allowed us to explore if 1 µM CsA was independently toxic in this model, and whether presence of CsA exacerbated cardiomyocyte injury secondary to doxorubicin.

As shown in fig. 5.6, we failed to identify any significant differences in cardiomyocyte death due to Dox alone, and cell-death due to co-treatment of Dox and CsA. We concluded from this experiment that presence of CsA offered no benefit against doxorubicin-induced injury, and therefore the mechanism of cell-death is likely to be independent of any increase in the vulnerability to mPTP transition. Further, the presence of CsA did not exacerbate Dox injury and CsA alone did not show any significant toxicity. We therefore concluded that the abrogation of CsA-responsive pore protection that we observed in Dox pre-treated cells is unlikely to be due to balances in ion fluxes, e.g. Ca^{2+}. The results discussed above are collated from seven repeat experiments (*n*=7), which allows considerable confidence in the results we observed. Our results differ from those noted by other groups. For example, Marechal et al (2011) noted a protection against the toxicity of Dox *in vivo* both after acute bolus injection (10mg/kg doxorubicin), as well as in an interrupted dosing model when CsA was administered (1mg/kg) in mice. The authors observed protection from Dox-induced ventricular dysfunction, as well as preservation of mitochondrial bioenegregtics, preserved transmitochondrial potential, and protection from Ca^{2+} induced mPTP transition. Similarly, Gharanei et al (2013a) demonstrated an exacerbation of the injury due to ischaemia-reperfusion in the presence of 1µM Dox in isolated rat Langendorff-perfused hearts, as well as in ex vivo papillary muscle contraction models. The presence oft of CsA (0.2 µM) abrogated this excess injury. Conversely in an *in vitro* model using H9C2 cardiomyobloasts, Merten et al (2006) were able to inhibit of Dox-induced calcineurin signalling with 100nM CsA, but were unable to prevent Dox-induced hypertrophy, which the authors demonstrated to be due to activation of the PI3K/Akt pathway. This

highlights that multiple protein-signalling cascades may be activated by anthracycline-treatment, and the pathological effect of the respective cascades ought to be correlated to the model under investigation. It ought to be highlighted that we did not include a separate positive control, with cell-death due to 1 µM CsA serving as an internal positive control. It may be argued that a dose-response study of cardiomyocyte-death due to CsA, and use of a toxic dose of CsA (if any) as a positive control may make the experiment more robust, and would allow better understanding and characterisation of the independent effect of CsA in the *in vitro* isolated cell-model we have used, and therefore allow a better interpretation of the effect of CsA on Dox-toxicity in our model. This may be explored in future work. Furthermore, to explore if Ca^{2+} signalling or overload is a factor in the toxicity of doxorubicin, in this *in vitro* approach, directly imaging free Ca^{2+} with Ca^{2+} probes may offer more clarity. These maybe considered limitations of this experiment, and future experiments particularly investigating the role of Ca^{2+} in this model of Dox-toxicity needs to include direct visualisations of ionic Ca^{2+} and explore the activation status of known Ca^{2+} signalling cascades induced by doxorubicin.

It is necessary to highlight that CsA interacts with other Cyclophilin molecules e.g. Cyp A, and inhibits Calcineurin signalling, which is a potential compounding factor (Bernardi and Di Lisa, 2015). Re-exploring cell-death and mPTP induction due to Dox in the presence of a different pore-protecting agent, Bongkrekic acid or Sanglifehrin A (SfA), may therefore offer more insight into the role of the mPTP in Dox cardiotoxicity. We did not use Bongkrekic acid due to its potential for inhibition of oxidative phosphorylation (Malekova et al, 2007). SfA and CsA both bind Cyp D with similar affinity, but SfA offers an advantage in avoiding activation of potential confounding factors, e.g. Calcineurin inhibition (Hausenloy et al, 2012) and maybe considered a suitable mPTP protective agent if the role of mPTP induction is re-explored in this model of Dox cardiotoxicity.

5.3.4. Hypoxic preconditioning protects against doxorubicin-induced cardiomyocyte death.

As mentioned earlier in introduction, Dox has been observed to modulate the signalling cascades PI3K/Akt and the MAPK ERK 1/2 cascades which are induced by HP. The exact role of these cascades in the toxicity of anthracyclines is far from clear, with some evidence, e.g., from *in vitro* cardiomyoblast cell-lines (Merten et al, 2006), *ex vivo* models (Deres et al, 2005, Gharanei et al, 2013) and *in vivo* approaches (Ichihara et al, 2007) noting an induction response. Conversely, other groups have noted attenuation responses to PI3K/Akt consequent to Dox-treatment, e.g., in *in vivo* rodent models, which has been correlated with symptomatic heart failure (Lou et al, 2005). Similarly, MAPK ERK 1/2 has been described in some experiments to play an injurious role, with data from, e.g., *in vitro* experiments using cardiomyopblast cell lines indicating a role in induction of apoptosis through the p53-mediated death pathway (Liu et al, 2008). Data from *ex vivo* models support the evidence of phosphorylation induction of MAPK ERK 1/2 as a consequence of Dox treatment, although the role this activation plays is unclear (Ghanaranei et al, 2013b). Contrasted with these repots, *in vitro,* neonatal rat cardiomyocytes display an induction of apoptosis on Dox treatment when ERK 1/2 is selectively inhibited (Zhu et al, 1999), while the potentiation of both MAPK ERK 1/2 (Su et al, 2006) as well as PI3K/Akt (Kitamura et al, 2014) has been observed to offer protection against doxorubicin-induced cardiac injury. Since both the PI3K/Akt and MAPK ERK 1/2 cascades are known to be activated by HP and exert a cardioprotective effect in IR-injury, we explored if HP could protect against the cardiotoxicity induced by doxorubicin. In the model of toxicity described, we had identified the second window of preconditioning (SWOP) as the most suitable pathway which may be capable of protecting against doxorubicin-induced toxicity. Importantly, although the key mediators and pathway in SWOP are still unclear, a key role is described for both PI3K as well as MAPK ERK 1/2. For example, inhibiting PI3K with the irreversible inhibitor Wortmannin abrogated SWOP in *in vivo* rabbit models of IR-injury (Kis et al, 2003; Raphael and Gozal, 2005).

Similarly, the delayed preconditioning effects of opioids have been linked to the activity of MAP Kinases p38 as well as ERK 1/2 (Fryer et al, 2001), while inhibiting PI3K and ERK 1/2 has been observed to abrogate pharmacologically induced SWOP in *ex vivo* murine models of IR-injury (Bell et al, 2005). The timescale of protection indicates this is likely to be mediated by alteration of protein synthesis. Therefore, we hypothesised that an early induction of the RISK proteins immediately prior to introducing Dox would offer a protection against cardiotoxicity of Dox in the timescale of cell-death that we observed in this model.

Consistent with this hypothesis, we found that HP protected cardiomyocytes against toxic concentrations of Dox. Cell-death in unprotected control cells showed a dose-dependent rise with increasing concentrations of doxorubicin, as was observed in previous characterising experiments, and was therefore internally consistent with previous data. The results were obtained from 5 repeat experiments (n=5). It ought to be re-iterated that in preceding experiments, we had not observed any role of oxidative stress or of mPTP induction in mediating cell-death due to doxorubicin. It may therefore be concluded that the protection offered by HP and indeed by SWOP is independent of any putative role HP may have against pathological oxidative stress, or of a role in protecting against mPTP induction (Hausenloy, 2013a). In this report, we have not investigated the redox state or the function of the mitochondrial respiratory chain. Further, we have not investigated the balance of pro-apoptotic and anti-apoptotic proteins of the BCL family or the status of p53 enzyme. These are potential pathways which may be influenced by both PI3K/Akt and by MAPK ERK 1/2.

Although direct myocardial preconditioning may be impractical in mitigating anthracycline-cardiotoxicity, the findings from the above experiments are interesting since various modes of preconditioning are possible without direct injury or access to the myocardium. Of particular note in this regard, remote ischaemic preconditioning (RIPC), where an ischaemic stimulus is

applied to a distal muscular organ, e.g., peripheral muscles or limb, have been observed to activate the RISK cascade and offer similar protective influence and, indeed, was observed to lower peak delayed troponin rise in myocardial infarction treated with thrombolysis (Yellon et al, 2015). Further, exercise, which may induce similar recurrent transient hypoxia in peripheral musculature as well as promote anaerobic adaptation in the myocardium, has been suggested to hold a preconditioning potential similar to remote ischaemic preconditioning in protecting against IR-injury (Powers et al, 1998). Interestingly, previous reports exploring cardioprotective strategies against anthracyclines note a role for aerobic-exercise induced preconditioning in cardioprotection against anthracycline-injury (Chicco et al, 2006a and 2006b, Hydock et al, 2008). For example, Hydock et al (2008) reported a protective effect of aerobic-exercise preconditioning against doxorubicin-induced left ventricular function deterioration *in vivo* as well as in isolated-perfused hearts in rats subjected to a bolus-regimen of toxicity of Dox. Subsequent work indicates this may in part be due to reduced cardiomyocyte-accumulation of Dox (Jensen et al, 2013). Exercise-induced preconditioning has also been suggested to upreguate myocardial levels of manganese superoxide dismutase (MnSOD) (Yamashita et al, 1999; Marini et al, 2007). This is interesting, since levels of MnSOD has previously been observed to further correlate with delayed ischaemic protection, or the second window of protection (SWOP) (Hoshida et al, 2002). This highlights that the protection against anthracycline-injury in cardiomyocytes activated by HP, RIPC and other cardioprotective interventions including exercise may be translated into clinical applications with a better understanding, particularly, of the molecular pathways activated in SWOP.

5.3.4.1. Investigating hypoxic preconditioning induced RISK pathway against doxorubicin toxicity.

SWOP is postulated to be mediated by a number of putative and confirmed signalling cascades including the components of RISK (PI3K/Akt and MAPK ERK 1/2), as well as other parallel and

interdependent pathways e.g. nitric oxide signalling, tyrosine kinases, and protein kinase C (PKC) (Hausenloy, 2013a). We therefore explored the relevance of PI3K/Akt and MAPK ERK 1/2 in protecting against Dox-cardiotoxicity by inhibiting the respective signalling cascades. We used the molecule LY294002 to inhibit PI3K/Akt, and PD98059 to inhibit MAPK ERK 1/2. A number of inhibitors of PI3K/Akt have been studied, including Wortmannin, LY294002, Quercetin, as well as derivatives of these compounds (McNamara and Degterev, 2011). Both Wortmannin and LY294002 has been used in our lab and are well studied (Bell and Yellon, 2003). However, Wortmannin is relatively nonspecific with broader cross-reactivity, and further it is more unstable and toxic in animals, limiting the potential for any future *in vivo* work. We therefore used LY294002 as an inhibitor of PI3K/Akt, at a working concentration of 10 μM, which has been reported in literature to offer potent attenuation of Akt phosphorylation (Aikawa et al, 2000). Similarly, we used the MEK1 inhibitor PD98059 as an inhibitor of MAPK ERK 1/2 phosphorylation since, of multiple kinase inhibitors, it is the most specific kinase inhibitor (Davies et al, 2000).

In these experiments using cell-death as a measure of Dox-toxicity, we observe that inhibition of PI3K/Akt pathway with LY294002 abrogated the protective effect of HP, but inhibition of the MAPK ERK 1/2 appeared to exert no discernible effect on HP-induced protection. This suggested that the protective effect of HP against Dox-toxicity required the activation of the PI3K/Akt signalling cascade. It ought to be highlighted that we did not use a separate positive control, e.g., insulin which may have served the role of a known inducer of PI3K/Akt and of MAPK ERK 1/2. In this context, the lack of any effect on HP-induced protection that is observed despite the presence of PD98059 is difficult to interpret. The suggestion may be raised that activation of MAPK ERK 1/2 had no role in the conferring the protection that was observed with HP, but require confirmation of phosphorylation induction of the ERK 1/2 pathway, which was not possible due to the lack of a positive control. The results we noted reflect the observations

of five repeat experiments (*n*=5). Of note, our results reflect the suggested protective role of activation of PI3K/Akt pathway against Dox-toxicity noted in wider literature. For example, Taniyama and Walsh (2002) had previously observed a protective effect using adenovirus-mediated consitutively active Akt in a rodent model of Dox-toxicity, whereby potentiating Akt pathway protected against deterioration of fractional shortening, decline in left ventricular dysfunction, and decline in cardiac mass. Similarly, Fu et al (2007) had previously reported a role for PI3K/Akt induced by Erythropoietin (Epo) in protecting neonatal rat ventricular myocytes (NRVMs) against the toxicity of Dox *in vitro*, but not MAPK ERK 1/2. In their report, Fu et al were able to abrogate the protection of Epo using 50 µM LY294002. By comparison, we used a lower concentration of LY294002 (10µM) to inhibit PI3K/Akt in the experiments, which is towards the lower end of a working concentration 1-100 µM. The protective role for HP-induced PI3K/Akt suggested by the cell-death data we observed, further, is consistent with the previously reported effect of potentiating PI3K pathways *in vivo*. For example, Kitamura et al (2014) observed that deleting ARIA (apoptosis regulator through modulating IAP expression), a plasma-membrane recruiter for the PI3K-phosphatase phosphatase and tensin homologue (pTEN) protein, protected against Dox-induced cardiac dysfunction and death in a murine model. However, these reports ought to be contrasted with the reported observations and role of PI3K/Akt phosphorylation-induction noted by other groups in Dox-toxicity. For example, as explained earlier, Merten et al (2006) had noted a phosphorylation response for protein kinase B (PKB), a downstream mediator of Akt. The authors noted an Akt-dependent hypertrophic response in cultured H9C2 cardiomyoblast derived cell lines, which they deemed to be reflective of a pathological response. In their experiments, Merten et al exposed the cardiomyoblasts to 1 µM Dox for upto 2 hours, and noted that the hypertrophic response could be abrogated by 20 µM LY294002. For comparison, we used an isolated adult rat ventricular myocyte model, and exposed these cells to 7.5µM Dox for 18 hours. Moreover, as discussed in

the next section, upon Western blotting we observed no evident Akt phosphorylation response in the after-sequence of Dox-treatment at time points of 15 minutes, 4 hours and 18 hours in this ARVM model. This differs from the sustained Akt phosphorylation that Merten et al observed for upto 360 minutes following exposure to Dox in their cardiomyoblast cell-model. The differences in the experimental set up, particularly the differences between a proliferating cardiomyoblast model and a terminally differentiated ARVM model may be a possible explanation, but this requires further experimental work and direct comparison under controlled conditions. This was beyond the scope of our current report. In a different experimental set up, Deres et al (2005) reported Akt phosphorylation-induction when isolated Langendorff-perfused rat hearts were subjected to 100 µM Dox for 60 minutes. The authors hypothesised this phosphorylation to be a possible response to activation of the kinase via nitration of tyrosine residues of receptor tyrosine kinases, secondary to reactive oxygen and nitrative species generation. Supporting this hypothesis, Akt phosphorylation in these experiments could be abrogated by concomitant perfusion with 200 µM dihydrolipoamide, an antioxidant. Similarly, Ichihara et al (2007) had noted increased phosphorylation of Akt in an *in vivo* model of toxicity, which could be inhibited by the administration of superoxide dismutase. It ought to be highlighted that in the model we characterised, we used a concentration of 7.5 µM Dox, significantly lower than that used by Deres et al. Moreover, the experiment we conducted exploring the role of N-acetyl cycsteine against doxorubicin-toxicity failed to show any protective effect, raising the suggestion that in the model we analyse, reactive oxygen specied may have a limited role in pathogenesis and induction of cell-death (discussed above). It is important to highlight that PI3K/Akt induction may be a stress response, and may serve to stabilise against mitochondrial fission. For example, in their 2013 report Gharanei et al (2013b) demonstrated activation of PI3K/Akt phosphorylation in response to Dox-treatment in a Langendorff-perfused rodent heart model, which increased when mitochondrial division

inhibitor mdivi-1 was coperfused with Dox. In a different report (Gharanei et al, 2013a) the group noted an increase in phosphorylated Akt content in rat heart when Dox was introduced in the reperfusion phase of an ischaemia-reperfusion protocol in a Langendorff-appratus. This upregulation could be inhibited by administration of 0.2 µM CsA. This may indicate that activation of PI3K/Akt noted in the after-sequence of Dox-treatment may be a stress-adaptation that aims to stabilise against the induction of mitochondrial apoptotic pathways (Ushio-Fukai et al, 1999). It is therefore worth considering a hypothesis that preactivation of PI3K/Akt may have a protective role against Dox-toxicity, which differs from the activation of PI3K/Akt observed in cells subjected to Dox-insult. This latter activation, as hypothesised by Deres et al, may be a consequence of nitration or amino acid Tyrosine residues as a consequence of reactive species accumulation. This hypothesis requires further exploratory work in the isolated ARVM model that we have used in our experiments, e.g., by sequential activation or inhibition of PI3K/Akt at different time points of Dox-treatment. However, this was again beyond the scope of the work reported here.

Concomitant with investigations into the role of PI3K/Akt pathway, we also explored the effect of inhibiting MAPK ERK 1/2 on HP-induced protection against Dox-induced cell-death. Hypoxic preconditioning is known to induce MAPK ERK 1/2 via the RISK-pathway. However, as explained in earlier sections the role of MAPK ERK 1/2 in Dox-induced cardiotoxicity is conflicting. Reports by different groups offer evidence in support of a deleterious role for pathway. For example, Liu et al (2008) reported an increase in ERK 1/2 phosphoprotein levels and nuclear translocation in H9C2 cardiomyoblasts in response to Dox treatment at a concentration of 1 µM, which the authors noted to be accompanied by nuclear translocation of phosphorylated p53 and induction of apoptotic pathway. The MEK1 inhibitor U0126 at 20 µM concentration inhibited both ERK 1/2 phosphorylation-induction as well as phosphorylated-p53 translocation to the nucleus, suggesting a role for ERK 1/2 induction in the apoptosis mediated by Dox on the cell-

lines. Similarly, Bien et al (2007) had noted a phosphorylation response of the ERK 1/2 cascade in an *in vivo* murine model of Dox cardiomyopathy. Gharanei et al, in their 2013 report (Gharanei et al, 2013a) had observed a phosphorylation induction of MAPK ERK 1/2 in a Langendorff-perfused rat heart model in the after-sequence of Dox-treatment, where IR-injury is used as an added stress. Other groups however report evidence indicating a protective or compensatory adaptation in cardiomyocytes via the induction of MAPK ERK 1/2. For example, as noted earlier in introduction, reports, e.g., by Lou et al (2005) noted a transient increase in ERK 1/2 phosphoprotein levels over 4 hours in a rodent model of Dox cardiomyopathy, followed by a decline over a period of three weeks. This reflected a decline in mRNA expression and accompanied clinically correlated heart failure in the experimental animals. Similarly, Wang et al (2012) noted a decrease in phosphorylated ERK 1/2 levels within five days of a bolus 20mg/kg Dox in a murine model of cardiotoxicity, along with an increased level of phosphorylated p53. These could be reversed by overexpression of the ubiquitin ligase chaperone protein C-terminal HSP70 interacting protein (CHIP) using a transgenic expression model, and was associated with decrease in markers of doxorubicin-induced cardiomyocyte apoptosis as well as ventricular dilatation. Since hypoxic preconditioning is known to induce MAPK ERK 1/2 via the RISK-pathway, we hypothesised this particular signalling pathway may have a role in mediation of the protective effect that HP offered against Dox-toxicity in the *in vitro* model of toxicity we characterised. We did not use a positive control agent to induce MAPK ERK 1/2 in our experiments exploring cell-death, e.g., insulin. This should be considered a limitation of the experimental design, and need addressed in future work. Our experimental data, however, reflect observations by other groups. For example, in an H9C2 cardiomyoblast model Spallarossa et al (2006) noted an increase matrix metalloproteinases (MMP) MMP-2 and MMP-9 in response to Dox-treatment, which could be attenuated with the β-blocker Carvedilol, with N-acetyl cysteine, and with Dexrazoxane. Dexrazoxane and Carvedilol both resulted in an

upregulation of phosphorylated MAPK ERK 1/2 levels, but inhibiting MAPK ERK 1/2 using pretreatment with 50 μM PD98059, the authors did not observe any differences in MMP-2 and MMP-9 protein expression and activity induced by the exposure to 0.5 μM Dox alone. This suggested the activation of MAPK ERK 1/2 was not consequential in the protective effect observed due to Carvedilol and NAC. Similarly a report by Fu et al (2007) noted phosphorylation induction of MAPK ERK 1/2, but the authors reported that the MEK1 inhibitor U0126 did not inhibit the protective effect of Epo. For comparison, we used 30 μM PD98059 as an inhibitor of MEK1-induced MAPK induction. It ought to be highlighted that repression of MAPK phosphatases by anthracycline compounds have been noted to induce upregulation of phosphorylation ERK 1/2, at least in breast epithelial and breast carcinoma cell lines (Small et al, 2003). Furthermore, ERK 1/2 may be induced by cellular stress including heat stress and substrate deprivation, while extracellular stress induced signalling e.g. as induced through lysis, mechanical agitation, and tensile stimuli, may lead to induction response in MAPK ERK 1/2 (Yamazaki et al, 1996). Moreover, ischaemic stress and reperfusion injury has been reported as stimuli capable of phosphorylation induction of ERK 1/2 (Araujo et al, 2001; Takeishi et al, 2001). Indeed, in subsequent Western blots (discussed further below), although phosphorylated ERK 1/2 was detected in response to HP as well as the positive control agent insulin, signals were also noted in control sample, and failed to reach statistical significance in the differences in p-ERK 1/2 levels between different samples. It ought to be emphasised therefore that the role of MAPK ERK 1/2 require further clarification in future work, where experimental design ought to include a positive control agent for induction of MAPK ERK 1/2 in cell-death experiments.

5.3.5. Western blots.

The analysis of the Western blot experiments we conducted were challenging. Although blot analysis detected phosphorylated protein content both for PI3K/Akt and MAPK ERK 1/2

following HP, crucially the increase in levels of phosphorylated proteins failed to reach statistical significance compared to control. Furthermore, in analysis of MAPK ERK 1/2 induction, p-ERK 1/2 inductions were also noted in control lysates. It ought to be highlighted that in our experimental setup, we evaluated phosphoprotein to total protein content as a ratio normalised to the loading controls in each sample in the respective blots. This protocol was established since, due to the small volume of protein content in the available cell cultures, we harvested protein by directly lysing cells with the loading buffer. We used GAPDH as loading control for Akt, and α-tubulin as loading control for blots exploring phosphorylation of ERK 1/2. The molecular weight of GAPDH (37 kDa) is distinct from that of Akt (56 kDa) and, in well resolved SDS-PAGE blots, would be expected to appear as a distinct signal with greater migration compared to that of Akt. Similarly, α-tubulin (molecular weight 50kDa) was chosen as loading control for ERK 1/2 (molecular weights 42 and 44 kDa) since the signal for α-tubuluin would be expected to migrate less compared to the two ERK 1/2 protein bands in a well-resolved SDS-PAGE membrane. Both GAPDH (Diez and Simm, 1998) and α-tubulin (Belmadani et al, 2002) are known to be expressed abundantly in adult rat ventricular myocytes and perform housekeeping roles, and has been reported from our lab previously (Hausenloy et al, 2005, Davidson et al, 2006). We used insulin as a positive control to induce phosphorylation of Akt and of ERK 1/2, and observed phosphorylation responses of both p-Akt and p-ERK which were consistent with previously reported data (Aikawa et al, 2000).

In these Western blot experiments, we observed phosphorylation of Akt both after HP and after insulin pre-treatment. As highlighted above, although the phosphorylation induction of Akt in response to HP and in response to insulin were consistently greater compared to control throughout the experiments, this failed to reach statistical significance. The sample size for the Western blots was 3 (n=3), which may be a factor in lack of sensitivity on statistical analysis. This ought to be considered a limitation of our experiments. However, we note that insulin

provided a very strong phosphorylation response, and 10 µM LY294002 attenuated this Akt phosphorylation, both of which was consistent with previous reports in Akt phosphorylation observed in *in vitro* neonatal rat cardiomyocyte models (Aikawa et al, 2000). Further, LY294002 has a broad specificity against PI3K, and has also been observed to inhibit additional pathways, e.g. lipid-kinases (Arrowsmith et al, 2015). More selective and sub-group specific inhibitors are available, and further work may include inhibition of respective components within the PI3K-induced cascades.

In subsequent Western blots, we explored the modulation of the respective phosphoprotein isoforms of Akt and ERK 1/2 due to Dox alone at various time points of treatment. However, our analyses were limited by poor quality blots despite optimising blot conditions. The results of our experiments revealed no discernible response for phosphorylation of PI3K/Akt 15 minutes, 4 hours, and 18 hours after introduction of Dox alone. This differs from data observed by other groups (Gharanei et al, 2013a). In this regard, it is necessary to highlight that the sample size with which we explored Dox-induced modulation of PI3K/Akt was small (n=2). Moreover, as our initial characterising experiments established, the volume of total and phosphoprotein content were low, and therefore strict adherence to protocol to limit sample volume and to optimise blotting conditions are necessary. Although the possibility exists that Dox-treatment alone does not induce PI3K/Akt phosphorylation in this model, particularly in light of divergence from a number of previously reported findings (Ichihara et al, 2007), more robust data with larger number of repeat experiments is necessary before confident conclusions can be drawn.

The Western blot analyses for MAPK ERK 1/2 that we carried out to analyse phosphorylation induction in response to HP were similarly challenging, owing to repeated poor signals in two out of three blots for non-phosphorylated (total or t) isoforms of ERK 1/2. This was despite

optimising experimental and blotting conditions. Similar to the blots for HP-induced Akt phosphorylation, statistical analysis failed to identify significance within the limits of the sample size we obtained (*n*=3). Although the levels of phospho-protein content for MAPK ERK 1/2 upon western blotting was most prominent (normalised to loading control α-tubulin levels) for HP, weaker signals were also noted with the positive control insulin and a weak signal was identified in control cells. All three signals were inhibited by PD98059. Since ERK 1/2 may be induced by extracellular stimuli including lysis, mechanical agitation, as well as by tensile stimuli, the stress during cell lysis itself may be a possible explanation for the p-ERK inductions we observed in control cardiomyocytes. Experimental conditions were optimised by incubating cells in ice during protein collection, and lysed in an environment with minimal agitation. However, it is recognised that a certain level of phosphorylation response may be inevitable. Repeat Western blot experiments for phosphoprotein expression for both phosphorylated and total ERK 1/2 may therefore confirm or refute the significance in HP-induced activation of the respective kinase cascades.

As with PI3K/Akt, we explored the phosphorylation status of MAPK ERK 1/2 at 15 minutes, 4 hours and 18 hours after subjecting cardiomyocytes to Dox-treatment. However, although we observed no clear signal to indicate p-ERK induction, caution ought to be exercised in particular light of the fact that the sample size in both experiments were two (*n*=2). As for the PI3K/Akt, it is not possible from this limited data to support or refute wether Dox-treatment alone in this model activates p-ERK, at least in the timescales we explored. This, therefore, requires more rigorous exploration with larger sample size and optimisation of Western blotting protocol to obtain standardised protein content in sample lysate, and to obtain clear signals for both proteins of interest and loading controls. This may be explored in more detail in future work.

Chapter 6. Conclusions, limitations, future directions and significance.

6.1. Summary, limitations, and future directions.

6.1.1. Summary.

In this thesis, we describe the development and characterisation of an *in vitro* primary adult rat cardiomyocyte model that allows us to investigate the cardiotoxicity of doxorubicin. Using this model, we identified hypoxic preconditioning (HP) as an intervention capable of protecting cardiomyocytes against Dox toxicity. We were further able to shed some light into the potential mechanisms through which this protection is mediated, identifying PI3K/Akt pathway as the protein-cascade of interest. Our results offer some support for the observations by other groups which show manipulation and potentiation of the PI3K/Akt pathway as having a role in the protection against anthracycline-cardiotoxicity. We were not, however, able to clarify the role of MAPK ERK 1/2 cascade in Dox-cardiotoxicity or in protection against this. Future work is required to explore further role and activation of status of MAPK ERK 1/2 induction in response to HP in this model, and to explore the respective role in mitigating Dox-toxicity against cardiomyocytes. Further future work is also necessary to clarify the phosphorylation induction of both PI3K/Akt and of MAPK ERK 1/2 *after* Dox treatment to explore the phosphorylation status of the respective kinases. The phosphorylation responses of both PI3K/Akt and of MAPK ERK 1/2 over longer timescales following HP ought to be explored. Further, future work ought to be carried out using more specific inhibitors of PI3K/Akt, and will be of immense interest.

Of the described mechanisms of toxicity of Dox that we explored, the experiments we carried out failed to identify a pathological role for oxidative stress, of alterations to the $\Delta\Psi_m$, or a role for increased vulnerability of the mPTP to transition as an explanation of doxorubicin-induced cardiomyocyte death in the model we developed and characterised. However, over the course

of our investigations, we found that Dox-treatment altered the capacity of CsA to protect the mPTP against induction from sensitising agents, possibly indicating a change to the levels or function of Cyp D. Whether such a change is reflective of a more widespread underlying mechanism, e.g. post-translational modification, is unclear. Investigation of the potential mechanisms including post-translational modifications of the proteins constituting the pore would be exciting, but is beyond the scope of this current work. Other putative death mechanisms, including the role of BCL group of death regulators and of p53-induced death pathways were not explored in this current work, but would also be a logical progression in planning of future experiments.

6.1.2. Limitations

A key general limitation in the work undertaken in preparing this report includes variations in the number of repeat experiments and unequal sample distribution. In some experiments, including in establishing initial cell-model of doxorubicin-toxicity, and in evaluating the effect of IR-injury in doxorubicin-stressed cardiomyocytes, the sample sizes (*n* value) were unequal and small, to the order of *n*=2. This reduces statistical power of the experiments (Kim, 2014). In our experimental set up, we attempted to address this potential problem by establishing all experiments in duplicate, and utilised Students *t*-test in statistical analysis where the *n* value in the experiments were very low. However, consistent observations in subsequent repeat experiments with similar treatment groups over the course of the experiments described above allowed us a measure of confidence in the results we observed. Future work ought to consider predefining acceptable significance levels (α-value) and precalculation of sample size in order to optimise experimental planning and robustness of the results.

A second limitation that ought to be highlighted is the lack of delineation between the canonical cell-death pathways, particularly between necrosis, apoptosis, and necroptosis. Further, contribution of altered autophagic flux in the injury due to Dox was not probed nor delineated

in this report. Emerging evidence suggest that anthracycline cardiotoxicity on the myocardium is the culmination of a complex interplay of these canonical death pathways, but characterising and investigating the individual contributions of these was beyond the scope of our work, in the model we characterised. Particularly, the lack of information on the extent of necrosis and apoptosis in this model necessitated a broad approach in exploring the known toxicity mechanisms. However, future work ought to consider the identification of necrotic or apoptotic death pathways as a key part of experimental setup, since this is directly relevant in light of our data which showed deviation from "classic" ANTC-toxicity descriptors, including a question over the role for ROS-scavenging and on the role of the mPTP in induction of cardiomyocyte-death in this model. Approaches currently in use in molecular biology, e.g., Cytochrome C levels, LDH assays or estimation of early markers of necrosis e.g., HMGB1 levels may be used to assess necrotic cell-death, while approaches e.g., annexin staining, TUNEL assay for DNA laddering, or Caspase 3 assay may provide insight into apoptotic death pathway in the model we have developed and characterised. Moreover, since Dox also induces early degradation of intracellular proteins, the role of autophagy maybe explored through e.g. myosin light chain isoform (LCII to I) ratios. These are potential topics that ought to be reflected on in future work.

In the work described above, we established an *in vitro* model of doxorubicin-toxicity on isolated cardiomyocytes. Anthracycline cardiotoxicity, as discussed earlier, is characterised by early asymptomatic sub-clinical changes which may reflect the physiological compensatory capacity of the intact heart. We used a pure culture of terminally differentiated adult mammalian ventricular cardiomyocyte as our model to investigate the cell-type predominantly at risk of injury, and known to concentrate anthracyclines the most within the intact myocardium. However, this necessarily limits the physiological translation of the results of our experiments. The adult mammalian heart is a composite not only of mature cardiomyocytes, but also of a support network of endothelial cells, fibroblasts, immune-cells including resident

and recruited macrophages, as well as a potential reservoir of smaller population of immature or senescent progenitor cells. It is therefore necessary to reconcile the results we observe in both other *in vitro* models, e.g., neonatal rat ventricular myocytes, as well as in higher physiological models, e.g. *ex vivo* models, for example Langendorff-apparatus perfursed heart systems. Exploring the work we describe in different cell model is particularly relevant since ARVMs display a high basal cell-death, although this phenomenon is particularly relevant in cell-culture established to time scales exceeding 24 hours (Louch et al, 2011). In our experiments, we attempted to address this by establishing minimum acceptability criteriae, and excluding experiments from analyses where basal cell-death exceeded 20% after 24 hours. It may be argued that an additional approach possible would have been to evaluate cell-death at beginning of the experiment and normalising this to basal-cell death at the end of experimental procedure. Moreover, in some experiments, e.g., evaluation of the role and induction of the RISK kinases in relation to doxorubicin-toxicity, our findings diverge from those described by other groups, some of which have been carried out in different models, e.g., *ex vivo* models used by Gharanei et al and Montaigne et al. Therefore, repeating our experiments in both immature cell-lines, e.g., NRVMs, as well as in *ex vivo* and *in vivo* models will alow examination of the robustness of the data we gathered, as well as reconciliation of the results and differences with those described by other groups in differing models. Further, in exploring the protective potential of HP against Dox-induced cell-death *in vitro*, we did not implement a positive control. In future experimental work, therefore, a known inducer of the RISK kinases, e.g., insulin, ought to be considered when evaluating the role of the respective protein cascades PI3K/Akt and MAPK ERK 1/2. The results should be of interest not only to the molecular biologist exploring mechanism of ANTC-cardiac injury, but also hold direct relevance to the clinical practice in oncology and cardiology today.

6.1.3. Clinical significance.

Approaches to potentiating PI3k cascade, such as genetic manipulation, e.g. as reported by Kitamura et al (2014), are impractical in humans as a cardioprotective intervention, and further unlikely to be cost-effective. However, these findings are exciting since it is well established that RISK pathway activation and cardioprotection is also elicited by the application of a preconditioning stimulus to an organ or limb remote from the heart (Hausenloy and Yellon, 2016). This intervention, called remote ischaemic preconditioning (RIPC), reduces ischaemia-reperfusion (IR) injury, and decreases peak troponin levels in patients undergoing thrombolysis for ST-elevation myocardial infarction (Yellon et al, 2015). The role of RIPC in protection against anthracycline-cardiotoxicity are indeed under investigation (Chung et al, 2015), and the results will be of immense interest. Moreover, lifestyle interventions, for example exercise preconditioning are postulated to share common biomolecular pathways to activation of what is considered the second window of preconditioning, and therefore will be of immense interest to both the clinican and the molecular biologist in translating into practical intervention against anthracycline-mediated cardiac injury.

Appendix a. Buffers for adult rat ventricular myocytes isolation.

a. Perfusion buffer.

Salts	Molarity (mM)	g/500ml	g/L	g/2L
NaCl	130	3.79	7.59	15.18
KCl	5.4	0.2	0.4	0.8
MgCl2	1.4	0.066	0.133	0.266
Na2HPO4 (anhydrous)	0.4	0.028	0.057	0.114
HEPES (not HEPES sodium)	4.2	0.5	1	2
pH to 7.3 at 37ºC				
Glucose †	10	0.9	1.8	3.6
Taurine †	20	1.25	2.5	5
Creatine †	10	0.655	1.31	2.62

Table 1. Composition of perfusion buffer solution used to isolate cardiac myocytes.

b. Isolation buffers.

Solution	Final concentration	Addition
1 (to clear heart of blood)	750µM $CaCl_2$	37.5µl of 1M $CaCl_2$
2 (to arrest heart)	100µM EGTA	2mg of EGTA
3 (to digest heart)	100µM $CaCl_2$ and 0.5mg/ml Collagenase	40µl of 100mM $CaCl_2$ 15-20mg of collagenase *18mg is good*
4 (to re-introduce $CaCl_2$)	0.5mM $CaCl_2$	12.5µl of 1M $CaCl_2$
5 (to re-introduce $CaCl_2$)	1m $CaCl_2$	25µl of 1M $CaCl_2$

Table 2. Solutions used and the purposes during isolation process for adult rat ventricular myocytes in modified Langendorff apparatus.

Appendix b. Representative photographs of cardiomyocytes following different treatment protocols.

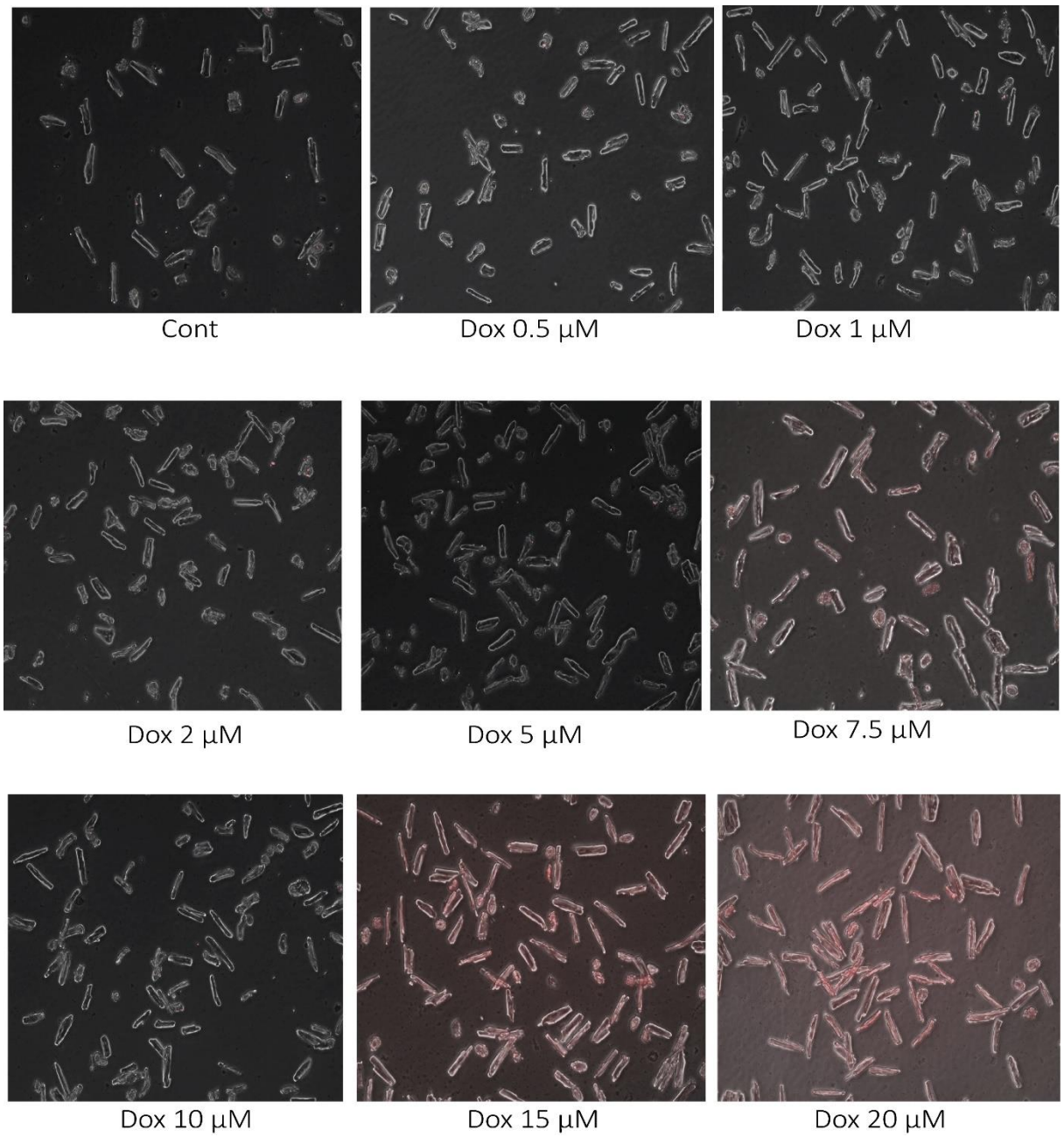

Fig. I. Cell-death following 4 h exposure to various concentrations of Doxorubicin.

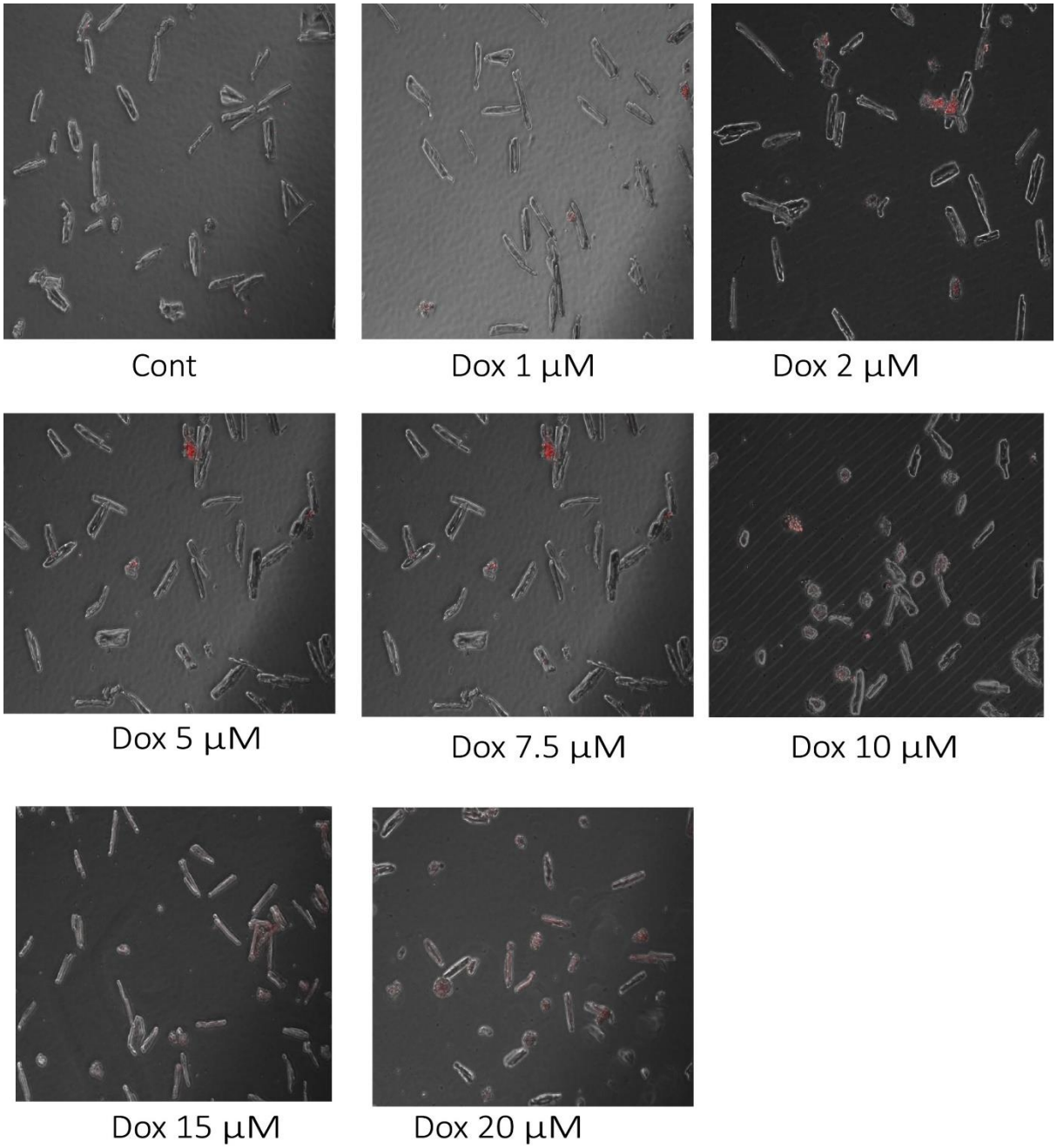

Fig. II. Cell-death with various concentrations of Doxorubicin after exposure for 18 h.

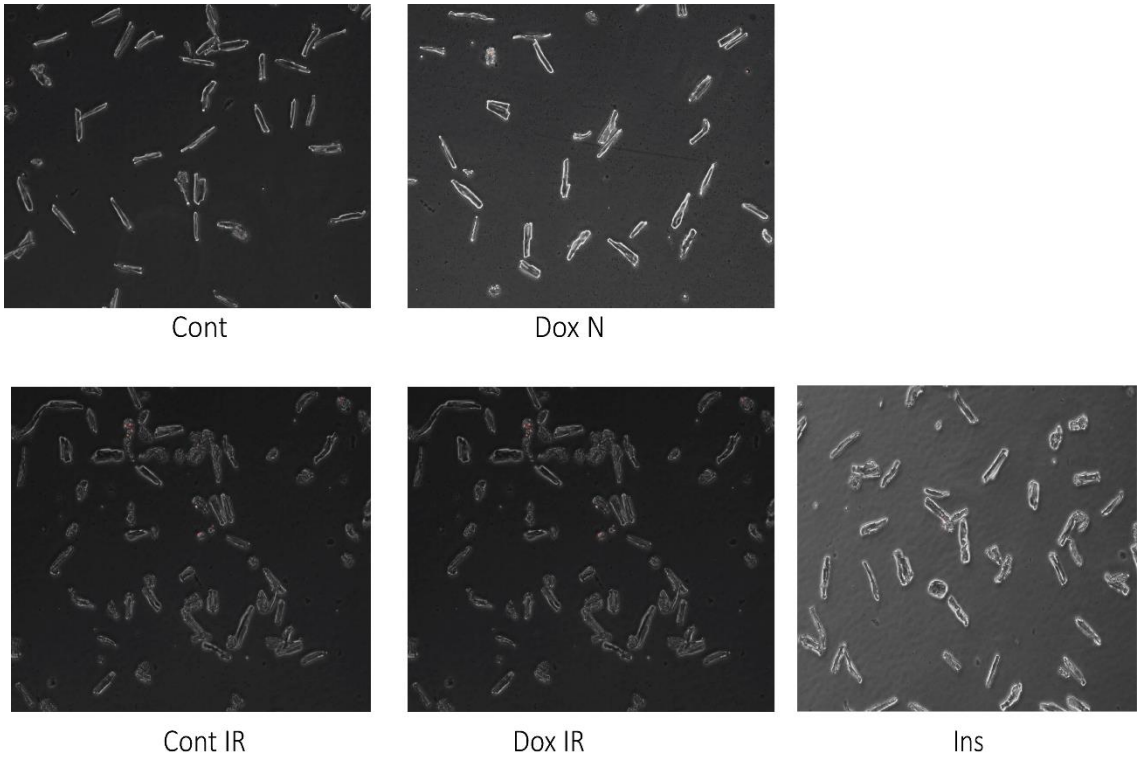

Fig. III. Ischaemia reperfusion induced cell-death following 4 h pretreatment with 2 µM Doxorubicin.

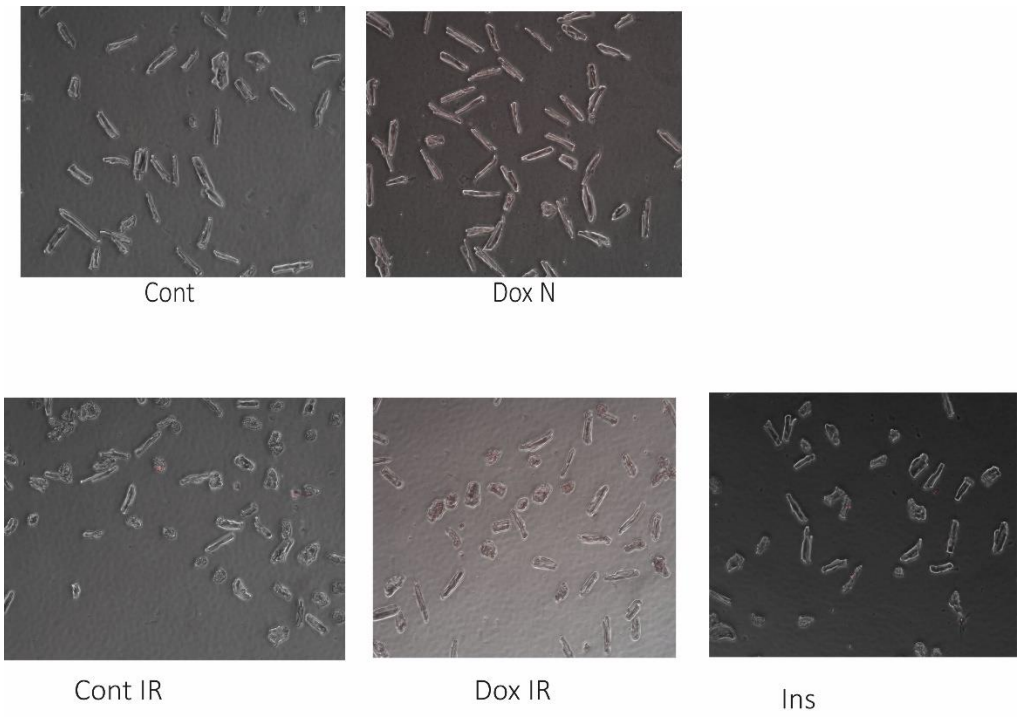

Fig. IV. Ischaemia reperfusion induced cell-death following 18 h pretreatment with 2 µM Doxorubicin.

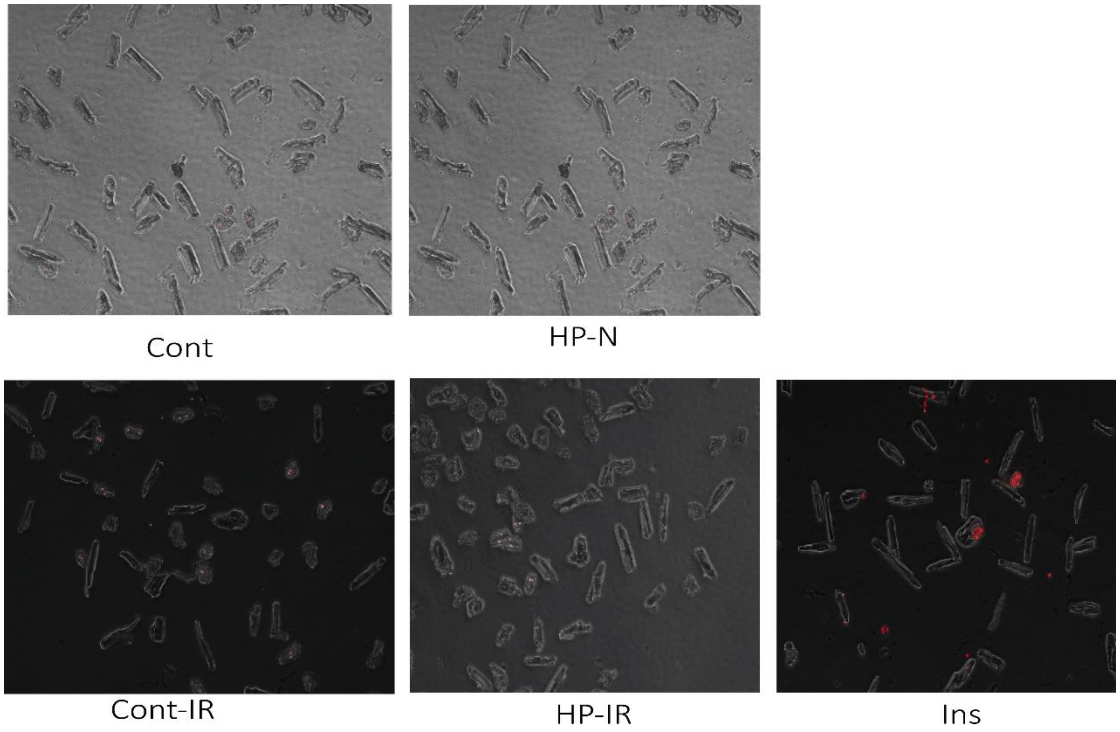

Fig. V. Ischaemia-reperfusion induced cell-death in preconditioned cardiomyocytes (HP protocol 1).

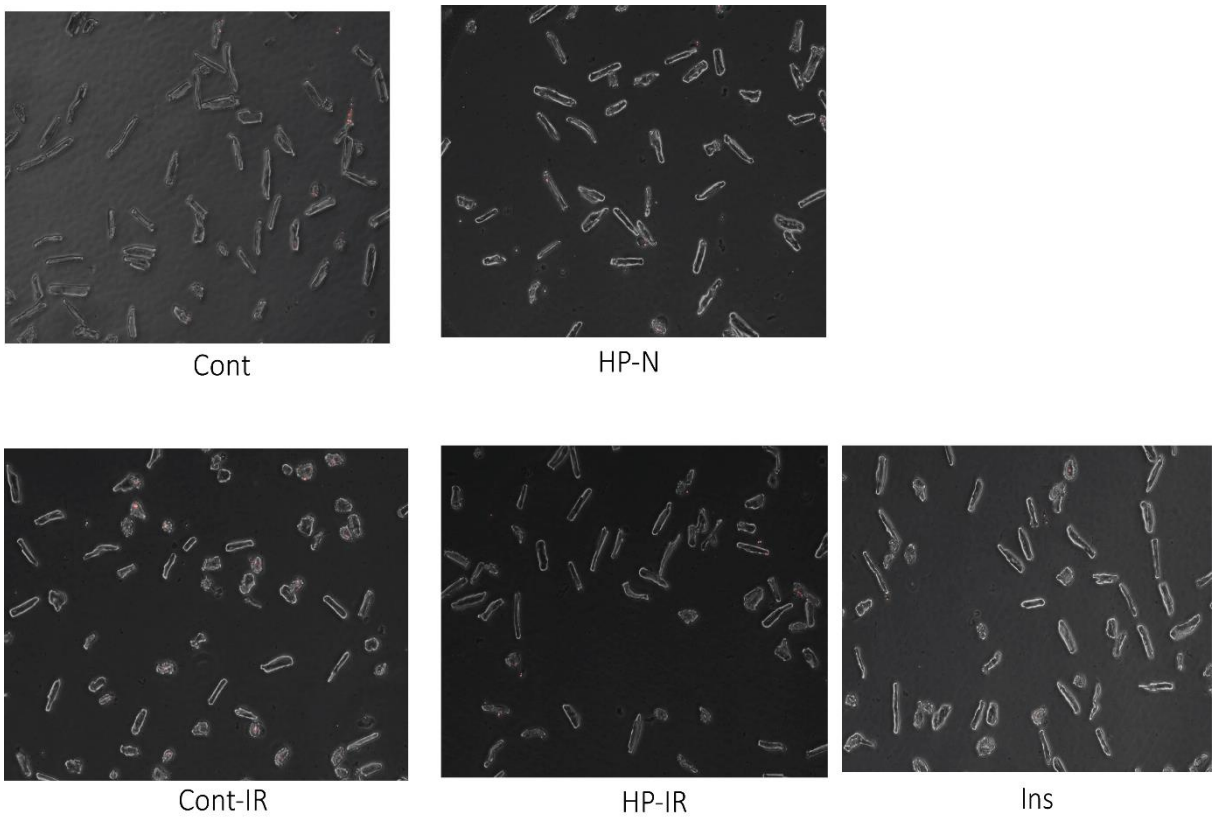

Fig. VI. Ischaemia-reperfusion induced cell-death in the second window in preconditioned cardiomyocytes (HP protocol 2).

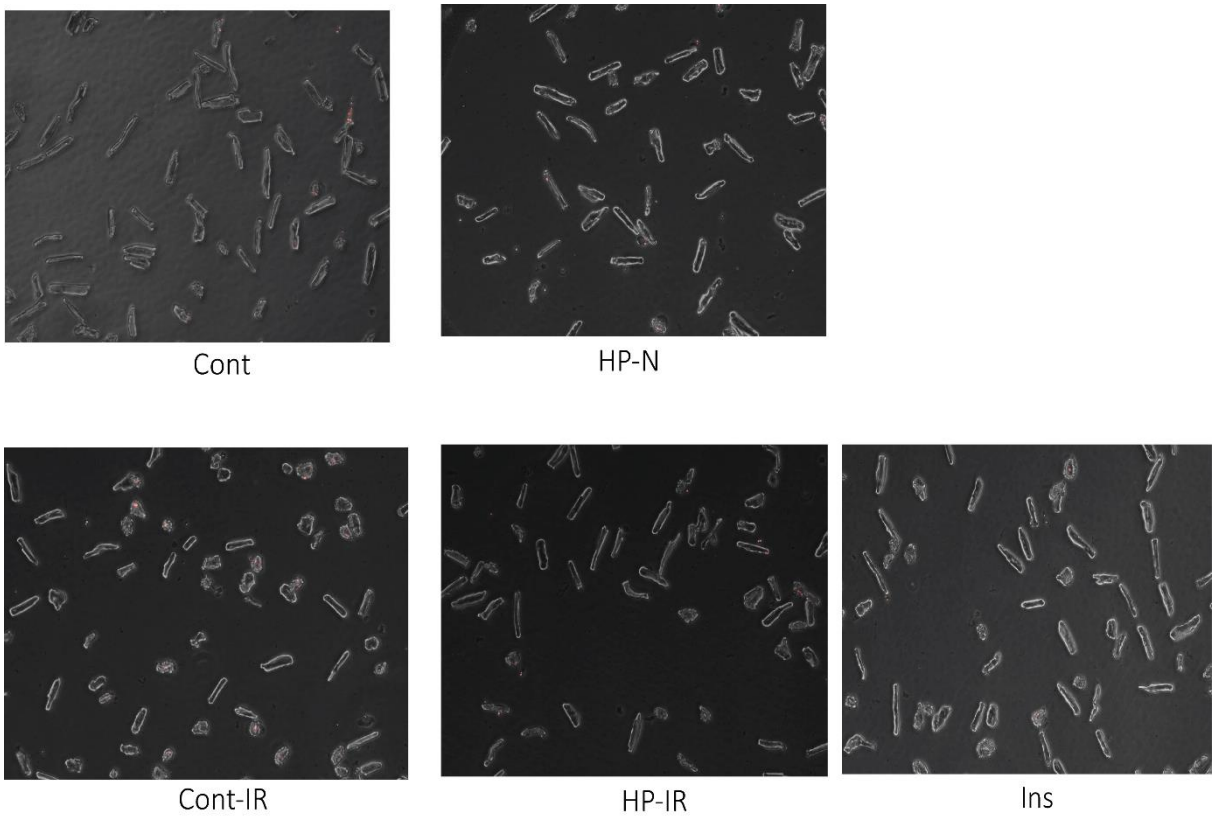

Fig. VII. Ischaemia-reperfusion induced cell-death in the first window in preconditioned cardiomyocytes (HP protocol 2).

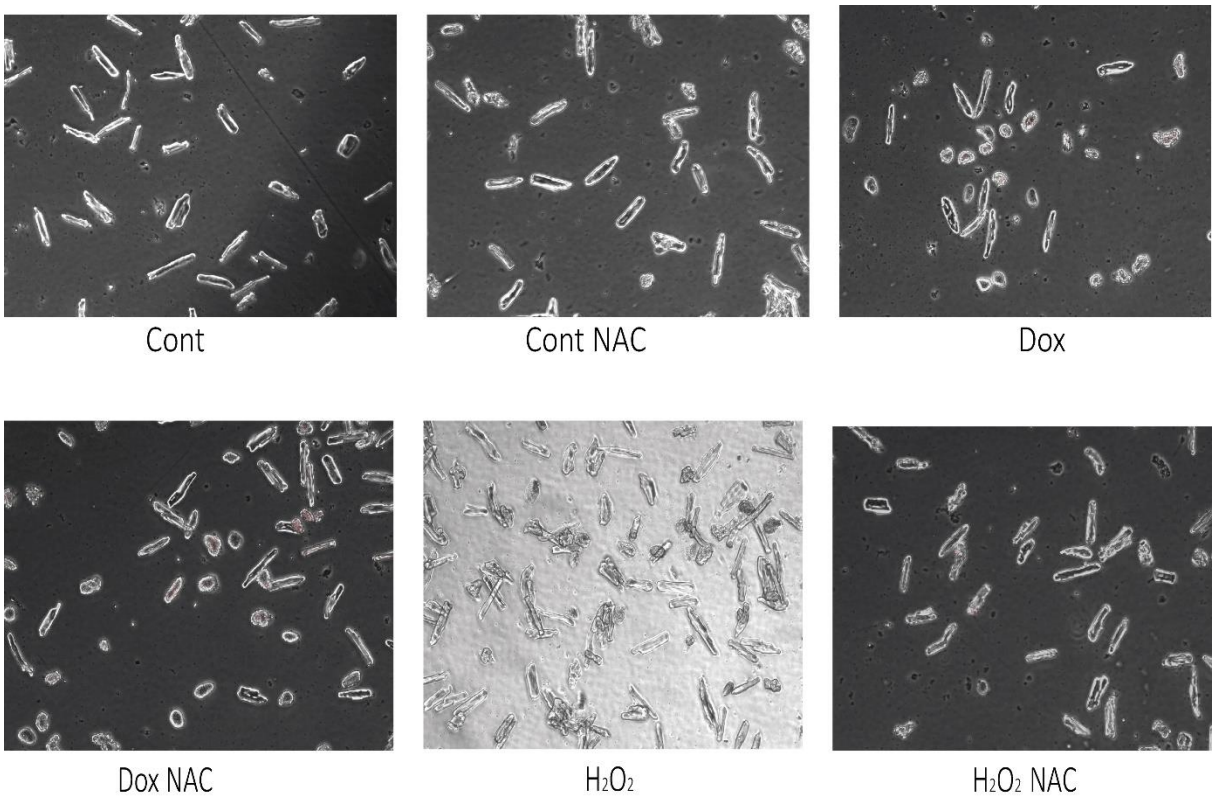

Fig. VIII. Cell-death in cardiomyocytes subjected to 7.5 µM Doxorubicin and to 1µMH_2O_2, with and without 250nM N-acetl cysteine (NAC) for 18 h.

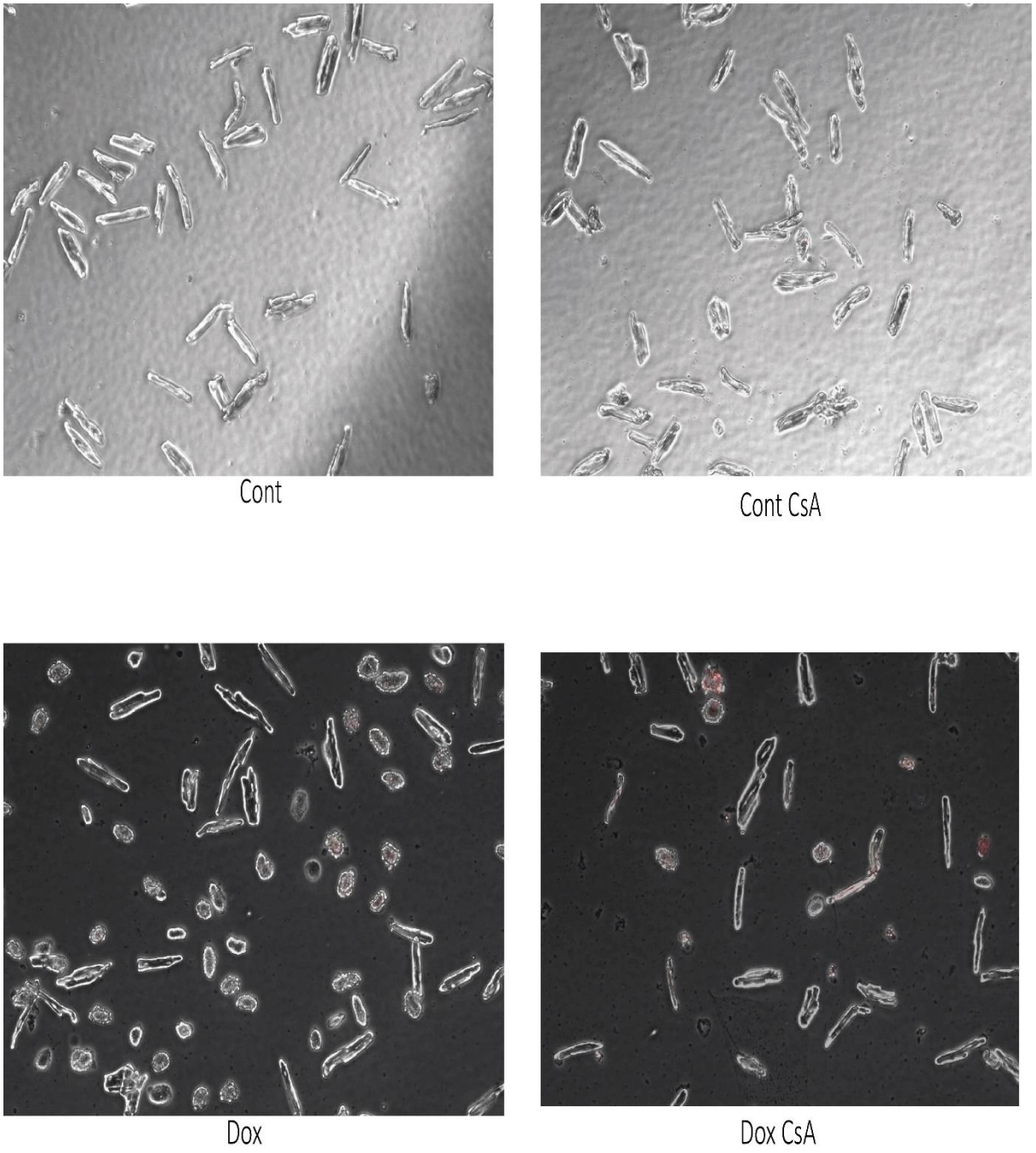

Fig. IX. Cell-death in cardiomyocytes subjected to 18 h of 7.5 µM Doxorubicin (Dox) with and without 1µM Ciclosporine A (CsA).

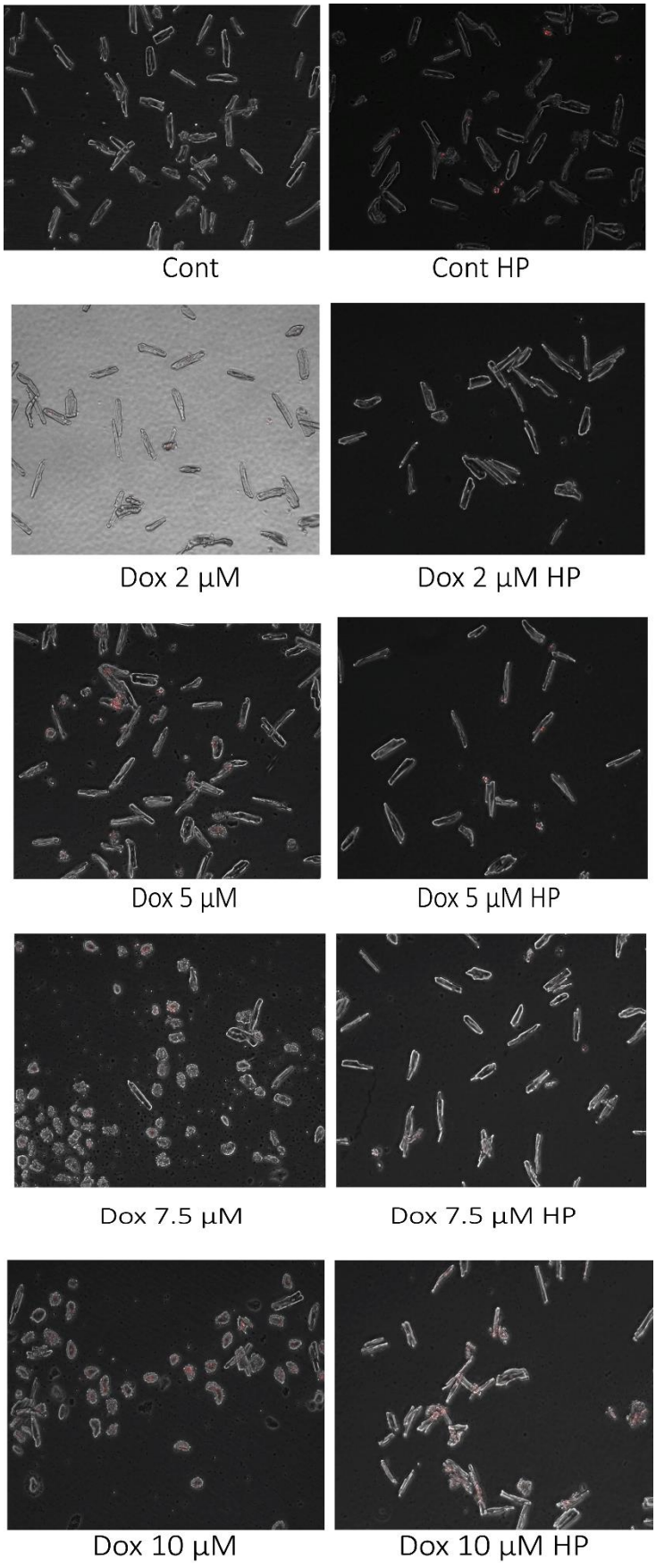

Fig. X. Cell-death after 18 h with various concentrations of Dox in preconditioned (HP) and non-preconditioned cells.

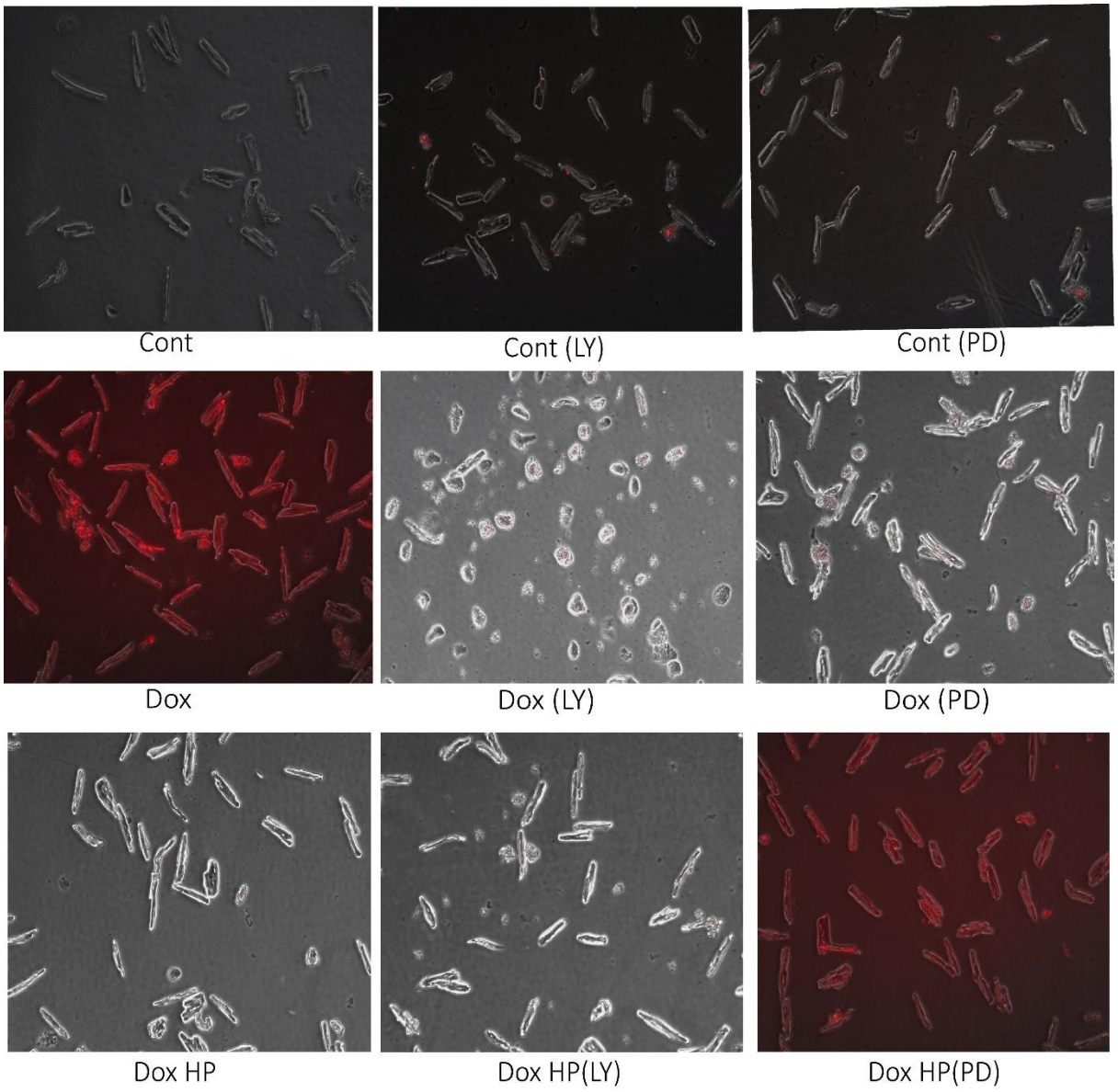

Fig. XI. Influence of 10 µM LY294002 (LY) and 30 µM PD98059 (PD) on preconditioned (HP) and non-preconditioned cells subjected to 18 h of 7.5 µM Doxorubicin (Dox).

References.

Agewall S, Giannitsis E. Troponin elevation in coronary ischemia and necrosis. Curr Atheroscler Rep. 2014 Mar;16(3):396.

Aikawa R, Nawano M, Gu Y, et al. Insulin prevents cardiomyocytes from oxidative stress-induced apoptosis through activation of PI3 kinase/Akt. Circulation. 2000 Dec 5;102(23):2873-9.

An J, Li P, Li J, et al. ARC is a critical cardiomyocyte survival switch in doxorubicin cardiotoxicity. J Mol Med (Berl). 2009 Apr;87(4):401-10.

Anaya P, Moliterno DJ. The evolving role of cardiac troponin in the evaluation of cardiac disorders. Curr Cardiol Rep. 2013 Nov;15(11):420.

Andreotti F, Pasceri V, Hackett DR, et al.Preinfarction Angina as a Predictor of More Rapid Coronary Thrombolysis in Patients with Acute Myocardial Infarction. N Engl J Med. 1996 Jan 4;334(1):7-12.

Araujo E, Bianchi C, Faro R, Sellke F. Oscillation in the activities of MEK ERK 1/2 during cardiopulmonary bypass in pigs. Surgery. 2001;130:182–91.

Armenian SH, Ding Y, Mills G et al. Genetic susceptibility to anthracycline-related congestive heart failure in survivors of haematopoietic cell transplantation. Br J Haematol 2013 Oct;163(2):205-13.

Arola OJ, Saraste A, Pulkki K, et al.Acute doxorubicin cardiotoxicity involves cardiomyocyte apoptosis. Cancer Res. 2000 Apr 1;60(7):1789-92.

Ascensão A, Lumini-Oliveira J, Machado NG, et al. Acute exercise protects against calcium-induced cardiac mitochondrial permeability transition pore opening in doxorubicin-treated rats. Clin Sci (Lond). 2011 Jan;120(1):37-49.

Badinloo M, Esmaeili-Mahani S. Phosphatidylinositol 3-kinases inhibitor LY294002 potentiates the cytotoxic effects of doxorubicin, vincristine, and etoposide in a panel of cancer cell lines. Fundam Clin Pharmacol. 2014 Aug;28(4):414-22.

Baines CP, Kaiser RA, Purcell NH, et al. Loss of cyclophilin D reveals a critical role for mitochondrial permeability transition in cell-death. Nature. 2005 Mar 31;434(7033):658-62.

Baines CP, Kaiser RA, Sheiko T, et al. Voltage-dependent anion channels are dispensable for mitochondrial-dependent cell death. Nat. Cell Biol. 2007;9:550–555.

Banerjee A, Locke-Winter C, Rogers KB, et al. Preconditioning against myocardial dysfunction after ischemia and reperfusion by an alpha 1-adrenergic mechanism. Circ Res. 1993 Oct;73(4):656-70.

Beckman JS, Koppenol WH. Nitric oxide, superoxide, and peroxynitrite: the good, the bad, and ugly. Am J Physiol. 1996 Nov;271(5 Pt 1):C1424-37

Bell RM, Yellon DM. Bradykinin limits infarction when administered as an adjunct to reperfusion in mouse heart: the role of PI3K, Akt and eNOS. J Mol Cell Cardiol. 2003 Feb;35(2):185-93.

Bell RM, Clark JE, Hearse DJ. Reperfusion kinase phosphorylation is essential but not sufficient in the mediation of pharmacological preconditioning: Characterisation in the bi-phasic profile of early and late protection. Cardiovasc Res. 2007 Jan 1;73(1):153-63.

Belmadani S, Poüs C, Ventura-Clapier R, et al. Post-translational modifications of cardiac tubulin during chronic heart failure in the rat. Mol Cell Biochem. 2002 Aug;237(1-2):39-46.

Berthiaume JM, Wallace KB. Adriamycin-induced oxidative mitochondrial cardiotoxicity. Cell Biol Toxicol. 2007 Jan;23(1):15-25.

Biondi R.M, Kieloch A, Currie R.A, et al. The PIF-binding pocket in PDK1 is essential for activation of S6K and SGK, but not PKB. EMBO J, 20 (2001), pp. 4380–4390.

Blanco JG, Leisenring WM, Gonzalez-Covarrubias VM, et al. Genetic polymorphisms in the carbonyl reductase 3 gene CBR3 and the NAD(P)H:quinone oxidoreductase 1 gene NQO1 in patients who developed anthracycline-related congestive heart failure after childhood cancer. Cancer. 2008 Jun 15;112(12):2789-95.

Boengler K, Hilfiker-Kleiner D, Heusch G, Schulz R. Inhibition of permeability transition pore opening by mitochondrial STAT3 and its role in myocardial ischemia/reperfusion. Basic Res Cardiol 105: 2010 Nov;105(6):771-85.

Brauchle E, Thude S, Brucker SY, Schenke-Layland K. Cell death stages in single apoptotic and necrotic cells monitored by Raman microspectroscopy. Sci Rep. 2014 Apr 15;4:4698.

Brew EC, Mitchell MB, Rehring TF, et al. Role of Bradykinin in cardiac functional protection after global ischemia-reperfusion in rat heart. Am J Physiol. 1995 Oct;269(4 Pt 2):H1370-8.

Bristow MR, Thompson PD, Martin RP, et al. Early anthracycline cardiotoxicity. Am J Med. 1978 Nov;65(5):823-32.

Brower M, Grace M, Kotz CM. Comparative analysis of growth characteristics of Sprague Dawley rats obtained from different sources. Lab Anim Res. 2015 Dec; 31(4): 166–173.

Burridge PW, Li YF, Matsa E, et al. Human induced pluripotent stem cell-derived cardiomyocytes recapitulate the predilection of breast cancer patients to doxorubicin-induced cardiotoxicity. Nat Med. 2016 May;22(5):547-56.

Cardinale D, Sandri MT, Martinoni A, et al. Left ventricular dysfunction predicted by early troponin I release after high-dose chemotherapy. J Am Coll Cardiol. 2000 Aug;36(2):517-22.

Cardinale D, Colombo A, Bacchiani G, et al. Early detection of anthracycline cardiotoxicity and improvement with heart failure therapy. Circulation. 2015 Jun 2;131(22):1981-8.

Chan FK, Shisler J, Bixby JG, et al. A role for tumor necrosis factor receptor-2 and receptor-interacting protein in programmed necrosis and antiviral responses. J Biol Chem. 2003 Dec 19; 278(51):51613-21.

Chatterjee K, Zhang J, Tao R, et al. Vincristine attenuates doxorubicin cardiotoxicity. Biochem Biophys Res Commun. 2008 Sep 5;373(4):555-60.

Charlier HA Jr, Olson RD, Et al. Investigations of calsequestrin as a target for anthracyclines: comparison of functional effects of daunorubicin, daunorubicinol, and trifluoperazine.. Mol Pharmacol. 2005 May;67(5):1505-12.

Cheung KG, Cole LK, Xiang B, et al. Sirtuin-3 (SIRT3) Protein Attenuates Doxorubicin-induced Oxidative Stress and Improves Mitochondrial Respiration in H9c2 Cardiomyocytes. J Biol Chem. 2015 Apr 24;290(17):10981-93.

Chicco AJ, Schneider CM, Hayward R. Exercise training attenuates acute doxorubicin-induced cardiac dysfunction. J Cardiovasc Pharmacol. 2006a. Feb;47(2):182-9.

Chicco AJ, Hydock DS, Schneider CM, Hayward R. Low-intensity exercise training during doxorubicin treatment protects against cardiotoxicity. J Appl Physiol (1985). 2006b Feb;100(2):519-27.

Childs AC, Phaneuf SL, Dirks AJ, et al. Doxorubicin treatment in vivo causes Cytochrome C release and cardiomyocyte apoptosis, as well as increased mitochondrial efficiency, superoxide dismutase activity, and BCL-2:Bax ratio. Cancer Res. 2002 Aug 15;62(16):4592-8.

Christiansen JR, Hamre H, Massey R et al. Left ventricular function in long-term survivors of childhood lymphoma. Am J Cardiol. 2014 Aug 1;114(3):483-90.

Chung R, Maulik A, Hamarneh A, et al. Effect of Remote Ischaemic Conditioning in ONCology patients undergoing chemotherapy: Rationale and design of the ERIC-ONC study - a single centre, blinded, randomised controlled trial. Clin Cardiol. 2016 Feb;39(2):72-82.

Cleveland JC Jr, Meldrum DR, Rowland RT, et al. Ischemic preconditioning of human myocardium: protein kinase C mediates a permissive role for alpha 1-adrenoceptors. Am J Physiol. 1997 Aug;273(2 Pt 2):H902-8.

Cohen MV, Baines CP, Downey JM. Ischemic preconditioning: from Adenosine receptor to KATP channel. Annu Rev Physiol. 2000;62:79-109.

Cohen MV, Yang XM, Liu GS, et al. Acetylcholine, Bradykinin, opioids, and phenylephrine, but not Adenosine, trigger preconditioning by generating free radicals and opening mitochondrial K(ATP) channels. Circ Res. 2001 Aug 3;89(3):273-8.

Costa ADT, Garlid KD. Intramitochondrial signaling: interactions among mitoKATP, PKCε, ROS, and MPT. Am J Physiol Heart Circ Physiol (2008). 295: H874–H882.

Cove-Smith L, Woodhouse N, et al An integrated characterization of serological, pathological, and functional events in doxorubicin-induced cardiotoxicity. Toxicol Sci. 2014 Jul;140(1):3-15.

Crompton M. On the involvement of mitochondrial intermembrane junctional complexes in apoptosis. Curr Med Chem. 2003 Aug;10(16):1473-84.

Crompton M. The mitochondrial permeability transition pore and its role in cell death. Biochem J. 1999 Jul 15; 341(Pt 2): 233–249.

Cummings BS, Schnellmann RG. Measurement of cell death in mammalian cells. Curr Protoc Pharmacol. 2004 Sep 1;Chapter 12:Unit 12.8.

Darrabie MD, Arciniegas AJ, Mantilla JG, et al. Exposing cardiomyocytes to subclinical concentrations of doxorubicin rapidly reduces their creatine transport. Am J Physiol Heart Circ Physiol. 2012 Sep 1;303(5):H539-48.

Darzynkiewicz Z, Zhao H. Detection of DNA strand breaks in apoptotic cells by flow- and image-cytometry. Methods Mol Biol. 2011; 682:91-101.

Das DK, Engelman RM, Kimura Y. Molecular adaptation of cellular defences following preconditioning of the heart by repeated ischaemia. Cardiovasc Res. 1993;27(4):578–84.

Dasgupta RK, Adamson PJ, Davies FE, et al. Polymorphic variation in GSTP1 modulates outcome following therapy for multiple myeloma. Blood. 2003 Oct 1;102(7):2345-50.

Datta S.R, Brunet A, Greenberg M.E. Cellular survival: a play in three Akts. Gene Dev, 13 (1999), pp. 2905–2927.

Davidson SM, Hausenloy D, Duchen MR, Yellon DM. Signalling via the reperfusion injury signalling kinase (RISK) pathway links closure of the mitochondrial permeability transition pore to cardioprotection. Int J Biochem Cell Biol. 2006 Mar;38(3):414-9.

Davies SP, Reddy H, Caivano M, and Cohen P (2000) Specificity and mechanism of action of some commonly used protein kinase inhibitors. Biochem J 351**:** 95–105

Day BJ. Antioxidants as Potential Therapeutics for Lung Fibrosis. Antioxidants and redox signaling. 2008;10(2):355-370.

De Angelis A, Piegari E, Cappetta D,et al. Anthracycline cardiomyopathy is mediated by depletion of the cardiac stem cell pool and is rescued by restoration of progenitor cell function. Circulation. 2010 Jan 19;121(2):276-92.

Delpy E, Hatem SN, Andrieu N, et al. Doxorubicin induces slow ceramide accumulation and late apoptosis in cultured adult rat ventricular myocytes. Cardiovasc Res. 1999 Aug 1;43(2):398-407.

Deres P, Halmosi R, Toth A, et al. Prevention of doxorubicin-induced acute cardiotoxicity by an experimental antioxidant compound. J Cardiovasc Pharmacol. 2005 Jan;45(1):36-43.

Dhingra R, Margulets V, Chowdhury SR, et al. Bnip3 mediates doxorubicin-induced cardiac myocyte necrosis and mortality through changes in mitochondrial signaling. Proc Natl Acad Sci U S A. 2014 Dec 23;111(51):E5537-44.

Diez C, Simm A. Gene expression in rod shaped cardiac myocytes, sorted by flow cytometry. Cardiovasc Res. 1998 Dec;40(3):530-7.

Drafts BC, Twomley KM, D'Agostino R Jr, et al. Low to moderate dose anthracycline-based chemotherapy is associated with early noninvasive imaging evidence of suBCLinical cardiovascular disease. JACC Cardiovasc Imaging. 2013 Aug;6(8):877-85.

Doble B.W, Woodgett J.R. GSK-3B -3: tricks of the trade for a multi-tasking kinase. J Cell Sci, 116 (2003), pp. 1175–1186.

Dongworth RK, Mukherjee UA, Hall AR, et al. DJ-1 protects against cell-death following acute cardiac ischemia-reperfusion injury. cell-death Dis. 2014 Feb 27;5:e1082.

Doroshow, J. H., and Davies K. J. Redox cycling of anthracyclines by cardiac mitochondria. II. Formation of super-oxide anion, hydrogen peroxide, and hydroxyl radical. JBC, (1986). 261(7), 3068–3074.

Downey JM, Davis AM, Cohen MV. Signaling pathways in ischemic preconditioning. Heart Fail Rev. 2007 Dec;12(3-4):181-8.

Edwards J, Mitry M, Laurent D. Doxorubicin may damage cardiomyocytes more than cardiac progenitor cells. FASEB J. 2016 Apr;30(1) S735.7

Elrod JW, Wong R, Mishra S, et al. Cyclophilin D controls mitochondrial pore-dependent Ca(2+) exchange, metabolic flexibility, and propensity for heart failure in mice. J Clin Invest. 2010 Oct;120(10):3680-7.

Elmore S. Apoptosis: A Review of Programmed Cell Death. Toxicol Pathol. 2007; 35(4): 495–516.

Faircloth M E, Redwood S R, Marber M S. Ischaemic preconditioning and myocardial adaptation to serial intracoronary balloon inflation: cut from the same cloth?
Heart. 2004 Apr; 90(4): 358–360.

Fan GC, Zhou X, Wang X, et al. Heat shock protein 20 interacting with phosphorylated Akt reduces doxorubicin-triggered oxidative stress and cardiotoxicity. Circ Res. 2008;103:1270–9.

Feldman AM, Combes A, Wagner D, et al. The role of tumor necrosis factor in the pathophysiology of heart failure. J Am Coll Cardiol. 2000 Mar 1;35(3):537-44.

Feng W, Liu G, Xia R, Abramson JJ, and Pessah IN (1999) Site-selective modification of hyperreactive cysteines of ryanodine receptor complex by quinones. Mol Pharmacol 55:821–831.

Ferreira AL, Yeum KJ, Matsubara LS, et al. Effect of Doxorubicin on Myocardial Concentration of Lycopene and its Metabolism in Wistar rats. FASEB J. 2007 Apr;21(5):A350.

Feola M, Garrone O, Occelli M, G et al. Cardiotoxicity after anthracycline chemotherapy in breast carcinoma: effects on left ventricular ejection fraction, troponin I and brain natriuretic peptide. Int J Cardiol.2011;148(2):194–198

Florio S, Ciarcia R, Crispino L, et al. Hydrocortisone has a protective effect on CyclosporinA-induced cardiotoxicity. Cell Physiol. 2003 Apr;195(1):21-6.

Frantz S, Kelly RA, Bourcier T. Role of TLR-2 in the activation of nuclear factor kappaB by oxidative stress in cardiac myocytes. J Biol Chem. 2001 Feb 16;276(7):5197-203.

Fryer RM, Hsu AK, Gross GJ, et al. ERK and p38 MAP kinase activation are components of opioid-induced delayed cardioprotection. Basic Res Cardiol. 2001 Apr;96(2):136-42.

Fu P, Arcasoy MO. Erythropoietin protects cardiac myocytes against anthracycline-induced apoptosis. Biochem Biophys Res Commun. 2007 Mar 9; 354(2): 372–378.

Ganz WI, Sridhar KS, Forness TJ. Detection of early anthracycline cardiotoxicity by monitoring the peak filling rate. Am J Clin Oncol. 1993 Apr;16(2):109-12.

Garciarena CD, Youm JB, Swietach P, et al. H^+-activated Na^+ influx in the ventricular myocyte couples Ca^{2+}-signalling to intracellular pH. J Mol Cell Cardiol. 2013 Aug;61:51-9.

Gharanei M, Hussain A, Janneh O, Maddock H. Doxorubicin induced myocardial injury is exacerbated following ischaemic stress via opening of the mitochondrial permeability transition pore. Toxicol Appl Pharmacol. 2013a Apr 15;268(2):149-56

Gharanei M, Hussain A, Janneh O, et al. Attenuation of doxorubicin-induced cardiotoxicity by mdivi-1: a mitochondrial division/mitophagy inhibitor. PLoS One. 2013b Oct 17;8(10):e77713.

Gianni L, Herman EH, Lipshultz SE, et al. Anthracycline cardiotoxicity: from bench to bedside. J Clin Oncol. 2008 Aug 1;26(22):3777-84.

Giorgio V., Bisetto E., Soriano M.E., et al. Cyclophilin D modulates mitochondrial F_0F_1-ATP synthase by interacting with the lateral stalk of the complex. J Biol Chem. 2009;284:33982–33988

Glukhov AV, Balycheva M, Sanchez-Alonso JL, et al. Direct Evidence for Microdomain-Specific Localization and Remodeling of Functional L-Type Calcium Channels in Rat and Human Atrial Myocytes. Circulation. 2015 Oct 8.

Gnapareddy B, Dugasani SR, Ha T, et al. Chemical and Physical Characteristics of Doxorubicin Hydrochloride Drug-Doped Salmon DNA Thin Films. Sci Rep. 2015 Jul 31;5:12722.

Goto K, Takemura G, Maruyama R, et al. Unique mode of cell-death in freshly isolated adult rat ventricular cardiomyocytes exposed to hydrogen peroxide. Med Mol Morphol. 2009 Jun;42(2):92-101.

Grenier MA, Lipshultz SE. Epidemiology of anthracycline cardiotoxicity in children and adults. Semin Oncol. 1998 Aug;25(4 Suppl 10):72-85.

Griffiths EJ, Halestrap AP. Protection by cyclosporin A of ischemia/reperfusion-induced damage in isolated rat hearts. J Mol Cell Cardiol. 1993;25:1461–1469

Gustafsson, Å.B., Gottlieb, R.A., 2003. Mechanisms of apoptosis in the heart. J. Clin. Immunol. 23, 447–459.

Hafner, A. V., Dai, J., Gomes, A. P., Xiao, C. Y., Palmeira, C. M., Rosenzweig, A., et al. (2010). Regulation of the mPTP by SIRT3-mediated deacetylation of Cyp D at lysine 166 suppresses age-related cardiac hypertrophy. *Aging (Albany NY)* 2, 914–923.

Hale SL, Kloner RA. Ischemic preconditioning and myocardial hypothermia in rabbits with prolonged coronary artery occlusion. Am J Physiol. 1999 Jun;276(6 Pt 2):H2029-34.

Halestrap AP, Pasdois P. The role of the mitochondrial permeability transition pore in heart disease. Biochim Biophys Acta. 2009;1787:1402–1415.

Halestrap AP, Richardson AP. The mitochondrial permeability transition: a current perspective on its identity and role in ischaemia/reperfusion injury. J Mol Cell Cardiol. 2015 Jan;78:129-41.

Hanna AD, Janczura M, Cho E. Multiple actions of the anthracycline daunorubicin on cardiac ryanodine receptors. Mol Pharmacol. 2011 Sep;80(3):538-49.

Harbeck N, Ewer MS, De Laurentiis M, et al. Cardiovascular complications of conventional and targeted adjuvant breast cancer therapy. Ann Oncol. 2011;22:1250-1258.

Hattori R, Maulik N, Otani H, et al. Role of STAT3 in ischemic preconditioning. J Mol Cell Cardiol 2001;33:1929-1936.

Hausenloy DJ, Duchen MR, Yellon DM. Inhibiting mitochondrial permeability transition pore opening at reperfusion protects against ischaemia-reperfusion injury. Cardiovasc Res. 2003a Dec 1;60(3):617-25.

Hausenloy DJ, Yellon DM. The mitochondrial permeability transition pore: its fundamental role in mediating cell-death during ischaemia and reperfusion. J Mol Cell Cardiol. 2003b;35:339–341

Hausenloy DJ, Tsang A, Mocanu M, Yellon DM. Ischemic Preconditioning Protects by Activating Pro-Survival Kinases at Reperfusion. Am J Physiol Heart Circ Physiol 2005; 288: H971H976.

Hausenloy DJ, Lim SY, Ong SG, et al. Mitochondrial cyclophilin-D as a critical mediator of ischaemic preconditioning. Cardiovasc Res. 2010 Oct 1;88(1):67-74.

Hausenloy DJ, Lecour S, Yellon DM. Reperfusion injury salvage kinase and survivor activating factor enhancement prosurvival signaling pathways in ischemic postconditioning: two sides of the same coin. Antioxid Redox Signal. 2011 Mar 1;14(5):893-907.

Hausenloy DJ, Boston-Griffiths E, Yellon DM. Cyclosporin A and cardioprotection: from investigative tool to therapeutic agent. Br J Pharmacol. 2012 Mar; 165(5): 1235–1245.

Hausenloy DJ. Cardioprotection techniques: preconditioning, postconditioning and remote conditioning (basic science). Curr Pharm Des. 2013;19(25):4544-63.

He H, Liu X, Lv L, et al. Calcineurin suppresses AMPK-dependent cytoprotective autophagy in cardiomyocytes under oxidative stress. cell-death Dis. 2014 Jan 16;5:e997.

Henninger C, Fritz G. Statins in anthracycline-induced cardiotoxicity: Rac and Rho, and the heartbreakers. Cell Death Dis. 2017 Jan 19;8(1):e2564.

Hudson MM, Rai SN, Nunez C, et al. Noninvasive evaluation of late anthracycline cardiac toxicity in childhood cancer survivors. J Clin Oncol. 2007 Aug 20;25(24):3635-43.

Von Hoff, D. D. et al. Risk factors for doxorubicin-induced congestive heart failure. Ann. Intern. Med. 1979. 91, 710–717.

Huang C, Yitzhaki S, Perry CN, Liu W, Giricz Z, Mentzer RM, Jr, et al. Autophagy induced by ischemic preconditioning is essential for cardioprotection. J Cardiovasc Transl Res. 2010;3:365–73.

Ichihara S, Yamada Y, Kawai Y, et al. Roles of oxidative stress and Akt signaling in doxorubicin cardiotoxicity. Biochem Biophys Res Commun. 2007 Jul 20;359(1):27-33.

Ichikawa Y, Bayeva M, Ghanefar M, et al. Disruption of ATP-binding cassette B8 in mice leads to cardiomyopathy through a decrease in mitochondrial iron export. Proc Natl Acad Sci U S A. 2012 Mar 13;109(11):4152-7.

Ichikawa Y, Ghanefar M, Bayeva M, et al. Cardiotoxicity of doxorubicin is mediated through mitochondrial iron accumulation. J Clin Invest. 2014 Feb 3;124(2): 617-30.

Iliodromitis EK, Lazou A, Kremastinos DT. Ischemic preconditioning: protection against myocardial necrosis and apoptosis. Vasc Health Risk Manag. 2007;3(5):629-37.

Inagaki K, Chen L, Ikeno F, et al. Inhibition of δ-protein kinase C protects against reperfusion injury of the ischemic heart in vivo. Circulation (2003a). 108: 2304–2307.

Jancsó G, Cserepes B, Gasz B, et al. Expression and protective role of heme oxygenase-1 in delayed myocardial preconditioning. Ann N Y Acad Sci. 2007 Jan;1095:251-61.

Jensen BT, Lien CY, Hydock DS, et al. Exercise mitigates cardiac doxorubicin accumulation and preserves function in the rat. J Cardiovasc Pharmacol. 2013 Sep;62(3):263-9.

Jia Y, Zuo D, Li Z, et al. Astragaloside IV inhibits doxorubicin-induced cardiomyocyte apoptosis mediated by mitochondrial apoptotic pathway via activating the PI3K/Akt pathway. Chem Pharm Bull (Tokyo). 2014;62(1):45-53.

Johnson BA, Cheang MS, Goldenberg GJ: Comparison of adriamycin uptake in chick embryo heart and liver cells in murine L5178Y lymphoblasts in vitro: role of drug uptake in cardiotoxicity. Cancer Res, 1986, 46, 218–223.

Juhaszova M, Zorov DB, Kim SH, et al. Glycogen synthase kinase-3β mediates convergence of protection signaling to inhibit the mitochondrial permeability transition pore. J Clin Invest. 2004; 113: 1535–1549.

Kalivendi SV, Konorev EA, Cunningham S, et al. Doxorubicin activates nuclear factor of activated T-lymphocytes and Fas ligand transcription: role of mitochondrial reactive oxygen species and calcium. Biochem J. 2005;389:527–539.

Kalam K, Marwick TH. Role of cardioprotective therapy for prevention of cardiotoxicity with chemotherapy: a systematic review and meta-analysis. Eur J Cancer. 2013 Sep;49(13):2900-9.

Karch J, Kwong JQ, Burr AR, et al. Bax and Bak function as the outer membrane component of the mitochondrial permeability pore in regulating necrotic cell death in mice. Elife. 2013;2:e00772.

Kawamura T, Hasegawa K, Morimoto T, et al. Expression of p300 protects cardiac myocytes from apoptosis in vivo. Biochem Biophys Res Commun. 2004 Mar 12;315(3):733-8.

Khawaja MZ, Cafferkey C, Rajani R, et al. Cardiac complications and manifestations of chemotherapy for cancer. Heart. 2014 Jul;100(14):1133-40.

Khiati S, Dalla Rosa I, Sourbier C, et al. Mitochondrial topoisomerase I (top1mt) is a novel limiting factor of doxorubicin cardiotoxicity. Clin Cancer Res. 2014 Sep 15;20(18):4873-81.

Kim KH, Oudit GY, Backx PH. Erythropoietin protects against doxorubicin-induced cardiomyopathy via a phosphatidylinositol 3-kinase-dependent pathway. J Pharmacol Exp Ther. 2008 Jan;324(1):160-9.

Kim HY. Analysis of variance (ANOVA) comparing means of more than two groups. Restor Dent Endod. 2014 Feb;39(1):74-7.

Kinnally KW, Peixoto PM, et al. Is mPTP the gatekeeper for necrosis, apoptosis, or both? Biochim Biophys Acta. 2011 Apr;1813(4):616-22.

King BA, Oh DH. Spatial control of reactive oxygen species formation in fibroblasts using two-photon excitation. Photochem Photobiol. 2004 Jul-Aug;80:1-6.

Kristiansen KA, Jensen PE, Møller IM, Schulz A. Monitoring reactive oxygen species formation and localisation in living cells by use of the fluorescent probe CM-H(2)DCFDA and confocal laser microscopy. Physiol Plant. 2009 Aug;136(4):369-83.

Kis A, Yellon D.M, Baxter G.F. Second window of protection following myocardial preconditioning: an essential role for PI3 kinase and p70S6 kinase. J Mol Cell Cardiol, 35 (2003), pp. 1063–1071.

Kitamura Y, Koide M, Akakabe Y, et al. Manipulation of cardiac phosphatidylinositol 3-kinase (PI3K)/Akt signaling by apoptosis regulator through modulating IAP expression (ARIA) regulates cardiomyocyte death during doxorubicin-induced cardiomyopathy. J Biol Chem. 2014 Jan 31;289(5):2788-800.

Kloner RA, Muller J, Davis V. Effects of previous angina pectoris in patients with first acute myocardial infarction not receiving thrombolytics. MILIS Study Group. Multicenter Investigation of the Limitation of Infarct Size. Am J Cardiol. 1995(a) Mar 15;75(8):615-7.

Kloner RA, Shook T, Przyklenk K, et al. Previous angina alters in-hospital outcome in TIMI 4. A clinical correlate to preconditioning? Circulation. 1995(b) Jan 1;91(1):37-45.

Kobara M, Tatsumi T, Matoba S, et al. Effect of ischemic preconditioning on mitochondrial oxidative phosphorylation and high energy phosphates in rat hearts. J Mol Cell Cardiol 1996; 28(2): 417-28

Koval OM, Guan X, Wu Y, et al. CaV1.2 beta-subunit coordinates CaMKII-triggered cardiomyocyte death and after depolarizations. Proc Natl Acad Sci USA. 2010;107:4996–5000

Kurrelmeyer KM, Michael LH, Baumgarten G, et al. Endogenous tumor necrosis factor protects the adult cardiac myocyte against ischemic-induced apoptosis in a murine model of acute myocardial infarction. Proc Natl Acad Sci U S A 2000;97:5456-5461.

Kwok JC, Richardson DR. Unexpected anthracycline-mediated alterations in iron-regulatory protein-RNA-binding activity: the iron and copper complexes of anthracyclines decrease RNA-binding activity. Mol Pharmacol. 2002;62(4):888–900.

Kwong JQ, Molkentin JD. Physiological and pathological roles of the mitochondrial permeability transition pore in the heart. Cell Metab. 2015 Feb 3;21(2):206-214.

Ky B, Putt M, Sawaya H, et al. Early increases in multiple biomarkers predict subsequent cardiotoxicity in patients with breast cancer treated with doxorubicin, taxanes, and trastuzumab. J Am Coll Cardiol. 2014 Mar 4;63(8):809-16.

Lacerda L, Somers S, Opie LH, Lecour S. Ischaemic postconditioning protects against reperfusion injury via the SAFE pathway. Cardiovasc Res. 2009. 84: 201–208.

Langenbach KJ, Rando TA. Inhibition of dystroglycan binding to laminin disrupts the PI3K/AKT pathway and survival signaling in muscle cells. Muscle Nerve. 2002 Nov;26(5):644-53.

Levin S, Bucci TJ, Cohen SM, et al. The nomenclature of cell death: recommendations of an ad hoc Committee of the Society of Toxicologic Pathologists. Toxicol Pathol. 1999;27:484–90

Levraut J, Iwase H, Shao ZH, et al. cell-death during ischemia: relationship to mitochondrial depolarization and ROS generation.Am J Physiol Heart Circ Physiol. 2003 Feb;284(2):H549-58.

Lebrecht D, Kirschner J, Geist A,et al. Respiratory chain deficiency precedes the disrupted calcium homeostasis in chronic doxorubicin cardiomyopathy. Cardiovasc Pathol. 2010 Sep-Oct;19(5): e167-74.

Lecour S, Smith RM, Woodward B, et al. Identification of a novel role for sphingolipid signaling in TNF alpha and ischemic preconditioning mediated cardioprotection. J Mol Cell Cardiol. 2002 May;34(5):509-18.

Lecour S, Suleman N, Deuchar GA, et al. Pharmacological preconditioning with tumor necrosis factor-alpha activates signal transducer and activator of transcription-3 at reperfusion without involving classic prosurvival kinases (Akt and extracellular signal-regulated kinase). Circulation 2005;112: 3911-3918.

Lecour S, James RW. When are pro-inflammatory cytokines SAFE in heart failure? Eur Heart J. 2011 Mar;32(6):680-5.

Lenčová-Popelová O, Jirkovský E, Mazurová Y, et al. Molecular remodeling of left and right ventricular myocardium in chronic anthracycline cardiotoxicity and post-treatment follow up. PLoS One. 2014 May 7;9(5):e96055.

Li H, Zhu H, Xu CJ, Yuan J. Cleavage of BID by caspase-8 mediates the mitochondrial damage in the Fas pathway of apoptosis. Cell. 1998;94:491–501.

Li M and Beg AA. Induction of Necrotic-Like Cell Death by Tumor Necrosis Factor Alpha and Caspase Inhibitors: Novel Mechanism for Killing Virus-Infected Cells. J Virol. 2000 Aug; 74(16): 7470–7477.

Li RC, Ping P, Zhang J, et al. PKCepsilon modulates NF-kappaB and AP-1 via mitogen-activated protein kinases in adult rabbit cardiomyocytes. Am J Physiol Heart Circ Physiol. 2000 Oct;279(4):H1679-89

Li H, Gu H, Sun B. Protective effects of pyrrolidine dithiocarbamate on myocardium apoptosis induced by adriamycin in rats. Int J Cardiol. 2007;114:159–165.

Lim CC, Zuppinger C, Guo Xet al. Anthracyclines induce calpain-dependent titin proteolysis and necrosis in cardiomyocytes. J Biol Chem. 2004 Feb 27;279(9):8290-9.

Lin Y, Choksi S, Shen HM, et al. Tumor necrosis factor-induced nonapoptotic cell death requires receptor-interacting protein-mediated cellular reactive oxygen species accumulation. J Biol Chem. 2004 Mar 12;279(11):10822-8.

Ling H, Gray CB, Zambon AC, et al. Ca2+/Calmodulin-dependent protein kinase II δ mediates myocardial ischemia/reperfusion injury through nuclear factor-κB. Circ Res. 2013 Mar 15;112(6):935-44.

Lipshultz SE, Lipsitz SR,09 Kutok JL, et al. Impact of hemochromatosis gene mutations on cardiac status in doxorubicin-treated survivors of childhood high-risk leukemia. Cancer. 2013a Oct 1;119(19):3555-62.

Lipshultz SE, Cochran TR, Franco VI, et al. Treatment-related cardiotoxicity in survivors of childhood cancer. Nat Rev Clin Oncol. 2013b Dec;10(12):697-710.

Lipshultz SE, Sambatakos P, Maguire M, et al. Cardiotoxicity and cardioprotection in childhood cancer. Acta Haematol. 2014;132(3-4):391-9.

Liu GS, Thornton J, Van Winkle DM, et al. Protection against infarction afforded by preconditioning is mediated by A1 Adenosine receptors in rabbit heart. Circulation. 1991 Jul;84(1):350-6.

Liu J, Mao W, Ding B, Liang CS. ERKs/p53 signal transduction pathway is involved in doxorubicin-induced apoptosis in H9c2 cells and cardiomyocytes. Am J Physiol Heart Circ Physiol. 2008 Nov;295(5):H1956-65.

Lo CA, Kays I, Emran F, et al. Quantification of Protein Levels in Single Living Cells. Cell Rep. 2015 Dec 22;13(11):2634-2644.

Lou H, Danelisen I, Singal PK. Involvement of mitogen-activated protein kinases in adriamycin-induced cardiomyopathy. Am J Physiol Heart Circ Physiol. 2005 Apr;288(4):H1925-30.

Louch WE, Sheehan KA, Wolska BM. Methods in cardiomyocyte isolation, culture, and gene transfer. J Mol Cell Cardiol. 2011 Sep;51(3):288-98.

Lu L, Wu W, Yan J, et al. Adriamycin-induced autophagic cardiomyocyte death plays a pathogenic role in a rat model of heart failure. Int J Cardiol. 2009;134:82–90.

Luo M, Anderson ME. Ca^{2+} Cycling in Heart Failure. Circ Res. 2013 August 30; 113(6): 690–708.

Ma Y, Zhang X, et al. Toll-like receptor (TLR) 2 and TLR4 differentially regulate doxorubicin-induced cardiomyopathy in mice. PLoS One. 2012;7(7):e40763.

Ma J, Wang Y, Zheng D, et al. Rac1 signalling mediates doxorubicin-induced cardiotoxicity through both reactive oxygen species-dependent and -independent pathways. Cardiovasc Res. 2013 Jan 1;97(1):77-87.

Maillet A, Tan K, Chai X, et al. Modeling Doxorubicin-Induced Cardiotoxicity in Human Pluripotent Stem Cell Derived-Cardiomyocytes. Sci Rep. 2016 May 4;6:25333.

Marber MS, Latchman DS, Walker JM, Yellon DM. Cardiac stress protein elevation 24 hours after brief ischemia or heat stress is associated with resistance to myocardial infarction. Circulation. 1993 Sep;88(3):1264-72.

Marechal X, Montaigne D, Marciniak C, et al. Doxorubicin-induced cardiac dysfunction is attenuated by ciclosporin treatment in mice through improvements in mitochondrial bioenergetics. Clin Sci (Lond). 2011 Nov;121(9):405-13.

Marini M, Lapalombella R, Margonato V, et al. Mild exercise training, cardioprotection and stress genes profile. Eur J Appl Physiol. 2007 Mar; 99(5):503-10.

Marshall KD, Edwards MA, Krenz M, et al. Proteomic mapping of proteins released during necrosis and apoptosis from cultured neonatal cardiac myocytes. Am J Physiol Cell Physiol. 2014 Apr 1;306(7):C639-47.

Martel C, Huynh le H, Garnier A. et al. Inhibition of the Mitochondrial Permeability Transition for Cytoprotection: Direct versus Indirect Mechanisms. Biochem Res Int.2012:213403

Mathur A, Hong Y, Kemp BK, et al. Evaluation of fluorescent dyes for the detection of mitochondrial membrane potential changes in cultured cardiomyocytes. Cardiovasc Res. 2000 Apr; 46(1):126-38

Mavroidis M, Panagopoulou P, Kostavasili I, et al. A missense mutation in desmin tail domain linked to human dilated cardiomyopathy promotes cleavage of the head domain and abolishes its Z-disc localization. FASEB J. 2008 Sep;22(9):3318-27.

McLeod CJ, Jeyabalan AP, Minners JO, et al. Delayed ischemic preconditioning activates nuclear-encoded electron-transfer-chain gene expression in parallel with enhanced postanoxic mitochondrial respiratory recovery. Circulation. 2004 Aug 3;110(5):534-9

McManus E.J, Collins B.J, Ashby P.R, et al. The in vivo role of PtdIns(3,4,5)P(3) binding to PDK1 PH domain defined by knockin mutation. EMBO J, 23 (2004), pp. 2076–2082.

McNamara CR, Degterev A.Small-molecule inhibitors of the PI3K signaling network.Future Med Chem. 2011 Apr; 3(5): 549–565.

Merino H, Singla DK. Notch-1 mediated cardiac protection following embryonic and induced pluripotent stem cell transplantation in doxorubicin-induced heart failure. PLoS One. 2014 Jul 2;9(7):e101024.

Merten KE, Jiang Y, Feng W, et al. Calcineurin activation is not necessary for Doxorubicin-induced hypertrophy in H9c2 embryonic rat cardiac cells: involvement of the phosphoinositide 3-kinase-Akt pathway. J Pharmacol Exp Ther. 2006 Nov;319(2):934-40.

Mihm MJ, Coyle CM, Schanbacher BL, et al. Peroxynitrite induced nitration and inactivation of myofibrillar creatine kinase in experimental heart failure. Cardiovasc Res. 2001; 49: 798–807.

Mihm MJ, Yu F, Weinstein DM, et al. Intracellular distribution of peroxynitrite during doxorubicin cardiomyopathy: evidence for selective impairment of myofibrillar creatine kinase. Br J Pharmacol. 2002; 135:581-588.

Minotti G, Mancuso C, Frustaci A, et al. Paradoxical inhibition of cardiac lipid peroxidation in cancer patients treated with doxorubicin. Pharmacologic and molecular reappraisal of anthracycline cardiotoxicity. J Clin Invest. 1996 Aug 1;98(3):650-61.

Minotti G, Ronchi R, Salvatorelli E,et al. Doxorubicin irreversibly inactivates iron regulatory proteins 1 and 2 in cardiomyocytes: evidence for distinct metabolic pathways and implications for iron-mediated cardiotoxicity of antitumor therapy. Cancer Res. 2001;61(23):8422–8428.

Minotti G, Menna P, Salatorelli E, et al. Anthracyclines: Molecular advances and pharmacologic developments I antitumour activity and cardiotoxicity. Pharmacol Rev. 2004 Jun;56(2):185-229.

Miyata M, Suzuki S, Misaka T, et al. Senescence marker protein 30 has a cardio-protective role in doxorubicin-induced cardiac dysfunction. PLoS One. 2013 Dec 31;8(12):e79093.

Moazeni S, Cadeiras M, Yang EH, et al. Anthracycline induced cardiotoxicity: biomarkers and "Omics" technology in the era of patient specific care. Clin Transl Med. 2017 Dec;6(1):17.

Morishita N, Kusachi S, Yamasaki S, et al. Sequential changes in laminin and type IV collagen in the infarct zone--immunohistochemical study in rat myocardial infarction. Jpn Circ J. 1996 Feb;60(2):108-14.

Montaigne D, Marechal X, Baccouch R, et al. Stabilization of mitochondrial membrane potential prevents doxorubicin-induced cardiotoxicity in isolated rat heart. Toxicol Appl Pharmacol. 2010 May 1;244(3):300-7.

Montaigne D, Marechal X, Preau S, et al. Doxorubicin induces mitochondrial permeability transition and contractile dysfunction in the human myocardium. Mitochondrion. 2011 Jan;11(1):22-6.

Montaigne D, Hurt C, Neviere R. Mitochondria death/survival signaling pathways in cardiotoxicity induced by anthracyclines and anticancer-targeted therapies. Biochem Res Int. 2012;2012:951539.

Moser EC, Noordijk EM, van Leeuwen FE, et al. Long-term risk of cardiovascular disease after treatment for aggressive non-Hodgkin lymphoma. Blood. 2006 Apr 1;107(7):2912-9. Epub 2005 Dec 8.

Murphy E, Eisner DA. Regulation of intracellular and mitochondrial sodium in health and disease. Circ Res. 2009 Feb 13;104(3):292-303.

Murry CE, Jennings RB, Reimer KA. Preconditioning with ischemia: a delay of lethal cell injury in ischemic myocardium. Circulation. 1986 Nov;74(5):1124-36.

Nakamura T, Ueda Y, Juan Y, et al. Fas-mediated apoptosis in adriamycin-induced cardiomyopathy in rats: In vivo study. Circulation. 2000 Aug 1;102(5):572-8.

Nakayama H, Chen X, Baines CP, et al. Ca^{2+} and mitochondrial-dependent cardiomyocyte necrosis as a primary mediator of heart failure. J Clin Invest. 2007 Sep;117(9):2431-44.

Nazareth W, Yafei N, Crompton M. Inhibition of anoxia-induced injury in heart myocytes by cyclosporin A. J Mol Cell Cardiol. 1991;23:1351–1354.

Niu J, Azfer A, Wang K, et al. Cardiac-targeted expression of soluble fas attenuates doxorubicin-induced cardiotoxicity in mice. J Pharmacol Exp Ther. 2009 Mar;328(3):740-8.

Nitiss KC, Nitiss JL. Twisting and ironing: Doxorubicin cardiotoxicity by mitochondrial DNA damage. Clin Cancer Res. 2014 Sep 15;20(18):4737-9.

Nozaki N, Shishido T,et al. Modulation of doxorubicin-induced cardiac dysfunction in toll-like receptor-2-knockout mice. Circulation. 2004 Nov 2;110(18):2869-74.

Olson RD, Gambliel HA, et al. Doxorubicin cardiac dysfunction: effects on calcium regulatory proteins, sarcoplasmic reticulum, and triiodothyronine. Cardiovasc Toxicol. 2005;5(3):269-83.

Ong SB, Hall AR, Dongworth RK, et al. Akt protects the heart against ischaemia-reperfusion injury by modulating mitochondrial morphology. Thromb Haemost. 2015 Mar;113(3):513-21.

Osada M, Netticadan T, Tamura K, Dhalla NS. Modification of ischemia-reperfusion-induced changes in cardiac sarcoplasmic reticulum by preconditioning. Am J Physiol. 1998 Jun;274(6 Pt 2):H2025-34.

Oudit GY, Sun H, Kerfant BG, et al. The role of phosphoinositide-3 kinase and PTEN in cardiovascular physiology and disease. J Mol Cell Cardiol. 2004; 37: 449–471.

Pacher P, Liaudet L, Bai P, et al. Potent metalloporphyrin peroxynitrite decomposition catalyst protects against the development of doxorubicin-induced cardiac dysfunction. Circulation. 2003 Feb 18;107(6):896-904.

Park AM, Nagase H, Liu L, et al. Mechanism of anthracycline-mediated down-regulation of GATA4 in the heart. Cardiovasc Res. 2011 Apr 1;90(1):97-104.

Peng YW, Buller CL, Charpie JR. Impact of N-acetylcysteine on neonatal cardiomyocyte ischemia-reperfusion injury. Pediatr Res. 2011 Jul;70(1):61-6.

Pinder MC, Duan Z, Goodwin JS, et al. Congestive heart failure in older women treated with adjuvant anthracycline chemotherapy for breast cancer. J Clin Oncol. 2007;25:3808-3815.

Ross RS, Borg TK. Integrins and the myocardium. Circ Res. 2001 Jun 8;88(11):1112-9.

Pedretti S, Raddatz E. STAT3α interacts with nuclear GSK3beta and cytoplasmic RISK pathway and stabilizes rhythm in the anoxic-reoxygenated embryonic heart. Basic Res Cardiol. 2011 May;106(3):355-69.

Peng W, Liu Y, Xu WJ, Xia QH. Role of Beclin 1-dependent autophagy in cardioprotection of ischemic preconditioning. J Huazhong Univ Sci Technolog Med Sci. 2013 Feb;33(1):51-6.

Perry SW, Norman JP, Barbieri J, et al. Mitochondrial membrane potential probes and the proton gradient: a practical usage guide. Biotechniques. 2011 Feb;50(2):98-115.

Pillai VB, Bindu S, Sharp W, et al. Sirt3 protects mitochondrial DNA damage and blocks the development of doxorubicin-induced cardiomyopathy in mice. Am J Physiol Heart Circ Physiol. 2016 Apr 15;310(8):H962-72.

Powers SK, Demirel HA, Vincent HK, et al. Exercise training improves myocardial tolerance to in vivo ischemia-reperfusion in the rat. Am J Physiol. 1998;275:R1468–77.

Quarrie R, Cramer BM, Lee DS, et al. Ischemic preconditioning decreases mitochondrial proton leak and reactive oxygen species production in the postischemic heart. J Surg Res. 2011 Jan;165(1):5-14.

Rakhit RD, Edwards RJ, Mockridge JW, et al. Nitric oxide-induced cardioprotection in cultured rat ventricular myocytes. Am J Physiol Heart Circ Physiol. 2000 Apr;278(4):H1211-7.

Ranek MJ, Wang X. Activation of the ubiquitin-proteasome system in doxorubicin cardiomyopathy. Curr Hypertens Rep. 2009 Dec;11(6):389-95.

Rieger AM, Hall BE, Luong le T, Schang LM, Barreda DR. Conventional apoptosis assays using propidium iodide generate a significant number of false positives that prevent accurate assessment of cell death. J Immunol Methods. 2010 Jun 30;358(1-2):81-92.

Reimer KA, Lowe JE, Rasmussen MM, Jennings RB. The wavefront phenomenon of ischemic cell-death. 1. Myocardial infarct size vs duration of coronary occlusion in dogs. Circulation. 1977 Nov;56(5):786-94.

Riad A, Bien S, Gratz M, et al. Toll-like receptor-4 deficiency attenuates doxorubicin-induced cardiomyopathy in mice. Eur J Heart Fail. 2008 Mar;10(3):233-43.

Romano S, Fratini S, Ricevuto E et al. Serial measurements of NT-proBNP are predictive of not-high-dose anthracycline cardiotoxicity in breast cancer patients. Br J Cancer 2011. 105(11):1663–1668.

Rose BA, Force T, Wang Y. Mitogen-activated protein kinase signaling in the heart: angels versus demons in a heart-breaking tale. Physiol Rev. 2010 Oct;90(4):1507-46.

Ross RS, Borg TK. Integrins and the myocardium. Circ Res. 2001 Jun 8;88(11):1112-9.

Rottenberg H, Wu S. Quantitative assay by flow cytometry of the mitochondrial membrane potential in intact cells. Biochim Biophys Acta. 1998;1404:393–404.

Rowland RT, Meng X, Cleveland JC Jr, et al. LPS-induced delayed myocardial adaptation enhances acute preconditioning to optimize postischemic cardiac function. Am J Physiol. 1997 Jun;272(6 Pt 2):H2708-15.

Sag CM, Köhler AC, et al. CaMKII-dependent SR Ca leak contributes to doxorubicin-induced impaired Ca handling in isolated cardiac myocytes. J Mol Cell Cardiol. 2011 Nov;51(5):749-59.

Said, M, Becerra, R, Valverde, CA, et al. Calcium-calmodulin dependent protein kinase II (CaMKII): a main signal responsible for early reperfusion arrhythmias. J Mol Cell Cardiol. 2011 Dec;51(6):936-44.

Salas MA, Valverde CA, Sánchez G, et al. The signalling pathway of CaMKII-mediated apoptosis and necrosis in the ischemia/reperfusion injury. J Mol Cell Cardiol. 2010 Jun;48(6):1298-306

Sand JM, Larsen L, Hogaboam C, et al. MMP mediated degradation of type IV collagen alpha 1 and alpha 3 chains reflects basement membrane remodeling in experimental and clinical fibrosis--validation of two novel biomarker assays. PLoS One. 2013 Dec 23;8(12):e84934

Sandhu R, Diaz RJ, Mao GD, Wilson GJ. Ischemic preconditioning: differences in protection and susceptibility to blockade with single-cycle versus multicycle transient ischemia. Circulation. 1997 Aug 5;96(3):984-95.

Sartoretto JL, Kalwa H, Shiroto T, et al. Role of Ca2+ in the control of H2O2 -modulated phosphorylation pathways leading to eNOS activation in cardiac myocytes. PLoS One. 2012;7(9):e44627.

Scaduto RC Jr, Grotyohann LW. Measurement of mitochondrial membrane potential using fluorescent rhodamine derivatives. Biophys J. 1999 Jan;76(1 Pt 1):469-77.

Schulman D, Latchman DS, Yellon DM. Urocortin protects the heart from reperfusion injury via upregulation of p42/p44 MAPK signaling pathway. Am J Physiol Heart Circ Physiol. 2002 Oct;283(4):H1481-8.

Schwartz RG, McKenzie WB, Alexander J, et al. Congestive heart failure and left ventricular dysfunction complicating doxorubicin therapy. Seven-year experience using serial radionuclide angiocardiography Am J Med. 1987 Jun;82(6):1109-18.

Seki K, Sanada S, Kudinova AY, et al. Interleukin-33 prevents apoptosis and improves survival after experimental myocardial infarction through ST2 signaling. Circ Heart Fail. 2009 Nov;2(6):684-91

Shulga, N., and Pastorino, J. G. Ethanol sensitizes mitochondria to the permeability transition by inhibiting deacetylation of cyclophilin-D mediated by sirtuin-3. J. Cell. Sci. 2010. 123, 4117–4127.

Shimojo T, Hiroe M, Ishiyama S, et al. Nitric oxide induces apoptotic death of cardiomyocytes via a cyclic-GMP-dependent pathway. Exp Cell Res. 1999 Feb 25;247(1):38-47.

Shulga, N., and Pastorino, J. G. (2010). Ethanol sensitizes mitochondria to the permeability transition by inhibiting deacetylation of cyclophilin-D mediated by sirtuin-3. *J. Cell. Sci.* 123, 4117–4127.

Siddall HK, Yellon DM, Ong SB, et al. Loss of PINK1 increases the heart's vulnerability to ischemia-reperfusion injury. PLoS One. 2013 Apr 29;8(4):e62400.

Simůnek T, Stérba M, Popelová O, et al. Anthracycline-induced cardiotoxicity: overview of studies examining the roles of oxidative stress and free cellular iron. Pharmacol Rep. 2009 Jan-Feb;61(1):154-71.

Small GW, Somasundaram S, Moore DT, et al. Repression of mitogen-activated protein kinase (MAPK) phosphatase-1 by anthracyclines contributes to their antiapoptotic activation of p44/42-MAPK. J Pharmacol Exp Ther. 2003 Dec;307(3):861-9.

Smith RM, Suleman N, Lacerda L, et al. Genetic depletion of cardiac myocyte STAT-3 abolishes classical preconditioning. Cardiovasc Res 2004;63:611-616.

Smith CC, Dixon RA, Wynne AM, et al. Leptin-induced cardioprotection involves JAK/STAT signaling that may be linked to the mitochondrial permeability transition pore. Am J Physiol Heart Circ Physiol. 2010 Oct;299(4):H1265-70.

Solem LE, Wallace KB. Selective activation of the sodium-independent, cyclosporin A-sensitive calcium pore of cardiac mitochondria by doxorubicin. Toxicol Appl Pharmacol. 1993 Jul;121(1):50-7.

Solem, LE, Henry TR, Wallace KB. Disruption of mitochondrial calcium homeostasis following chronic doxo rubicin administration. Toxicol Appl Pharmacol. 1994 Dec; 129(2), 214–222.

Solenkova NV, Solodushko V, Cohen MV, Downey J. Endogenous Adenosine protects preconditioned heart during early minutes of reperfusion by activating Akt. Am J Physiol Heart Circ Physiol. 2006 Jan;290(1):H441-9.

Spallarossa P, Altieri P, Garibaldi S, et al. Matrix metalloproteinase-2 and -9 are induced differently by doxorubicin in H9c2 cells: The role of MAP kinases and NAD(P)H oxidase. Cardiovasc Res. 2006 Feb 15;69(3):736-45.

Stěrba M, Popelová O, Lenčo J, et al. Proteomic insights into chronic anthracycline cardiotoxicity. J Mol Cell Cardiol. 2011 May;50(5):849-62.

Stoddard MF, Seeger J, Liddell NE, et al. Prolongation of isovolumetric relaxation time as assessed by Doppler echocardiography predicts doxorubicin-induced systolic dysfunction in humans. J Am Coll Cardiol. 1992;20(1):62–69.

Suter TM, Ewer MS. Cancer drugs and the Heart: importance and management. Eur Heart J. 2013 Apr;34(15):1102-11.

Su HF, Samsamshariat A, Fu J,et al. Oleylethanolamide activates Ras-ERK pathway and improves myocardial function in doxorubicin-induced heart failure. Endocrinology. 2006 Feb;147(2):827-34.

Sun X, Gu J, Chi M, et al. Activation of PI3K-Akt through taurine is critical for propofol to protect rat cardiomyocytes from doxorubicin-induced toxicity. Can J Physiol Pharmacol. 2014 Feb;92(2):155-61.

Tacar O, Indumathy S, Tan ML, et al. Cardiomyocyte apoptosis vs autophagy with prolonged doxorubicin treatment: comparison with osteosarcoma cells. J Pharm Pharmacol. 2015 Feb;67(2):231-43.

Takeishi Y, Huang Q, Wang T, et al. Src family kinase and Adenosine differentially regulate multiple MAP kinases in ischemic myocardium: Modulation of MAP kinases activation by ischemic preconditioning. J Mol Cell Cardiol. 2001;33:1989–2005.

Tang J, Wang G, Liu Y, et al. Cyclosporin A induces cardiomyocyte injury through calcium-sensing receptor-mediated calcium overload. Pharmazie. 2011 Jan;66(1):52-7.

Tanno M, Gorog DA, Bellahcene M, et al. Tumor necrosis factor-induced protection of the murine heart is independent of p38-MAPK activation. J Mol Cell Cardiol. 2003 Dec;35(12):1523-7.

Temsah RM, Netticadan T, Chapman D, et al. Alterations in sarcoplasmic reticulum function and gene expression in ischemic-reperfused rat heart. Am J Physiol. 1999 Aug;277(2 Pt 2):H584-94.

Temsah RM, Kawabata K, Chapman D, Dhalla NS. Preconditioning prevents alterations in cardiac SR gene expression due to ischemia-reperfusion. Am J Physiol Heart Circ Physiol. 2002 Apr;282(4):H1461-6.

Thompson-Gorman SL, Zweier JL. Evaluation of the role of xanthine oxidase in myocardial reperfusion injury. J Biol Chem. 1990;265:6656–6663.

Tian S, Hirshfield KM, Jabbour SK, et al. Serum biomarkers for the detection of cardiac toxicity after chemotherapy and radiation therapy in breast cancer patients. Front Oncol. 2014 Oct 9;4:277.

Tokarska-Schlattner M, Zaugg M, Zuppinger C, et al. New insights into doxorubicin-induced cardiotoxicity: the critical role of cellular energetics. J Mol Cell Cardiol. 2006 Sep;41(3):389-405.

Tong H, Chen W, Steenbergen C, Murphy E. Ischemic preconditioning activates phosphatidylinositol-3-kinase upstream of protein kinase C. Circ Res 2000; 87(4): 309-15.

Tong H, Imahashi K, Steenbergen C, Murphy E. Phosphorylation of glycogen synthase kinase-during preconditioning through a phosphatidylinositol-3-kinase-dependent pathway is cardioprotective. Circ Res. 2002; 90: 377–379

Tsuchida A, Liu GS, Mullane K, Downey JM. Acadesine lowers temporal threshold for the myocardial infarct size limiting effect of preconditioning. Cardiovasc Res. 1993 Jan;27(1):116-20.

Ushio-Fukai M, Alexander RW, Akers M, et al. Reactive oxygen species mediate the activation of Akt/protein kinase B by angiotensin II in vascular smooth muscle cells. J Biol Chem. 1999; 274: 22699-22704

van Dalen EC, Caron HN, Dickinson HO, Kremer LC. Cardioprotective interventions for cancer patients receiving anthracyclines. Cochrane Database Syst Rev. 2011 Jun 15;(6):CD003917.

van den Doel MA, Gho BC, Duval SY, et al. Hypothermia extends the cardioprotection by ischaemic preconditioning to coronary artery occlusions of longer duration. Cardiovasc Res. 1998 Jan;37(1):76-81.

van Loo G, van Gurp M, Depuydt B, et al. The serine protease Omi/HtrA2 is released from mitochondria during apoptosis. Omi interacts with caspase-inhibitor XIAP and induces enhanced caspase activity. Cell Death Differ. 2002 Jan;9(1):20-6

Vicencio JM, Yellon DM, Sivaraman V, et al. Plasma exosomes protect the myocardium from ischemia-reperfusion injury. J Am Coll Cardiol. 2015 Apr 21;65(15):1525-36.

Vila-Petroff M, Salas MA, Said M, et al. CaMKII inhibition protects against necrosis and apoptosis in irreversible ischemia-reperfusion injury. Cardiovasc Res. 2007 Mar 1;73(4):689-98.

Wang Y, Lyu YL, Wang JC. Dual localization of human DNA topoisomerase IIIalpha to mitochondria and nucleus. Proceedings of the National Academy of Sciences of the United States of America. 2002;99:12114–9.

Wang S, Kotamraju S, Konorev E, et al. Activation of nuclear factor-kappaB during doxorubicin-induced apoptosis in endothelial cells and myocytes is pro-apoptotic: the role of hydrogen peroxide. Biochem J. 2002;367:729–740.

Wang XL, Liu HR, Tao L, et al. Role of iNOS-derived reactive nitrogen species and resultant nitrative stress in leukocytes-induced cardiomyocyte apoptosis after myocardial ischemia/reperfusion. Apoptosis. 2007 Jul;12(7):1209-17.

Wang L, Zhang TP, Zhang Y, et al. Protection against doxorubicin-induced myocardial dysfunction in mice by cardiac-specific expression of carboxyl terminus of hsp70-interacting protein. Sci Rep. 2016 Jun 21;6:28399.

Weinstein DM, Mihm MJ, Bauer JA. Cardiac peroxynitrite formation and left ventricular dysfunction following doxorubicin treatment in mice. J Pharmacol Exp Ther. 2000; 294: 396–401.

Westermann D, Lettau O, Sobirey M, et al. Doxorubicin cardiomyopathy-induced inflammation and apoptosis are attenuated by gene deletion of the kinin B1 receptor. Biol Chem. 2008 Jun;389(6):713-8.

Wonders KY, Hydock DS, Schneider CM, et al. Acute exercise protects against doxorubicin cardiotoxicity. Integr Cancer Ther. 2008 Sep;7(3):147-54.

Xia Y, Zweier JL. Substrate control of free radical generation from xanthine oxidase in the postischemic heart. J Biol Chem. 1995;270:18797–18803.

Xu S, Wang P, Zhang H, et al. CaMKII induces permeability transition through Drp1 phosphorylation during chronic β-AR stimulation. Nat Commun. 2016 Oct 14;7:13189.

Yamashita N, Nishida M, Hoshida S, et al. Induction of manganese superoxide dismutase in rat cardiac myocytes increases tolerance to hypoxia 24 hours after preconditioning. J Clin Invest. 1994 Dec;94(6):2193-9.

Yamashita N, Hoshida S, Otsu K, et al. Exercise provides direct biphasic cardioprotection via manganese superoxide dismutase activation. J Exp Med. 1999 Jun 7; 189(11):1699-706.

Yamashita N, Hoshida S, Otsu K, et al. The involvement of cytokines in the second window of ischaemic preconditioning. Br J Pharmacol. 2000 Oct;131(3):415-22.

Yamazaki T, Komuro I, Shiojima I, Yazaki Y. Angiotensin II mediates mechanical stress-induced cardiac hypertrophy. Diabetes Res Clin Pract. 1996;30(Suppl):107–11.

Yan W, Xuan C, Xuan L, et al. BN52021 protects rat cardiomyocyte from doxorubicin-induced cardiotoxicity. Int J Clin Exp Pathol. 2015 Feb 1;8(2):1719-24.

Yang JT, Qian LB, Zhang FJ, et al. Cardioprotective effects of luteolin on ischemia/reperfusion injury in diabetic rats are modulated by eNOS and the mitochondrial permeability transition pathway. J Cardiovasc Pharmacol. 2015 Apr;65(4):349-56.

Yano N, Suzuki D, Endoh M,et al. Beta-adrenergic receptor mediated protection against doxorubicin-induced apoptosis in cardiomyocytes: the impact of high ambient glucose. Endocrinology. 2008 Dec;149(12):6449-61.

Yao Y, Chen R, Ying C, et al. Interleukin-33 attenuates doxorubicin-induced cardiomyocyte apoptosis through suppression of ASK1/JNK signaling pathway. Biochem Biophys Res Commun. 2017 Nov 25;493(3):1288-1295.

Yellon DM, Baxter GF. A “second window of protection” or delayed preconditioning phenomenon: future horizons for myocardial protection? 1995. J Mol Cell Cardiol. 27:1023–34.

Yuan F, Xie Q, Wu J, et al. MST1 promotes apoptosis through regulating Sirt1-dependent p53 deacetylation. J Biol Chem. 2011 Mar 4;286(9):6940-5.

Zeiss CJ. The apoptosis-necrosis continuum: insights from genetically altered mice. Vet Pathol. 2003;40:481–95

Zhai, L, Guo C, Cao Y, et al. Long-term results of pirarubicin versus doxorubicin in combination chemotherapy for aggressive non-Hodgkin's lymphoma: single center, 15-year experience. Int J Hematol. 2010 Jan;91(1):78-86.

Zhang YW, Shi J, Li YJ, Wei L. Cardiomyocyte death in doxorubicin-induced cardiotoxicity. Arch Immunol Ther Exp (Warsz). 2009 Nov-Dec;57(6):435-45.

Zhang Y, Kang YM, Tian C, et al. Overexpression of Nrdp1 in the heart exacerbates doxorubicin-induced cardiac dysfunction in mice. PLoS One. 2011a;6(6):e21104.

Zhang C, Feng Y, Qu S, et al. Resveratrol attenuates doxorubicin-induced cardiomyocyte apoptosis in mice through SIRT1-mediated deacetylation of p53. Cardiovasc Res. 2011s. Jun 1;90(3):538-45.

Zhang S, Liu X, Bawa-Khalfe T, Lu LS, Identification of the molecular basis of doxorubicin-induced cardiotoxicity. Nat Med. 2012 Nov;18(11):1639-42.

Zhang XQ, Tang R, Li L, Szucsik A, et al. Cardiomyocyte-specific p65 NF-κB deletion protects the injured heart by preservation of calcium handling. Am J Physiol Heart Circ Physiol. 2013 Oct 1;305(7):H1089-97.

Zhang H, Shang W, Zhang X, et al. β-adrenergic-stimulated L-type channel Ca^{2}+ entry mediates hypoxic Ca^{2}+ overload in intact heart. J Mol Cell Cardiol. 2013 Dec;65:51-8.

Zhang T, Zhang Y, Cui M, et al. CaMKII is a RIP3 substrate mediating ischemia- and oxidative stress-induced myocardial necroptosis. Nat Med. 2016 Feb;22(2):175-82.

Zhao L, Zhang B. Doxorubicin induces cardiotoxicity through upregulation of death receptors mediated apoptosis in cardiomyocytes. Sci Rep. 2017 Mar 16; 7: 44735.

Zhou S, Palmeira CM, Wallace KB. Doxorubicin-induced persistent oxidative stress to cardiac myocytes. Toxicol Lett. 2001 May 19;121(3):151-7.

Zhu W, Zou Y, Aikawa R, et al. MAPK superfamily plays an important role in daunomycin-induced apoptosis of cardiac myocytes. Circulation. 1999 Nov 16;100(20):2100-7.

Zhu J, Zhang J, Zhang L, et al. Interleukin-1 signaling mediates acute doxorubicin-induced cardiotoxicity. Biomed Pharmacother. 2011 Oct;65(7):481-5.

Zorov DB, Filburn CR, Klotz LO, et al. Reactive oxygen species (ROS)-induced ROS release: a new phenomenon accompanying induction of the mitochondrial permeability transition in cardiac myocytes. J Exp Med. 2000;192:1001–1014.